THE UNIVERSITY OF CHICAGO

THE ROLE OF H3K79ME2 IN LEUKEMIA AND ALTERNATIVE SPLICING

A DISSERTATION SUBMITTED TO

THE FACULTY OF THE DIVISION OF THE BIOLOGICAL SCIENCES

AND THE PRITZKER SCHOOL OF MEDICINE

IN CANDIDACY FOR THE DEGREE OF

DOCTOR OF PHILOSOPHY

GRADUATE PROGRAM IN CELL AND MOLECULAR BIOLOGY

BY

WILLIAM FRANK RICHTER, JR.

CHICAGO, ILLINOIS

MARCH 2021

Dedicated to my mother, who always supported me in my endeavors and helped spark my interest in science.

TABLE OF CONTENTS

LIST OF FIGURES

LIST OF TABLES

ACKNOWLEDGEMENTS

I would like to thank Dr. Alexander Ruthenburg for his guidance and mentorship. His enthusiasm for science inspired me to attempt to answer difficult and exciting questions about what makes us all tick. I would also like to thank the members of my thesis committee: Dr. Jonathan Staley, Dr. Douglas Bishop and Dr. Benjamin Glick for their wisdom and thoughtful assessments of my work. I would like to thank the members of the Ruthenburg lab, some truly incredible people who made the long hours pass quickly and the, at times, seemingly sisyphusian tasks bearable. Most of all, I'd like to thank Connie for her support and love and William for his ability to lift my spirits in even the most difficult of times with his bright smile and bear hugs.

This work was made possible by funding from the National Institutes of Health including the NIH Molecular and Cellular Biology Training Grant 2T32GM007183-37.

ABSTRACT

Methylation at lysine 79 of histone H3 regulates a variety of nuclear functions necessary for embryogenesis, hematopoiesis and cardiac development while playing crucial roles in cell cycle regulation, DNA repair, transcriptional activation and alternative splicing (Bernt et al., 2011; Daigle et al., 2011; Deshpande et al., 2013; Huyen et al., 2004; Jones et al., 2008; McLean et al., 2014). Surprisingly, given the abundance of studies of this mark (W. Kim et al., 2014; McLean et al., 2014; Vlaming & van Leeuwen, 2016), little is known about the mechanisms by which it affects cellular processes and importantly, the proteins that recognize it. For instance, in the current model of MLL-rearranged (MLL-r) leukemogenesis, knockout or inhibition of DOT1L, the enzyme that deposits H3K79me2, reduces expression of *HOXA9* and *MEIS1*, the leukemic oncogenes that drive proliferation, through depletion of activating H3K79me2, thereby reducing cell survival (Bernt et al., 2011; Guenther et al., 2008; Milne et al., 2005; Stubbs et al., 2008). This model however, is unable to explain key observations such as reductions in the proliferation of leukemia cells at DOT1L inhibitor concentrations that do not affect the expression of the canonical driver oncogenic drivers *HOXA9* and *MEIS1*. Additionally, H3K79me2 depletion also affects alternative splicing in MLL-r cell lines through repression of exon skipping but, the mechanism behind this effect and the proteins involved are unknown. In MLL-r leukemia, I find that the FLT3-ITD/STAT5A and PRC2 pathways are disrupted by low-dose pinometostat (10 nM), a concentration that reduces proliferation of the MLL-r MV4;11 cell line without affecting *HOXA9* and *MEIS1* expression. At this low-dose inhibitor concentration I also identify 71 events of differential alternative splicing. Using quantitative ICeChIP-seq, I observe profound H3K79me2 depletion at downregulated MLL-r targets, and alternatively spliced genes, with resulting increases in transcriptionally activating H3K4me3 at MLL-r target

promoters, increases in H3K36me3 in gene bodies and global reductions in repressive H3K27me3. Although downregulation of polycomb components modestly contributes to reductions in proliferation, overexpression of constitutively active *STAT5A*, a target of FLT3-ITD-signalling, nearly completely rescues proliferation, accounting for the bulk of cytotoxicity from H3K79me2 depletion. I also observe a dependence of FLT3-ITD/STAT5A signaling on MLL1 function, suggesting that the *FLT3* locus is exquisitely sensitive to both H3K79me2 and H3K4me3 depletion and arguing that combinations of DOT1L, MLL1 and FLT3 inhibitors should be explored for treating the ~30% of all leukemias that carry *FLT3* mutations. Additionally, I identify several splicing factors that recognize H3K79me2 through modified nucleosome pulldowns from nuclear extract followed by tandem mass spectrometry. Knocking down one of these factors, PTBP1 results in similar effects on alternative splicing as DOT1L inhibition, suggesting that PTBP1 facilitates H3K79me2-mediated alternative splicing and providing the first mechanistic understanding of how H3K79me2 affects alternative splicing

1. INTRODUCTION

1.1 HISTONE POST-TRANSLATIONAL MODIFICATIONS

The organization and compaction of eukaryotic DNA within the nucleus is accomplished through association with histone proteins in a complex called the nucleosome core particle. Nucleosomes are composed of 147 base pairs of DNA wrapped around a histone octamer comprised of 2 copies each of 4 histone proteins: H2A, H2B, H3 and H4 (Cutter & Hayes, 2015; Kornberg & Lorch, 1999). But, beyond facilitating the storage and accessibility of the genetic blueprint these histone proteins themselves carry information crucial to the proper dissemination and maintenance of the genetic code in the form of post-translational modifications (Strahl & Allis, 2000).

The core histone proteins are highly conserved (Arents & Moudrianakis, 1995; Sullivan & Landsman, 2003), containing several alpha helices that facilitate interactions among histone proteins, basic patches where histones coordinate DNA binding and long, unstructured C-terminal tails. It is the C-terminal tails that harbor the vast majority of post-translational modifications including methylation, acetylation, phosphorylation and sumoylation to name just a few of a growing list of over 500 distinct modification types found on all 4 core histones and histone variants (Zhao & Garcia, 2015). Some of these modifications can exist in multiple states at a single residue. For example, lysines can be mono-, di- or trimethylated through processive or non-processive enzymatic processes at the same nitrogen atom (Zhao & Garcia, 2015).

Histone post-translational modifications were discovered in 1964 with the observation that residues could be methylated and acetylated, fostering an earlier and deeper understanding

of these two types of modifications (ALLFREY et al., 1964). Recent advancements in mass spectrometry and molecular biology are responsible for a surge in the discovery of the types and locations of histone modifications however, we as yet understand very little about the functional significance of the vast majority of these modifications (Zhao & Garcia, 2015).

Many histone modifications such as H3K4me3, H3K79me2 and H2Bub are evolutionarily conserved from yeast to humans (Zhang et al., 2015). Over 50 years of investigations into just a few of these modifications have ascribed a variety of important functions. For instance: lysine acetylation promotes transcription through the disruption of higher order chromatin structure and the promotion of transcription factor binding (Tse et al., 1998; Vettese-Dadey et al., 1996); Histone 3 lysine 10 phosphorylation is involved in both chromatin condensation during mitosis and transcriptional activation during interphase (Clayton et al., 2000; Hendzel et al., 1997); and two of the most extensively studied modifications- histone methylation at lysine 4 (H3K4me3) and lysine 27 (H3K27me3) can recruit proteins to facilitate transcriptional activation (Vermeulen et al., 2007) and repression (R. Cao et al., 2002), respectively.

Histone modifications populate a dynamic landscape in which marks can be deposited by enzymes characterized as “writers” removed by “erasers” and recognized by “readers”. To date, dozens of enzymes have been discovered that deposit and remove some of the more thoroughly studied modifications such as acetylation, phosphorylation and methylation (Q. Jin et al., 2011; Lee & Workman, 2007; Nagy & Tora, 2007; Ruthenburg et al., 2007; Sassone-Corsi et al., 1999). Several H3K4 methyltransferases have been discovered in humans including: MLL1-4, SETD1A, ASH1, SMYD3 and PRDM9 (Ruthenburg et al., 2007). Interestingly, as is the case with many highly conserved modifications such as H3K4me3, the modification is deposited by

only one enzyme in yeast (Set1), and by several homologs in mammalian cells, performing overlapping yet non-redundant functions necessary for the development of more complex organisms (Ruthenburg et al., 2007; Zhang et al., 2015). For instance, while SETD1A/B are responsible for depositing the majority of H3K4me2/3 in human cells (Hu et al., 2013), PRDM9 is a meiosis-specific H3K4 methyltransferase involved in the selection of recombination hot spots and MLL1 is involved in homeotic gene regulation (Hayashi et al., 2005; A. Yokoyama et al., 2004). An interesting counterexample of this is Dot1/DOT1L, the methyltransferase responsible for depositing mono-, di- and trimethylation of H3K79, where one enzyme is responsible for deposition of this highly conserved modification in yeast, humans and many other eukaryotic organisms (McLean et al., 2014). Notable exceptions are *Trypanosoma brucei* and Caenorhabditis elegans which possess 2 and 5 Dot1 homologs, respectively (W. Kim et al., 2014).

Timely and effective removal of histone modifications can be just as crucial as their deposition. In the case of H3K4me3 with its demonstrated role in gene activation (P.-Y. Chang et al., 2010; Vermeulen et al., 2007), it's necessary to remove this modification from homeotic target genes for efficient silencing and temporal control of expression to ensure proper vertebrate body patterning and development (Shen et al., 2017; B. D. Yu et al., 1995). There are nearly a dozen histone demethylases capable of removing H3K4 methylation including LSD1-2 and the JARID1A-D family of enzymes. Histone deacetylases are also crucial regulators of gene expression. Histones can be acetylated at many different lysine residues including H3K9ac, H3K14ac and H3K27ac, promoting an open chromatin conformation that facilitates gene activation and making these modifications the hallmarks of active promoters and enhancers (Karmodiya et al., 2012). Histone deacetylases (HDACs) remove these modifications to

facilitate gene silencing or inactive enhancers. The HDAC SIRT1 removes H3K9ac, making that residue available for methylation by the SUVAR39H1 methyltransferase which can then methylate and silence gene targets by facilitating heterochromatinization (C. W. Chen et al., 2015).

The functions of histone modifications must be carried out by proteins that recognize or "read" specific modifications. These proteins typically have characteristic folds that mediate interactions with specific marks. For example, proteins typically bind methylated lysine residues using one of several common binding domain structures such as a Tudor, chromodomain, PHD, PWWP, MBT, WD40 and Ankyrin Repeats among others (Yun et al., 2011). Structural analyses of several of these domains have revealed the use of aromatic cages to coordinate interactions with the small, uncharged methylation modifications (Yun et al., 2011). Proteins that recognize acetylated lysines almost always mediate the interaction with a variation of the bromodomain fold. Often, multiple modification-binding domains can be found within the same protein or complex. The TFIID transcription initiation factor binds H3K4me3 via a PHD finger of the TAF3 subunit, while also recognizing H4K5ac and H4K12ac through double bromodomains via the TAf1 subunit (Jacobson et al., 2000; Vermeulen et al., 2007). Coexistence of these domains and others that recognize phosphorylation, ubiquitination and additional histone marks within a single protein or protein complex suggests that multiple modifications could be simultaneously recognized by a specific protein or complex. Observations such as these led Strahl and Allis to formulate the "histone code" hypothesis around 20 years ago, which postulates that two or more unique histone modifications can be recognized by protein effectors to produce an outcome distinct from either of the modifications alone, meaning that specific combinations of modifications could "code" for different effector outputs (Strahl & Allis, 2000).

In addition to the coexistence of modifications within regions of chromatin, there is ample evidence of crosstalk through dependence and antagonism of histone modifications. For instance, histone H2B ubiquitination is a prerequisite for the installation of both H3K4me3 and H3K79me2, modifications involved in transcriptional activation (Dover et al., 2002; Ng et al., 2002). Often, modifications with opposing functions in gene regulation can antagonize one another. The H3K27me3 mark involved in gene silencing and heterochromatinization inhibits the methyltransferase activity of SET1-like complexes that deposit H3K4me3 (D.-H. Kim et al., 2013). H3K27me3 also inhibits DOT1L, the histone methyltransferase that deposits H3K79me1/2/3, marks found at transcriptionally active chromatin, through an interaction with the PZP domain of its complex subunit AF10 (S. Chen et al., 2015). But antagonism among these modifications is bidirectional and both H3K4me3 and H3K36me2/3, additional modifications found at transcriptionally active chromatin, inhibit deposition of H3K27me3 through an interaction with the PRC2 complex subunit SUZ12 (Schmitges et al., 2011). This dynamic interplay helps establish chromatin domains where the modifications involved in gene activation or silencing reinforce the enrichment of like-functioning marks, further enhancing and fine-tuning the regulation of gene expression, meiotic recombination and other important functions (Dixon et al., 2016).

Although much as been learned about chromatin modifications in the last 50 years, there is still so much that we don't understand about how these marks influence one another as well as the maintenance and dissemination of the genetic code. Investigations using peptide fragments carrying particular modifications in pulldowns from nuclear extract have worked well to identify binders of marks on the unstructured histone tails such as H3K4me3 and H3K27me3 (Vermeulen et al., 2010). However, this strategy has not worked as well to identify proteins that recognize

modifications found on the structured nucleosome core such as H3K79me2 and we still know very little about what proteins bind many of these modifications. Further investigations and new approaches will be necessary to fully understand the functions of these histone core modifications as well as the hundreds of other new modifications that have only recently come to light.

1.2 DOT1L AND METHYLATION OF LYSINE 79 OF HISTONE H3

Unlike some of the better understood modifications found on histone tails such as H3K4me3 and H3K27me3, methylation at lysine 79 of histone 3 (H3K79me) is located at a solvent-exposed interface at the structured nucleosome core (Van Leeuwen et al., 2002). Lysine 79 resides on a loop between alpha helices at the intersection of the H3/H4 tetramer and the H2A/H2B dimer (Van Leeuwen et al., 2002). H3K79me is conserved from yeast to humans and has been implicated in a multitude of cellular processes including DNA repair, embryogenesis, transcriptional activation and carcinogenesis (Bernt et al., 2011; Daigle et al., 2011; Deshpande et al., 2013; Huyen et al., 2004; Jones et al., 2008; McLean et al., 2014). H3K79me is found in the bodies of actively transcribed genes and methylation levels directly correlate with transcriptional activity (Steger et al., 2008). H3K79 can be mono-, di- or trimethylated and over 90% of the yeast genome bears H3K79 methylation (Van Leeuwen et al., 2002). Interestingly, the human genome shows the opposite enrichment where a little over 10% of the genome is methylated (Sweet et al., 2010). Observations by mass spectrometry, quantifying the different methylation states of lysine 79 in HeLa cells, revealed that of total cellular H3, 11% is monomethylated, 1.5% is demethylated and <0.1% is trimethylated (Sweet et al., 2010; Vlaming & van Leeuwen, 2016). Monomethylation at H3K79 (H3K79me1) is distributed throughout the

entire gene body and can also be found at inactive or "poised" genes. However, H3K79me2 and me3 are enriched in the 5' regions of active genes downstream of the TSS and taper off far into the gene body (Barski et al., 2007; Steger et al., 2008). The scarcity of H3K79me3 on chromatin as determined by mass spectrometry measurements, suggests a less prominent role for this modification in functions attributed to H3K79me and is a key factor in the predominant focus on dimethylation in the field (Sweet et al., 2010; Vlaming & van Leeuwen, 2016).

Dot1 (Disruptor of Telomere Silencing), the histone methyltransferase (HMT) responsible for depositing H3K79me2, was first identified in yeast in a genetic screen for components necessary for telomere silencing (van Welsem et al., 2008). Germ line knockouts of the mammalian homolog *Dot1l* (Dot1-like) in mice result in embryonic lethality due to heart and yolk sack defects (Jones et al., 2008). *Dot1l* knockout in mouse cells leads to a global loss of H3K79 methylation, suggesting it is the only enzyme responsible for depositing this modification (Bernt et al., 2011; Deshpande et al., 2013).

Dot1/DOT1L is the only lysine HMT that doesn't have a SET catalytic domain. Instead, DOT1L has a domain similar to arginine methyltransferases but, is not capable of modifying arginine residues in vitro (Min et al., 2003; Van Leeuwen et al., 2002). Unlike HMTs that target the histone tails, Dot1 has very low activity on peptide fragments and requires the full nucleosome to be present for in vitro methylation (Fingerman et al., 2007; Van Leeuwen et al., 2002). This enzymatic activity is stimulated by a basic patch on histone H4 and ubiquitination of lysine 123 of H2B (120 in humans), interactions that are required for di- and tri-methylation (Anderson et al., 2019; Fingerman et al., 2007). These findings suggest that DOT1L takes advantage of the unique position of H3K79 within the nucleosome for inter-histone interactions to provide specificity.

The highly structured nucleosome core region, replete with potential binding interfaces, may be necessary for recognition of H3K79me by potential binders, just as it is necessary for DOT1L methyltransferase activity. This may explain why pulldowns with peptide fragments containing this modification but, lacking the structured nucleosome environment have failed to identify binders that could be validated by rigorous and thorough investigations of the specific affinity of these proteins for H3K79me (Vlaming & van Leeuwen, 2016). The handful of studies that purport to have identified H3K79me binders lack strong biochemical evidence for a specific and direct interaction and some of them have been refuted by subsequent investigations. Huyen et al. suggest that 53BP1, a protein necessary for the repair of DNA double strand breaks, recognizes H3K79me2 through its tandem Tudor domain with little biochemical evidence (Huyen et al., 2004; Panier & Boulton, 2014). However, a later study that included crystallographic and NMR structural analyses as well as isothermal titration calorimetry provided compelling evidence that the Tandem Tudor domain of 53BP1 instead recognizes H4K20me2 with a KD of 19.7 +/- 0.7 μM compared to ~ 2 mM for H3K79me2 (Botuyan et al., 2006). Another study suggested the survival motor neuron (SMN) protein bound H3K79me1/2 from pulldowns of biotinylated peptides lacking sufficient negative controls and with particularly high background of the unmethylated peptide (Sabra et al., 2013). To date, there isn't strong evidence for any direct and specific protein binders of H3K79me2.

DOT1L has been purified in several complexes involved in transcriptional elongation (Bitoun et al., 2007; Mohan et al., 2010; Mueller et al., 2007, 2009). Two of these complexes were identified by mass spectrometry from immunoprecipitations of the transcriptional elongation components ENL (ENL associated proteins) and AF4 (Bitoun et al., 2007; Mueller et al., 2007, 2009). A third complex (Dotcom) is a conglomeration of Wnt pathway members and

transcriptional elongation components (Mohan et al., 2010). Knocking down ENL, a subunit of two of these complexes, leads to a global reduction in both transcriptional activity and H3K79me2 (Mueller et al., 2007). This suggests that H3K79 methylation is deposited in association with the transcriptional elongation complex. These studies also point to a role for H3K79me in transcriptional elongation. P-TEFb, a cyclin dependent kinase that phosphorylates ser2 of the pol II alpha-CTD subunit to facilitate the transition to transcriptional elongation was found in all 3 complexes with DOT1L (Bitoun et al., 2007; Mohan et al., 2010; Mueller et al., 2007, 2009). Additionally, overexpression of any of the four components of the complex identified by Bitoun et al. (AF4, AF9, AF10 and ENL) increased H3K79me2 and P-TEFb-dependent transcriptional elongation (Bitoun et al., 2007).

Unlike other HMTs, DOT1L isn't a processive enzyme and only increases the H3K79 methylation state after separate, additional encounters with each residue (Frederiks et al., 2008). This could mean that the different methylation states are only a product of repetitive encounters of nucleosomes with DOT1L associated with a passing elongation complex, suggesting that the different methylation states may have redundant functions. However, resolving this issue will be difficult without knowing the protein binders. The apparent existence of only one known methyltransferase responsible for H3K79me1/2/3 has allowed for much to be indirectly learned about the downstream effects of H3K79 methylation from knockdown/out and inhibition of DOT1L.

H3K79 methylation states vary throughout the cell cycle and in different ways depending on the organism (W. Kim et al., 2014). In yeast, only H3K79me2 changes significantly with the cell cycle and in mice, H3K79me2 and me3 emerge at different stages of embryogenesis (W. Kim et al., 2014). H3K79me2 also fluctuates throughout the cell cycle in HeLa cells. H3K79me2

is highest in G1 and decreases through S and G2 and rises again in M phase (Q. Feng et al., 2002). H3K79 methylation itself is important for regulation of the cell cycle. Dot1 knockout or H3K79 mutants are defective in the G1/S checkpoint arrest in response to IR in budding yeast and exhibit reduced recruitment of the DNA repair protein 53BP1 to double-strand breaks (Huyen et al., 2004). Additionally, during mouse embryo development H3K79 methylation is at very low levels until the blastocyst stage. Germline knockout of DOT1L results in embryonic lethality by day 10.5 and these embryos display numerous cardiovascular defects (Jones et al., 2008).

Active transcription is necessary to maintain H3K79me2 but, this modification can also activate transcription, although how it is able to do this is not well understood (Bernt et al., 2011; Daigle et al., 2011; Mueller et al., 2007). H3K79me2-mediated gene activation is exemplified in MLL-rearranged leukemia where MLL-fusion proteins aberrantly recruit DOT1L to HOX genes resulting in H3K79 hypermethylation and transcriptional activation of oncogenes necessary for leukemogenesis (Bernt et al., 2011; C. W. Chen et al., 2015; Guenther et al., 2008; Milne et al., 2005; Stubbs et al., 2008).

One possible mechanism of H3K79me2-mediated activation of gene expression could be indirect, through antagonism of gene silencing. This modification may function similarly in humans as it does in yeast, where H3K79me2 prevents chromatin association of sirtuin proteins, effectors of gene silencing and heterochromatinization, in order to prevent spurious gene silencing (van Welsem et al., 2008). Chen et al. observed that H3K79me2 prevents association of the SIRT1 HDAC with MLL-fusion targets, preventing loss of acetylation, subsequent increases in repressive H3K9me3 and gene silencing (C. W. Chen et al., 2015). Thus, the deposition of H3K79me2 by DOT1L in complex with the transcriptional elongation complex may prevent the

association of repressive complexes at active genes, thereby promoting transcription.

The variety of effects observed from perturbations of DOT1L expression and H3K79me deposition underscore the importance of this modification in the development and survival of higher eukaryotes. However, there is much we don't know about this highly conserved histone modification. No binders of this modification have yet been identified and supported with conclusive evidence from rigorous experimentation and we are left with little understanding of the mechanisms through which H3K79me fulfills its many roles. Of particular importance to human health would be a better understanding of how H3K79me2 activates gene expression in MLL-rearranged leukemia and the downstream pathways that facilitate leukemogenesis, a topic I will discuss further in the next section.

1.3 MLL-REARRANGEMENTS AND HISTONE METHYLATION IN LEUKEMIA

MLL1-rearrangements (MLL-r) account for ~10% of all leukemia cases and are particularly refractory to current treatment regimens with an event-free survival rate of 35% compared to 45% for non-MLL-r leukemia (Jabbour et al., 2015; Marks et al., 2013). MLL-r lesions are especially prominent in children where 70-80% of infant leukemias harbor MLL-rearrangements and bear a very poor prognosis (Mann et al., 2010; Pieters et al., 2007; Winters & Bernt, 2017).

These translocations are readily identifiable through in situ hybridization or qPCR and are often considered prognostic indicators for treatment. However, treatment regimens based on the presence of MLL-rearrangements alone may be ill-informed as our understanding of how these translocations result in disease is far from complete. For instance, it is unclear if MLL1-rearrangements are able to induce leukemogenesis through the combined ability of genes involved in normal hematopoietic development to aberrantly target and deregulate gene expression at multiple gene targets or if they require additional mutations to induce a leukemic

disease state. A growing body of evidence suggests that MLL-rearrangements alone may be insufficient to cause disease and that additional mutations are required (Corral et al., 1996; Forster et al., 2003; Ono et al., 2005). The susceptibilities of MLL-r cell lines to pharmacological treatments that disrupt MLL-fusion protein-mediated activation of disease-driving oncogenes sometimes differs by orders of magnitude and mutations affecting growth-signaling receptors and their downstream targets often coincide with translocations in leukemia patients (Daigle et al., 2013; Grossmann et al., 2013; Liang et al., 2006; López et al., 2016). MLL-fusions in mouse models cause leukemias with longer-than-expected latencies, and patients with chemotherapy induced MLL-translocations develop the disease about 3-5 years after treatment, suggesting that additional mutations are required (Corral et al., 1996; Forster et al., 2003; Ono et al., 2005). However, few studies have examined the genetic or physiological context of MLL-fusion proteins and how additional lesions may cooperate to promote disease.

MLL1 translocations fuse the amino terminus of the Mixed Lineage Leukemia protein (KMT2A), a histone H3 lysine methyltransferase involved in regulating HOX gene expression during development and normal hematopoiesis to the C-terminus of a growing list of over 130 different fusion partners (Meyer et al., 2018). The resulting fusion protein contains the N-terminus of MLL1 harboring the CXXC domain, DNA-binding AT hook motifs and MENIN and LEDGF binding regions but lacks the catalytic SET methyltransferase domain (Birke, 2002; Milne et al., 2010; Akihiko Yokoyama et al., 2005; Zeleznik-Le et al., 1994; L. Zhu et al., 2016). Through one or a combination of the aforementioned domains, the fusion protein is targeted to a slew of MLL1-regulated genes (El Ashkar et al., 2018; Milne et al., 2002, 2010; Akihiko Yokoyama et al., 2005).

The MLL-fusions form large multimeric protein complexes that spread far into the gene bodies of MLL-fusion target loci (Kerry et al., 2017). A small subset of patient cases involve fusion partners that are not transcriptionally activating, instead relying on their ability to self-dimerize to induce leukemogenesis (Biswas et al., 2011; Milne et al., 2005). However, in > 75% of cases of MLL-r acute myeloid leukemia and > 90% of cases of MLL-r acute lymphoblastic leukemia the MLL-fusion partner is one of 7 members of the transcriptional elongation complex (Marschalek, 2011). These MLL-fusion proteins copurify with components of the transcriptional elongation complex including DOT1L, the histone methyltransferase responsible for methylation of lysine 79 of histone H3 (Mohan et al., 2010). The carboxy-terminal elongation factor portion of the fusion protein aberrantly recruits the transcriptional elongation complex including DOT1L to the HOXA gene cluster and a multitude of other MLL1 target genes (Okada et al., 2005). DOT1L hypermethylates these genes and the consequent increase in H3K79 methylation, through some as yet incompletely understood mechanism, activates gene expression (Bernt et al., 2011; C. W. Chen et al., 2015; Guenther et al., 2008; Milne et al., 2005; Stubbs et al., 2008). This generates a unique expression profile for MLL-r leukemias with a surprising amount of target gene overlap across different MLL-fusions (Armstrong et al., 2002).

Among the fusion protein's upregulated targets are the oncogenic transcription factors *HOXA9* and *MEIS1* (Zeisig et al., 2004). These pleiotropic transcription factors are important regulators of hematopoiesis with high expression in early hematopoietic lineages that decreases as cells differentiate (Lawrence et al., 2005). Recombination-induced expression of MLL-AF9 alone or co-expression of both *HOXA9* and *MEIS1* in mouse bone marrow progenitors is sufficient to cause acute leukemia (Calvo et al., 2002; M. J. Chang et al., 2010; Corral et al., 1996; Jo et al., 2011; Kroon et al., 1998). Interestingly, exogenous expression of MLL-AF9 in

mice requires a long latency period (4-9 months) before leukemia onset and patients with chemotherapy induced MLL-translocations develop the disease about 3-5 years after treatment, suggesting that additional cooperating mutations may be necessary to induce leukemogenesis (Corral et al., 1996; Dobson et al., 1999).

In the prevailing model, MLL-fusions recruit DOT1L to hypermethylate and activate expression of *MEIS1* and *HOXA9,* a common core of homeobox transcription factors sufficient to cause leukemia (Bernt et al., 2011; Daigle et al., 2011; Deshpande et al., 2013; Guenther et al., 2008; Okada et al., 2005). MLL-r leukemias are uniquely sensitive to disruptions of DOT1L histone methyltransferase activity. DOT1L deletion in mouse MLL-AF6 or MLL-AF9-transformed hematopoietic progenitors results in global ablation of H3K79me2, disrupting the MLL-fusion target gene expression profile and downregulating *HOXA9* and *MEIS1*, resulting in reductions in proliferation and induction of apoptosis and differentiation (Bernt et al., 2011; Deshpande et al., 2013).

MLL-r leukemia's reliance on H3K79me2 makes it uniquely sensitive to disruption of this modification, providing an excellent therapeutic target. To this end, dozens of small molecule DOT1L inhibitors have been developed, with only a select few of the more effective molecules further studied as potential treatments for MLL-r leukemia (Anglin & Song, 2013). The high specificity of many of these inhibitors is likely owed to the fact that DOT1L is the only lysine HMT that doesn't have a SET catalytic domain. The DOT1L catalytic domain is unique among lysine methyltransferases and resembles something closer to an arginine methyltransferase (Min et al., 2003; Van Leeuwen et al., 2002). In fact, some of the more effective inhibitors that function as S-adenosylmethionine (SAM) competitors are highly specific (Anglin & Song, 2013; Daigle et al., 2011, 2013; W. Yu et al., 2012). EPZ004777, an effective

(K_i = 0.3 nM), small molecule DOT1L inhibitor has greater than 1,000-fold selectivity over its closest related paralogs and a host of other lysine and arginine methyltransferases (Anglin & Song, 2013; Daigle et al., 2011). Using EPZ0004777 as a lead compound, two other more highly effective derivatives were subsequently developed- SGC0946, a brominated version of EPZ0004777, with increased effectiveness (K_i = 0.06) and pinometostat (EPZ5676) (K_i < 0.07), an inhibitor that has extremely high specificity for DOT1L (37,000-fold) (Anglin & Song, 2013; Daigle et al., 2011, 2013; W. Yu et al., 2012).

Studies of the effects of these inhibitors on MLL-r leukemia provided hope for their use as potential treatments for the disease. Treating a panel of MLL-r and non-MLL-r leukemia cells as well as non-cancerous cell types with EPZ0004777 resulted in severe toxicity to the MLL-r leukemia cells only, with little effect on the proliferation of non-MLL-r leukemias or non-cancerous cell types (Daigle et al., 2011). EPZ0004777 treatment resulted in the near total depletion of H3K79me2 genome-wide, the subsequent downregulation of MLL-fusion targets including *HOXA9* and *MEIS1*, reduced proliferation and induction of apoptosis and differentiation (Daigle et al., 2011). These effects were consistent with those observed by *Dot1l* deletion in mouse models (Bernt et al., 2011; Deshpande et al., 2013). Both SGC0946 and pinometostat show remarkably similar effects as EPZ0004777 on MLL-r leukemia cell survival and MLL-fusion-induced gene expression but at much lower concentrations (Anglin & Song, 2013; Daigle et al., 2013). The pinometostat IC_{50} for the MV4;11 cell type is 3.5 ± 0.7 nM, a much improved effect over the EPZ0004777 IC_{50} of 170 nM (0.15-0.19, 95% confidence interval). Pinometostat also shrank tumors in rat xenograft experiments and improved overall longevity (Daigle et al., 2013). However, the observed effects from pinometostat treatment present inconsistencies with the current model of MLL-fusion-mediated leukemogenesis. For

example, the MLL-r cell lines MV4;11, SEM and RS4;11 all have the *MLL-AF4* translocation but display pinometostat sensitivities that differ by nearly 3 orders of magnitude (Daigle et al., 2013). Most surprisingly, the MV4;11 pinometostat IC_{50} for proliferation is 20 times lower than that for *HOXA9* and *MEIS1* expression (Daigle et al., 2013), suggesting that these drivers of leukemogenesis and proliferation may not be contributing to cell-type specific effects at low DOT1L inhibitor concentrations and that other genes are involved. Knowing the answers to these questions may improve treatment options for MLL-r leukemia and help resolve issues of pinometostat-acquired resistance in leukemia patients (Stein et al., 2018).

Phase I clinical trials with pinometostat for the treatment of MLL-r leukemia resulted in poor outcomes due to resistance-mediated relapse (Stein et al., 2018). A subsequent study of conditioned immunity in MLL-r leukemia cell lines identified overexpression of the efflux transporter ABCB1 as a potential mechanism of resistance in only one of two cell lines analyzed, while source(s) of resistance in the second cell line were undetermined (Campbell et al., 2017). Surprisingly, no mutations were identified in DOT1L itself, a typical means of acquired resistance from inhibitors of other enzymes such as FLT3 and EZH2 (Gibaja et al., 2016; Weisberg et al., 2010).

Another modification necessary for MLL-r leukemogenesis is H3K4me3, a mark involved in transcriptional activation and necessary for HOX gene activation in normal hematopoietic progenitors (F. Cao et al., 2014; Milne et al., 2002, 2005; Ruthenburg et al., 2007). The MLL-fusion protein does not contain the MLL1 catalytic SET domain and lacks methyltransferase ability, however, a functional copy of the MLL1 gene is necessary to deposit H3K4me3 at MLL-fusion target genes to induce leukemogenesis (F. Cao et al., 2014; Milne et al., 2005). Knockdown of *MLL1* by shRNA in the human MLL-r cell line THP-1 (MLL-AF9

translocation) results in downregulation of HOX genes and reduced proliferation (Thiel et al., 2010). Similar effects were observed through knockdown or knockout of *Mll1* in MLL-AF9-transformed mouse bone marrow progenitors (Thiel et al., 2010).

Just as with DOT1L, there has been a push to develop MLL1 inhibitors as treatments for MLL-r leukemia, resulting in some promising candidates (Borkin et al., 2015; F. Cao et al., 2014). These small molecule MLL1 inhibitors are potent and effective treatments for MLL-r leukemia that specifically affect the leukemic gene expression profile induced by the MLL-fusion protein (Borkin et al., 2015; F. Cao et al., 2014). Two small-molecules that reduce H3K4me3 and specifically kill MLL-r leukemia cells inhibit MLL1 function in different ways. The compound MI-503 disrupts the binding of MENIN to MLL1, an interaction that is necessary for MLL1 and MLL-fusion protein localization to target genes and leukemogenesis but not required for normal hematopoiesis (Borkin et al., 2015; B. E. Li et al., 2013; Akihiko Yokoyama et al., 2005). The molecule MM-401 inhibits the methyltransferase activity of MLL1 by disrupting its interaction with WDR5, an MLL1 complex member necessary for full enzymatic activity of MLL1 but not MLL2-4 (F. Cao et al., 2014). Treatment with MM-401 and MI-503 specifically reduce MLL-r leukemia cell survival and inhibit leukemogenesis in mouse models. Both inhibitors abrogate the expression profile induced by the MLL-fusion protein similar to MLL1 deletion, downregulating the oncogenes *HOXA9, MEIS1, FLT3* and *BCL2* (Borkin et al., 2015; F. Cao et al., 2014).

There is growing evidence that histone methylation at another residue- H3K36me2/3 plays an important role in MLL-r leukemogenesis (A. K. Andersson et al., 2015; X. Zhu et al., 2014). The SETD2 enzyme methylates the H3K36me2 substrate to yield H3K36me3 and provides the vast majority of the H3K36me3 modification genome-wide (Wagner & Carpenter,

2012). Interestingly, 15 to 22% of MLL-r leukemia patients have coinciding mutations in the SETD2 methyltransferase, suggesting that *SETD2* loss-of-function mutations cooperate with MLL-fusion to induce leukemogenesis (A. K. Andersson et al., 2015; X. Zhu et al., 2014). In fact, knockdown of *Setd2* decreases the latency and increases the severity of disease in mice transplanted with MLL-AF9 knock-in hematopoietic progenitor cells (X. Zhu et al., 2014). *Setd2* knockdown not only decreases H3K36me3 genome-wide but results in a global increase in H3K79me2 in mouse MLL-AF9 knock-in hematopoietic progenitors (Bu et al., 2018). Overexpression of *Setd2* in those same cells increases global levels of H3K36me3 while causing a decrease in H3K79me2 (Bu et al., 2018). *Setd2* knockdown increased the expression of the *Meis1* and *Mef2c* oncogenes and increases Mll1 but not MLL-fusion localization to fusion targets (Bu et al., 2018; L. Zhu et al., 2016). Knockdown of the *Ash1l*, the histone methyltransferase responsible for H3K36me2 at many MLL-fusion targets resulted in reduced MLL1 localization and expression of *Hoxa9* (L. Zhu et al., 2016). These observations suggest there is cooperation between MLL-rearrangements and *SETD2* loss of function mutations as well as crosstalk between the H3K36me3 and H3K79me2 histone modifications that affect the expression of key leukemic oncogenes.

Perturbations to global H3K36me2/3 levels potentially affect the localization of the MLL-fusion complex to gene targets through the complex member LEDGF (PSIP1). LEDGF, through its PWWP domain binds H3K36me2/3 and is necessary for recruiting both MLL1 and the MLL-fusion complex to target genes (Okuda et al., 2014; Pradeepa et al., 2012; L. Zhu et al., 2016). However, there are conflicting observations as to which methylation state of H3K36 is recognized by LEDGF (Okuda et al., 2014; Pradeepa et al., 2012; L. Zhu et al., 2016). Okuda et al. find that LEDGF binds both H3K36me2/3 (Okuda et al., 2014), Pradeepa et al show that the

LEDGF PWWP domain is specific for H3K36me3 (Pradeepa et al., 2012) and Zhu et al. observe specific recognition of only H3K36me2 (L. Zhu et al., 2016). These conflicting observations could be due to the use of different experimental approaches. Pradeepa et al. determine binding affinities by introducing the PWWP domain into a peptide array (Pradeepa et al., 2012), a highly artificial environment rich in epitope which can yield vastly different apparent affinities than analyses under conditions closer to the native environment (Shah et al., 2018). Zhu et al. use NMR (L. Zhu et al., 2016) as well as pulldowns from nuclear extract followed by blotting for the distinct modifications, using antibodies for each modification state that could potentially have widely different affinities that would affect the apparent enrichments by blotting (Okuda et al., 2014; Pradeepa et al., 2012; L. Zhu et al., 2016).

Whether specific for H3K36me2 or -3, the interaction of LEDGF with methylated H3K36 is necessary for recruitment of the MLL-fusion complex to target genes (Okuda et al., 2014). LEDGF binds MLL1 indirectly through the protein Menin (Akihiko Yokoyama & Cleary, 2008). Introduction of an MLL-ENL fusion protein in which the Menin binding motif was substituted for the H3K36me3-binding PWWP domain of LEDGF resulted in transformation of mouse hematopoietic progenitor cells, suggesting that the interaction with H3K36me2/3 is necessary for leukemogenesis (Okuda et al., 2014). In fact, the authors of the study were able to design a minimal mutant protein composed only of the PWWP domain, the MLL1 CXXC domain, involved in targeting to CpG-rich sites and the transcriptionally activating domain of AF4 that was able to activate *Hoxa9* expression and transform mouse myeloid progenitor cells (Birke, 2002; Okuda et al., 2014).

Given the crucial involvement of several histone modifications associated with transcriptional activation in MLL-r leukemogenesis, many important questions about the roles of

these marks in this disease are still unanswered. It is unclear if or how these modifications might cooperate or affect each other's distribution to activate the MLL-fusion gene expression profile and promote disease. With reductions in H3K36me3 through perturbations to *SETD2* expression resulting in anticorrelative changes in H3K79me2 there is some evidence for crosstalk but, it is not known if this antagonism occurs in the opposite direction. Does depletion of H3K79me2 result in an increase in H3K36me3? Does some of the toxicity in MLL-r cells lines resulting from targeted depletion in these modifications result from redistribution of other histone marks? Answering these questions could provide crucial therapeutic options for treating this disease.

1.4 FLT3 LESIONS IN LEUKEMIA

FMS-Like Tyrosine Kinase 3 (FLT3) is a class III receptor tyrosine kinase that is expressed on the surface of hematopoietic stem and progenitor cells (Kikushige et al., 2008). When bound to its cognate ligand FL, FLT3 dimerizes and autophosphorylates, activating its tyrosine kinase domain and allowing it to activate a variety of signaling pathways through PI3K, AKT, the STAT proteins and MAP kinases and has well-defined roles in hematopoeisis and proliferation (Dosil et al., 1993; Gary Gilliland & Griffin, 2002). Treating mice, or $CD34^+$ cells in culture with FL stimulates the proliferation of these early hematopoietic progenitors (Gary Gilliland & Griffin, 2002). However, proliferation is only weakly affected unless combined with other growth factors such as c-kit and gp130, where the combined stimulation results in synergy and appreciable population growth (Gary Gilliland & Griffin, 2002). Although highly expressed in early progenitors, *FLT3* expression decreases as hematopoietic cells differentiate (Kikushige et al., 2008).

FLT3 is mutated in about 30% of acute myeloid leukemia (AML) patients, making it one of the most common mutations found in leukemia (M. Levis & Small, 2003; Papaemmanuil et al., 2016). *FLT3* internal tandem duplications (*FLT3-ITD*) occur in ~20% of AML and are caused by an in-frame duplication in the juxtamembrane domain, resulting in ligand-independent dimerization and constitutively active signaling that promotes proliferation (Mizuki et al., 2003; Nakao et al., 1996; Papaemmanuil et al., 2016). Mutations in the FLT3 activation loop occur in about 7% of patients and include small deletions and substitutions of aspartic acid for histidine (D835H) or tyrosine (D835Y), resulting in a similarly hyperactive receptor that functions independently of its cognate ligand (Nagel et al., 2017; Y. Yamamoto et al., 2001). FLT3-ITD activates a transcriptional program that more closely resembles IL-3 signaling than FL-induced signaling by aberrantly hyperactivating STAT3 and STAT5A and downregulating the Pu.1 and C/EBPα transcription factors that are activated by wild-type FLT3 and repressing wild-type FLT3-dependent differentiation (Mizuki et al., 2003; Sandhöfer et al., 2016).

Much of the *FLT3-ITD*-driven effects on proliferation, inhibition of apoptosis and differentiation have been attributed to its downstream target STAT5A (Mizuki et al., 2003; Rosen et al., 2010; Spiekermann et al., 2003; J. Zhou et al., 2009). Previous studies have shown that virally transducing human CD34+ progenitor cells with constitutively active murine *Stat5a* can phenocopy the hyperproliferative and dedifferentiated cellular state consistent with exogenous expression of *FLT3-ITD* (Moore et al., 2007). Other studies have elucidated that expression of a constitutively active *Stat5a* can render Ba/F3 cells growth factor-independent and resistant to apoptosis through activation of Akt and upregulation of the *Pim1-2* protooncogenes (Fathi et al., 2012; Mizuki et al., 2003; Onishi et al., 1998; Santos et al., 2001).

As is common in leukemia, *FLT3* mutations often coincide with other genetic lesions in patient samples including *NPM1*, *DNMT3A* and *MLL1*-rearrangments (Grossmann et al., 2013; Metzeler et al., 2012; Papaemmanuil et al., 2016). Several studies have observed cooperation between MLL-rearrangements and *FLT3* mutations. Ono et al. observed that transplanting mice with hematopoietic progenitors expressing *MLL-SEPT6* fusions resulted in a myeloproliferative disease with a long latency but, when the cells were transduced with both *MLL-SEPT6* and *FLT3-ITD,* the mice developed an acute leukemia with a short latency (Ono et al., 2005). *FLT3* mutations also cooperate with *MLL-AF9* and *MLL-ENL* to decrease the latency of leukemia onset in mice (Armstrong et al., 2002, 2003; Ono et al., 2005; Stubbs et al., 2008). The *FLT3* gene is a common target of MLL-fusion proteins and MLL-r cell lines overexpressing *FLT3* or carrying the *FLT-ITD* mutation are particularly sensitive to FLT3 inhibition (Armstrong et al., 2002; Guenther et al., 2008; Kerry et al., 2017). However, it is unclear how mutant or overexpressed *FLT3* cooperates mechanistically with MLL-rearrangements to induce leukemia.

Because *FLT3* is highly expressed in 70-100% of AML and ALL cases and is one of the most commonly mutated genes in leukemia (Gary Gilliland & Griffin, 2002; M. Levis & Small, 2003; Papaemmanuil et al., 2016), there has been considerable interest and effort invested in developing inhibitors of the signaling kinase and several are currently in clinical trials.

All FLT3 inhibitors interact with the ATP binding site but are classified into two categories based on their mode of action. Type I inhibitors bind the ATP-binding site when the receptor is in the active conformation, while type II inhibitors bind a hydrophobic pocket that is only accessible when the receptor is inactive, preventing its activation (Larrosa-Garcia & Baer, 2017). Because some D835 point mutations in the tyrosine kinase domain result in a sustained

adoption of the active state, type II inhibitors are generally only used for treating cases with FLT-ITD mutations (C C Smith et al., 2015).

The first generation of FLT3 inhibitors including sorafenib, tandutinib (MLN518), sunitinib and midostaurin are extremely potent but, are not very specific and often inhibit other tyrosine kinases in the same or parallel pathways such as VEGFR, PDGFR and KIT (Larrosa-Garcia & Baer, 2017). Several of the first generation of inhibitors, as forerunners, have amassed an extensive catalogue of publications exploring their mechanism of action. For instance, we know a great deal about tandutinib (MLN518), its effectiveness against FLT3 kinase activity, and how it mediates reductions in the phosphorylation of downstream FLT3 targets such as STAT5A (Clark et al., 2004). The second generation of inhibitors including quizartinib, crenolanib and gilteritinib have higher specificity for FLT3 but are also often plagued by off-target effects on similar receptors such as PDGFR (Galanis et al., 2014).

Many of these inhibitors are in clinical trials however, emergent resistance is a consistent and considerable problem. The development of tyrosine kinase domain mutations in response to treatment of *FLT3-ITD* leukemias to class II inhibitors is common (Catherine C Smith et al., 2012). Another mechanism of resistance is the upregulation of the downstream FLT3 target *PIM1*, a kinase that also stabilizes FLT3 activation in a feedback loop (Green et al., 2015; Larrosa-Garcia & Baer, 2017). One way to surmount the problem of resistance is through combination therapy. Interestingly, FLT3 inhibitors have shown strong synergistic effects in combination with HDAC inhibitors (Pietschmann et al., 2012). This raises the possibility that FLT3 inhibitors in combination with inhibitors of other histone modification pathways involved in leukemogenesis may yield synergistic effects, perhaps providing much needed treatment options for *FLT*3-mutant leukemia.

1.5 THE ROLES OF HISTONE POST-TRANSLATIONAL MODIFICATIONS IN ALTERNATIVE SPLICING

Splicing is the process of removing an intron from an RNA transcript by the spliceosome, a large, dynamic ribonucleoprotein complex involving between 150 and 300 different proteins (Rappsilber et al., 2002; Z. Zhou et al., 2002) and 5 snRNAs (Wahl et al., 2009). There are on average about 8 introns per gene in the human genome (Sakharkar et al., 2004) and most splicing is constitutive in which the same splice sites are consistently used to remove an intron. However, approximately 95% of multi-exonic genes in humans are alternatively spliced, where the removal of at least one intron involves the differential use of splice sites (Pan et al., 2008). Alternative splicing vastly increases protein diversity, allowing complex organisms to achieve the multitude of functions crucial to the establishment of different cell types and tissue specific characteristics without enormously expanding the genome (Nilsen & Graveley, 2010; Pan et al., 2008; Rosenfeld et al., 1982; E. T. Wang et al., 2008).

Alternative splicing can result in many different transcripts from a single gene, yielding proteins with unique functions (Linares et al., 2015; Navaratnam et al., 1997; Rosenblatt et al., 1997). In one extreme case, the human *KCNMA1* gene, encoding a potassium channel in the hair cells of the inner ear, undergoes extensive alternative splicing to yield more than 500 different mRNA isoforms, believed to help establish the range of soundwave frequencies that can be detected (Navaratnam et al., 1997; Rosenblatt et al., 1997). Many alternative splicing events are tissue specific, encoding proteins with altered or unique functions in different cell types (Rosenfeld et al., 1982; E. T. Wang et al., 2008). An excellent example of cell type-specific expression and the regulation of differentiation by alternative splicing involves the splicing

factor PTBP1, a protein with well-described roles in exon exclusion (Ling et al., 2016; Luco et al., 2010). PTBP1 is highly expressed in embryonic stem cells but, is downregulated during neuronal development, relieving repression of exon 7 of the transcription factor PBX1 (Linares et al., 2015). The protein encoded by the isoform of PBX1 containing exon 7 is then able to activate genes that promote neuronal differentiation, whereas PBX1 isoforms lacking this exon cannot (Linares et al., 2015).

Our understanding of the mechanisms regulating alternative splicing is still far from complete but previous observations have shown that splice site sequence, the rate of transcription, availability of the splicing machinery, and the differential recruitment of hundreds of splicing factors with diverse effects on splicing all contribute to splice site choice (De La Mata et al., 2003; Linares et al., 2015; Muñoz et al., 2009; Nilsen & Graveley, 2010; Uemura et al., 2017). Of all of the crucial factors contributing to alternative splicing, our understanding of how splicing factors are differentially recruited to modulate splice site choice is far from complete.

Unlike yeast, which have clearly defined splice site consensus sequences and very few instances of alternative splicing, splice sites in higher eukaryotes are poorly defined by RNA sequence and the positioning and efficiency of splicing depends on the recruitment of splicing factors for constitutive as well as alternative splicing, where these factors can both increase or decrease the usage of a specific site (Herzel et al., 2017). Splicing factors regulate alternative splicing in myriad ways including: recruitment of the spliceosome, modulating splice site communication, blocking splice sites and affecting the rates of splicing steps (Nilsen & Graveley, 2010). Proper regulation of this process is crucial, as perturbations through mutations in splice site sequences, splicing factors and splicing factor consensus binding sequences can result in cancer, cystic fibrosis, spinal muscular atrophy and other diseases (Bonnal et al., 2020;

Luco et al., 2011; Scotti & Swanson, 2016). However, many splicing factor consensus sequences are degenerative and ill-defined and the expression differences of these factors between cell types cannot alone explain the abundance of observed differential splicing, suggesting that other factors affect recruitment of proteins involved in alternative splicing (Dvinge, 2018; Hui et al., 2005; Ule et al., 2006).

Most of the 100,000 or more estimated events of alternative splicing that occur in human cells are still mechanistically unexplored but, the sheer volume of events suggests there are, as yet, unknown layers of splicing regulation (Nilsen & Graveley, 2010). Splicing occurs cotranscriptionally, and chromatin characteristics can affect alternative splicing, representing an important layer of splicing regulation that remains to be explored (Carrillo Oesterreich et al., 2016; Herzel et al., 2017). Several studies have provided both direct and indirect evidence that histone post translational modifications have significant effects on the regulation of alternative splicing (Guo et al., 2014; T. Li et al., 2018; Luco et al., 2010; Pradeepa et al., 2012).

Observations that histone modifications are differentially distributed within introns and exons suggest these modifications play a role in splicing (R. Andersson et al., 2009; Schwartz et al., 2009; Spies et al., 2009). Andersson et al. observed that H3K36me3, H3K79me1, and H3K27me1/2/3 levels were higher in exons than in the following introns (R. Andersson et al., 2009). While Huff et al. found that the 5' regions up through the end of the first intron, which is usually the largest intron in a gene, are enriched for H2B ubiquitylation (H2Bub), H3K23ac, H3K4me1/2, H3K9me1, H4K20me1, H2BK5me1 and H3K79me1/2/3, while H3K36me3 is enriched after the first intron into the gene body (Huff et al., 2010). And yet another study found that H3K27me2 and H3K36me3 were enriched in exons as well (Spies et al., 2009). Though these observed correlations of histone modifications with introns and exons do not demonstrate a

functional role in splicing, they do suggest the possible scope of the variety of modifications that could be involved in splicing and warrant further investigation.

While many histone modifications have been indirectly implicated in splicing regulation, H3K79me2 and H3K36me3 have been observed to play a more direct role in alternative splicing (Guo et al., 2014; T. Li et al., 2018; Luco et al., 2010; Pradeepa et al., 2012). Both H3K79me2 and H3K36me3 are deposited by enzymes in complex with the transcriptional elongation complex, DOT1L and SETD2, respectively (Bitoun et al., 2007; Kizer et al., 2005; Mohan et al., 2010; Mueller et al., 2007, 2009; Steger et al., 2008), and are found in actively transcribed genes but, with the opposite enrichment patterns-- H3K79me2 is enriched at the 5' end of the gene body and tapers off toward the end of the gene while H3K36me3 begins in the 5' end of the gene but builds toward the 3' transcription termination site (Barski et al., 2007). Interestingly, in addition to the transcriptional machinery, both DOT1L and SETD2 have been found in complex with splicing factors (Brown et al., 2012). DOT1L associates with HNRNPM, HNRNPU and Ally/Ref and SETD2 was found in complex with HNRNPL and Ally/Ref (Brown et al., 2012). If feedback from splicing regulates the activity of these histone methyltransferases, this could perhaps explain the enrichment of H3K79me2 and H3K36me3 within exons. In fact, disrupting splicing through depletion of the core splicing component SF3B3 or pharmacological inhibition reduces SETD2 recruitment to chromatin and H3K36me3 levels (Brown et al., 2012). The deposition of these modifications in actively transcribed genes, associations with active transcription and splicing factors and apparent enrichment within exons were indicators of potential roles in splicing that were confirmed and expanded upon through further examination.

An expansive study by Li et al., looking at H3K79me2 patterns in 34 cancerous and non-cancerous cell lines, observed that this modification was enriched at sites of exon exclusion

compared to those same sites in other cell lines where the exon is included in the transcript (T. Li et al., 2018). Inhibition or knockdown of the H3K79 methyltransferase DOT1L in the MV4;11 and MOLM14 leukemia cell lines decreased H3K79me2 and increased exon inclusion, suggesting that H3K79me2 functions in alternative splicing, potentially through recruitment of a splicing factor that promotes exon exclusion (T. Li et al., 2018). However, to date there is no strong evidence of an interaction between H3K79me2 and known splicing factors and how this modification affects splicing is unknown. As splicing often occurs cotranscriptionally, one possible explanation is that H3K79me2 may affect alternative splicing indirectly by modulating the rate of transcription (Carrillo Oesterreich et al., 2016; Herzel et al., 2017). DOT1L interacts with components of the transcriptional elongation complex including p-TEFb and AF4, suggesting that H3K79 methylation may play a role in transcriptional elongation (Bitoun et al., 2007; Mohan et al., 2010; Mueller et al., 2007, 2009). If H3K79me2 affects transcriptional elongation it could modulate splice site choice just as changes in the rate of transcriptional elongation through expression of a slower mutant RNA Pol II or DNA-damage-induced phosphorylation of the alpha-CTD subunit have been previously observed to affect alternative splicing (De La Mata et al., 2003; Muñoz et al., 2009).

Unlike H3K79me2, we know a great deal about how H3K36me3 regulates alternative splicing, providing a framework for understanding how H3K79me2 and other modifications might affect splice site choice. H3K36me3 is enriched at the chromatin encoding alternatively spliced exons such as the mutually exclusive exons iiib and iiic of the *FGFR2* gene (Luco et al., 2010). The chromodomain-containing protein MRG15 binds H3K36me3 at the *FGFR2* locus to recruit the splicing factor PTBP1, resulting in exclusion of the iiib exon and inclusion of iiic in human mesenchymal stem cells. Exon iiib is more often included in *FGFR2* transcripts in

prostate epithelium cells where H3K36me3 levels are lower. Through this mechanism, H3K36me3 facilitates cell type-dependent recruitment of PTBP1 to affect splice site choice at many other loci as well (Luco et al., 2010). However, this modification is also recognized by ZMYND11, a splicing factor that binds H3K36me3 through its PWWP domain. Ironically, ZMYND11 facilitates intron retention and is recruited by H3K36me3 to sites throughout the genome. Knockdown of *ZMYND11* or *SETD2* affects alternative splicing at over 200 genes in HeLa cells, mainly through decreased intron retention (Guo et al., 2014). Given that PTBP1 and ZMYND11 have seemingly opposing effects on alternative splicing, weakly-defined consensus binding sequences and are both recruited by H3K36me3, it is unclear at present how these proteins are recruited to specific splicing events (Guo et al., 2014; Ling et al., 2016; Luco et al., 2010). Additional modes of recruitment unique to each splicing factor are likely involved. H3K36me3 is also recognized by the PWWP domain of LEDGF (PSIP1), a protein involved in transcriptional activation and alternative splicing through interactions with dozens of splicing factors including SRSF1 and PTBP1 (Pradeepa et al., 2012; Singh et al., 2015). LEDGF can recruit the splicing factor SRSF1 in an H3K36me3-dependent manner to regulate splicing at 95 alternative exons in mouse embryonic fibroblasts (Pradeepa et al., 2012), providing yet another mechanism through which this histone modification can affect alternative splicing.

There is still much that we don't know about how H3K79me2 and H3K36me3 affect alternative splicing. The H3K36me3-binder LEDGF interacts with several splicing factors and future investigations may determine if any of them are involved in H3K36me3-mediated alternative splicing at other loci (Pradeepa et al., 2012; Singh et al., 2015). Additionally, it is currently not understood how H3K79me2 affects alternative splicing and further studies are

needed to determine if the recruitment of splicing factors to modulate splice site choice is a shared mechanism.

2 NON-CANONICAL PATHWAYS REGULATING GROWTH SIGNALING AND HISTONE METHYLATION MEDIATE THE SENSITIVITY OF MLL-REARRANGED LEUKEMIA TO LOW-DOSE DOT1L INHIBITION

2.1 INTRODUCTION

MLL1-rearrangements (MLL-r) account for ~10% of all leukemia cases and are especially prominent in infants (70-80%) and, lacking an effective standard of care, bear a very poor prognosis (Jabbour et al., 2015; Mann et al., 2010; Marks et al., 2013; Pieters et al., 2007; Winters & Bernt, 2017). A growing body of evidence suggests that MLL-rearrangements rely on additional mutations to cause leukemia. Leukemia patients with MLL-fusions often have additional mutations that affect growth signaling pathways (Armstrong et al., 2003; Grossmann et al., 2013; Liang et al., 2006) and MLL-fusions in mouse models cause leukemias with longer-than-expected latencies, suggesting that additional mutations are required for full progression (Corral et al., 1996; Forster et al., 2003; Ono et al., 2005). Yet few studies have examined the genetic context of MLL-fusion proteins and how additional lesions may cooperate to promote disease at the molecular level.

MLL1 (Mixed Lineage Leukemia protein, also known as *KMT2A*) is a histone H3 lysine methyltransferase involved in regulating *HOX* gene expression during development and normal hematopoiesis (Hess, 2004). Translocations of MLL1 fuse its amino terminus to the carboxy-terminus of a growing list of over 130 different fusion partners (Meyer et al., 2018). Although these MLL-fusions lack methyltransferase activity, a functional copy of the MLL1 gene is necessary to target and hypermethylate H3K4 at MLL-fusion target genes to induce leukemogenesis (F. Cao et al., 2014; Milne et al., 2005, 2010). In more than 75% of acute

myeloid leukemia (AML) cases and > 90% of acute lymphoblastic leukemia (ALL) cases involving MLL translocations, the MLL-fusion partner is one of 7 members of the transcriptional elongation complex, most commonly, AF9 and AF4 respectively (Marschalek, 2011). These fusion partners aberrantly recruit DOT1L, the sole histone H3 lysine 79 methyltransferase to MLL1 target genes including the HOXA gene cluster (Kerry et al., 2017; Mohan et al., 2010; Okada et al., 2005). By mechanisms that remain unclear, DOT1L-mediated hypermethylation of H3K79 promotes expression of MLL-fusion targets (Bernt et al., 2011; C. W. Chen et al., 2015; Guenther et al., 2008; Milne et al., 2005; Stubbs et al., 2008), establishing an expression profile with a surprising degree of target gene overlap across different MLL-fusions (Armstrong et al., 2002). Ablation of H3K79 methylation through knockout or pharmacological targeting of *DOT1L* abrogates the MLL-fusion target gene expression profile, selectively induces apoptosis and differentiation of leukemia cells in culture and dramatically extends the survival of mice in xenograft experiments (Bernt et al., 2011; Daigle et al., 2013).

Viral co-transduction of the MLL-AF4 targets (Zeisig et al., 2004) *HOXA9* and *MEIS1* is sufficient to cause acute leukemia in mouse bone marrow progenitors, arguing that these transcription factors represent a major etiologic pathway in MLL-r leukemia (Calvo et al., 2002; M. J. Chang et al., 2010; Corral et al., 1996; Jo et al., 2011; Kroon et al., 1998). However, exogenous expression of *MLL-AF9* in mice requires a long latency period (4-9 months) and chemotherapy induced MLL-translocations cause disease 3-5 years after treatment, suggesting that additional mutations are required for leukemagenesis (Corral et al., 1996; Dobson et al., 1999). In the prevailing model, MLL-fusions recruit DOT1L to hypermethylate and activate expression of *MEIS1* and *HOXA9* (Figure 2.1A) (Bernt et al., 2011; Daigle et al., 2011; Deshpande et al., 2013; Guenther et al., 2008; Okada et al., 2005). However, the genetic

manipulations used to define this paradigm may have missed more subtle and graded effects afforded by kinetically-staged antagonism with highly-specific small-molecule inhibitors. Therefore, to better understand the direct effects of H3K79me2 in several MLL-r cell lines we employed pharmacologic inhibition of DOT1L methyltransferase activity.

Pinometostat (EPZ5676), a highly specific DOT1L inhibitor (Anglin & Song, 2013; Daigle et al., 2011; W. Yu et al., 2012) displays 37,000-fold selectivity over its closest related paralogs and a host of other lysine and arginine methyltransferases[6]. Interestingly, several cell lines that all have the *MLL-AF4* translocation display pinometostat sensitivities that differ by nearly 3 orders of magnitude (Daigle et al., 2013). One of these lines (MV4;11) displays a pinometostat IC50 for proliferation that is 20 times lower than the IC50 for *HOXA9* and *MEIS1* expression (Daigle et al., 2013), suggesting that these drivers of leukemogenesis, though downregulated at higher concentrations (1 μM) (Daigle et al., 2013), may not contribute to cell-type specific effects at lower concentrations.

I sought to understand low-dose pinometostat effects by treating a variety of MLL-r cell lines with a concentration that reduces proliferation in only a subset, with MLL-r cell lines harboring *FLT3-ITD* mutations being the most susceptible. Under these conditions, *HOXA9* and *MEIS1* expression remain unaffected, presenting a clear exception to the existing paradigm, but found thousands of other differentially expressed genes, including the *PBX3* and *FLT3* oncogenes. Capitalizing on the sensitivity of internally calibrated ChIP-seq (ICeChIP-seq) (Grzybowski et al., 2015, 2019), I observed larger reductions in H3K79me2 density at a subset of MLL-AF4 targets, a genome-wide reduction in H3K27me3 and stark H3K4me3 increases at transcription start sites. Remarkably, I could nearly completely rescue not only pinometostat- but also MLL1 inhibitor-induced effects on proliferation and apoptosis through expression of a

constitutively active form of the downstream FLT3-ITD target *STAT5A* (*STAT5A-CA*), arguing that disruptions to this pathway represent the main source of toxicity from low-dose DOT1L inhibition. In addition, DOT1L inhibition also downregulated the *EZH2* and *EED* components of the PRC2 complex, likely accounting for global reductions in H3K27me3 and imparting modest, but distinct effects on proliferation and a correspondingly moderate proliferation rescue from EZH2 overexpression. Collectively, my data argue that the FLT3-ITD signaling and PRC2 pathways, are more sensitive to disruptions of MLL-fusion-mediated gene activation than the canonical oncogenic drivers in MLL-r, $FLT3^{ITD}$ leukemias, defining a new molecular understanding of how MLL-fusions cooperate with other oncogenic factors to induce leukemia.

2.2 RESULTS

2.2.1 MLL-r leukemia is sensitive to DOT1L inhibition via a non-canonical pathway

Leukemias harboring MLL-rearrangements are uniquely susceptible to DOT1L inhibition and MV4;11, a biphenotypic leukemia cell line harboring an MLL-AF4 translocation, is one of the most sensitive (Daigle et al., 2013). To determine the basis of this susceptibility I systematically examined how low-dose regimes of pinometostat affect proliferation and global H3K79me2 levels in cells treated for 7 days with 1-50 nM pinometostat. This range of concentrations encompasses the previously determined MV4;11 proliferation IC50 (3.5 nM) but is well below the 1 μM or higher typically used in published investigations of the effects of H3K79me ablation

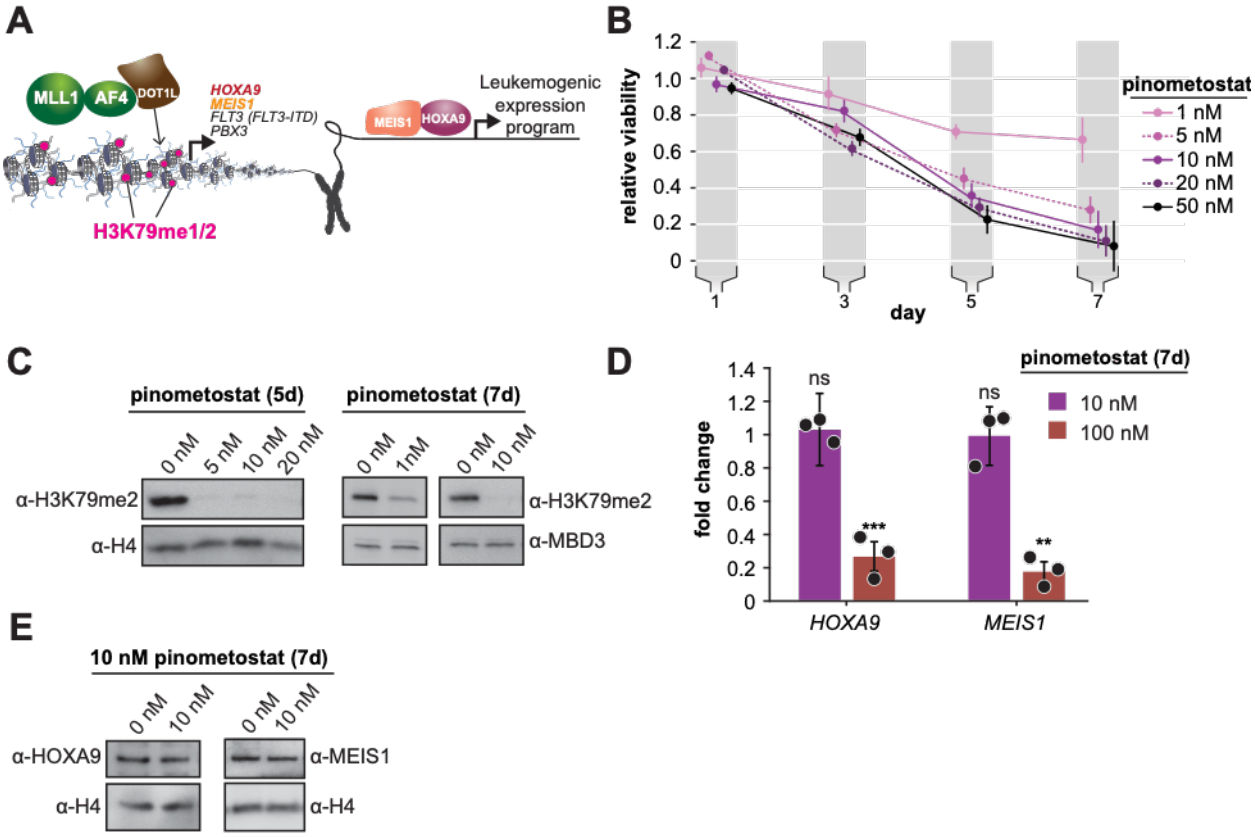

Figure 2.1 Low doses of DOT1L inhibitor ablate bulk H3K79me2 and curtail MV4;11 proliferation without impacting expression of canonical target genes.
A. Conventional model depicting how DOT1L methyltransferase activity activates transcription of key proliferative oncogenic transcription factors(Armstrong et al., 2002; Bernt et al., 2011; Guenther et al., 2008; Kroon et al., 1998; Okada et al., 2005; Zeisig et al., 2004). **B.** Proliferation assay of MV4;11 cells treated with the indicated concentrations of the DOT1L inhibitor pinometostat (EPZ5676). Cell viability was assayed every two days, starting one day after treatment commenced using the CellTiter Glo 2.0 reagent. Relative cell viability is presented as the mean fraction of pinometostat versus cells treated with the equivalent volume of DMSO from three independent experiments ± S.E.M. **C.** Western blots for H3K79me2 with H4 or MBD3 loading controls in MV4;11 cells treated with 1 to 20 nM pinometostat for 5 or 7 days. **D.** RT-qPCR analysis of *HOXA9* and *MEIS1* expression fold-change in MV4;11 cells treated with 10 or 100 nM pinometostat for 7 days. Results are shown as mean ± S.E.M. of three independent experiments. Student's t-test (ns $p > 0.05$, ** $p \leq 0.01$, *** $p \leq 0.001$). **E.** Western blot of HOXA9 and MEIS1 with H4 as a loading control from MV4;11 cells treated with 10 nM pinometostat for 7 days.

(Daigle et al., 2013; Godfrey et al., 2019; Okuda et al., 2017). Consonant with previous findings

(Daigle et al., 2013), pinometostat concentrations as low as 1 nM significantly reduce global

levels of H3K79me2 and cause a 30% ± 10% reduction in MV4;11 proliferation, while 10 nM inhibitor reduced cell proliferation by 80% ± 10% (Figure 2.1B and C). Notably, after treating MV4;11 cells with 10 nM inhibitor for 7 days I observed no discernable effect on the expression of *HOXA9* and *MEIS1* (Figure 2.1D and E), despite the emphasis on these genes as the critical mediators of DOT1L's effects in MLL-r leukemia (Bernt et al., 2011; Daigle et al., 2011; Deshpande et al., 2013; Guenther et al., 2008; Okada et al., 2005). Consistent with prior observations (Daigle et al., 2013), a much higher dose of 100 nM pinometostat significantly downregulates both *HOXA9* and *MEIS1* expression (Figure 2.1D).

2.2.2 DOT1L inhibition at low concentrations downregulates leukemic oncogenes

With the extant model (Bernt et al., 2011; Daigle et al., 2011; Deshpande et al., 2013; Guenther et al., 2008; Okada et al., 2005) unable to explain reductions in proliferation caused by the DOT1L inhibitor in this concentration regime, I reasoned that the expression of other genes crucial to the survival of these cells are likely affected. To define these genes, I performed RNA-seq in MV4;11 cells that had been treated with 10 nM pinometostat for 7 days and observed that 1916 genes were downregulated and 2007 genes were upregulated (Figure 2.2A) relative to a DMSO treated control. To account for any handling biases, I included 4 RNA "spike-in" controls and found no significant differences in read counts between treatment groups (Figure 2.3A). The downregulated genes significantly overlap with MLL-AF4 targets identified by Kerry et al. by ChIP-seq in MV4;11 cells (Kerry et al., 2017) (Figure 2.2B). Relative to prior high-dose (3 μM) treatment with a compound structurally related to pinometostat in MV4;11 cells, the numbers of differentially expressed genes are similar, and there is marked overlap

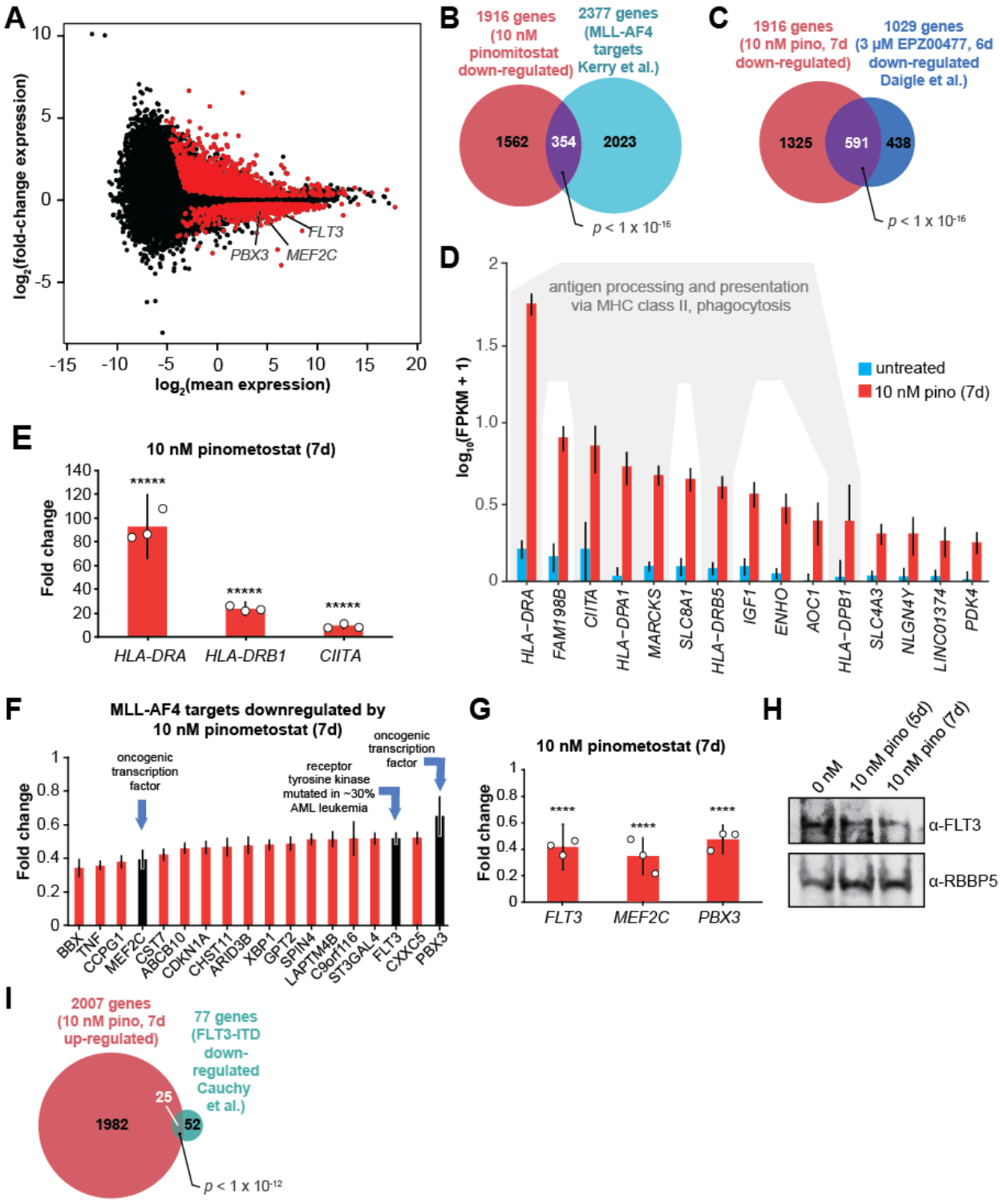

Figure 2.2 DOT1L inhibition downregulates a subset of MLL-AF4 targets including the leukemic oncogene FLT3.

A. MA plot showing genes differentially expressed in MV4;11 cells treated with 10 nM pinometostat or DMSO 7 days as $\log_2$-mean of expression (FPKM) of the DMSO and pinometostat treated samples versus the $\log_2$-fold change of the mean normalized pinometostat

Figure 2.2, continued.
versus DMSO treated FPKM for three independent replicates. Red represents genes that meet the significance threshold, with an FDR-adjusted $p \leq 0.5$. **B.** Venn diagram depicting overlapping genes between those downregulated by 10 nM pinometostat and MV4;11 MLL-AF4 targets identified by Kerry et al.(Kerry et al., 2017), *p*-value computed by two-tailed Fisher Exact test. **C.** Venn diagram displaying the overlap between genes downregulated in MV4;11 cells by 10 nM pinometostat treatment (7 days) and treatment with 3 μM of the pinometostat-related compound EPZ004777 for 6 days(Daigle et al., 2011). *p*-value computed by two-tailed Fisher Exact test. **D.** Bar plot depicting upregulated genes with the highest fold changes from RNA-seq analysis of 3 independent experiments of DMSO- (blue) or pinometostat-treated (red) MV4;11 cells with uncertainty presented as the standard deviation computed by CuffDiff(Trapnell et al., 2013) with immune response genes outlined in gray. **E.** RT-qPCR analysis showing the fold-change for *HLA-DRA, HLA-DRB1* and *CIITA* gene expression in MV4;11 cells ± 10 nM pinometostat treatment for 7 days. Results are shown as mean ± S.E.M. of three independent experiments. Student's t-test (*****$p \leq 0.00001$) **F.** Bar plot depicting the top pinometostat-downregulated genes from the RNA-seq analysis that are previously described MLL-AF4 targets(Guenther et al., 2008) including the oncogenes *MEF2C, FLT3* and *PBX3*. **G.** RT-qPCR analysis of *MEF2C, FLT3* and *PBX3* expression in MV4;11 cells ± with 10 nM pinometostat for 7 days. Results are displayed as mean fold-change ± S.E.M. of three independent experiments; Student's t-test (**** $p \leq 0.0001$). **H.** Western blot for FLT3 with RBBP5 as loading control in MV4;11 cells treated with 10 nM pinometostat for 5 or 7 days. **I.** Venn diagram displaying the overlap between genes upregulated in MV4;11 cells by 10 nM pinometostat treatment (7 days) and genes downregulated in leukemic cells from patients with *FLT3-ITD* vs normal *FLT3* karyotypically normal AML(Cauchy et al., 2015). *p*-value computed by two-tailed Fisher Exact test.

between the sets, particularly the downregulated cohort (Daigle et al., 2011) (Figure 2.2C and 2.3B). Consistent with my RT-qPCR measurements, *HOXA9* was unaltered in its expression (Figure 2.3C) and *MEIS1* displayed extremely modest mRNA reduction (20%) not observed by RT-qPCR and not reflected in apparent protein levels (Figure 2.1D-E). Of the other *HOXA* cluster genes only *HOXA11* and *HOXA13* exhibited expression changes with a 1.7-fold decrease and 2.5-fold increase, respectively (Figure 2.3C).

Although H3K79me2 is considered transcriptionally activating, the upregulated genes had much larger expression fold-changes. 906 genes were upregulated at least 2-fold (and some > 80-fold), while only 86 genes were downregulated ≥ 2-fold (Figure 2.2A). The list of upregulated transcripts include MHC class II and innate immune response genes (Figure 2.2D). I

confirmed the expression increases of *CIITA* (the master regulator of interferon-inducible MHC class II genes), and the MHC class II genes *HLA-DRA* and *HLA-DRB1* by RT-qPCR (Figure 2.2E). Gene ontology analysis of the upregulated genes indicated enrichment for "immune

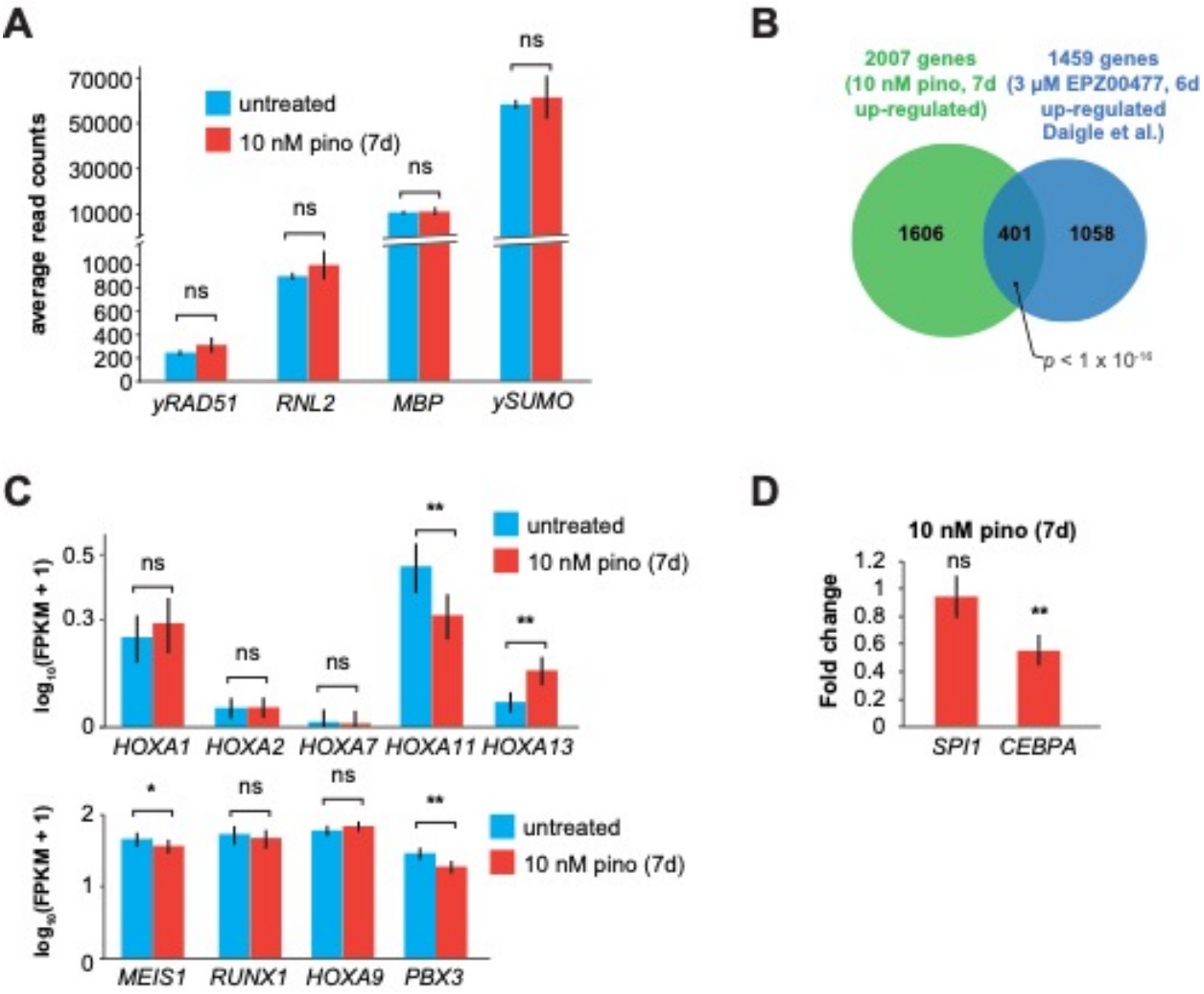

Figure 2.3 Low dose DOT1L inhibition downregulates several oncogenes without affecting the expression of HOXA9 and MEIS1.
A. RT-qPCR analysis of non-native RNA "spike-ins" for ± 10 nM pinometostat cDNA libraries used for RNA-seq from MV4;11 cells. Bar graphs represent the average of 3 independent experiments ± S.E.M. Student's t-test **(**ns $p > 0.05$). **B.** Venn diagram displaying the overlap between genes upregulated in MV4;11 cells by 10 nM pinometostat treatment (7 days) and treatment with 3 μM of the pinometostat-related compound EPZ004777 for 6 days(Daigle et al., 2011). **C.** Bar graph of Cuffdiff(Trapnell et al., 2013) output for the expression of HOXA cluster genes and HOX domain-containing oncogenes *MEIS1*, *RUNX1* and *PBX3* from RNA-seq in MV4;11 cells ± 10 nM pinometostat. Values are represented as log(10) FPKM + 1 for 3 independent experiments with standard deviation. Student's t-test **(**ns $p > 0.05$, * $p < 0.05$, ** $p <$

Figure 2.3, continued.
0.01). **D.** RT-qPCR analysis of *SPI1* and *CEBPA* expression from three independent experiments of MV4;11 cells treated with 10 nM pinometostat for 7 days. Fold change over DMSO-treated cells is depicted ± S.E.M. Student's t-test (ns $p > 0.05$, ** $p < 0.01$).

response" and "interferon-gamma signaling pathway" (Figure 2.4A) (D. W. Huang et al., 2009a, 2009b).

Despite there being no discernable effect on interferon-gamma (*IFNG*) expression in the RNA-seq analysis (Figure 2.4B), marked activation of IFN-γ-inducible genes is apparent. I hypothesize that this may be due to perturbations to signaling effectors of the IFN-γ pathway which includes the STAT family of transcription factors that are often aberrantly expressed in leukemia and other cancers (Caldarelli et al., 2013; Muhlethaler-Mottet et al., 1998; Spiekermann et al., 2002). The activation of so many genes involved in antigen processing and presentation as well as macrophage cell surface markers (Figure 2.4C) may indicate that these cells are undergoing differentiation towards a more macrophage-like state, consistent with apparent differentiation observed in other DOT1L loss-of-function paradigms (Bernt et al., 2011; Daigle et al., 2011). By Gene Set Enrichment Analysis (GSEA)(Mootha et al., 2003; Subramanian et al., 2005) the set of differentially expressed genes were enriched for hematopoietic differentiation factors and anticorrelated with hematopoietic progenitor expression signatures (Figure 2.4D). Notably, the cytokine receptors CSF1R and CSF3R, critical signaling inducers of hematopoietic differentiation, were upregulated (Figure 2.4E) (Klimiankou et al., 2017; Mossadegh-Keller et al., 2013).

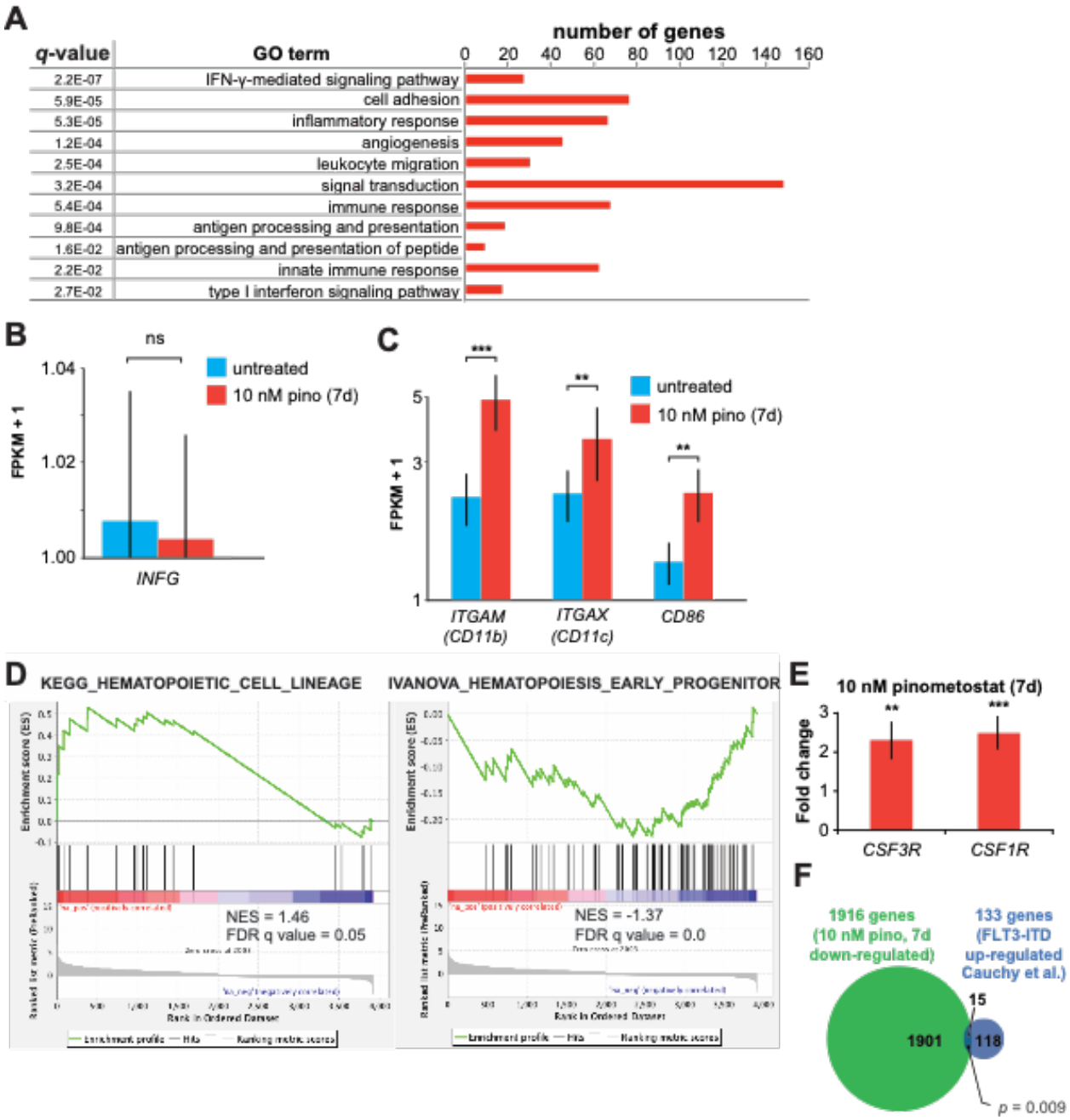

Figure 2.4 DOT1L inhibition upregulates components of the IFN-γ pathway and markers of differentiation.

A. Gene Ontology analysis (DAVID)(D. W. Huang et al., 2009b, 2009a) of pinometostat-upregulated genes showing top functional classification categories and the number of genes in each category that are significantly upregulated. **B.** Bar graph of Cuffdiff(Trapnell et al., 2013) output for the expression of *INFG* (IFN-γ) from RNA-seq in MV4;11 cells ± 10 nM pinometostat. Values are represented as FPKM + 1 for 3 independent experiments with standard deviation. Student's t-test (ns $p > 0.05$). **C.** RT-qPCR analysis of *ITGAM (CD11b), ITGAX (CD11c)* and CD86 macrophage cell surface marker expression in MV4;11 cells ± 10 nM pinometostat for 7 days. Results are displayed as mean fold-change vs. DMSO-treated cells ±

Figure 2.4, continued.
S.E.M. of three independent experiments. Student's t-test (** $p < 0.01$, *** $p \leq 0.0001$). **D.** GSEA(Mootha et al., 2003; Subramanian et al., 2005) of the set of differentially expressed genes in MV4;11 cells ± 10 nM pinometostat compared to KEGG_HEMATOPOIETIC_CELL_LINEAGE and IVANOVA_HEMATOPOIESIS_CELL_LINEAGE gene sets from the MSigDB data base. NES - normalized enrichment score. **E.** RT-qPCR analysis of *CSF3R* and *CSF1R* expression in MV4;11 cells ± 10 nM pinometostat for 7 days. Results are displayed as mean fold-change vs. DMSO-treated cells ± S.E.M. of three independent experiments. Student's t-test (** $p < 0.01$, *** $p \leq 0.0001$). **F.** Venn diagram displaying the overlap between genes downregulated in MV4;11 cells by 10 nM pinometostat treatment (7 days) and genes upregulated in leukemic cells from patients with *FLT3-ITD* vs normal *FLT3* karyotypically normal AML(Cauchy et al., 2015). *p*-value computed by two-tailed Fisher Exact test.

Among the most downregulated genes were many MLL-AF4 target genes (Guenther et al., 2008; Kerry et al., 2017; Wilkinson et al., 2013) including the oncogene FMS-Like Tyrosine Kinase 3 (*FLT3*), the protooncogene Myocyte Enhancer Factor 2C (*MEF2C*) and Pre-B-cell leukemia homeobox 3 (*PBX3)* (Figure 2.2F). These genes all have previously described roles in the development of MLL-rearranged leukemias (Krivtsov et al., 2006; Z. Li et al., 2016; Nagel et al., 2017; Stubbs et al., 2008). FLT3 is a receptor tyrosine kinase that regulates proliferation and cell survival via STAT and other signaling pathways. Mutations that constitutively activate FLT3 by internal tandem duplication of its juxtamembrane domain (*FLT3-ITD*) or point mutations within its kinase domain collectively represent the most frequently occuring genetic lesions in acute myeloid leukemia (M. Levis & Small, 2003; Mizuki et al., 2003; Nagel et al., 2017). MV4;11 cells are homozygous for the *FLT3-ITD* mutation and highly sensitive to FLT3 inhibition (Armstrong et al., 2003; Mark Levis et al., 2002). The transcription factor *MEF2C* cooperates with *SOX4* to induce leukemogenesis in mouse models and *MLL-AF9*-expressing hematopoietic progenitors to promote colony formation (Du et al., 2005; Krivtsov et al., 2006). PBX3 is a transcription factor that acts to stabilize both HOXA9 and MEIS1 localization at a subset of target genes and coexpression of either oncogene with *PBX3* can cause leukemogenesis

(Z. Li et al., 2013, 2016; G. G. Wang et al., 2006). I verified the reductions in *FLT3, MEF2C* and *PBX3* expression with pinometostat by RT-qPCR and examined FLT3 protein levels by Western blot (Figure 2.2G-H).

I wondered if downregulation of one or more of these genes could be responsible for the reductions in cell proliferation from low-dose pinometostat treatment. Using previously published datasets of MEF2C and FLT3-regulated genes, I first looked at the expression of 15 genes that were downregulated by MEF2C knockout in mouse hematopoietic progenitors (Stehling-Sun et al., 2009). Of these genes, only FLT3 was downregulated in my pinometostat-treated cells. Because the expression of nearly all of the set of MEF2C-regulated genes was unaffected in my analysis I moved my focus to FLT3. Previous work by Cauchy et al. identified 138 genes significantly upregulated in karyotypically normal *FLT3-ITD*+ AML compared to WT *FLT3* AML patient samples (Cauchy et al., 2015). A comparison of those FLT3-ITD-upregulated genes to my pinomeostat downregulated genes yielded a small but significant overlap (Figure 2.4F). I saw a more pronounced overlap between genes downregulated in FLT3-ITD+ patient samples and those upregulated by pinometostat, including 10 MHC class II receptors (Figure 2.2I). *PBX3* is the only MLL-AF4 target upregulated in the *FLT3-ITD* samples, suggesting it could be a crucial convergence point of the MLL-AF4 and FLT3-ITD pathways. Collectively, these data suggest that FLT3-ITD may represent an important pathway through which DOT1L inhibition reduces leukemia cell survival. Before delving further into the delineation of the responsible molecular pathways, I first sought to quantitatively define the consequences of low dose DOT1L inhibition on the distribution of the H3K79me2 mark and its causal connection to these gene expression-level changes.

2.2.3 MLL-AF4 targets downregulated by low dose DOT1L inhibition are highly enriched for H3K79me2

Despite extensive global reductions in H3K79me2 levels, only a subset of MLL-AF4 targets were downregulated by 10 nM pinometostat, necessitating more nuanced measurement of the mark, particularly MLL-AF4 target genes. The current model, that MLL-AF4 recruits DOT1L to target genes resulting in aberrantly high levels of H3K79me2 and transcriptional activation (Bernt et al., 2011; Daigle et al., 2013; Guenther et al., 2008), has not been rigorously examined by quantitative methods that would be sensitive to small changes. Indeed, the limitations of conventional ChIP-seq preclude unambiguous quantitative analyses for direct comparisons of histone modifications upon global depletion (Grzybowski et al., 2015; Orlando et al., 2014). To circumvent these problems, I used ICeChIP-seq, a form of native ChIP that uses barcoded internal-standard modified nucleosomes to permit direct quantitative comparison of histone modification density (HMD) at high resolution across samples (Grzybowski et al., 2015, 2019; Shah et al., 2018).

With ICeChIP I was able to measure a positive correlation ($R^2 = 0.53$) between transcript abundance and H3K79me2 levels in MV4;11 cells (Figure 2.5A), consistent with the speculated role for H3K79me2 in transcriptional activation (Bernt et al., 2011; C. W. Chen et al., 2015; Daigle et al., 2011; Okada et al., 2005). However, only 30 of the 250 most highly-expressed genes, including only 3 MLL-AF4 targets, were downregulated by 10 nM pinometostat treatment, suggesting that H3K79me2 is not necessary to maintain high levels of gene expression

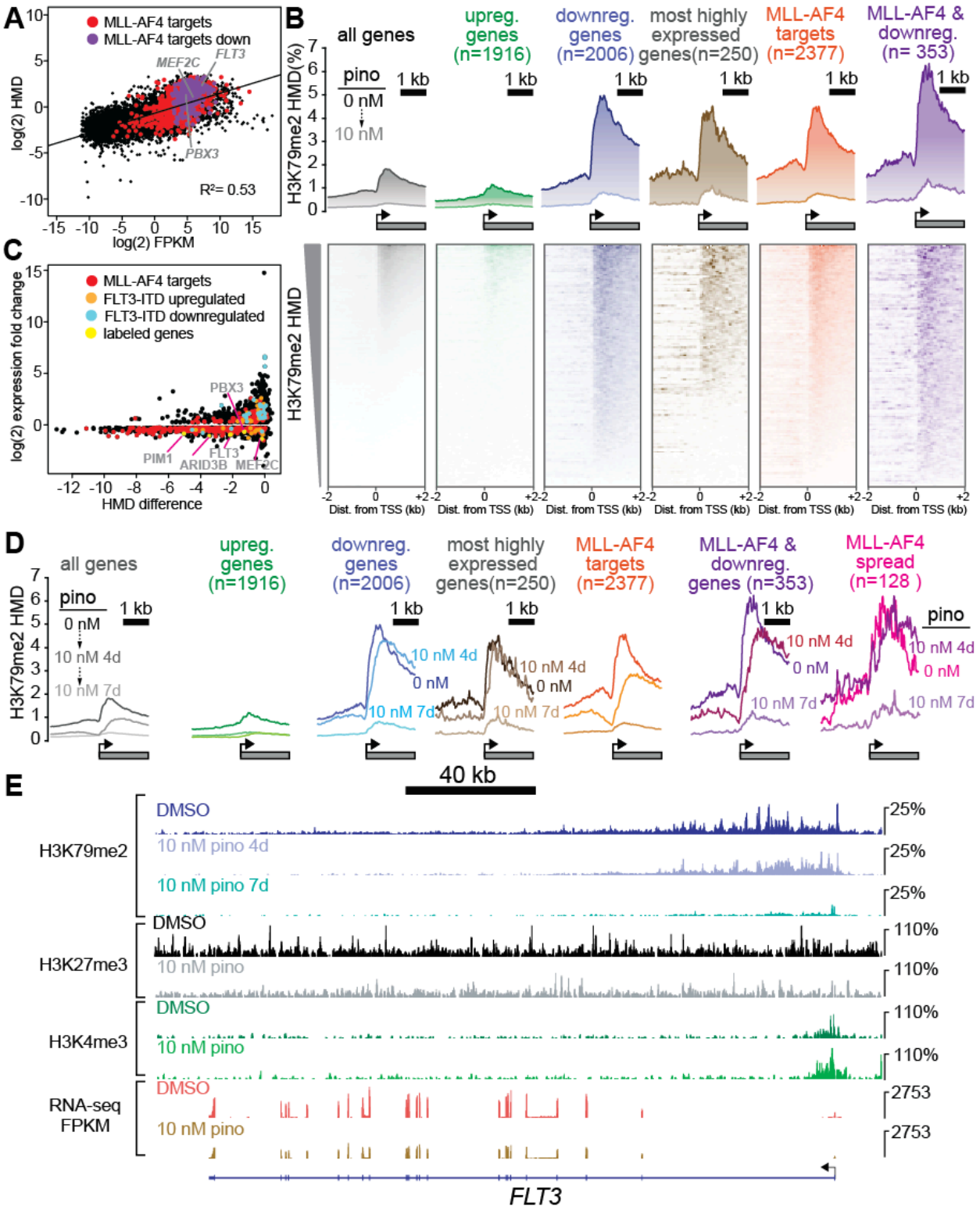

Figure 2.5 Low dose DOT1L inhibition disrupts H3K79me2 with more pronounced effects on downregulated MLL-AF4 targets.

Figure 2.5, continued.
A. Scatterplot of the mean normalized log_2-FPKM (three independent replicates) of genes expressed in DMSO-treated MV4;11 cells plotted versus the log_2-HMD (H3K79me2) for +1000 bp from the TSS. Colors signify: red, MLL-AF4 targets(Kerry et al., 2017); purple, MLL-AF4 targets downregulated by 10 nM pinometostat. **B.** (top) Quantitative measurement of H3K79me2 modification density from ICeChIP-seq of MV4;11 cells treated with 10 nM pinometostat for 7 days contoured over the promoters (-2000 to 2000 bp from the TSS) of indicated gene sets, including genes up- or down-regulated by 10 nM pinometostat, the most highly-expressed genes, MLL-AF4 target genes(Kerry et al., 2017) as well as those MLL-AF4 targets downregulated by 10 nM pinometostat. (bottom) Heatmaps depicting H3K79me2 density (HMD) for the gene promoter regions shown above ranked by HMD. **C.** Scatterplot of genes in MV4;11 cells downregulated by 10 nM pinometostat depicting log_2-fold change H3K79me2 HMD (+1000 bp from TSS) versus the log_2-fold change of the mean normalized FPKM (three independent replicates) for 10 nM pinometostat or DMSO treated cells. Colors signify: red, MLL-AF4 targets(Kerry et al., 2017); orange, FLT3-ITD upregulated genes(Cauchy et al., 2015); blue, FLT3-ITD downregulated genes(Cauchy et al., 2015); yellow, labeled genes in gray font. **D.** Same as A. but includes 1 nM pinometostat treatment and the subset where this complex spreads(Kerry et al., 2017). **E.** The FLT3 locus as representative of an MLL-AF4 target(Guenther et al., 2008; Kerry et al., 2017) downregulated by 10 nM pinometostat, displaying MV4;11 ICeChIP-seq tracks for H3K79me2 10 nM pinometostat 4 and 7 day treatment and H3K27me3 and H3K4me3 tracks from 10 nM pinometostat 7 day treatment as well as DMSO control-treated cells and an RNA-seq track (FPKM) from a single replicate of 10 nM pinometostat 7 day treatment and DMSO-treated cells.

at all sites where it is enriched. The genes that were downregulated by 10 nM pinomeostat had higher H3K79me2 levels compared to upregulated genes or all expressed genes, rivalling the most highly expressed genes (Figure 2.5B). Although previous conventional ChIP-seq measurements observed enrichment of H3K79me2 at MLL-fusion target genes (Bernt et al., 2011; Guenther et al., 2008), my ICe-ChIP-seq analysis revealed equivalent average density at MLL-AF4 targets and 250 most highly expressed genes (Figure 2.5B). Given that only 12 MLL-AF4 targets are included in that highly expressed gene list, this higher H3K79me2 density is likely due to very efficient recruitment of DOT1L by MLL-AF4 rather than deposition via the transcriptional apparatus (Guenther et al., 2007; Schübeler et al., 2004). Interestingly, the subset of MLL-AF4 targets that are downregulated by 10 nM pinometostat exhibit still higher levels of H3K79me2 than even MLL-AF4 targets as a whole and appear to be more dependent on

H3K79me2 for their expression (Figure 2.5A and B). The only other group of genes analyzed with comparable peak H3K79me2 levels were "MLL-spreading" genes which display a binding profile that stretches further downstream into the gene body (Kerry et al., 2017).

In all gene categories I examined, 10 nM pinometostat dramatically reduced apparent H3K79me2 density in gene bodies, eliminating the sharp peaks near the TSS and proportionally

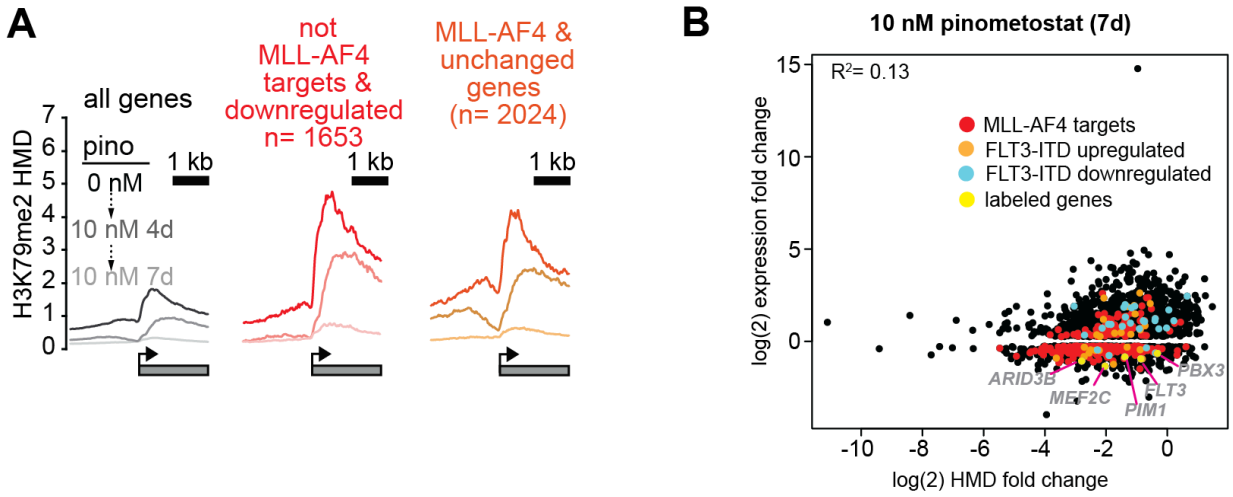

Figure 2.6 H3K79me2 is depleted genome-wide by low dose pinometostat.
A. Plots of H3K79me2 density from ICeChIP-seq in MV4;11 cells treated with 10 nM pinometostat for 4 or 7 days. H3K79me2 modification density (HMD) is displayed from ± 2000 bp of the TSS of all gene expressed, non-MLL-AF4 targets (Kerry et al., 2017) downregulated by 10 nM pinometostat and MLL-AF4 targets not downregulated by 10 nM pinometostat. **B.** Scatterplot of genes downregulated by 10 nM pinometostat plotted as the log(2) fold-change in gene expression vs the log(2) fold-change in HMD with MLL-AF4 targets in red, FLT3-ITD upregulated genes(Cauchy et al., 2015) in orange, FLT3-ITD downregulated genes(Cauchy et al., 2015) in cyan and labeled genes highlighted in yellow. Regression analysis of all genes (R^2 = 0.13) or the MLL-AF4 target subset (R^2 = 0.20), reveals poor correlation between log fold changes of H3K79me2 and RNA expression.

reducing methylation as it tapers toward the 3' end of the gene body (Figure 2.5B). The upregulated gene set displayed lower-than-average density both before and after treatment, consistent with the transcriptional upregulation occurring as an indirect effect of the dosing. Whereas the 10 nM pinometostat downregulated genes, 250 highest expressed genes and MLL-

AF4 targets all experienced similar reductions in H3K79me2 HMD. The similar reductions in methylation at gene groups that had such different overall responses to gene expression from pinometostat treatment suggests that the expression of some genes is more dependent on H3K79me2-mediated transcriptional activation. Given the modest correlation between H3K79me2 early in the gene body and transcriptional output, I observed an unexpectedly poor linear correlation between fold-change in H3K79me2 HMD versus fold-change in gene expression of differentially expressed genes ($R^2 = 0.13$) (Figure 2.6B). However, comparing the absolute differences in HMD to fold-change of gene expression more clearly reveals some interesting trends (Figure 2.5C). Those genes with the largest reductions in HMD (including MLL-AF4 targets) are nearly uniformly downregulated though not in proportion to HMD loss. Conversely, MLL-AF4 targets with smaller HMD reductions are more evenly distributed between both up- and downregulated genes. FLT3-ITD-upregulated genes identified in patient samples (Cauchy et al., 2015) have only small reductions in HMD, suggesting their downregulation is not a direct result of HMD loss but, instead, a secondary effect of FLT3 downregulation.

Interestingly, the MLL-AF4 targets downregulated by low-dose pinometostat (Figure 2.2B) had the largest reductions in H3K79me2 of any gene category examined (Figure 2.5A). These data show that a subset of MLL-AF4 targets have higher levels of H3K79me2 and greater reductions from DOT1L inhibition and are more dependent on this methylation for even moderate levels of expression. Gene expression sensitivity to low-dose DOT1L inhibition may more accurately define “true” MLL-AF4 target genes whose expression is upregulated by the fusion protein and H3K79me2 hypermethylation than those genes that merely align with MLL1 and AF4 ChIP-seq peaks.

To further define the H3K79me2 depletion trajectory, we also examined the distribution of this modification within gene bodies at an earlier timepoint of pinometostat treatment. Treating MV4;11 cells with 10 nM pinometostat for 4 days had little effect on H3K79me2 HMD at the most highly expressed genes, which likely depend more on DOT1L recruitment by the transcriptional apparatus than by the MLL-fusion protein (Figure 2.5D). Pinometostat treatment for 4 days diminished the 5' H3K79me2 peak at genes downregulated by 7-day pinometostat treatment and at MLL-AF4 targets while only slightly reducing H3K79me2 levels within gene bodies of MLL-AF4 targets. Within the gene bodies of 10 nM (7 day) pinometostat-downregulated genes there was actually an increase in H3K79me2 HMD at the 4-day timepoint. This 3' shift in methylation density away from the transcription start site was even more evident in "MLL-spreading" genes, which showed little reduction in peak methylation levels seen in other groups. The shifting and near total depletion of H3K79me2 density from 4-day and 7-day 10 nM pinometostat treatment respectively, is exemplified by several MLL-AF4 target loci (Figure 2.12D, 2.12F, and 2.12G).

The absence of a correlation between H3K79me2 loss and reductions in gene expression suggests that this modification does not have a universal and proportionate effect on gene activation. Rather, it appears some MLL-AF4 targets have higher levels of H3K79me2 and are more sensitive to its depletion. It is possible that the higher methylation levels result in greater dependence on this modification for gene expression at a subset of MLL-AF4 targets. Given the correlation of H3K79me2 depletion with *FLT3-ITD* expression (Figure 2.5E), I next sought to determine if these consequences were direct, and whether the functional consequences of DOT1L inhibition can be explained by this pathway.

2.2.4 MLL-r cells with FLT3-ITD mutations are hypersensitive to both FLT3 and DOT1L inhibition

As my mechanistic analyses relied on MV4;11 cells (*MLL-AF4*, *FLT3*$^{ITD/ITD}$), I investigated the effects of low dose DOT1L inhibition on 3 other cell lines to determine whether *FLT3-ITD* could account for increased sensitivity to H3K79me2 ablation. Unlike MV4;11, the MOLM13 cell line harbors an *MLL-AF9* translocation and is heterozygous for the *FLT3-ITD* mutation (Quentmeier et al., 2003), lesions that have been shown to cooperate to reduce the latency of leukemia onset in mice (Stubbs et al., 2008). I also examined two MLL-translocation cell lines without *FLT3* mutations: THP-1 (*MLL-AF9*); and SEM (*MLL-AF4*). I note that previous studies of DOT1L inhibitor dosing sensitivity of some MLL-r cell lines (Daigle et al., 2013) could be explained by the *FLT3* mutational status, although given the many other genetic background differences in outgrown cell lines it is reasonable that this correlation was not noted.

I treated all four cell lines with 10 nM pinometostat for 7 days. When comparing each cell line to its counterpart with the same MLL-translocation, those with the *FLT3-ITD* mutation were significantly more sensitive to DOT1L inhibition than those with normal *FLT3* alleles (Figure 2.7A, left). After 7 days of 10 nM pinometostat treatment MV4;11 viability was drastically reduced by 74% ± 3% while the viability of SEM, its *MLL-AF4* counterpart with intact *FLT3*, was unaltered within experimental error. MOLM13 viability was somewhat reduced (21% ± 3%) while there was no significant difference in the viability of THP-1 cells. As in MV4;11 cells, MOLM13 cells displayed no change in *HOXA9* or *MEIS1* expression under these conditions (Figure 2.8A).

If the heightened sensitivity of MLL-r cell lines to DOT1L inhibition is indeed mediated by reduced *FLT3-ITD* expression, then I would expect to see a similar heightened sensitivity to

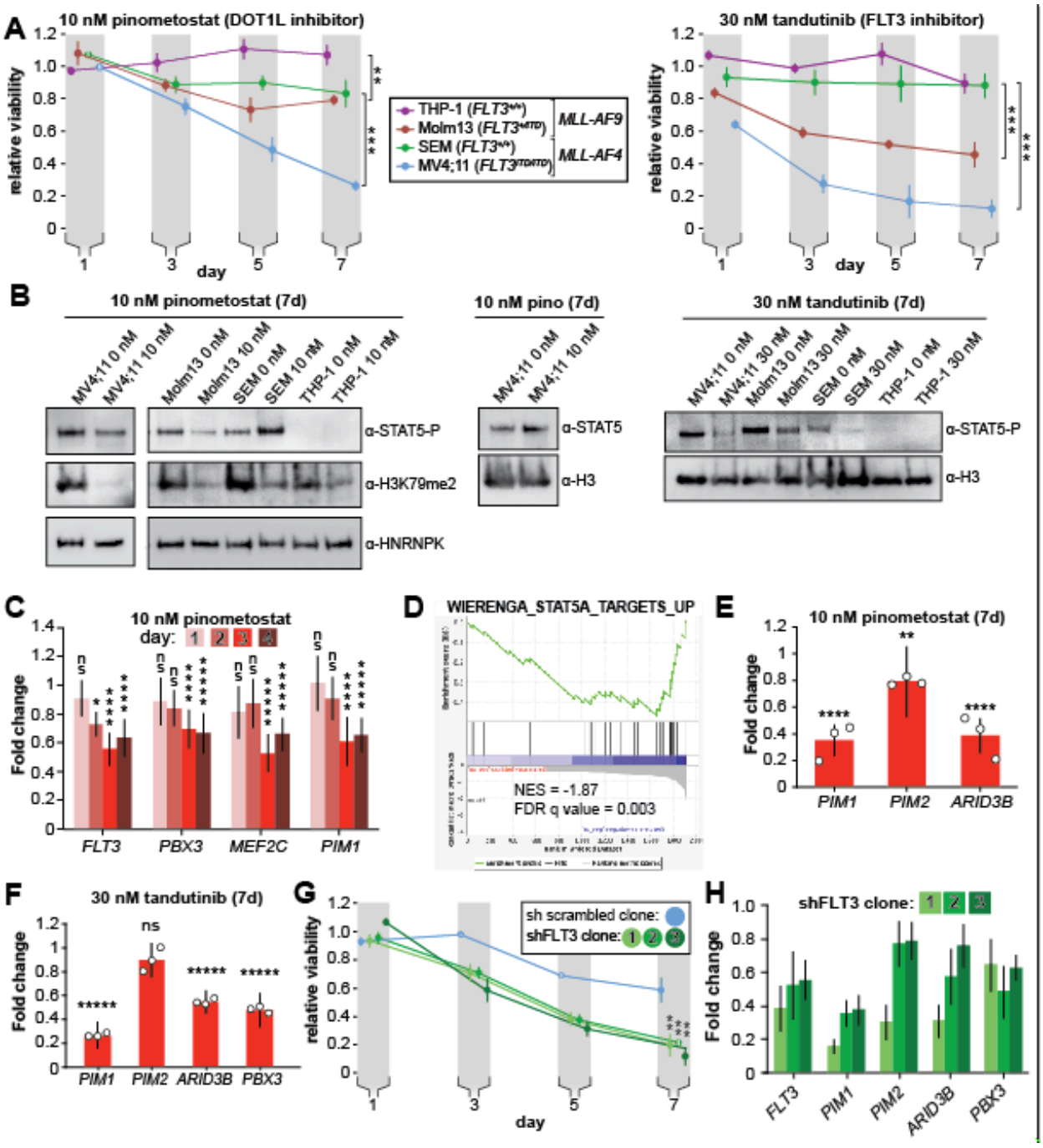

Figure 2.7 DOT1L inhibition reduces STAT5A activation and downregulates STAT5A targets in FLT3-ITD leukemia lines.

A. MLL-rearranged leukemia lines with genotypes indicated were treated with 10 nM pinometostat (left panel, DOT1L inhibitor) or 30 nM tandutinib (right panel, FLT3 inhibitor MLN518), and relative growth monitored by CellTiter Glo 2.0 assay on the indicated days. Relative viability presented is the mean fraction of luminescence of treated versus side-by-side mock treated cultures (same volume of DMSO) for three independent replicates ± S.E.M. Student's t-test (** $p \leq 0.01$, *** $p \leq 0.001$). **B.** Western blots of phosphorylated STAT5

Figure 2.7, continued.
(active) or total STAT5A with H3 or HNRNPK as loading controls across the cell lines from panel A treated as indicated; H3K79me2 is monitored in pinometostat lines to confirm inhibition. **C.** Time course of gene expression by RT-qPCR, presented as mean fold-change of *FLT3, PBX3, PIM1* and *MEF2C* in MV4;11 cells ± 10 nM pinometostat at each time point indicated ± S.E.M.; n = 3; Student's t-test (ns $p > 0.05$, * $p \leq 0.05$, **** $p \leq 0.0001$, ***** $p < 0.00001$). **D.** Gene Set Enrichment Analysis (GSEA)(Mootha et al., 2003; Subramanian et al., 2005) of the set of downregulated genes in MV4;11 cells ± 10 nM pinometostat compared to genes upregulated by exogenous expression of constitutively active STAT5A in the WIERENGA_STAT5A_TARGETS_GROUP1 gene set(Wierenga et al., 2008) from the MSigDB database. **E-F.** DOT1L and FLT3 inhibition downregulate STAT5A targets in *FLT3-ITD*. RT-qPCR expression analysis presented as mean fold-change ± S.E.M. for the indicated transcript in MV4;11 cells treated with indicated inhibitor versus mock-treatment for 7 days. Student's t-test (** $p < 0.01$, **** $p < 0.0001$, ***** $p < 0.00001$). **G.** Proliferation assay as in panel A, with 3 clonal populations of MV4;11 cells virally transduced, selected, then induced to express shRNA to FLT3 or a scrambled shRNA control by 1 μg/mL doxycycline. Means of fractional viability relative to uninduced cells ± S.E.M. are shown for 3 independent experiments; Student's t-test (** $p < 0.01$). **H.** RT-qPCR analysis of *PIM1, PIM2* and *ARID3B* expression in MV4;11 cells expressing an inducible shRNA targeting FLT3 for 7 days. Results are depicted as fold-change expression of shGFP expressing control cells.

disruption of FLT3 signaling. The small molecule tandutinib (MLN518) inhibits FLT3 kinase activity, severely reducing phosphorylation-mediated activation of downstream targets such as STAT5A (Clark et al., 2004). I treated the MLL-r cell lines with 30 nM tandutinib for 7 days. As with the DOT1L inhibition experiments, cell lines with *FLT3-ITD* mutations were significantly more susceptible to the inhibitor's effects (Figure 2.7A, right). Given the variety of other genetic differences amongst these cell lines, these observations can at best be taken as consistent with the hypothesis that the co-occurring *FLT3-ITD* mutations may sensitize MLL-r leukemias to DOT1L inhibition, motivating us to seek more direct examination of FLT3 signaling.

2.2.5 Reduced FLT3 signaling by DOT1L inhibition culminates in reduced transcription of STAT5A target genes

The *FLT3-ITD* mutation allows FLT3 to phosphorylate STAT5A, a transcription factor that is not activated by wild type FLT3 (Choudhary et al., 2005). This aberrant STAT5A phosphorylation licenses translocation to the nucleus to drive target gene transcription, resulting in a hyperproliferative state necessary for leukemia cell survival (Choudhary et al., 2007; Onishi et al., 1998). We hypothesized that *FLT3-ITD* downregulation by DOT1L inhibition would thereby reduce STAT5A phosphorylation. Indeed, pinometostat treatment reduced STAT5 phosphorylation in MV4;11 cells without affecting STAT5A protein levels (Figure 2.7B). Pinometostat treatment slightly reduced STAT5 phosphorylation in MOLM13 cells, consistent with the lower *FLT3-ITD* allele dose, whereas lines with wild type *FLT3* (THP-1, SEM) did not display these effects. As a point of direct comparison, small molecule inhibition of FLT3 signaling yielded markedly reduced STAT5 phosphorylation in lines bearing the *FLT3-ITD* (MV4;11 and MOLM13), with a more modest reduction in SEM cells while phospho-STAT5 was barely detectable in THP-1 cells (Figure 2.7B).

To examine whether FLT3 effects precede other pro-proliferation pathways, I obtained more granular expression kinetics of several downregulated MLL-AF4 targets that have been implicated in leukemogenesis. Expression of *FLT3, PBX3, PIM1* and *MEF2C* was significantly reduced after 72 hours treatment with pinometostat (Figure 2.7C), however, *FLT3* was the only gene whose expression was reduced 48 h after treatment, suggesting it is more sensitive to H3K79me2 reductions than the others examined. Though *FLT3* and *MEF2C* are targets of the HOXA9-MEIS1-PBX3 complex, these genes are all targets of the MLL-fusion protein (Kerry et al., 2017). The reduction in *FLT3* expression in advance of decreased *PBX3* or *MEF2C*

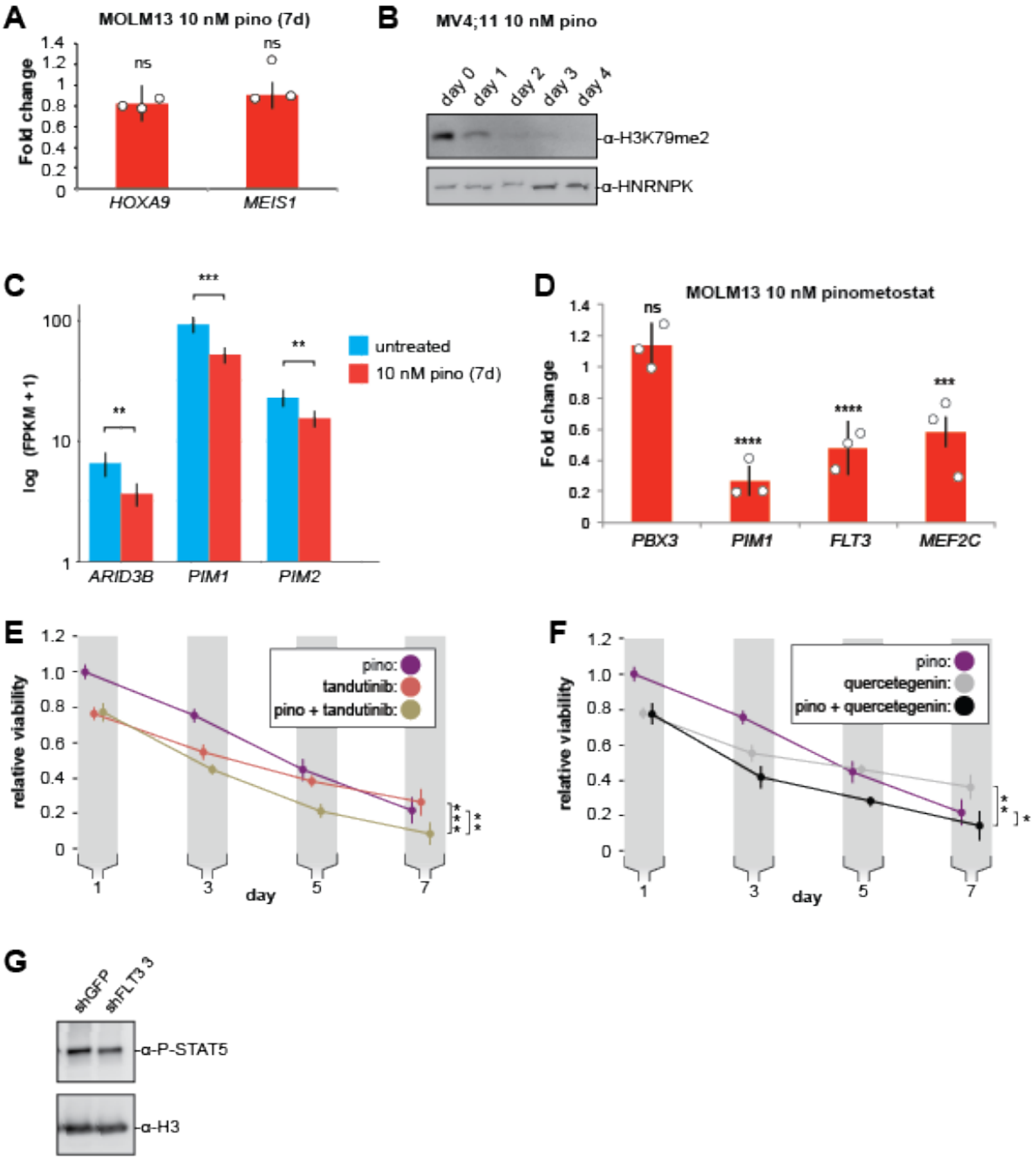

Figure 2.8 STAT5A target genes are downregulated by 10 nM pinometostat.
A. RT-qPCR analysis of *HOXA9* and *MEIS1* expression from three independent experiments of MOLM13 cells treated with 10 nM pinometostat for 7 days. Fold change over DMSO-treated cells is depicted ± S.E.M. Student's t-test **(**ns $p > 0.05$). **B.** Western blots of cell extract from MV4;11 cells treated with 10 nM pinometostat for the indicated number of days and then blotted for H3K79me2 and HNRNPK as a loading control. **C.** Bar graph of Cuffdiff(Trapnell et al., 2013) output for the expression of STAT5A targets *ARID3B*, *PIM1* and *PIM2* from RNA-seq in MV4;11 cells ± 10 nM pinometostat. Values are represented as log(10) FPKM + 1 for 3 independent experiments with standard deviation. Student's t-test **(**** $p < 0.01$, *** $p < 0.001$).

Figure 2.8, continued.
D. RT-qPCR analysis of *PBX3*, *PIM1, FLT3* and *MEF2C* expression from three independent experiments of MOLM13 cells treated with 10 nM pinometostat for 7 days. Fold change over DMSO-treated cells is depicted ± S.E.M. Student's t-test (ns $p > 0.05$, *** $p < 0.001$, **** $p < 0.0001$). **E.** Proliferation assay of MV4;11 cells treated with DOT1L or FLT3 inhibitors alone or in combination using CellTiter Glo 2.0 to measure viability, showing the luminescence fraction of inhibited over uninhibited cells. Data are represented as mean ± SE of three independent experiments. Student's t-test for significance of day 7 values: 10 nM pinometostat vs. combined ** $p < 0.01$, 30 nM tandutinib vs combined *** $p < 0.001$. **F.** Same as E but cells were treated with DOT1L and PIM1 inhibitors alone or in combination. Student's t-test for significance of day 7 values: 10 nM pinometostat vs. combined * $p < 0.05$, 10 μM quercetagenin vs combined ** $p < 0.01$. **G.** Western blots of MV4;11 cell extract from clonal cell lines expressing shRNA to FLT3 (clone 3) or GFP blotted for phosphorylated STAT5 or histone H3 as a loading control.

expression lends tentative support to the possibility that DOT1L inhibition directly affects *FLT3* gene expression independently of *PBX3* or *MEF2C*.

Given the early reductions in FLT3-ITD expression and reduced phosphorylation of its target STAT5A, I hypothesized that the pinometostat-induced reductions in proliferation were due to a loss of STAT5A signaling. I performed GSEA (Mootha et al., 2003; Subramanian et al., 2005) with the pinometostat-downregulated genes and genes upregulated by STAT5A overexpression in human CD34+ hematopoietic progenitors (Wierenga et al., 2008) and observed a negative correlation indicative of significant pathway overlap (NES = -1.87, FDR = 0.003, Figure 2.7D). I then reexamined my RNA-seq data for previously described STAT5A target genes downregulated by pinometostat and found several, including *PIM1* and *ARID3B* (K. T. Kim et al., 2005; Ribeiro et al., 2018)(Figure 2.8C). The PIM proteins are a family of 3 protooncogene serine/tyrosine kinases (PIM1-3) that are upregulated in, and indicative of poor prognosis in leukemia, prostate, mesothelioma and other cancers (Amson et al., 1989; Cibull et al., 2006; Deneen et al., 2003; K. T. Kim et al., 2005; Mizuki et al., 2003; Peltola et al., 2009). However, only *PIM1* and *PIM2* expression is increased in FLT3 inhibitor-resistant *FLT3-ITD*

patient samples and exogenous expression of either *PIM1* or *PIM2* can rescue proliferation defects caused by loss of FLT3 activity in MOLM14 cells (*MLL-AF9*, *FLT3-ITD* heterozygous) (Adam et al., 2006; Green et al., 2015). Although *PIM1* and *PIM2* are both downregulated in my RNA-seq analysis (Figure 2.8C) I observed a much greater reduction in *PIM1* expression by RT-qPCR (Figure 2.7E). Similarly, treating MV4;11 cells with tandutinib (FLT3 inhibitor) resulted in downregulation of *PIM1*, *ARID3B* and *PBX3* but not *PIM2* (Figure 4F). Treating MOLM13 cells with pinometostat also reduced expression of *MEF2C, FLT3* and *PIM1,* but caused no change in *PBX3* expression (Figure 2.8D).

If the FLT3 and DOT1L inhibitors have overlapping functions through inhibition or downregulation of *FLT3,* respectively, then I could potentially observe synergy in the effects on MV4;11 proliferation if I treated with both inhibitors simultaneously. The DOT1L inhibitor has a delayed effect compared to the PIM1 and FLT3 inhibitors, which complicates comparisons, but nonetheless, I observed small but significant differences in proliferation when using inhibitors singly or in combination at day 7 (Figures 2.8E and 2.8F).

To directly interrogate the effects of *FLT3* on MLL-r leukemia proliferation without complications from different genetic backgrounds, I used viral transduction to insert a tet-inducible shRNA targeting *FLT3* into MV4;11 cells. With modest knockdown of *FLT3* (Figure 2.7H) I observed significant reductions in the proliferation of 3 different clonal lines as compared to a scrambled shRNA (Figure 2.7G). *FLT3* knockdown reduces MV4;11 proliferation and STAT5A phosphorylation (Figure 2.8G), analogous to the effects of pinometostat treatment. Akin to the DOT1L and FLT3 inhibitors (Figure 2.7E-F), *FLT3* knockdown also significantly reduced the expression of the STAT5A target genes *PIM1* and *ARID3B*, with *PIM2* expression reduced in only 1 of 3 clones (Figure 2.7H). Interestingly, *FLT3* knockdown also resulted in

PBX3 downregulation, suggesting that FLT3 can regulate the expression of this oncogenic transcription factor, in line with previous observations (Cauchy et al., 2015). Unfortunately, overexpression of *FLT3-ITD* for an attempted rescue of DOT1L inhibition proved technically challenging, as retrovirally introduced ectopic expression was rapidly silenced or dropped out during selection as has been observed in other contexts (Spiekermann et al., 2002). To further interrogate this pathway's functional significance, I sought to perturb signaling downstream of FLT3-ITD via STAT5A alterations.

2.2.6 Overexpression of constitutively active STAT5A rescues proliferation and target gene expression defects caused by DOT1L inhibition

To potentiate STAT5A activity, I overexpressed a constitutively active STAT5A mutant to examine whether this could counteract the reduction of upstream FLT3-ITD levels by DOT1L inhibition. STAT5A is "activated" through phosphorylation at multiple sites, facilitating translocation into the nucleus and activation of gene targets. Previous work showed that H299R and S711F mutations create a constitutively active murine *Stat5a* able to activate target genes independently of upstream signaling (Onishi et al., 1998), which phenocopies the effects of exogenous *FLT3-ITD* expression including hyperproliferation and inhibition of myeloid maturation (Moore et al., 2007). I used a lentiviral system to generate individual MV4;11 clonal cell lines with stably-incorporated, inducible human *STAT5A* mutated at the corresponding residues H298R and S710F (*STAT5A-CA*), all of which exhibit several-fold induction with doxycycline (Figure 2.9A and Figure 2.10A). Ectopic expression of *STAT5A-CA* was able to partially rescue proliferation when challenged with 30 nM FLT3 inhibitor tandutinib, confirming the capacity of this mutant to complement impaired FLT3-ITD signaling (Figure 2.10B).

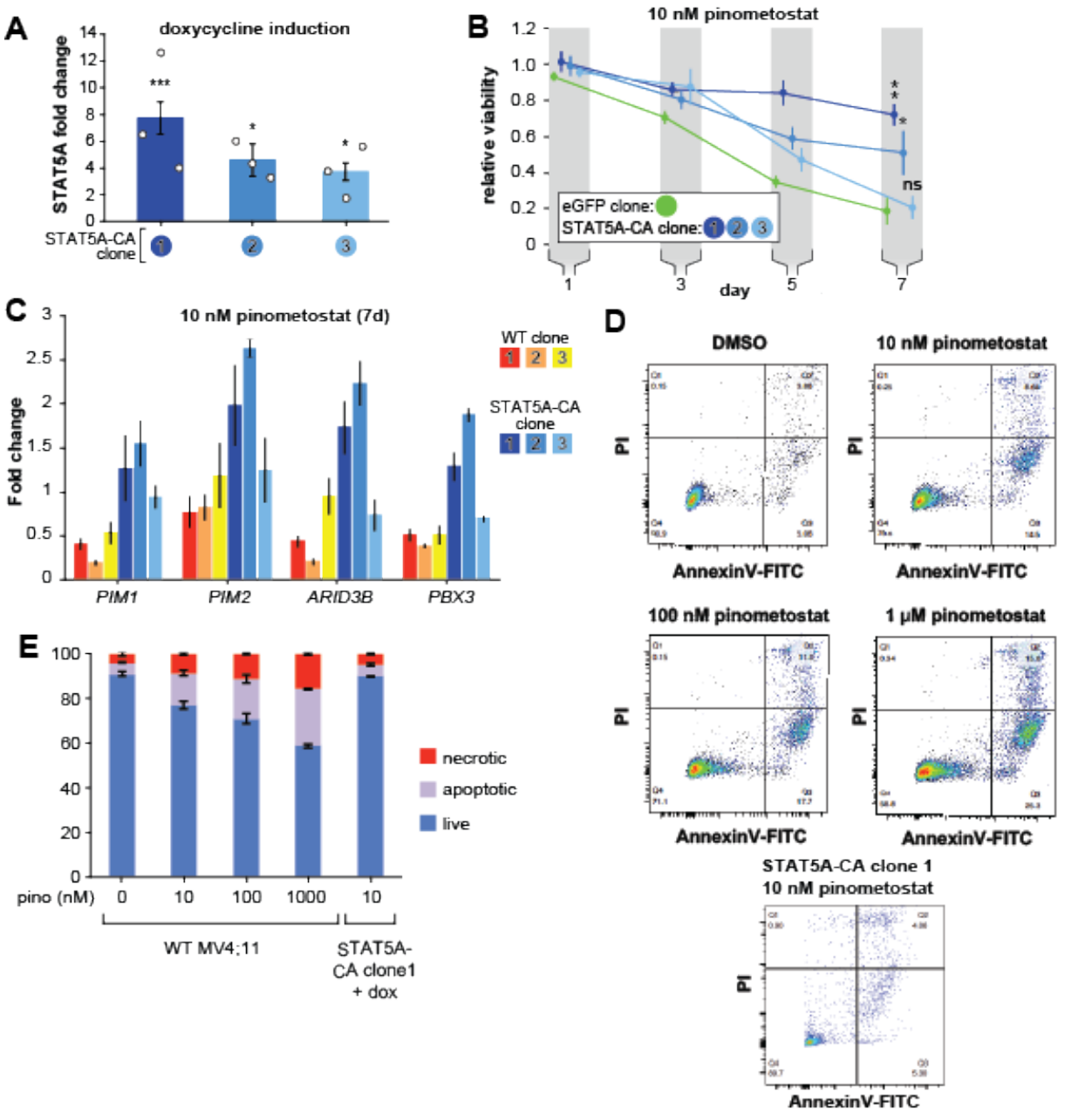

Figure 2.9 Exogenous expression of constitutively active STAT5A partially rescues proliferation and gene expression effects of DOT1L inhibition.
A. RT-qPCR analysis of *STAT5A* expression from 3 monoclonal isolates of MV4;11 cells virally transduced with a tet-inducible constitutively active *STAT5A* (*STAT5A-CA*) depicted as fold-change over untransduced cells with standard error of the mean. Student's t-test (* $p < 0.05$, *** $p < 0.001$). **B.** Proliferation assay of MV4;11 clonal isolates from panel A. induced to express *STAT5A-CA* or eGFP with 1 µg/mL doxycycline and treated concomitantly with 10 nM pinometostat. We determined the fractional viability of each clone as the luminescence from a CellTiter Glo 2.0 assay with pinometostat-treatment normalized to DMSO-treated cells, both induced to express *STAT5A-CA or eGFP*, to accommodate for any potential increases in viability. Means ± SE are shown for 3 independent experiments with Student's t-test for

Figure 2.9, continued.
significance of day 7 values (**** $p \leq 0.0001$). **C.** Gene expression analysis by RT-qPCR of STAT5A target genes in WT MV4;11 cells or MV4;11 *STAT5A-CA* clones from A. induced with 1 μg/mL doxycycline and treated with 10 nM pinometostat for 7 days. Results are displayed as fold-change over DMSO-treated WT cells. **D.** Quantitative measurement by flow cytometry of live, apoptotic (Annexin V-FITC) and necrotic cells (propidium iodide) of WT MV4;11 cells or cells exogenously expressing *STAT5A-CA* (clone 1) and treated with increasing concentrations of pinometostat. Images of gated FITC vs. PI signal are shown for 1 of 3 independent experiments that are quantified in the bar plot in E.

Remarkably, *STAT5A-CA* overexpression also rescued pinometostat-induced proliferation reductions (Figure 2.9B) in proportion to each clone's *STAT5A-CA* expression level (Figure 2.9A). Clone 3 was unable to rescue proliferation substantially, possibly because it had the lowest expression of *STAT5A/STAT5A-CA* (Figure 5A). As another control, I similarly overexpressed MEF2C, yet it displayed no effect on the viability of MV4;11 cells treated with 10 nM pinometostat (Figure 2.10C).

To gain a molecular understanding of how ectopic *STAT5A-CA* expression could rescue proliferation of inhibitor-treated cells, I measured expression of the STAT5A targets *PIM1*, *PIM2* and *ARID3B* by RT-qPCR. Expression of *STAT5A-CA* restored expression of *PIM1*, *PIM2* and *ARID3B* in both DOT1L inhibitor- and FLT3 inhibitor-treated MV4;11 cells (Figure 2.9C and 2.10D).

Because ectopic expression of *STAT5A-CA* is able to rescue proliferation of MV4;11 cells and the expression of STAT5A targets including the anti-apoptotic *PIM1* oncogene, I examined whether *STAT5A-CA* overexpression could rescue MV4;11 cells from apoptosis. A previous study observed that ~30% of MV4;11 cells treated with 1 μM pinometostat for 6 days were undergoing apoptosis (Daigle et al., 2013). I analyzed apoptosis in MV4;11 cells treated with increasing concentrations of pinometostat for 7 days (Figures 2.9D and E). I observed 25.5% ± 0.3% apoptotic cells when treating with 1 μM pinometostat and a still sizeable proportion (15%

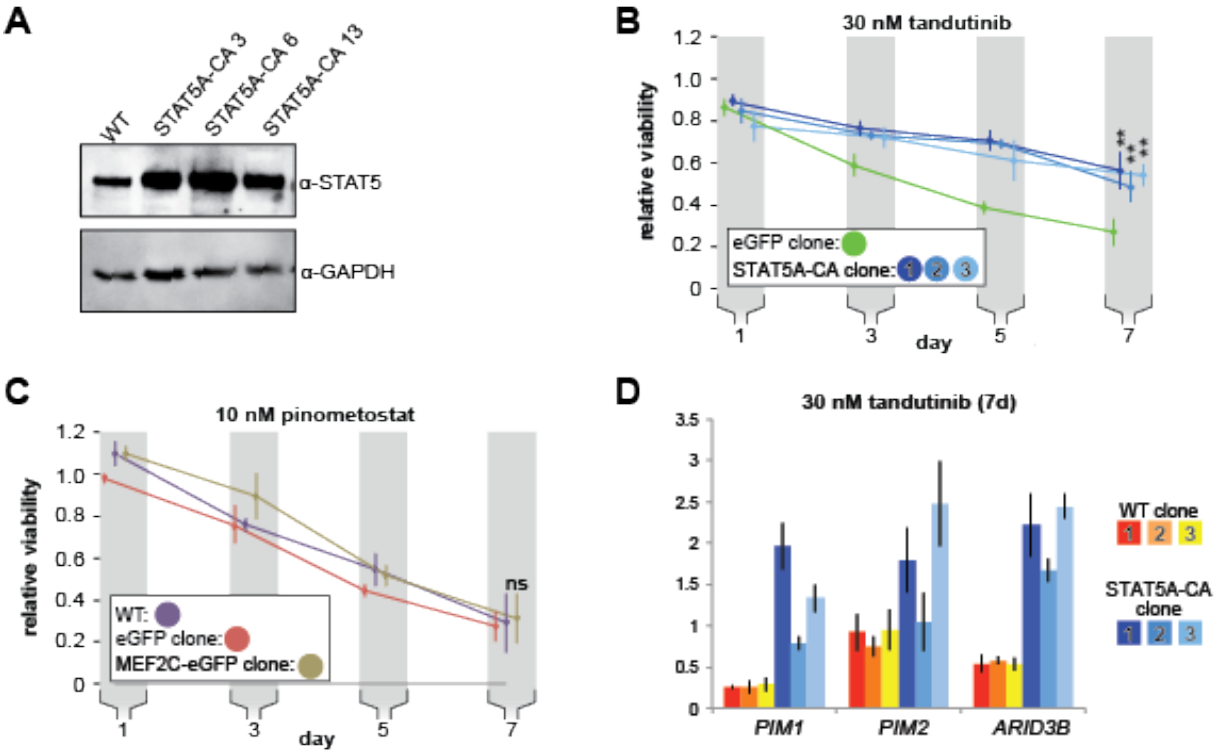

Figure 2.10 Ectopic STAT5A expression rescues the proliferation of MV4;11 cells treated with FLT3 inhibitor.
A. Western blots of whole cell extracts from WT MV4;11 cells or 3 monoclonal populations isolated from MV4;11 cells virally transduced with constitutively active *STAT5A* (*STAT5A-CA*). Membranes were blotted for STAT5 or GAPDH as a loading control. **B.** Proliferation assay of MV4;11 clonal isolates overexpressing *STAT5A-CA* or GFP through induction with 1 µg/mL doxycycline and treated with 30 nM tandutinib using CellTiter Glo 2.0 to measure viability, showing the luminescence fraction of inhibited over uninhibited cells, both with induced transgene (either STAT5A-CA or eGFP). Means ± SE are shown for 3 independent experiments. Student's t-test of day 7 values: ** $p < 0.01$. **C.** Proliferation assay done as in B. with MV4;11 WT or virally transduced with *GFP* or *MEF2C-GFP* and induced to express either construct with 1 µg/mL doxycycline and treated with 10 nM pinometostat. Means ± SE are shown for 3 independent experiments. Student's t-test of day 7 values: ns $p > 0.05$. **D.** Gene expression analysis by RT-qPCR of STAT5A target genes in WT MV4;11 cells or MV4;11 *STAT5A-CA* clones from A. induced with 1 µg/mL doxycycline to express STAT5A-CA and treated with 30 nM tandutinib for 7 days. Results are displayed as fold-change over DMSO-treated WT cells.

± 1%) of apoptotic cells when treating with just 10 nM pinometostat. Yet upon treatment of STAT5A-CA clone 1 with 10 nM pinometostat for 7 days, I observed no significant induction of apoptosis as compared to the DMSO control (Figure 2.9D and E). Thus, I concluded that recovering STAT5A function can rescue MV4;11 cells from apoptosis induced by 10 nM

pinometostat. It is striking that despite marked gene expression changes caused by low-dose DOT1L inhibition, one signaling pathway, FLT3-ITD to STAT5A, is able to account for the bulk of the phenotypic and molecular changes I measured. Given that the rescue was nevertheless incomplete, I investigated other potential secondary contributors to the proliferation and gene expression consequences of low-dose DOT1L inhibition.

2.2.7 An ancillary DOT1L-dependent pathway limits proliferation through PRC2 signaling

Although H3K79me2 potentiates transcription, my RNA-seq analysis revealed the upregulation of thousands of genes when treating with pinometostat. One potential explanation for this effect is the downregulation of the repressive PRC2 complex members EZH2 and EED and consequent reductions in global levels of the transcriptionally repressive H3K27me3 mark (Figures 2.11A-B, 2.12A). PRC2 deposits the facultative heterochromatin H3K27me3 modification and, though antagonistic to MLL1 and H3K4me3 deposition (D.-H. Kim et al., 2013), is necessary for MLL-r leukemogenesis (Neff et al., 2012; Shi et al., 2013; J. Zhou et al., 2011). Analysis by quantitative ICeChIP revealed that 10 nM pinometostat decreased H3K27me3 genome-wide (Figure 6C). Promoter H3K27me3 levels are reduced by 2-5% on average with more pronounced decreases observed among downregulated genes and MLL-AF4 targets than upregulated or all genes (Figure 2.11C). However, H3K27me3 levels in untreated cells were much higher in pinometostat-upregulated genes, perhaps indicating that these genes are more reliant on PRC2 to buffer their expression. H3K27me3 levels are lower throughout gene bodies in DOT1L inhibited cells, as apparent at individual loci (Figure 2.5E, 2.12D-G).

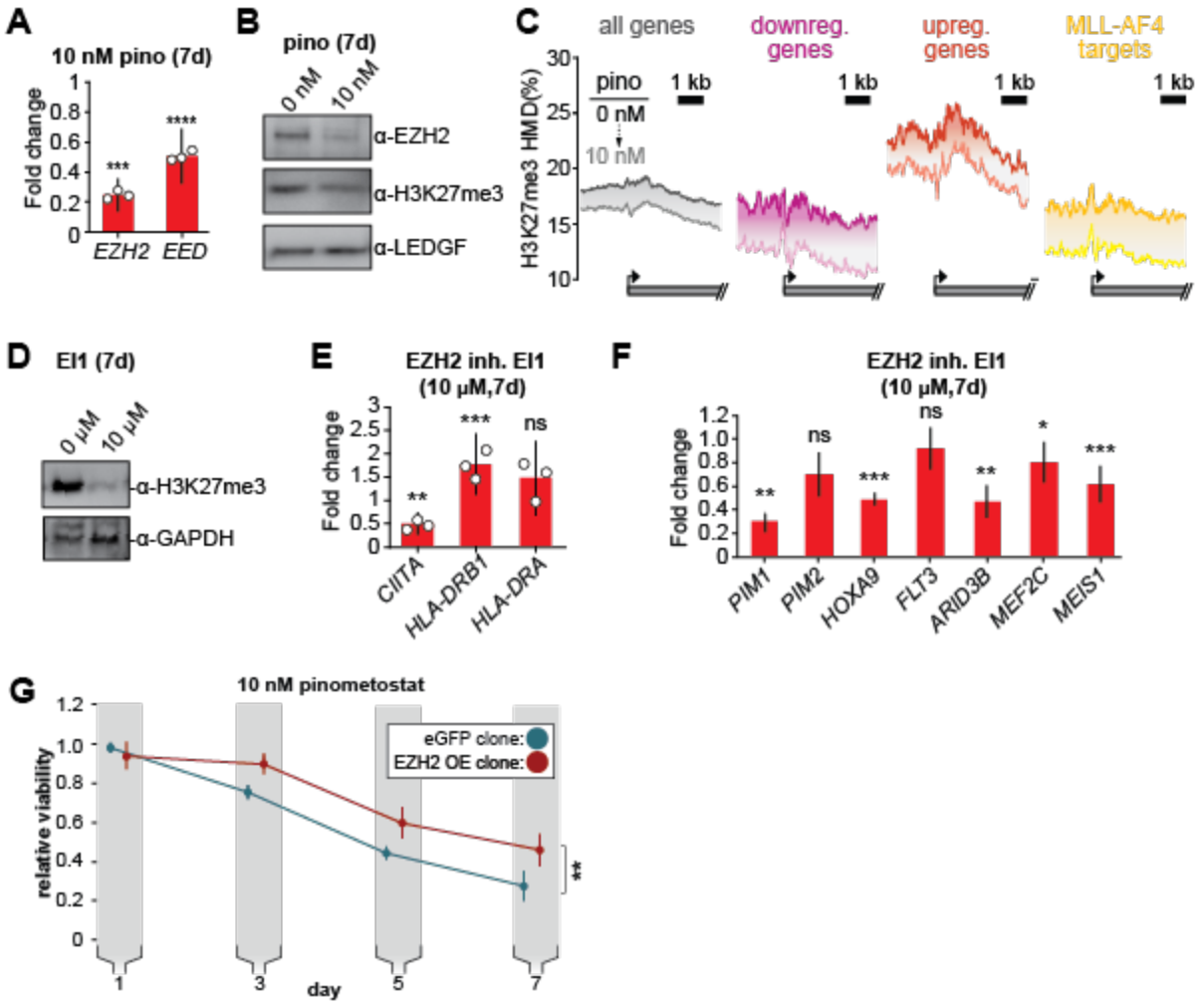

Figure 2.11 PRC2 function is an ancillary pathway dependent on DOT1L and necessary for leukemia proliferation.

A. RT-qPCR analysis of the components of the polycomb complex *EZH2* and *EED* expression in MV4;11 cells ± 10 nM pinometostat for 7 days. Results are displayed as mean fold-change vs. DMSO-treated cells ± S.E.M. of three independent experiments. Student's t-test for significance (*** $p < 0.001$, **** $p < 0.0001$). **B.** Western blot of EZH2, H3K27me3 and LEDGF as loading control in MV4;11 cells treated ± 10 nM pinometostat for 7 days. **C.** Quantitative Ice-ChIP-seq from MV4;11 cells treated with 10 nM pinometostat for 7 days displaying H3K27me3 histone methylation density contoured over promoters from -2000 to +4000 of the TSS of either all expressed genes, genes up- or downregulated by 10 nM pinometostat or MLL-AF4 target genes(Kerry et al., 2017). **D.** Western blot for H3K27me3 with GAPDH as a loading control in MV4;11 cells treated with EI1 for 7 days. **E.** RT-qPCR analysis of MHC class II genes and master regulator *CIITA* expression from MV4;11 cells ± 10 μM EZH2 inhibitor EI1. Results are displayed as mean fold-change vs. DMSO-treated cells ± S.E.M. of three independent experiments. Student's t-test for significance (** $p = 0.01$, *** $p = 0.001$). **F.** Fold change of RT-qPCR analysis of gene expression MV4;11 cells ± 10 μM EZH2 inhibitor EI1. Results are the average 3 independent experiments ± S.E.M. Student's t-test (* $p < 0.05$, ** $p < 0.01$, *** $p =$

Figure 2.11, continued.
0.001). **G.** Proliferation assay of MV4;11 cells virally transduced with tet-inducible EZH2 or eGFP treated with 10 nM pinometostat and induced with 1 μg/mL doxycycline to express EZH2 or eGFP for 7 days showing the luminescence fraction of inhibited over uninhibited from a CellTiter Glo 2.0 assay. Means ± SE are shown for 3 independent experiments. Student's t-test of day 7 values (** $p = 0.01$).

I next sought to interrogate the functional impact of the PRC2 signaling axis by experimental perturbation. As PRC2 is necessary for repression of *IFNG* (IFN-γ) and proper differentiation in T-cells (Tumes et al., 2013), I wondered if the upregulated genes found in my RNA-seq analysis, many of which are components of the IFN-γ-response, were upregulated as a result of a loss of H3K27me3-mediated repression. To investigate this possibility, I treated MV4;11 cells with 10 μM EI1 EZH2 inhibitor (Qi et al., 2012) and observed dramatically reduced global H3K27me3 (Figure 2.11D) and proliferation (Figure 2.12B), consistent with previously observed sensitivities of MOLM13 and MV4;11 (Ueda et al., 2014). EI1 treatment had comparatively little effect on the class of genes massively overexpressed during DOT1L inhibition (Figure 2.11E, compare to Figures 2.2D and E). Surprisingly, EZH2 inhibition downregulated *HOXA9* and *MEIS1* expression (which only occurs with higher doses of pinometostat (Daigle et al., 2013)), with no changes in *FLT3* expression (Figure 2.11F) or STAT5 phosphorylation (Figure 2.12C). The greater reduction in global H3K27me3 from 10 μM EI1 than 10 nM pinometostat may account for the lack of effect on *HOXA9* and *MEIS1* expression by pinometostat. Collectively, these data argue that the PRC2 pathway is largely independent of the FLT3-ITD-STAT5A pathway, culminating in distinct target gene expression consequences, that may converge for only a few targets, such as *PIM1* and *ARID3B*.

Next, I queried the functional consequences of rescuing EZH2 expression in the context of low-dose DOT1L inhibition. Inducible overexpression of *EZH2* was only able to partially

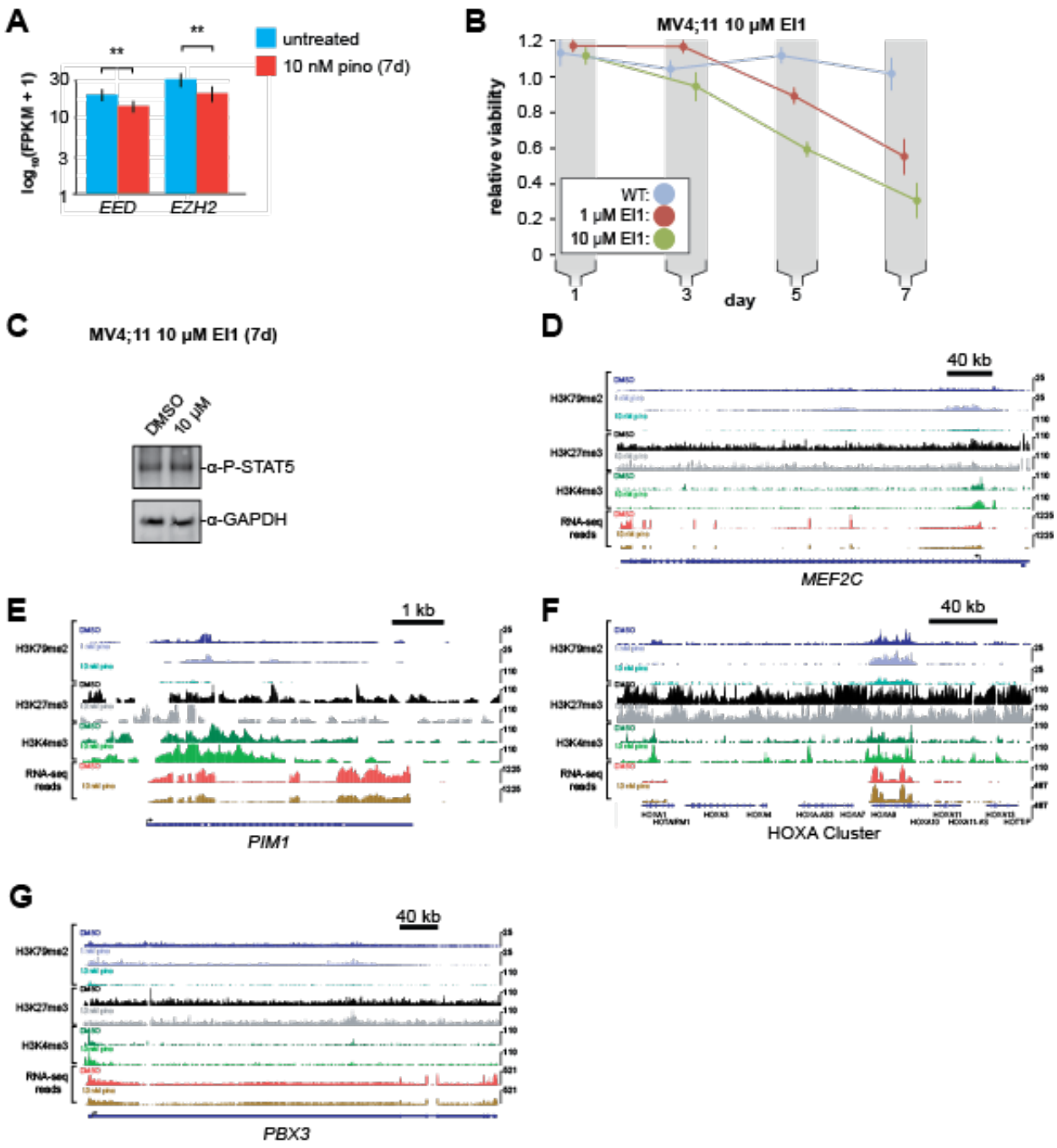

Figure 2.12 PRC2 components are downregulated by 10 nM pinometostat.
A. Bar graph of Cuffdiff(Trapnell et al., 2013) output for the expression of polycomb complex members *EED* and *EZH2* from RNA-seq in MV4;11 cells ± 10 nM pinometostat for 7 days. Values are represented as log(10) FPKM + 1 for 3 independent experiments with standard deviation. Student's t-test (** $p < 0.01$). **B.** Proliferation assay of MV4;11 cells treated with 10 µM EI1 EZH2 inhibitor using CellTiter Glo 2.0 to measure viability, showing the luminescence fraction of inhibited over DMSO-treated cells. Means ± SE are shown for 3 independent experiments. Student's t-test of day 7 values: * $p < 0.05$, ** $p < 0.01$. **C.** Western blot of extract from MV4;11 cells treated with 10 µM EI1 for 7 days and blotted for phosphorylated

Figure 2.12, continued.
STAT5 or GAPDH as a loading control. **D-G.** ICeChIP-seq tracks of H3K79me2, H3K27me3 and H3K4me3 HMD and an RNA-seq track (FPKM) from a single replicate for MV4;11 cells treated with 10 nM pinometostat or DMSO for 7 days for MLL-AF4(Kerry et al., 2017) and STAT5A(Moore et al., 2007) target genes: **D.** *MEF2C*; **E.** the HOXA gene cluster; **F.** *PIM1* and **G.** *PBX3*.

rescue proliferation in MV4;11 cells treated with pinometostat, suggesting that a small portion of the effects on MV4;11 viability is due to reduced PRC2 function (Figure 2.11G). The nearly complete rescue from intervening in the FLT3-ITD-STAT5A pathway compared to the modest rescue from PRC2, suggests that the former is the predominant source of pinometostat-induced effects on proliferation in this leukemia background.

2.2.8 STAT5A-CA overexpression rescues the viability of MV4;11 cells treated with MLL1 inhibitors

My observations suggest that most of the toxicity from low-dose DOT1L inhibition in MLL-r, *FLT3-ITD+* leukemia cell lines stems from downregulation of *FLT3* and subsequent loss of STAT5A phosphorylation. I wanted to know if this effect was specific to H3K79me2 depletion, or attributable to disruption of MLL-fusion-induced gene activation. To distinguish between these two mechanisms, I employed small-molecule MLL1 inhibitors, potent and effective treatments for MLL-r leukemia (Borkin et al., 2015; F. Cao et al., 2014), as orthologous means of disrupting MLL-fusion function. These compounds inhibit MLL1 in different ways but both disrupt the leukemic gene expression profile, specifically downregulating the oncogenes *HOXA9*, *MEIS1*, *FLT3* and *BCL2* (Borkin et al., 2015; F. Cao et al., 2014). MI-503 competitively antagonizes binding of MENIN to MLL1, an interaction that is necessary for MLL-fusion complex localization to target genes and leukemogenesis (Borkin et al., 2015; Akihiko Yokoyama et al., 2005). Another small molecule, MM-401 inhibits the methyltransferase activity

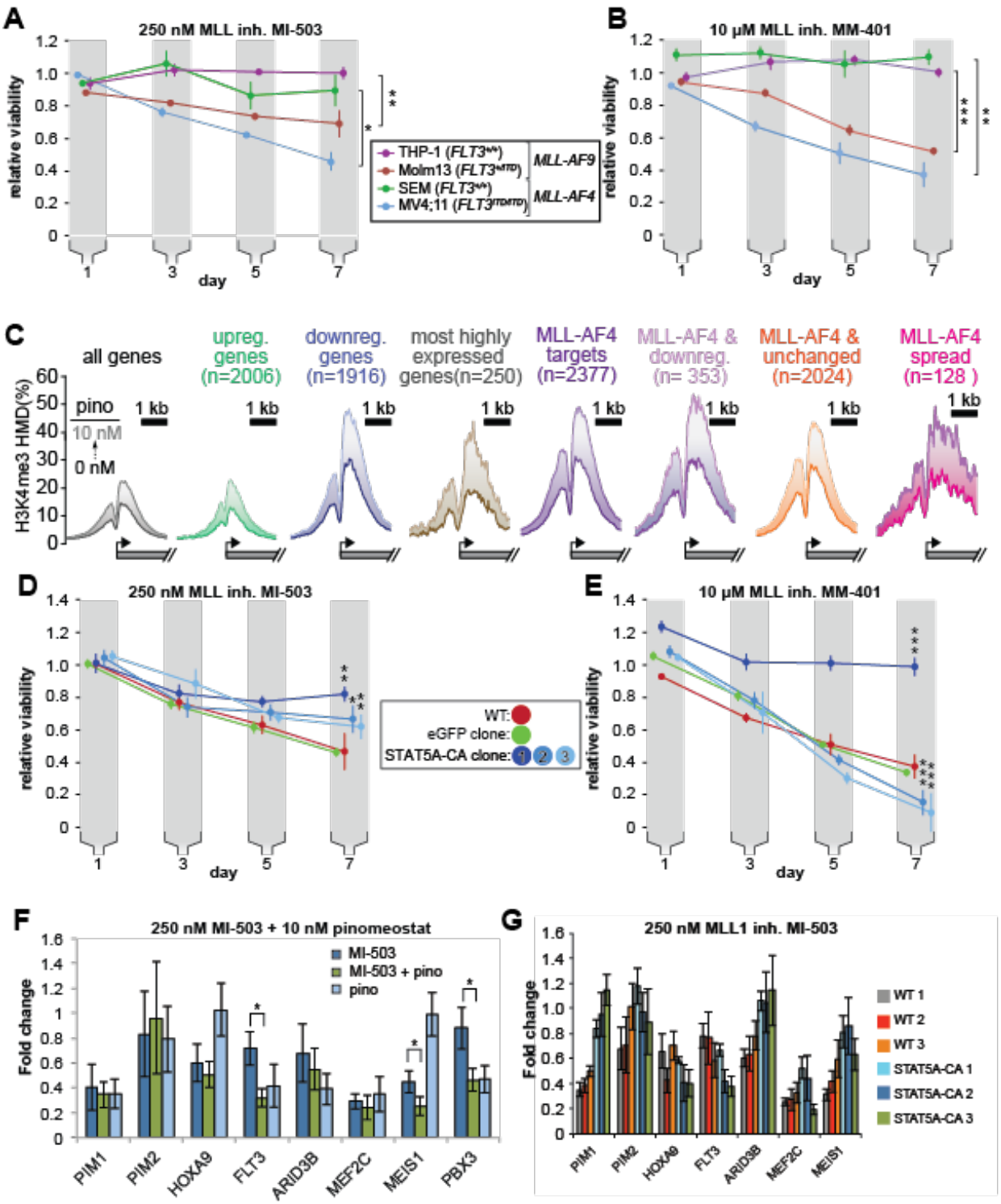

Figure 2.13 STAT5A-CA overexpression rescues the viability of MV4;11 cells treated with MLL1 inhibitors.

Proliferation assay of MLL-r cell lines treated with **A.** 250 nM MI-503 (MLL1-Menin interaction inhibitor) or **B.** 10 µM MM-401 (MLL1 histone methyltransferase inhibitor) for 7 days. Viability was measured by CellTiter Glo 2.0 assay and results are displayed as the fraction of

Figure 2.13, continued.
luminescence of inhibitor-treated over DMSO-treated cells. Means ± SE are shown for 3 independent experiments. Student's t-test (* $p < 0.05$, ** $p < 0.01$, *** $p < 0.001$). **C.** H3K4me3 histone methylation density from -2000 to +2000 of the TSS from quantitative ICeChIP-seq from MV4;11 cells treated with 10 nM pinometostat for 7 days for genes up- or down-regulated by 10 nM pinometostat, the most highly-expressed genes, MLL-AF4 target genes(Kerry et al., 2017) as well as those MLL-AF4 targets downregulated by 10 nM pinometostat. **D. and E.** Proliferation assay of MV4;11 *STAT5A-CA* clonal isolates induced to express *STAT5A-CA* or eGFP with 1 µg/mL doxycycline and treated with **D.** 250 nM MI-503 or **E.** 10 µM MM-401. Viability was measured and results displayed as in A and B. Means ± SE are shown for 3 independent experiments. Student's t-test (* $p < 0.05$, ** $p < 0.01$, *** $p < 0.001$). **F.** Gene expression analysis by RT-qPCR of MLL-fusion and STAT5a targets in MV4;11 cells treated with 250 nM MI-503 MLL1 inhibitor, 10 nM pinometostat DOT1L inhibitor or a combination for 7 days. Means ± S.E.M. are shown for 3 independent experiments (* $p < 0.05$). **G.** Gene expression analysis by RT-qPCR of MLL-fusion and STAT5A targets in WT and STAT5A-CA MV4;11 cells treated with 250 nM MI-503 MLL1 inhibitor for 7 days. Means ± S.E.M. are shown for technical replicates of individual experiments.

of MLL1 by disrupting its interaction with WDR5, a complex member necessary for full enzymatic activity of MLL1 but not MLL2-4 or SET1 complexes (F. Cao et al., 2014). I treated MLL-r cell lines with low concentrations of MI-503 or MM-401 and observed greater reductions in the proliferation of *MLL-r*, *FLT3-ITD*+ cells than their WT *FLT3* counterparts (Figure 2.13A and B).

Given the similar effects of DOT1L and MLL1 inhibitors on MLL-r cell proliferation and gene expression, that both histone modifications are involved in transcriptional activation and the extensive literature describing dynamic cross-talk between chromatin modifications (S. Chen et al., 2015; D.-H. Kim et al., 2013; Schmitges et al., 2011; Voigt et al., 2012) I was curious as to how perturbations in H3K79 methylation might affect the distribution of H3K4me3. In order to accurately quantify histone methylation and observe differences in modification densities I performed ICeChIP-seq for H3K4me3 in MV4;11 cells treated with pinometostat. H3K4me3 is deposited at promoters during active transcriptional initiation and promotes gene expression

through several established mechanisms (Krogan et al., 2002; Vermeulen et al., 2007; A. Yokoyama et al., 2004). Surprisingly, pinometostat treatment increased H3K4me3 at transcription start sites (TSS's) genome-wide, with the largest increases at genes downregulated by pinometostat (Figure 2.13C). Pinometostat-downregulated MLL-AF4 targets had the highest H3K4me3 levels of all gene categories examined (Figure 2.13C), not only at the TSS but spreading downstream into the gene body, suggesting that the MLL-fusion protein is driving this increase. Potentially indicative of a previously undescribed form of antagonistic histone mark cross-talk, I observed a striking anti-correlation between pinometostat-induced reductions in H3K79me2 and increases in H3K4me3, which was most evident at MLL-AF4 targets downregulated by 10 nM pinomeostat. Despite gains of the H3K4me3 mark during treatment, these genes are downregulated, consistent with a decoupling of active transcription initiation from productive elongation, the latter of which is more effectively correlated with H3K79me2 and H3K36me3 (Guenther et al., 2007).

Intriguingly, the putative antagonism between modifications is not apparent in global H3K4me3 levels during DOT1L inhibition (Figure 2.14A). However, reductions in H3K4me3 from MLL1 inhibitor treatment are also not readily apparent by Western blot, similar to what has been observed in other studies (F. Cao et al., 2014) (Figure 2.14B). Conversely, global increases in H3K79me2 are more pronounced when treating cells with the MLL1 inhibitors (Figure S7C). Treatment with the MLL1 inhibitors also reduced STAT5A phosphorylation, suggesting that this orthologous means of disrupting MLL-fusion gene activation also reduces FLT3-ITD/STAT5A signaling (Figure 2.14C).

As with the DOT1L and FLT3 inhibitors, overexpression of *STAT5A-CA* was able to partially rescue survival of MV4;11 cells treated with MI-503 (Figure 2.13D), with the degree of

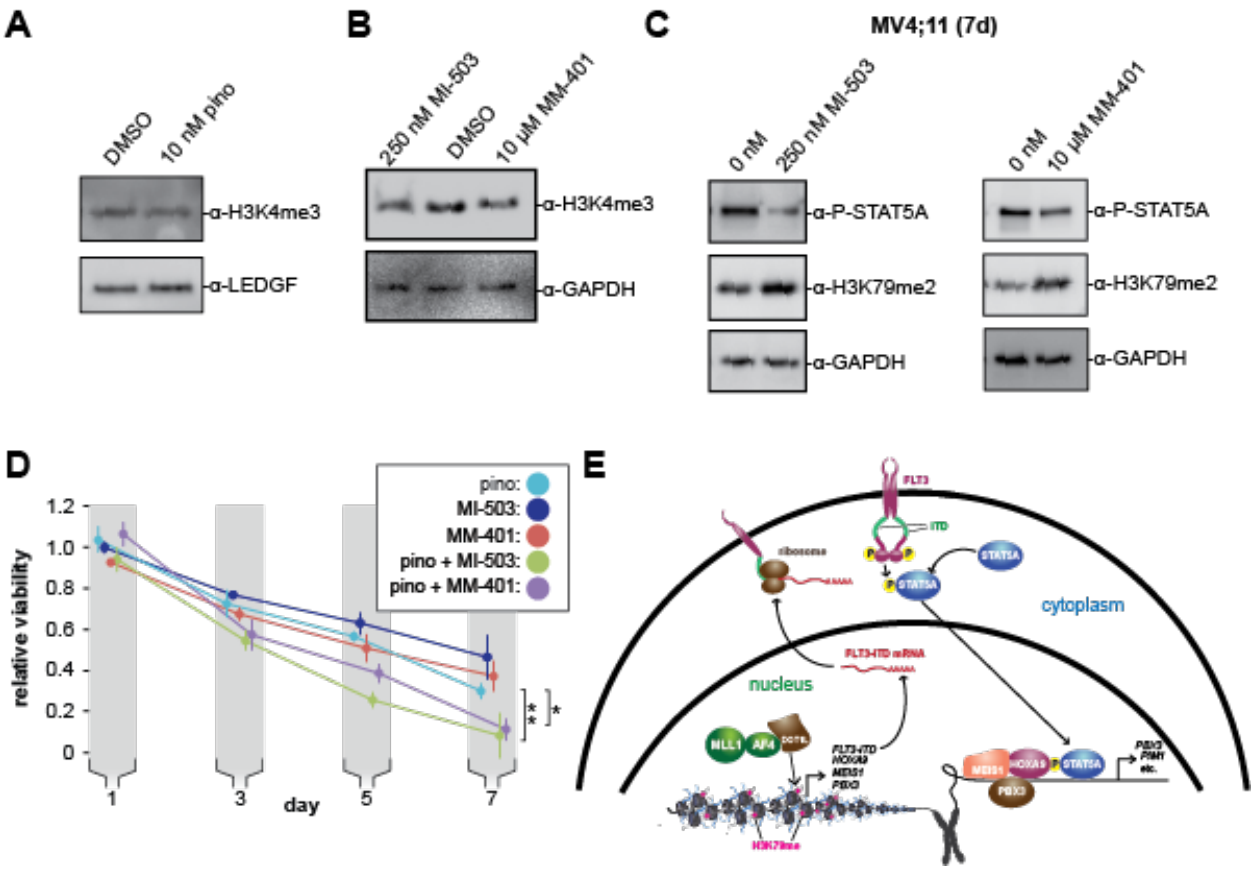

Figure 2.14 MLL1 inhibition reduces STAT5A activation.
A. Western blots of whole cell extract from MV4;11 cells treated with 10 nM pinometostat for 7 days and blotted for H3K4me3 or LEDGF as a loading control. **B.** Western blots of whole cell extract from MV4;11 cells treated with MLL1 inhibitors MI-503 (250 nM) or MM-401 (10 μM) or DMSO for 7 days and blotted for histone H3 lysine 4 trimethylation (H3K4me3) or GAPDH as a loading control. **C.** Western blots of MV4;11 cell extract treated with MLL1 inhibitors MI-503 (250 nM) or MM-401 (10 μM) for 7 days and blotted for phosphorylated STAT5, histone H3 lysine 79 dimethylation (H3K79me2) or GAPDH as a loading control. **D.** MV4;11 cells were treated with DOT1L or MLL1 inhibitors alone or in combination for 7 days. Viability was analyzed using CellTiter Glo 2.0, showing the luminescence fraction of inhibited over DMSO-treated cells. Means ± SE are shown for 3 independent experiments. Student's t-test of day 7 values: 10 nM pinometostat vs. 10 nM pinometostat + 250 nM MI-503 ** $p < 0.01$ 10 nM pinometostat vs. 10 nM pinometostat + 10 μM MM-401 * $p < 0.05$). **E.** Model of MLL-fusion-mediated activation of HOXA9/MEIS1 and STAT5A co-targets in MLL-r, *FLT3-ITD*+ leukemia. MLL-AF4 activates *HOXA9*, *MEIS1* and *FLT3-ITD* gene expression through recruitment of DOT1L and H3K79me2 hypermethylation (fuchsia). FLT3-ITD phosphorylates STAT5A allowing it to translocate to the nucleus to cooperatively bind HOXA9/MEIS1 targets with PBX3 and facilitate gene activation.

rescue corresponding to the amount of *STAT5A* expression in each clone (Figure 2.9A). When treated with the MM-401 inhibitor, STAT5A-CA clone 1 (with the highest exogenous *STAT5A-CA* expression), completely rescued proliferation (Figure 2.13E). Unexpectedly, clones 2 and 3, that express *STAT5A-CA* at lower levels both displayed reduced proliferation when treated with MM-401 compared to WT or GFP expressing cells (Figure 2.13E).

I observed an additive effect when MV4;11 cells were co-treated with the MLL1 and DOT1L inhibitors (Figure 2.14D), suggesting that the inhibitors affect different sets of genes through different mechanisms, or have an additive effect on the same genes. To distinguish between these two models, I compared gene expression of several MLL-AF4 and STAT5A targets in MV4;11 cells treated with MI-503 alone or MI-503 with pinometostat for 7 days (Figure 2.13F). Akin to low dose DOT1L inhibitor treatment, MI-503 reduced expression of *FLT3*, *MEF2C, ARID3B* and *PIM1*. The reduction in *FLT3* expression was only 30% ± 10% but doubled to 60% ± 10% when both inhibitors were used, recapitulating the 60% reduction observed with pinometostat alone. MI-503 had no significant effect on *PBX3* expression but both inhibitors reduced *PBX3* expression to 50% ± 10%, the same as the DOT1L inhibitor alone. However, unlike low dose pinometostat, MI-503 treatment starkly reduced expression of *HOXA9* and *MEIS1* and combination treatment further reduced *MEIS1* expression from 40% to 30%. In summation, low dose MLL1 and DOT1L inhibitors downregulate different, yet partially overlapping sets of genes (with *FLT3*, *MEF2C*, and *PIM1* in common), that are necessary for MLL-rearranged leukemia.

I wondered whether the *STAT5A-CA*-mediated rescue of proliferation in MV4;11 cells treated with MI-503 coincided with a rescue of STAT5A target genes. I examined expression of these targets in my 3 *STAT5A-CA* clones after treating cells with MI-503 for 7 days and observed

increased the expression of the STAT5A target genes *PIM1, PIM2* and *ARID3B* (Figure 2.13G). Collectively, these data suggest that downregulation of *FLT3-ITD*, and crucially, reductions in STAT5A phosphorylation and gene activation are more sensitive to perturbations of MLL-fusion-mediated gene activation and are the main source of inhibitor effects on leukemia cell survival when expression of the canonical MLL-r proliferation mediators *HOXA9* and *MEIS1* are not substantially affected (model, Figure 2.14E).

2.3 DISCUSSION

Little is known about why MLL-r leukemia cell lines have such disparate sensitivities to DOT1L inhibitors or how MLL-fusions might cooperate with co-occurring lesions. By investigating the effects of a DOT1L inhibitor at a low, as yet unexplored concentration, I revealed that MLL-r cell lines carrying *FLT3-ITD* lesions are more sensitive to DOT1L inhibition. I observed that a subset of MLL-AF4 targets, including *FLT3,* have aberrantly high H3K79me2 and that low-dose inhibitor treatment downregulates these genes, dramatically depleting H3K79me2, while resulting in increased H3K4me3 at promoters and reduced H3K27me3 genome-wide. My findings illustrate how MLL-fusions can cooperate mechanistically with *FLT3-ITD* mutations to facilitate leukemogenesis and how PRC2 function is necessary for that disease state. FLT3-ITD-mediated STAT5A activation is crucial to the MLL-AF4 expression profile, potentially through direct interaction of STAT5A with HOXA9 and coactivation of some targets such as *PIM1*.

2.3.1 The FLT3-ITD signaling pathway accounts for the bulk of low-dose DOT1L inhibitor toxicity

A subset of MLL-AF4 targets were downregulated by low-dose DOT1L inhibition and the FLT3 locus was impacted earlier than other MLL-AF4 targets. *FLT3* expression was downregulated after only 2 days of low-dose pinometostat treatment, coinciding with reduced proliferation, increased apoptosis and gene expression changes consistent with differentiation. Reductions in *FLT3-ITD* expression precede reductions in other MLL-AF4 targets including *PBX3* and *MEF2C*, arguing that these effects are more primary or sensitive to DOT1L function. Although PBX3 interacts with both HOXA9 and MEIS1 to facilitate leukemogenesis and regulate the expression of common targets including *FLT3* (Z. Li et al., 2013, 2016) I observed that *PBX3* expression could also be reduced by either FLT3 knockdown or inhibition (Figure 2.7F and H). These results are in agreement with previous findings that *PBX3* was significantly upregulated in *FLT3-ITD*+ compared to WT *FLT3,* karyotypically normal AML patient samples (Cauchy et al., 2015).

The FLT3 receptor has an outsized effect on myeloid differentiation and proliferation through its regulation of several myeloid transcription factors (Mizuki et al., 2003; Rosen et al., 2010), accounting for its predominance in AML patients (M. Levis & Small, 2003; Mizuki et al., 2003; Nagel et al., 2017). Although stable transfection of *FLT3-ITD* has been observed to downregulate the PU.1 and C/EBPα transcription factors and regulators of myeloid differentiation (Mizuki et al., 2003), I detected no discernable change in *SPI1* (PU.1) expression and a surprising ~2-fold downregulation of *CEBPA* (C/EBPα) in MV4;11 cells (Figure 2.3D) treated with low-dose pinometostat. Much of the *FLT3-ITD*-driven effects on proliferation, inhibition of apoptosis and differentiation have been attributed to the activation of STAT5A

(Mizuki et al., 2003; Moore et al., 2007; Rosen et al., 2010; Spiekermann et al., 2003; J. Zhou et al., 2009). Constitutively active *Stat5a* can render mouse Ba/F3 cells growth factor-independent and resistant to apoptosis through upregulation of the *Pim1-2* protooncogenes[76,110,111]. I observe that 10 nM pinometostat downregulates *FLT3-ITD* with concomitant reductions in STAT5A phosphorylation and diminished expression of the STAT5A target genes *PIM1* and *ARID3B,* suggesting that low-dose DOT1L inhibition is able to disrupt FLT3-ITD-mediated signaling and downstream oncogene activation.

Exogenous expression of constitutively active human *STAT5A* (*STAT5A-CA*) in MV4;11 cells treated with 10 nM pinometostat rescues cells from apoptosis, almost completely rescues proliferation, and restores *PIM1* and *ARID3B* gene expression, suggesting that most of the toxicity from low-dose DOT1L inhibition is through loss of STAT5A activation. The ability of ectopic *STAT5A-CA* expression to rescue orthologous perturbations to MLL-fusion-mediated gene activation and proliferation from MLL1 inhibitors suggests that STAT5A activation is necessary for leukemogenesis and maintenance of the proliferative gene expression profile including *PIM1* in this context. Interestingly, *PIM1* is a downstream target of both FLT3-ITD and HOXA9 (Y. Huang et al., 2012; K. T. Kim et al., 2005). Though both factors regulate *PIM1* expression, the FLT3-ITD axis is more sensitive and is responsible for *PIM1* downregulation with low-dose DOT1L inhibitor treatment in MLL-r leukemia also bearing the *FLT3-ITD* mutation. FLT3-ITD-mediated activation of STAT5A may promote HOXA9 localization to the *PIM1* locus or complement it, thereby facilitating expression of this common target and leukemogenesis.

PIM1 activation by both STAT5A and HOXA9 represents a common coregulation scenario for these hematopoietic transcription factors. Indeed, De Bock et al. discovered that

HOXA9 binding sites have significant overlap with STAT5A, PBX3 and C/EBP targets genome-wide (de Bock et al., 2018). I observed downregulation of both *PBX3* and *C/EBPA* by 10 nM DOT1L inhibition. It is possible that the dependence of MLL-r, *FLT3-ITD*+ leukemia on *FLT3-ITD* expression may be due to HOXA9 requiring STAT5A and/or PBX3 and C/EBPA to cooperatively bind select target genes. Huang et al. found that HOXA9 and MEIS1 preferentially localized to enhancer regions enriched with STAT5 binding motifs (Y. Huang et al., 2012) and identified STAT5A and C/EBPA in complex with HOXA9. Furthermore, *HOXA9* knockdown reduced STAT5A binding at common target sites (Y. Huang et al., 2012). If HOXA9 depends on STAT5A for chromatin localization then low dose DOT1L inhibition may reduce HOXA9 binding at enhancer regions, reducing HOXA9 target gene activation without affecting *HOXA9* expression.

In addition to gene activation, STAT5A phosphorylation also results in gene repression, modulating the immune response and differentiation (Moore et al., 2007; J. Zhu et al., 2003). Viral transduction of constitutively active *Stat5a* affects T cell differentiation by repressing IFN-γ production (Rani & Murphy, 2016; J. Zhu et al., 2003). I found 2007 genes upregulated with 10 nM pinometostat treatment, including many MHC class II genes with large fold-changes that significantly overlapped with a set of genes consistently downregulated in FLT3-ITD+ (KN) leukemia samples (Cauchy et al., 2015). Indeed, GO analysis of the pinometostat-upregulated genes indicated significant enrichment for the "IFN-γ-mediated signaling pathway" and other immune-related categories (Figure 2.4A). Despite the increase in expression of IFN-γ-regulated genes we saw barely measurable levels of *IFNG* (IFN-γ) and no increase in expression with pinometostat treatment (Figure 2.4B). Many components of the IFN-γ pathway, such as IRF4 and IRF5 are involved in macrophage differentiation, a functional consequence of *DOT1L*

deletion or inhibition that has been observed in other studies (Bernt et al., 2011; Daigle et al., 2011; Mossadegh-Keller et al., 2013; M. Yamamoto et al., 2011). With pinometostat treatment I observed upregulation of *CSF1R* and *CSF3R,* targets of IRF4 and critical signaling inducers of macrophage and neutrophil differentiation, respectively (Figure 2.4D) (Klimiankou et al., 2017; Mossadegh-Keller et al., 2013). Additionally, expression increases in the macrophage cell surface markers *ITGAM* (CD11b), *ITGAX* (CD11c) and *CD86* suggest these cells are differentiating to a more macrophage-like state (Figure 2.4C), consistent with previous observations from DOT1L deletion and from a study using the DOT1L inhibitor EPZ004777(Bernt et al., 2011; Daigle et al., 2011).

2.3.2 Extensive histone modification cross-talk contributes to the survival of MLL-r, FLT3-ITD+ leukemia

FLT3 is part of a subset of MLL-AF4 targets that are more sensitive to reductions in H3K79me2 than even the *HOXA9* and *MEIS1* oncogenes. I observed that MLL-AF4 targets (Kerry et al., 2017) that are downregulated by 10 nM pinometostat have higher levels of H3K79me2 than even the most highly expressed genes and show the largest reductions in methylation when treated with pinometostat. (Figure 2.5A). The greater reductions in H3K79me2 levels at downregulated genes is likely a contributing factor to their loss of gene expression. H3K79me2 hypermethylation antagonizes SIRT1 localization to MLL-AF4 targets, preventing H3K9ac and H3K16ac deacetylation, thereby facilitating gene expression (C. W. Chen et al., 2015). However, there are stark differences in methylation density and susceptibility to DOT1L inhibition even among MLL-fusion targets. MLL-AF4 “spreading” genes (Kerry et al., 2017) had H3K79me2 levels comparable to those MLL-AF4 targets whose expression was

downregulated by pinometostat. Yet only 31% of "spreading genes" were downregulated by 10 nM pinometostat, suggesting that effects on gene expression from depletion of H3K79me2 could be governed by other factors including changes to the distribution of other chromatin modifications.

To my surprise, the pinometostat-induced activation of MHC class II genes I observed did not appear to result from a loss of H3K27me3-mediated repression, despite PRC2 subunit downregulation. Treatment with PRC2 inhibitor EI1 had no effect on *CIITA* or MHC class II gene expression but significantly reduced proliferation in MV4;11 cells (Figure 2.11E and 2.12B). A growing body of evidence supports an essential role for the PRC2 complex in MLL-r leukemogenesis-- PRC2 is necessary for *MLL-AF9*-induced leukemogenesis in mouse progenitor cells and cooperates with MLL-AF9 to promote self-renewal of acute myeloid leukemia cells (Neff et al., 2012; Shi et al., 2013). The observed downregulation of the MLL-AF4 target oncogenes upon EZH2 inhibition (Figure 2.11F), suggests that MLL-fusion-mediated gene activation is in some way dependent on PRC2 methyltransferase activity. Consistent with this idea, ectopic expression of *EZH2* was able to provide a small but significant proliferation rescue when treating cells with 10 nM pinometostat (Figure 6G).

I identified pinometostat-induced increases in H3K4me3 at TSS's genome-wide (Figure 2.13C). Although H3K4me3 is transcriptionally activating (P.-Y. Chang et al., 2010; Vermeulen et al., 2007), the largest H3K4me3 increases were at downregulated MLL-AF4 targets that had the largest decreases in H3K79me2. Though DOT1L inhibition reduces global H3K27me3, this is unlikely to explain the massive increases in H3K4me3 that I observe (Hanson et al., 1999; D.-H. Kim et al., 2013). Studies in human embryonic stem cells and mouse preadipocytes observed no genome-wide increases in H3K4me3 upon *EZH2* knockout and reductions in H3K27me3

(Collinson et al., 2016; L. Wang et al., 2010). Rather, the increases in H3K4me3 may be due to either reduced antagonism from loss of H3K79me2 or hypermethylation due to a stalled transcriptional complex containing MLL1 near the TSS. The former scenario could function to localize H3K4me3 at the TSS, preventing spurious transcription initiation within the gene. In the latter scenario, if H3K79me2 does indeed facilitate the transition from transcription initiation to elongation (Wood et al., 2018), its depletion could increase in H3K4me3 through greater dwelling time of RNAPII at the TSS. Indeed, given the global increases in H3K79me2 I observed upon treatment with MLL1 inhibitors (Figure 2.14C) it seems probable that there is a reciprocal antagonism of these two modifications on either's deposition, potentially through H3K79me2-mediated recruitment of LSD1. Previous studies have observed that knockout or inhibition of LSD1, the H3K4me2-histone demethylase and component of the MLL-supercomplex, results in apoptosis and differentiation of MLL-r cells, inhibits leukemogenesis in mouse models and increases H3K4me2/3 at MLL-target genes (Fang et al., 2017; Z. Feng et al., 2016; Harris et al., 2012; McGrath et al., 2016).

2.3.3 Broader Clinical implications

In light of the heightened sensitivity of the *FLT3-ITD* lesion to DOT1L inhibition, small molecules such as pinometostat may prove effective in treating non-MLL-r leukemias with *FLT3-ITD* mutations. Although several FLT3 inhibitors have undergone clinical trials, drug resistance has emerged as a formidable and so far, insurmountable barrier to an effective treatment. A previous study observed that siRNAs targeting *FLT3* expression increased the efficacy of the FLT3 inhibitor tandutinib (Walters et al., 2017). As a way of circumventing the difficulties associated with siRNA delivery, DOT1L inhibitors that reduce *FLT3* expression

could serve as part of an effective combinatorial treatment with drugs that target FLT3 function. My mechanistic studies provide important impetus for exploration of these ideas in pre-clinical or patient-derived *FLT3-ITD* leukemias.

2.4 MATERIALS AND METHODS

2.4.1 Accession numbers

The ICeChIP and RNA-seq data has been reported in the Gene Expression Omnibus with accession number GSE162441.

2.4.2 Cell Culture

Human MV4;11 and MOLM13 leukemia cells and MLL1 inhibitor MM-401 were gifts from the laboratory of Yali Dou at the University of Michigan. Human THP-1 leukemia cells (cat # TIB-202) were purchased from American Type Culture Collection (ATCC). Human SEM leukemia cells (ACC546) were obtained from DSMZ- the German Collection of Microorganisms and Cell Cultures GmbH. Cells were cultured in RPMI-1640 medium containing 10% (v/v) FBessence (Seradigm cat # 3100-500), 1% L-glutamine at 37°C in humidified air containing 5% CO_2. DOT1L inhibitor pinometostat (EPZ5676, Cayman Chemical cat # 16175), EZH2 inhibitor EI1 (Cayman Chemical cat # 19146-1), FLT3 inhibitor tandutinib (MLN518) (Selleckchem cat # S1043), MI-503 (Selleckchem cat # S7817) and PIM1 inhibitor Quercetagenin (MedChemExpress cat # HY-15604) were resuspended in DMSO. Doxycycline (Alfa Aesar cat # J60422) was resuspended in water.

2.4.3 RNA-seq and Gene Expression Analysis

Exponentially growing MV4;11 cells were grown in 150 mm^2 tissue culture-treated plates (Corning cat # 0877224) in 30 ml media ± 10 nM pinometostat for 7 days. Every 2 days cells were spun down at 500 x g 5 min. then resuspended in media ± 10 nM pinometostat. On day 7 1 x 10^7 cells were spun down at 500 x g 5 min. then cells were resuspended in 1 ml Trizol reagent (Life Technologies cat# 15596018), incubated 5 min. at RT then 200 µl chloroform was added and samples were shaken rigorously for 15 sec. then incubated 3 min. at RT and spun down 12,000 x g 15 min. at 4 °C. The aqueous layer (~ 500 µl) was removed and mixed with 500 µl EtOH and added to a Zymo Research RNA Clean and Concentrator column (cat # 11-353B) and spun 12,000 x g 1 min.. 100 µl DNase I (1:10 in buffered dH20) (Thermo Fisher Scientific cat # en0521) was added to the column and then spun 500 x g 5 min., incubated 15 min. at RT and then spin 12,000 x g for 30 sec. Combined 200 µl RNA binding buffer with 300 µl EtOH and then spun 12,000 x g for 30 sec. and the flow through was discarded. After each of the following were added to the column, it was spun down 12,000 x g for 30 sec. and the flow through was discarded: 400 µl RNA prep buffer; 700 µl RNA wash buffer; and 400 µl RNA wash buffer. RNA was eluted from column with 30 µl RNase-free dH2O. Added RNA standards to 2 µg of each RNA sample- Add the equivalent of 10 copies/cell yeast RAD51; 30 copies/cell RNL2; 200 copies/cell E coli MBP; and 2000 copies/cell yeast SUMO to each sample then proceed with rRNA removal Ribo Zero Gold kit (Illumina cat # MRZ11124C) according to manufacturer's protocol. Libraries were prepared using the NEBNext Ultra Directional RNA Library prep kit (NEB cat # E7420S). Libraries were then sequenced on the Illumina NextSEQ500. Reads were aligned to the hg38 genome assembly using HISAT2(D. Kim et al., 2015) and differential gene expression analysis was done with Cufflinks (Trapnell et al., 2013).

2.4.4 Reverse Transcription and Quantitative real-time PCR

RNA was extracted from 10^6 cells using 500 µl Trizol and following the manufacturer's protocol. 1 µg RNA was used for reverse transcription with 0.5 µl MMLV HP reverse transcriptase (Lucigen cat # RT80125K) per 20 µl rxn. RNA was then degraded by alkaline hydrolysis by adding 40 µl 150 mM KOH, 20 mM tris base and heating 95 °C 10 min. then cooling on ice and quenching with 40 µl 150 mM HCl and then adding 100 µl TE. Gene expression was assayed by real-time PCR in 10 µl reactions with 0.5 µl cDNA and 5 µl PowerUP SYBR Green master mix (Applied Biosystems cat # A25742) per reactions. qPCR was run on the Bio-Rad thermocycler CFX96 or CFX384 using the program: 50 °C 2:00, 95 °C 2:00, then 40 cycles 95 °C 0:15, then 60 °C 1:00. Data was normalized to 18S rRNA. Primer sets are listed in Table 4.2.

2.4.5 Cell Proliferation Assay

Cells were seeded at 10^5 cells/ml in 80 µl in clear bottom 96-well plates (Corning 07200566) in 3 replicates. Everyday 40 µl of culture was transferred to 40 µl media in a new plate. On odd days 30 µl of Cell TiterGlo 2 (Promega cat # G924A) was added to the remaining 40 µl culture and incubated 10 min. at room temperature on a shaker at 600 rpm. Luminescence was measured on a Tecan Infinite F200 Pro plate reader and fraction viability was determined from the luminescence of treated over untreated cells.

2.4.6 Apoptosis Assay

Exponentially growing cells were incubated with increasing concentrations of pinometostat for 7 days in 3ml media in 6-well plates in 3 experimental replicates. 10^6 were harvested from each plate and washed twice in 1 ml PBS then resuspended in 1 ml binding buffer as per BD Biosciences manufacturer's protocol. Add 5 µl FITC-conjugated Annexin V

(BD Biosciences cat# 556420) and 2 µl propidium iodide (Alfa Aesar cat # J66584) to 100 µl cells and incubate 15 min. at RT in the dark. Cells were then sorted on the BD FACSAriaII device for propidium iodide or FITC (Annexin V) positive cells. Data was analyzed using FlowJo software (Tree Star).

2.4.7 Calibrated chromatin immunoprecipitation sequencing (ICeChIP-seq)

Native, internally calibrated ICeChIP-seq was carried out as described previously for H3K4me3 and H3K27me3(Grzybowski et al., 2015, 2019). A modified protocol was used for H3K79me2 that included cross-linking and denaturation, because of greater difficulty in immunoprecipitation of this modification, likely due to reduced accessibility of this mark within the more highly-structured nucleosome core. Briefly, nuclei were obtained from 20 million MV4;11 cells and processed to obtain HAP-purified mononucleosomal chromatin. 150 µl of 280 µl total HAP-purified chromatin was removed for denaturative ICeChIP and crosslinked in 0.25% formaldehyde for 8 min. on a nutator at RT, then quenched by adding 1M Tris pH 7.5 to 200 mM and incubating 5 min. at RT on a nutator. 50 µl of cross-linked chromatin was used for denaturation and 2.5 ul 20% SDS was added to 1% SDS final concentration and sample was incubated 1 min. at 55 °C, then IMMEDIATELY put on ice. This was then diluted with 9 volumes water (450 ul) and 100 µl was used for each IP. Antibodies for both the DMSO- and pinometostat-treated samples were processed together (12 µl antibody-bound beads per IP). 3 µg of anti-H3K79me2 (Abcam cat # ab3594, lot # GR173874); 3 µg of anti-H3K4me3 (Abcam cat # 12209, lot # GR275790-1); and 0.6 µg of anti-H3K27me3 (Cell Signaling cat # 9733, lot # 8) were used per IP. For crosslinked IPs include 1 hour 65 °C after proteinase K digest. Libraries were prepared using the NEBNext Ultra II DNA Library prep kit (NEB cat # E7645). 3 cycles of PCR amplification were used for native inputs and H3K36me3 IPs, 4 cycles for denaturated

inputs and H3K27me3 IPs, 7 cycles for H3K4me3 IPs and 10 cycles for H3K79me2 IPs. The following primer indices were used: denatured DMSO-treated input (index 8), denatured pinometostat-treated input (index 12), DMSO-treated H3K79me2 IP (index 9), pinometostat-treated H3K79me2 IP (index 11), native DMSO-treated input (index 8), native pinometostat-treated input (index 12), DMSO-treated H3K36me3 IP (index 9), pinometostat-treated H3K36me3 IP (index 11), DMSO-treated H3K4me3 IP (index 9), pinometostat-treated H3K4me3 IP (index 11), DMSO-treated H3K27me3 IP (index 2), pinometostat-treated H3K27me3 IP (index 7). Analysis of histone methylation density (HMD) was carried out using the scripts and workflow from Grzybowski et al.(Grzybowski et al., 2019)

2.4.8 Western blotting

10 ul whole cell extracts of 2 x 10^5 cells in 40 µl 6X SDS loading buffer were run on 4-14% bis-tris gel (Invitrogen cat # NP0335). Membranes were transferred by semi-dry apparatus (Bio-Rad Transblot cat # 170-3940) at 200 mA, 25 V for 35 min to 0.45 µm nitrocellulose membrane (Millipore cat # IPVH00010). Membranes were then blocked for 1 h with TBS-T 1% ECL Prime blocking reagent (GE Healthcare cat # RPN418) at RT on an orbital shaker and blotted with primary antibody for 1 h at RT with gentle agitation. Membranes were then washed 3 times for 5 min. while shaking with TBS-T and then incubated with secondary antibody at RT for 1 h while shaking. A complete list of antibodies used in this study can be found in Table 4.3.

2.4.9 Plasmid generation

pCMV-Gag-Pol plasmid, encoding HIV-1 derived *gag*, and *pol,* the pCMV-VSV-G vector encoding VSV-G envelope gene, pTRIPZ-EZH2 and Tet-pLKO were purchased from Addgene. pTRIPZ-STAT5a-CA and pTRIPZ-FLT3-ITD were created by cloning *STAT5A* and *FLT3-ITD* from cDNA from MV4;11 cells. STAT5A-CA mutations were introduced at H298R

and S710F and genes were inserted into the pTRIPZ plasmid at restriction sites AgeI and MluI. shRNA constructs were created by inserting annealed oligos of shRNA sequences (Table 4.2) purchased from IDT into Tet-pLKO at the AgeI and EcoRI restriction sites.

2.4.10 Transfection for lentiviral particle generation

Lentiviral particles were produced by Fugene (Promega cat # E2311) transfection of the 293T packaging cell line in a 6-well plate at ~70% confluency with pCMV-Gag-Pol, pCMV-VSV-G and 2 μg of the plasmid encoding the gene or shRNA of interest using a 3:1:4 ratio, respectively. Lentiviral particle enriched supernatants were collected 72 hours after transfection for immediate transduction.

2.4.11 Lentiviral transduction

4 x 10^5 MV4;11 cells suspended in 1 ml RPMI-1640 medium containing 10% FBessence in a 6-well plate were transduced by adding 2.5 ml of 0.45 μm filtered viral supernatants from 293T cells. Then 0.8 μl polybrene (EMD Millipore cat. # TR-1003-G)/ml transduction reagent was added to the media and the plates were wrapped with parafilm and spun down at 2000 rpm for 2 hours at room temperature then incubated O/N at 37°C in humidified air containing 5% CO_2. After 12 hours cells were spun down and resuspended in RPMI-1640 10% FBessence. After 24 h 0.5 μg/ml puromycin was added to the wells and this selection media was refreshed every 3 days to select for transduced cells. Individual clones were purified by diluting cell cultures to 1 cell/100 μl and then plating 100 μl aliquots in a 96-well plate. Wells were visually assessed for individual clones and then grown out.

3 DOT1L INHIBITION IMPACTS ALTERNATIVE SPLICING THROUGH RECRUITMENT OF THE SPLICING FACTOR PTBP1

3.1 INTRODUCTION

Alternative splicing of mRNA is a means of extending protein diversity to provide for the complex functions necessary to sustain higher eukaryotes without dramatically expanding the size of the genome (Nilsen et al. 2010, Pan and Shai et al. 2008, Rosefeld et al. 2010, Wang and Sandberg et al. 2008). It is estimated that over 95% of all human genes are alternatively spliced, often in a tissue-specific manner, enormously expanding the proteomic catalogue and necessitating regulation for tens of thousands of splicing events (Pan and Shai et al. 2008, Wang and Sandberg et al. 2008).

Unlike yeast, which have clearly defined splice site consensus sequences, the less-defined splice site sequences in higher eukaryotes require a complex regulatory network of splicing factors to define and regulate splice site usage (Herzel et al., 2017). This process must be executed efficiently and accurately as the fidelity of splicing is crucial to the proper dissemination of the genetic code and the creation of functional proteins. Mutations in splicing factors and their binding sites are commonly found in many diseases including cancer, cystic fibrosis and spinal muscular atrophy (Bonnal et al., 2020; Luco et al., 2011; Scotti & Swanson, 2016). Just how these splicing factors are differentially recruited to thousands of loci throughout the genome in a cell- and tissue-specific manner is not well understood. At present, the mechanisms behind the majority of the estimated > 100,000 alternative splicing events in human cells are unexplored (Nilsen et al. 2010), however, the sheer number of events suggests that additional, as yet unidentified regulatory mechanisms are at work. Chromatin modifications are

emerging as a crucial source of alternative splicing regulation that we are only beginning to understand (Guo et al., 2014; T. Li et al., 2018; Luco et al., 2010; Pradeepa et al., 2012).

Observations of the tissue-specific, differential distribution of the H3K36me3, H3K27me2 and H3K79me2 histone modifications, among others, within introns and exons suggests that a variety of chromatin modifications may be involved in splicing (R. Andersson et al., 2009; Schwartz et al., 2009; Spies et al., 2009). While the association of many histone modifications with alternative splicing is correlative, both H3K79me2 and H3K36me3 have more direct effects (Guo et al., 2014; T. Li et al., 2018; Luco et al., 2010; Pradeepa et al., 2012). H3K79me2 and H3K36me3 are enriched in the bodies of actively transcribed genes, deposited by the methyltransferases DOT1L and SETD2, respectively, in association with the transcriptional elongation complex (Bitoun et al., 2007; Kizer et al., 2005; Mohan et al., 2010; Mueller et al., 2007, 2009; Steger et al., 2008). However, these marks have different distributions within genes- H3K79me2 is enriched slightly downstream of the TSS at the 5' end of the gene body and decreases toward the end of the gene, while H3K36me3 is least enriched at the 5' end of the gene but increases toward the end of the gene body (Barski et al., 2007).

Several mechanisms of H3K36me3-mediated regulation of alternative splicing have been elucidated (Guo et al., 2014; Luco et al., 2010; Pradeepa et al., 2012). H3K36me3 is enriched at alternatively spliced exons in some cell types and recruits the splicing factors PTBP1, ZMYND11 and SRSF1 to regulate alternative splicing at hundreds of genes (Guo et al., 2014; Luco et al., 2010; Pradeepa et al., 2012). PTBP1, a splicing factor that promotes exon exclusion (Ling et al., 2016), is indirectly recruited by the MRG15 protein, which binds H3K36me3 through its PWWP domain, to hundreds of loci enriched in H3K36me3 to repress the splicing of cell type-specific exons (Luco et al., 2010). The splicing factor ZMYND11 is directly recruited

by H3K36me3 through its PWWP domain to facilitate intron retention in HeLa cells (Guo et al., 2014). The LEDGF protein also recognizes H3K36me3 through its PWWP domain and interacts with dozens of splicing factors including SRSF1, which it recruits to alternatively spliced exons to promote both exon inclusion and exclusion, depending on the locus (Pradeepa et al., 2012). Interestingly, PTBP1, ZMYND11 and SRSF1 are all recruited by H3K36me3 to facilitate disparate effects on alternative splicing at different genes, suggesting that additional regulatory mechanisms are necessary to yield such targeted and specific outcomes (Guo et al., 2014; Luco et al., 2010; Pradeepa et al., 2012).

H3K79me2 also plays a role in alternative splicing however, the mechanism(s) behind its observed effects on splice site selection are unknown. A broad analysis of ChIP-seq in 34 human cancerous and non-cancerous cell lines revealed that H3K79me2 is highly enriched at loci in cell types where alternative exons are excluded from the transcript (T. Li et al., 2018). Furthermore, leukemia cell lines containing MLL-rearrangements (MLL-r) such as MV4;11 and MOLM14 had particularly high levels of H3K79me2 at sites of alternative splicing with MV4;11, by far, the most enriched. *DOT1L* knockdown in these cell lines increased exon inclusion at several H3K79me2-enriched, alternatively spliced genes (T. Li et al., 2018). A similar and dose-dependent effect on exon inclusion was observed with treatment of increasing concentrations of the DOT1L inhibitor pinometostat. Pinometostat concentrations of 0.5, 1 and 2 μM resulted in 58, 60 and 73 events of exon inclusion respectively (T. Li et al., 2018). But, unlike H3K36me3, there is no evidence of an interaction of H3K79me2 and splicing factors and it is unknown how H3K79me2 affects alternative splicing.

DOT1L inhibitors such as pinometostat, used in the Li et al. study, are highly effective and specific antagonists of DOT1L methyltransferase activity (Daigle et al., 2011, 2013; W. Yu

et al., 2012). Pinometostat itself, is an extremely effective and specific inhibitor with 37,000-fold greater selectivity over its closest paralogs from an extensive list of other lysine and arginine methyltransferases (Daigle et al., 2013). Unlike gene knockout or knockdown, DOT1L inhibition is adjustable and directly targets the methyltransferase activity of the DOT1L enzyme, allowing more precise depletion of H3K79me2 levels.

Pinometostat, and other DOT1L inhibitors were developed as treatments for MLL-rearranged leukemia and these small molecules can selectively kill MLL-r cells in culture (Daigle et al., 2013). *Dot1l* knockout decreases the expression of *HOXA9* and *MEIS1*, the leukemic oncogenes that drive proliferation, through depletion of activating H3K79me2, thereby reducing cell survival (Bernt et al., 2011; Guenther et al., 2008; Milne et al., 2005; Stubbs et al., 2008). Importantly, pinometostat treatment recapitulates the effects of *DOT1L* knockout by reducing proliferation and the MLL-fusion leukemic expression signature and inducing apoptosis and differentiation (Bernt et al., 2011; Daigle et al., 2013; Kerry et al., 2017). Although both proliferation and alternative splicing are affected by H3K79me2 depletion in MLL-r cell lines, it is unknown whether H3K79me2-dependent alternative splicing contributes to MLL-rearranged leukemogenesis.

To answer some of these outstanding questions, I sought to achieve a more mechanistic understanding of the role of H3K79me2 in regulating splice site selection by examining the effects of low-dose DOT1L inhibitor treatment on splicing in MV4;11 cells. The MV4;11 MLL-r cell line has extremely high global H3K79me2 levels, providing a larger range of methylation density to observe how depletion of this modification might affect alternative splicing (T. Li et al., 2018). At 10 nM pinometostat, a much lower concentration than those used in the previous study (0.5-2 μM) (T. Li et al., 2018), and closer to 1 nM, where global depletion of H3K79me2

is first evident (Daigle et al., 2013), the effects of H3K79me2 depletion are readily apparent and I had previously observed the differential expression of thousands of genes and reductions in proliferation, increased apoptosis and expression of surface markers of differentiation in MV4;11 cells.

At low-dose DOT1L inhibition I observe 71 instances of changes in alternative splicing compared to DMSO-treated cells, with exon inclusion making up the vast majority of the effects. Using calibrated ICeChIP-seq to quantify H3K79me2 and H3K36me3 genome-wide I observe that genes with pinometostat-induced effects on alternative splicing have higher H3K79me2 levels than the highest expressed genes or MLL-AF4 targets and experience profound reductions in H3K79me2 from pinometostat treatment. I also find that H3K36me3 density is almost as high at alternatively spliced genes as the highest expressed genes and that surprisingly, 10 nM pinometostat treatment results in an increase in H3K36me3 in gene bodies genome-wide but is especially high at pinometostat-induced alternatively spliced genes. I find the splicing factor PTBP1, with a known role in exon exclusion, interacts with H3K79me2 through nucleosome pulldowns from HEK293 nuclear extract. Further, I observe that PTBP1 knockdown recapitulates pinometostat-induced effects on alternative splicing and reductions in proliferation from DOT1L inhibitor treatment, suggesting that pinometostat-mediated changes in alternative splicing are due to reduced PTBP1 recruitment through H3K79me2 depletion and that PTBP1 function is necessary for leukemia survival. Finally, I find that H3K79me2 depletion affects alternative splicing at the *PTEN* tumor suppressor gene to increase PTEN protein levels with coinciding reductions in phosphorylated AKT, a PTEN target and inducer of proliferation. Here I provide the first mechanistic understanding of how H3K79me2 regulates alternative splicing to affect the expression of a tumor suppressor and growth signaling pathway.

3.2 RESULTS

3.2.1 DOT1L inhibition results in greater exon inclusion of alternatively spliced genes

I sought to identify specific alternative splicing events regulated by H3K79me2 that I could then explore mechanistically. I chose to examine how disruptions to H3K79me2 affects splicing in MV4;11 cells, an MLL-r leukemia cell line with abnormally high levels of H3K79me2 and potentially a large dynamic range of effects from perturbation to H3K79me2 density. I surveyed transcription though RNA-seq in MV4;11 cells that had been treated with 10 nM pinometostat (for 7 days), a concentration that I previously found had dramatically depleted H3K79me2 at gene bodies genome-wide and resulted in the differential expression of thousands of genes, reductions in proliferation and the induction of apoptosis and differentiation (Figures 2.1B, 2.2A, 2.4C and 2.9D). I then analyzed my RNA-seq data for changes in alternative splicing between pinometostat and DMSO-treated cells using the Leafcutter software package (Y. I. Li et al., 2018) and observed 71 instances of differential alternative splicing (Figure 3.1A and Table 4.1). This number that is likely to be conservative as the Leafcutter software uses a more definitive, yet less sensitive method for determining splicing events by looking at exon-exon junctions rather than exon frequency, as some other splicing software packages do (Ding et al., 2017; Y. I. Li et al., 2018; Rasche et al., 2014; Trapnell et al., 2009).

A previous study by Li et al. reanalyzed publicly available RNA-seq data from SEM cells, an MLL-r cell line with an MLL-AF4 translocation, treated with 0.5, 1 and 2 μM pinometostat and observed changes in exon usage at 58, 60 and 73 genes, respectively, with only 14 genes overlapping among the three treatment groups (T. Li et al., 2018). I find no overlap of those 14 genes with the genes from my set of 71 alternative splicing events observed from 10 nM

pinometostat treatment in MV4;11 cells, a similar MLL-r leukemia cell line that also contains an MLL-AF4 translocation. This discrepancy may result from differential effects on alternative splicing from inhibitor concentrations that differ by orders of magnitude, cell-line specific effects on splicing or differences in detection from the way alternative splicing was analyzed (i.e. Leafcutter vs. MISO analysis software) (T. Li et al., 2018).

I categorized the types of differential alternative splicing I observed and found that exon inclusion was by far the most frequent (52%) (Figure 3.1A). Alternative start site usage was the second most frequently occurring event at 21% of the total followed by the "other" category which includes mutually exclusive exons, alternative splice site choice, and events that included multiple coinciding splicing events and made up 18% of the total. Finally, making up just 9% of the total, was exon exclusion. Our results indicated that reductions in global H3K79me2 caused changes in alternative splicing at dozens of genes, resulting most frequently in exon inclusion. Although there was no overlap of alternatively spliced genes between the Li et al. study and mine, increases in exon inclusion were the dominant effect from pinometostat treatment in both studies (T. Li et al., 2018).

I examined three different types of alternative splicing events identified in my Leafcutter analysis by RT-qPCR of MV4;11 cells treated with 10 nM pinometostat for 7 days and using primers specific to the differentially incorporated mRNA regions (Figure 3.1B). My RT-qPCR analyses confirmed increased exon inclusion at the *ABI1* gene, changes in the frequency of mutually exclusive exons at the *H2AFY* gene and differences in the alternative start site of the *SATB1* gene which shifts to greater usage of the isoform 209 start site in place of the isoform 205 start site upon pinometostat treatment (Figure 3.1C).

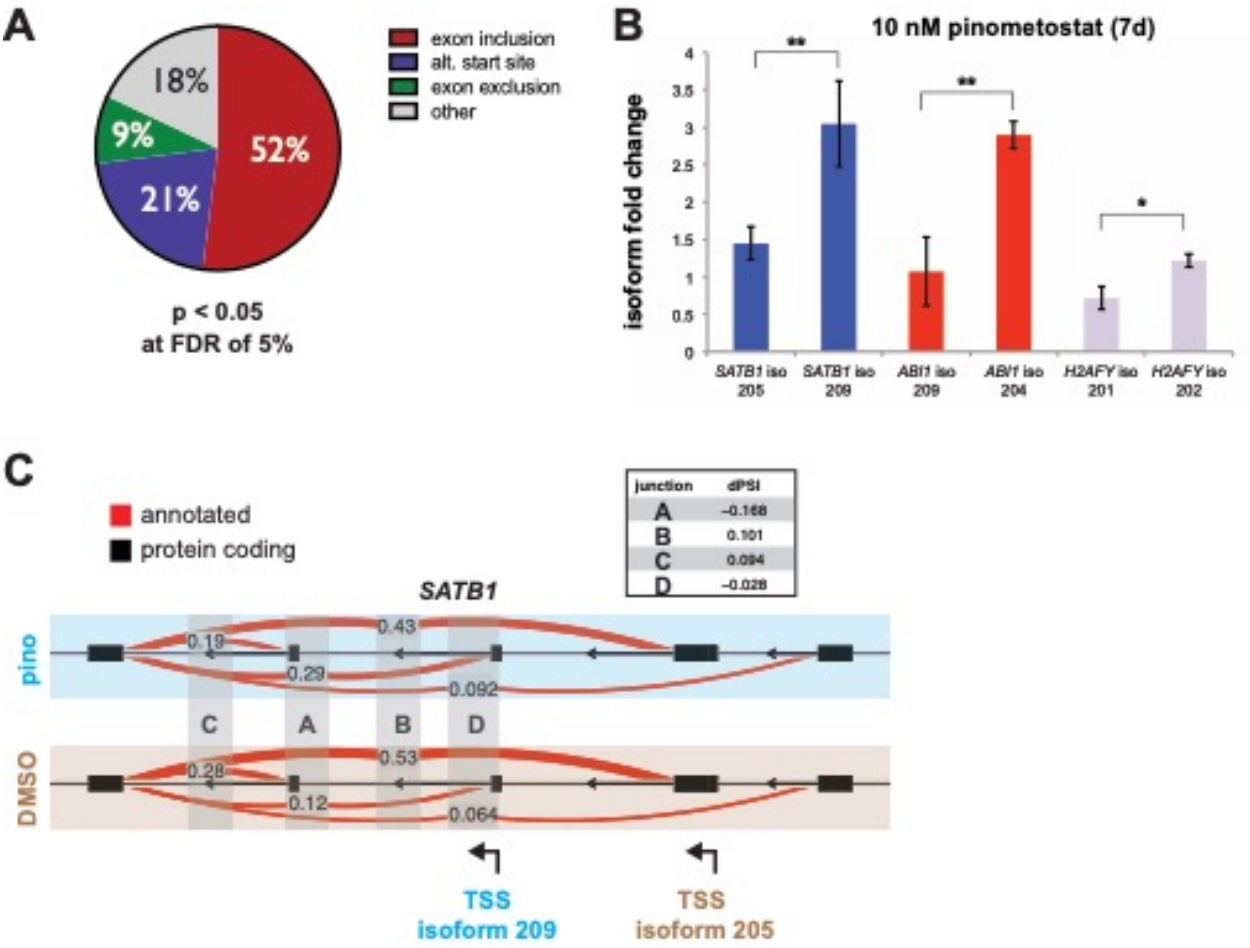

Figure 3.1 Low dose DOT1L inhibitor causes changes to alternative splicing that primarily promote exon inclusion.
A. A pie chart breakdown of types of differential alternative splicing in MV4;11 cells treated with 10 nM pinometostat for 7 days. RNA-seq data for 3 biological replicates was analyzed using the Leafcutter software package and 72 genes had some form of alternative splicing ($p < 0.05$ at FDR of 5%). **B.** RT-qPCR analysis of expression of different isoforms of SATB1, ABI1 and H2AFY representing alternative start site, exon inclusion and mutually exclusive exons respectively, using primers specific to the differentially incorporated mRNA regions in MV4;11 cells treated with 10 nM pinometostat or DMSO for 7 days. Results are shown as mean ± S.E.M. of three independent experiments. Student's t-test (* $p < 0.05$, ** $p \leq 0.01$). **C.** Image from the Leafviz visualization software component of Leafcutter depicting splicing changes at the first 5 exons if the SATB1 locus in MV4;11 cells treated with 10 nM pinometostat (blue box) vs. DMSO (brown box) for 7 days. The thickness of the red arches indicates the relative frequency of exon junctions with the percent splicing for each isoform in the middle of the arch. The difference of the percent spliced in (dPSI) is tabulated at right.

3.2.2 Splicing factors including PTBP1 are enriched in H3K79me2-modified nucleosome pulldowns from nuclear extract

Because H3K79me2 depletion resulted in genome-wide changes in alternative splicing with an emphasis on exon inclusion, I wanted to know if splicing factors interacted with H3K79me2. Proteins that recognize histone tail modifications have been identified from pulldowns using peptide fragments that contain the modification of interest (Vermeulen et al., 2010). However, this strategy has not worked to identify binders of H3K79me2, likely due to its location, not on the unstructured histone tail but, within a highly structured, solvent exposed region of the nucleosome core (Van Leeuwen et al., 2002). Just as DOT1L requires many interactions with neighboring interfaces such as a basic patch on H4 and ubiquitilation of H2B, any potential binder of H3K79me2 may require additional interactions within the nucleosome core (Anderson et al., 2019; Fingerman et al., 2007). To better recreate the native environment, I reconstituted nucleosomes using unmodified histone H3 or H3 bearing dimethylation at lysine 79 of histone H3 (Z. Chen et al., 2015) and biotinylated DNA (Figure 3.2A) and used these in pulldowns from HEK293 nuclear extract. In order to mitigate indirect associations mediated through RNA interactions we treated the H3K79me2-labeled nucleosome pulldown with RNase. I ran our pulldown samples by SDS-page and cut out bands that were enriched in the RNase-treated H3K79me2 compared to unmodified nucleosome pulldowns (Figure 3.2B). I then identified, by tandem mass spectrometry, proteins that were enriched in the H3K79me2 vs. the unmodified nucleosome pulldowns (Figure 3.2B and C). All but one of the H3K79me2-enriched proteins (EEF1A1) had known roles in RNA processing and splicing. There were several proteins involved in RNA splicing including HNRNPU, HNRNPK, DDX5 and PTBP1.

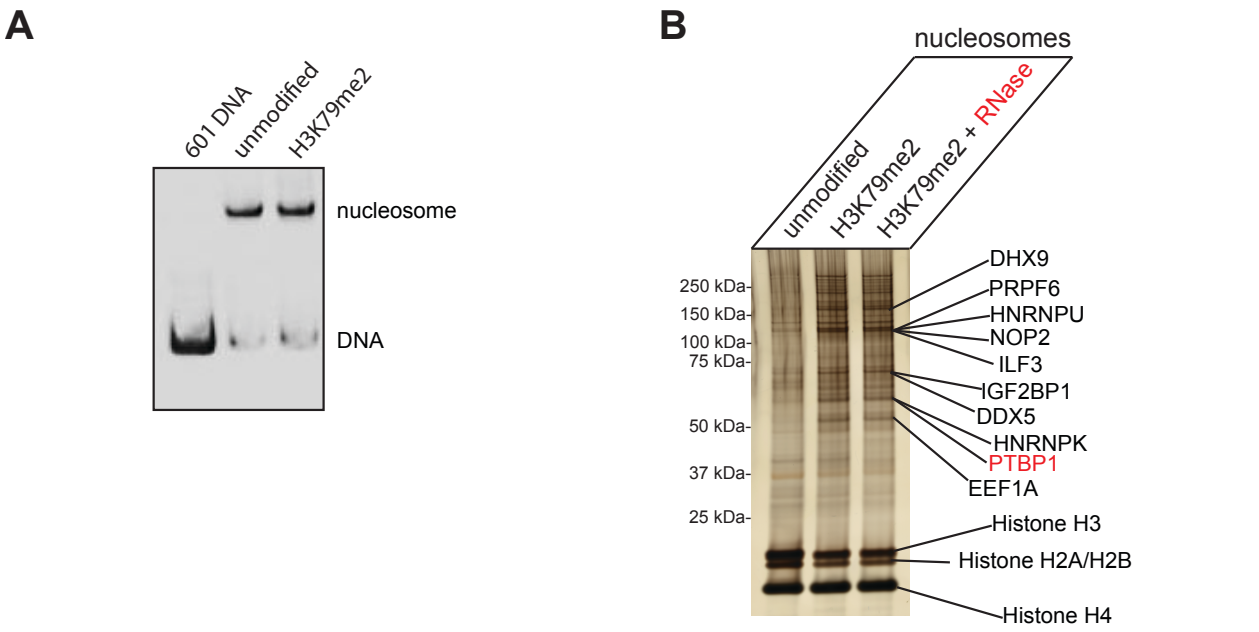

C

protein	total peptides unmodified	H3K79me2	MW
DHX9	4	22	140.87
HNRNPU	3	6	90.53
NOP2	3	8	89.25
PRPF6	0	10	106.86
DDX5	3	10	69.1
IGF2BP1	5	12	63.44
PTBP1	0	6	57.19
HNRNPK	4	28	50.94
EEF1A1	1	7	50.11

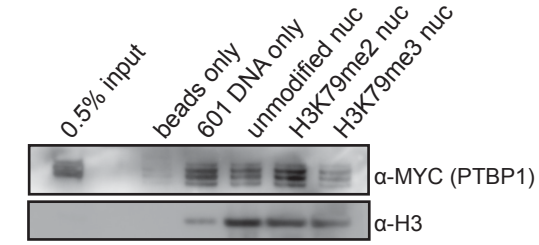

Figure 3.2 PTBP1 recognizes H3K79me2 in a nucleosomal context.
A. Image from a SYBR Gold-stained native 5% polyacrylamide gel of 601 DNA or unmodified and H3K79me2-labeled reconstituted nucleosomes used for the nucleosome pulldowns in B. **B.** Silver-stained 4-12% bis-tris denaturing gel of nucleosome pulldowns from HEK293 nuclear extract ± RNase treatment. Proteins listed to the right include several splcing factors (PTBP1 in red) were identified by tandem mass spectrometry analysis of the bands indicated and enriched in H3K79me2 nucleosome pulldowns both with/out RNase treatment over the unmodified nucleosome pulldown. **C.** Table of proteins enriched in mass spec analyses of H3K79me2 + RNase compared to unmodified nucleosomes from A. **D.** Western blot using antibodies detecting MYC (PTBP1) and histone H3 as a loading control from nucleosome pulldowns containing the indicated modifications from nuclear extract of HEK293 cells transfected with MYC-tagged PTBP1. Beads and DNA only pulldowns are included as controls for non-specific binding.

Interestingly, the polypyrimidine tract-binding protein (PTBP1, enriched by 6 peptide counts to 0 of H3K79me2 vs. unmodified nucleosome pulldowns, Figure 3.2C), has a previously observed role in exon exclusion (Linares et al., 2015; Ling et al., 2016; Luco et al., 2010). Specifically, PTBP1 represses cryptic and alternative exons that are often tissue and cell-type specific (Linares et al., 2015; Luco et al., 2010). PTBP1, is highly expressed in undifferentiated cell types and is involved in repressing alternative exons in genes such as *PBX1* that promote neuronal differentiation (Linares et al., 2015; Ling et al., 2016). I validated the mass spectrometry analyses through nucleosome pulldowns with unmodified, H3K79me2 and H3K79me3 nucleosomes from nuclear extract from HEK293 cells transfected with MYC-tagged PTBP1. MYC-tagged PTBP1 was enriched in the H3K79me2 nucleosome pulldowns but not unmodified or H3K79me3, suggesting the interaction is methyl-form specific (Figure 3.2D).

3.2.3 Pinometostat-induced alternatively spliced genes have aberrantly high H3K79me2 and show stark increases in H3K36me3 upon pinometostat treatment

Before characterizing the role of PTBP1 in H3K79me2-mediated alternative splicing I was keen to observe how DOT1L inhibition affected the distribution of H3K79me2, and to see if any changes in the distribution could explain the effects on alternative splicing. For this analysis I used ICeChIP-seq, a calibrated form of ChIP with internal nucleosome standards that permits the quantification of histone modification levels genome-wide and allows for direct comparisons of modifications within and across experiments (Grzybowski et al., 2015, 2019; Shah et al., 2018). I reanalyzed quantitative ICeChIP-seq data of H3K79me2 I previously acquired from MV4;11 cells to determine H3K79me2 density at different gene groups including genes that were downregulated by 10 nM pinometostat treatment from my previous study in MV4;11 cells

(Figure 3.3A). I previously observed that pinomeostat-downregulated genes and MLL-AF4 targets had abnormally high H3K79me2 levels (Figure 3.3A). Surprisingly, the genes with changes in alternative splicing had higher peak levels of H3K79me2 than most highly expressed genes or even the pinometostat-downregulated genes in the untreated cells. About 1 kb downstream of the TSS, the peak subsided and the amount of H3K79me2 within the gene body was similar among the three gene groups. Ie observed that 20 of the genes with changes in alternative splicing were also downregulated by 10 nM pinometostat, a significant overlap (Figure 3.3B), compared to only 5 alternatively spliced genes that were upregulated. MLL-fusion targets have aberrantly high levels of H3K79me2 and are highly-dependent on this modification for expression (Bernt et al., 2011; Daigle et al., 2013). I also observed a significant overlap with fusion targets as 28 MLL-AF4 targets were among the differentially alternatively spliced genes (Kerry et al. 2016) (Figure 3.3C). This suggests that abnormally high levels of H3K79me2, found in genes downregulated by low-dose pinometostat and MLL-AF4 targets induce changes in alternative splicing and that pinometostat-induced effects on gene expression and alternative splicing may be occurring by a common mechanism.

Treating MV4;11 cells with 10 nM pinometostat for 7 days drastically reduced H3K79me2 at all gene categories. Just as with the downregulated genes, the highest-expressed

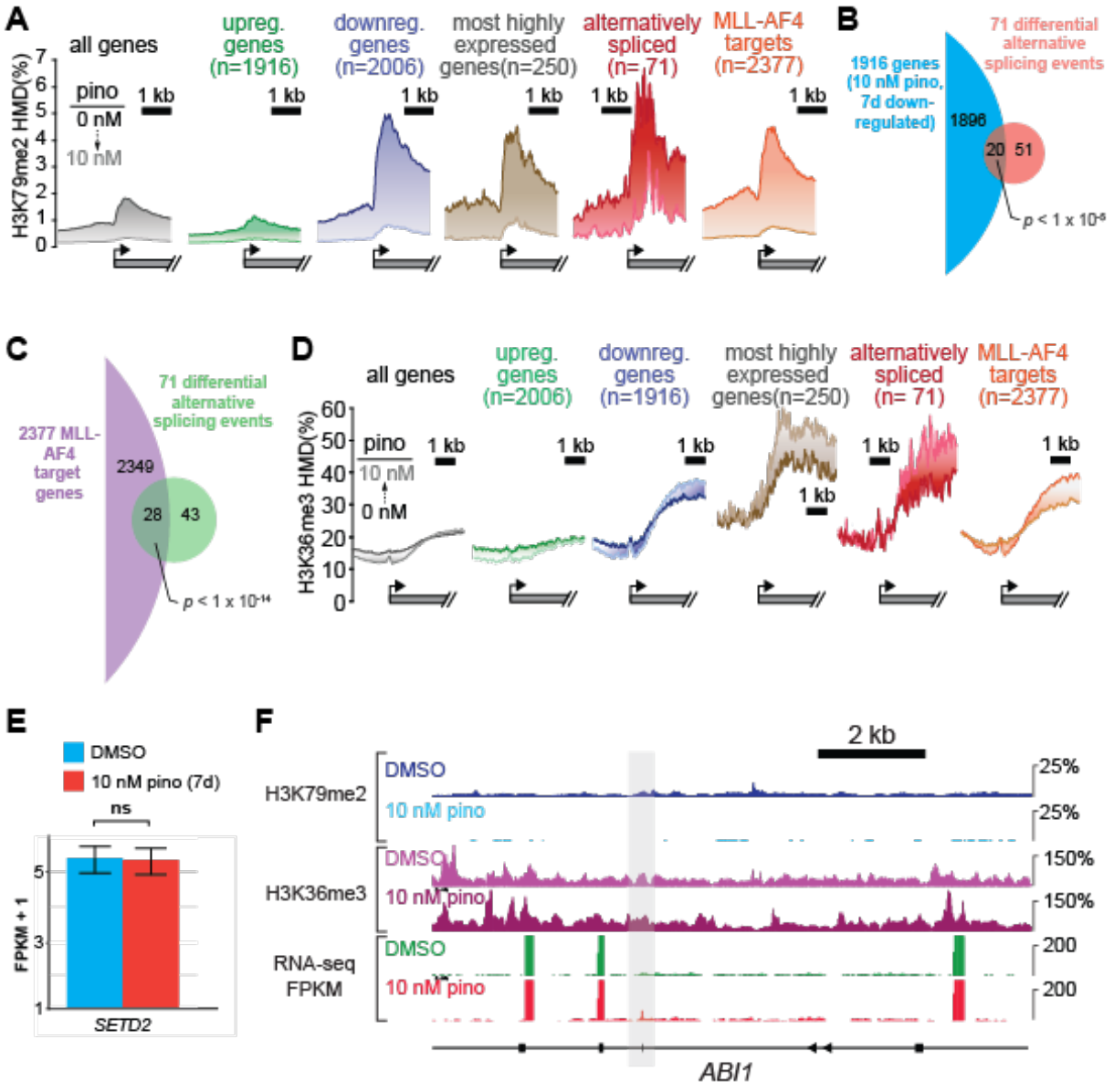

Figure 3.3 Pinometostat-induced alternatively spliced genes have abnormally high H3K79me2 that is severely reduced by pinometostat treatment.
A. Quantitative measurement of H3K79me2 modification density from ICeChIP-seq of MV4;11 cells treated with 10 nM pinometostat for 7 days contoured over the promoters (-2000 to 2000 bp from the TSS) of indicated gene sets, including genes up- or down-regulated by 10 nM pinometostat, the most highly-expressed genes, and genes with changes in alternative splicing. **B.** Venn diagram displaying the overlap between genes downregulated in MV4;11 cells by 10 nM pinometostat treatment (7 days) and genes with changes in alternative splicing. *p*-value computed by two-tailed Fisher Exact test. **C.** Venn diagram displaying the overlap between MLL-AF4 targets (Kerry et al., 2017) and genes with changes in alternative splicing. *p*-value computed by two-tailed Fisher Exact test. **D.** ICeChIP-seq of H3K36me3 HMD from MV4;11 cells treated with 10 nM pinometostat for 7 days contoured over the promoters (-2000 to 4000 bp from the TSS) of the same gene sets from A. **E.** Bar graph of Cuffdiff (Trapnell et al., 2013)

Figure 3.3. continued.
output for the expression of *SETD2* from RNA-seq in MV4;11 cells ± 10 nM pinometostat. Values are represented as FPKM + 1 for 3 independent experiments with standard deviation. Student's t-test **(**ns $p > 0.05$). **F.** A section of the ABI1 locus depicting an alternatively spliced exon (outlined in gray) whose inclusion is increased by 10 nM pinometostat treatment, displaying MV4;11 ICeChIP-seq tracks for H3K79me2 and H3K36me3 tracks from 10 nM pinometostat as well as DMSO control-treated cells and an RNA-seq track (FPKM) from a single replicate of 10 nM pinometostat- and DMSO-treated cells. All treatments were for 7 days.A portion of the ABI1 locus depicting an alternative exon (outlined in gray) whose inclusion is increased by 10 nM pinometostat treatment, displaying MV4;11 ICeChIP-seq tracks for H3K79me2 and H3K36me3 tracks from 10 nM pinometostat as well as DMSO control-treated cells and an RNA-seq track (FPKM) from a single replicate of 10 nM pinometostat- and DMSO-treated cells. All treatments were for 7 days.

genes and the MLL-AF4 targets, the alternatively spliced genes had large reductions in H3K79me2, suggesting the H3K79me2-depletion mediated effects on alternative splicing at these genes is direct (Figure 3.3D).

A previous study observed crosstalk between H3K79me2 and H3K36me3 (Bu et al., 2018), another modification associated with active transcription and with known roles in splicing (Guo et al., 2014; Luco et al., 2010). Bu et al. observed that knockdown of *Setd2*, the H3K36me3-methyltransferase caused a resulting increase in H3K79me2 genome-wide in MLL-AF9 expressing mouse hematopoietic progenitors (Bu et al., 2018). Interestingly, PTBP1 is recruited by H3K36me3 through the MRG15 protein to affect tissue-specific alternative splicing at specific genes (Luco et al., 2010). Given the observed crosstalk between these two histone modifications I wanted to see if there was a change in H3K36me3 upon pinometostat-induced H3K79me2 depletion. I once again performed ICeChIP-seq for a quantitative, high resolution comparison of H3K36me3 density across pinometostat-treated and control samples for the same gene groups from Figure 3.3A (Figure 3.3B). SETD2 associates with the transcriptional elongation complex and deposits H3K36me3 during active transcription (Kizer et al., 2005) and H3K36me3 roughly tracks with transcriptional activity. However, in untreated cells H3K36me3

levels in genes with pinometostat-induced differential alternative splicing were almost as high as the 250 highest expressed genes and only 2 of the alternatively spliced genes are among the 250 highest expressed genes.

Pinometostat treatment resulted in decreases in H3K36me3 near the TSS of all gene groups examined but, surprisingly, caused methylation levels to increase further into the gene body compared to DMSO control (Figure 3.3D). The gene group with splicing changes had the greatest increase in H3K36me3 and were followed closely by the highest expressed genes after pinometostat treatment. MLL-AF4 targets and the set of genes downregulated by pinometostat had much smaller H3K36me3 increases. I previously observed the differential expression of thousands of genes with 10 nM pinometostat treatment (Figure 2.1) however, I observed no changes in the expression of *SETD2* in our RNA-seq analysis (Figure 3.3E), suggesting that this increase in H3K36me3 is potentially due to the release of an antagonistic effect of H3K79me2. These reciprocal trends in histone methylation where decreasing H3K79me2 is accompanied by increased H3K36me3 are apparent at the ABI1 locus where inclusion of an exon is increased upon pinometostat treatment (highlighted in gray) (Figure 3.3F). Although the exon is encoded far downstream of the H3K79me2 peak near the TSS there is a reduction in H3K79me2 and an increase in H3K36me3 around the site of the alternative exon. In summation, pinometostat-induced alternatively spliced genes have aberrantly high initial H3K79me2 and H3K36me3 levels and H3K36me3 is starkly increased upon 10 nM pinometostat treatment.

3.2.4 PTBP1 knockdown reproduces pinometostat-induced effects on alternative splicing and reduces leukemia cell viability

Having observed that pinometostat-induced alternatively spliced genes are highly enriched for H3K79me2 and that this methylation is severely depleted upon 10 nM pinometostat treatment (Figure 3.3A), I wondered if a splicing factor that I observed to preferentially recognize H3K79me2-modified nucleosomes was involved in pinometostat-mediated changes in alternative splicing. Due to its previously observed effects on exon exclusion, I focused on PTBP1 (Linares et al., 2015; Luco et al., 2010). I virally transduced a tet-inducible shRNA targeting *PTBP1* into MV4;11 cells and then isolated individual clones as stable, inducible *PTBP1* knockdown cell lines. Upon doxycycline induction *PTBP1* expression was drastically reduced (Figure 3.4A). I treated MV4;11 PTBP1 shRNA cells with doxycycline for 7 days to induce knockdown of *PTBP1* and then analyzed alternative splicing at the same loci from Figure 3.1B. Interestingly, I observed similar effects on alternative splicing as pinometostat treatment with changes in the start site of *SATB1*, exon exclusion at *ABI1* and exon switching at *H2AFY* (Figure 3.4B), suggesting that *PTBP1* knockdown and H3K79me2 are affecting alternative splicing through the same mechanism. I examined *PTBP1* expression and saw no discernable difference in expression with pinometostat treatment (Figure 3.4C), suggesting that H3K79me2 depletion does not affect PTBP1-mediated effects on splicing by reducing *PTBP1* expression.

Surprisingly, when I looked at how *PTBP1* knockdown affected the viability of MV4;11 cells I observed significant reductions in the proliferation of 3 different clonal cell lines upon doxycycline induction of *PTBP1*-targeting shRNA as compared to a control shRNA targeting *GFP* (Figure 3.4D). When I treated those same PTBP1 shRNA clones with both doxycycline for shRNA induction and 10 nM pinometostat I observed no additional decrease in viability (Figure

3.4E), suggesting that H3K79me2 and *PTBP1* knockdown are affecting MV4;11 cell viability through the same pathway.

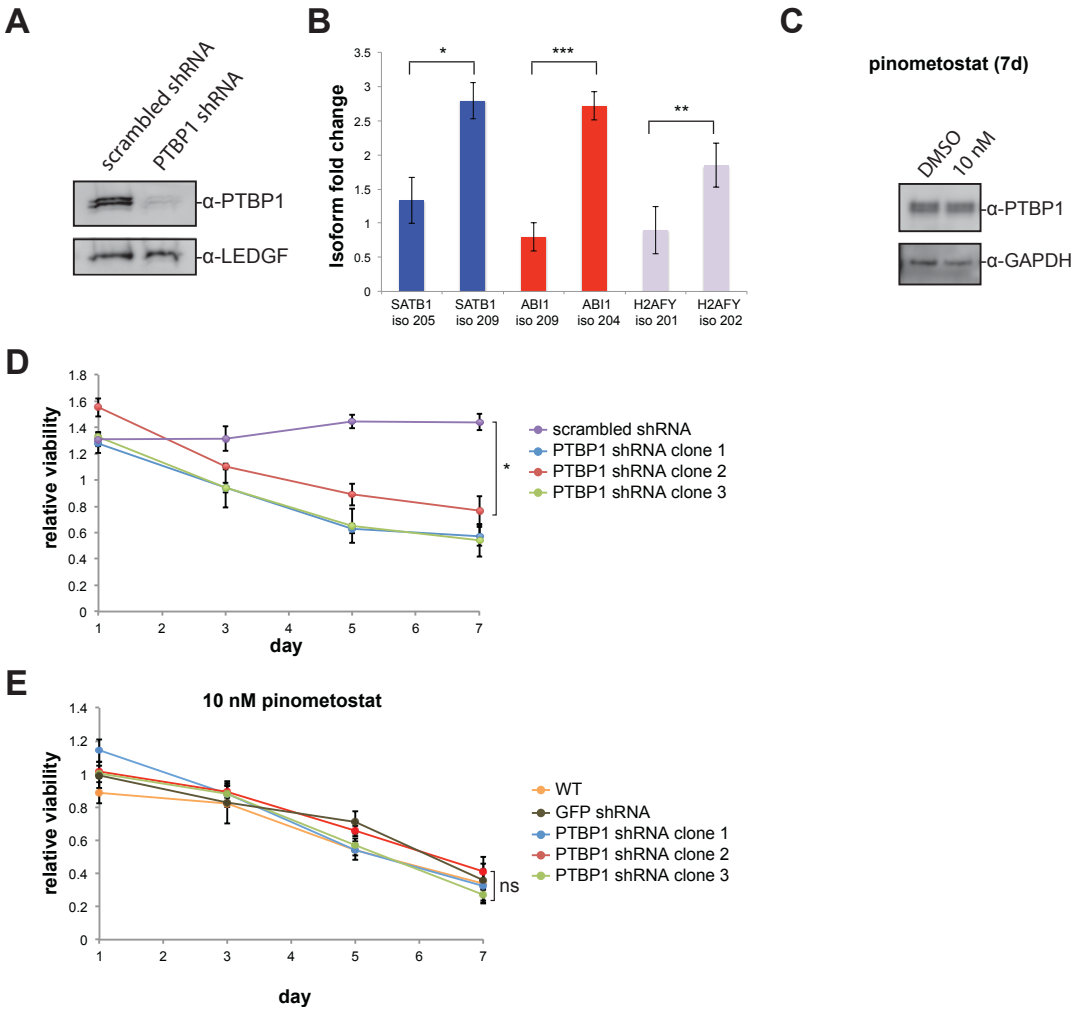

Figure 3.4 PTBP1 knockdown causes similar effects on alternative splicing as DOT1L inhibition. **A.** Western blot for PTBP1 and LEDGF (loading control) in WT or an MV4;11 clonal isolate virally transduced with a tet-inducible shRNA to *PTBP1* or a scrambled shRNA induced with doxycycline to express the indicated shRNAs. **B.** RT-qPCR analysis of the expression of different isoforms of SATB1, ABI1 and H2AFY as in Figure 1B, from 3 monoclonal isolates of MV4;11 cells virally transduced with a tet-inducible shRNA to *PTBP1* or a scrambled shRNA control and induced by 1 µg/mL doxycycline for shRNA expression. Results are shown as mean ± S.E.M. of three clonal isolates. Student's t-test (* $p < 0.05$, ** $p \leq 0.01$, *** $p \leq 0.001$). **C.** Western blot for PTBP1 and GAPDH (loading control) in MV4;11 cells treated for 7 days with 10 nM pinometostat or DMSO. **D.** Proliferation assay of the 3 MV4;11 clonal isolates from panel A induced with 1 µg/mL doxycycline to express an shRNA to PTBP1 and compared to a cell line expressing a scrambled shRNA. Y axis represents the luminescence fraction of shRNA clones over WT cells from a CellTiter Glo 2.0 assay. Means ± SE are shown for 3 independent experiments with Student's t-test for significance of day 7 values (** $p \leq 0.01$). **E.** Proliferation

Figure 3.4, continued.
assay of the 3 MV4;11 clonal isolates from panel C with an inducible shRNA to PTBP1 or cells virally transduced with an shRNA targeting GFP or WT cells induced with 1 μg/mL doxycycline for shRNA expression and treated with 10 nM pinometostat. Y axis represents the luminescence fraction of cells treated with 1 μg/mL doxycycline and 10 nM pinometostat over cells treated with 1 μg/mL doxycycline and DMSO from a CellTiter Glo 2.0 assay. Means ± SE are shown for 3 independent experiments with Student's t-test for significance of day 7 values (ns $p > 0.05$).

3.2.5 H3K79me2 depletion results in alternative splicing of the PTEN tumor suppressor, increased PTEN protein levels and reduced AKT signaling

This dependency of MLL-r leukemia cells on PTBP1 for survival has been observed in other cancer types where PTBP1 is necessary for the proliferation of prostate, breast and ovarian cancers (He et al., 2007, 2014; W. Jin et al., 2000; C. Wang et al., 2008; X. Wang et al., 2018). A study by Wang et al. found that *PTBP1* knockdown in breast cancer MDA-MB-231 cells reduced proliferation and increased expression of the *PTEN* tumor suppressor, resulting in reductions in phosphorylated AKT and growth signaling (X. Wang et al., 2018). Interestingly, I observe increased inclusion of an alternatively spliced exon at the *PTEN* locus upon H3K79me2 depletion (Table 4.1). I find no significant changes in *PTEN* expression in our RNA-seq analysis from pinometostat treatment (Figure 3.5A) but observed an increase in PTEN protein levels (Figure 3.5B), suggesting that the increase in PTEN protein levels may be somehow mediated by an increase in the isoform containing the alternative exon. PTEN antagonizes PI3K/AKT growth signaling, an important driver of proliferation in malignancies and PTEN is one of the most frequently mutated genes in cancer (Dillon & Miller, 2014; Haddadi et al., 2018). I observe that phosphorylated AKT is strongly reduced with 10 nM pinometostat treatment (Figure 3.3C), providing a potential mechanism through which H3K79me2/PTBP1-mediated alternative splicing might affect leukemia proliferation.

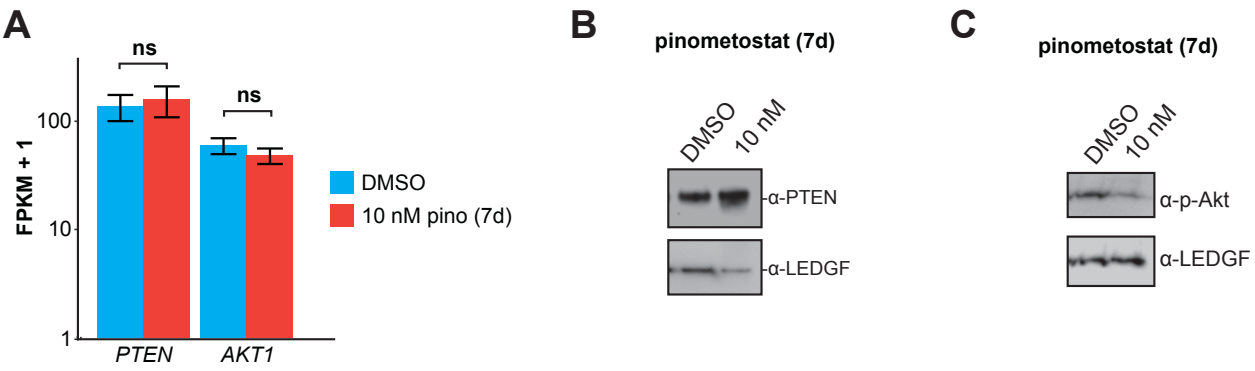

Figure 3.5 Pinometostat-induced alternative splicing of the PTEN tumor suppressor coincides with increased protein levels and reduced activation of AKT.
A. Bar graph of Cuffdiff(Trapnell et al., 2013) output for the expression of *PTEN* and *AKT1* from RNA-seq in MV4;11 cells ± 10 nM pinometostat. Values are represented as FPKM + 1 for 3 independent experiments with standard deviation. Student's t-test (ns $p > 0.05$). **B.** Western blot for PTEN or **C.** phospho-Akt and LEDGF (loading control) in MV4;11 cells treated for 7 days with 10 nM pinometostat or DMSO.

3.3 DISCUSSION

3.3.1 H3K79me2 is recognized by splicing factors including PTBP1, and depleting H3K79me2 or PTBP1 results in similar effects on splicing

Here, I present the first evidence of an interaction between H3K79me2 and a splicing factor and a common pathway for how this modification and PTBP1 regulate alternative splicing in an MLL-r leukemia cell line. I observed 71 instances of alternative splicing in the MV4;11 MLL-r leukemia cell line treated with low-dose (10 nM) DOT1L inhibitor, with instances of exon-inclusion making up the majority (52%) of these events. Through quantitative ICeChIP-seq I revealed that these alternatively spliced genes have higher levels of H3K79me2 than even the highest expressed genes or MLL-AF4 targets (Figure 3.3B). 10 nM pinometostat treatment drastically depletes H3K79me2 but causes an increase in H3K36me3 in gene bodies that is particularly high at alternatively spliced genes (Figure 3.3A and D). I observe that the splicing

factor PTBP1 interacts with H3K79me2 in the context of the nucleosome and that *PTBP1* knockdown has a similar effect on alternative splicing as H3K79me2 depletion, suggesting that H3K79me2 and PTBP1 affect pinometostat-induced alternative splicing through the same mechanism. I find that *PTBP1* knockdown reduces MV4;11 proliferation, an effect consistent with the observation that pinometostat-induced alternative splicing increases exon inclusion at the PTEN tumor suppressor, potentially causing an observed increase in PTEN protein levels and coinciding reductions in the activation of its target, the growth signaling protein AKT.

The 71 H3K79me2-regulated alternative splicing events I identified in MV4;11 cells mostly involved exon inclusion, consistent with the Li et al. study that observed 191 differentially alternatively spliced genes in SEM cells treated with 0.5 to 2 μM pinometostat (T. Li et al., 2018). However, only 14 genes overlapped among those 3 concentrations of pinometostat in the Li et al. study and there was no overlap with the alternatively spliced genes in my analysis of 10 nM pinometostat treatment in MV4;11 cells. MV4;11 and SEM cells are similar, MLL-r cell lines with MLL-AF4 translocations and significant overlap in MLL-AF4 targets with aberrantly high H3K79me2 levels (Kerry et al., 2017). I observe a significant overlap of H3K79me2-regulated alternatively spliced genes and MLL-AF4 targets (Figure 3C), suggesting that H3K79 hypermethylation resulting from that aberrant recruitment of DOT1L affects splicing. The absence of an overlap between the pinometostat-altered alternative splicing events in my set and the Li et al. study could be the result of the use of different alternative splicing detection software. Li et al. used MISO which employs a probabilistic framework, relying on Baynesian inference to assign exonic reads to specific isoforms (Katz et al., 2010) while I used Leafcutter, software that relies on reads that span exon junctions to identify splice sites (T. Li et al., 2018). Because the number of detected differential alternative splicing events

in the Li et al. study didn't increase at higher pinometostat concentrations from 0.5 to 1 to 2 μM yet, instead resulted in relatively similar numbers of poorly-overlapping alternatively spliced genes (58, 60 and 73 genes respectively), suggests that the analysis may have lacked sensitivity, missing perhaps the majority of H3K79me2-regulated splicing events. Interestingly, the H3K79me2-regulated alternative splicing events in the Li et al. study were also primarily exon inclusion events, enriched for PTBP1 consensus binding sequences (T. Li et al., 2018), suggesting the events they identified likely have a similar dependence on PTBP1 function. Still yet another study by Ye et al. also found higher H3K79me2 at sites of exon exclusion that were enriched for PTBP1 consensus sequences (Ye et al., 2014). Each of PTBP1's 4 RNA binding domains can recognize PTBP1 consensus sequences that consist of polypyrimidine tracks, CU repeats that range from pentamers to more than 30 nucleotides (Ling et al., 2016; Oberstrass et al., 2005). The length of the CU track appears to affect PTBP1 localization and H3K79me2-mediated recruitment could be an additional means of differentially recruiting the splicing factor to specific loci (Ling et al., 2016).

I find that H3K79me2 is recognized by several splicing factors including DDX5 and HNRNPK and PTBP1 (Figure 3,2A). Because almost all of the proteins enriched in H3K79me2 nucleosome pulldowns have known roles in RNA splicing, it is possible that many or all of these proteins are present as a complex that could be recruited by H3K79me2 to actively transcribed genes. My analysis of the available structural information for these proteins in the literature did not reveal any of the canonical methyllysine-binding domains (Tudor, chromodomain, PHD, PWWP, MBT, WD40 and Ankyrin Repeats etc.) (Yun et al., 2011) that could potentially implicate any of them in a direct interaction with H3K79me2. However, I cannot rule out the possibility of an unrecognized canonical domain or an uncharacterized methyl-lysine binding

domain within one or several of these proteins. A possible mechanistic explanation is provided by Luco et al. who found that PTBP1 is recruited indirectly to sites of alternative splicing enriched with H3K36me3 through the PWWP domain of MRG15 to promote exon exclusion (Luco et al., 2010). Following this model, it is likely that PTBP1 and many, if not all of these proteins that interact with H3K79me2 are doing it indirectly and the specific binder has not yet been identified.

3.3.2 PTBP1 knockdown decreases MV4;11 MLL-r leukemia viability, consistent with its role in promoting proliferation in other malignancies

I observe a reduction in the proliferation of MV4;11 cells upon knockdown of *PTBP1*, similar to and not exacerbated by treatment with pinometostat (Figure 3.4E), suggesting that this splicing factor is necessary for leukemia survival. Furthermore, the lack of additional toxicity from *PTBP1* knockdown coupled with pinometostat treatment suggests that PTBP1 may be involved in H3K79me2-mediated leukemogenesis.

Interestingly, downregulation of PTBP1 during neuronal differentiation relieves PTBP1-mediated repression of a neuron-specific exon of the transcription factor PBX1 (Linares et al., 2015). Splicing of this exon through reduced PTBP1-mediated repression yields an isoform of PBX1 that is capable of activating neuronal genes. In addition to its role in neuronal development, PBX1 is involved in hematopoiesis and leukemogenesis as a cofactor of the *MEIS1* oncogene. Alternative splicing, mediated by H3K79me2 recruitment of PTBP1 to the *PBX1* locus might affect leukemogenesis through targeting of the PBX1-MEIS1 complex (Dardaei et al., 2014). Although I didn't observe alternative splicing of *PBX1* in our analysis, alternative splicing at *PBX1* should be more closely examined for potential effects on leukemogenesis.

PTBP1 is already implicated in the pathogenesis and maintenance of a growing list of malignancies (He et al., 2007, 2014; W. Jin et al., 2000; C. Wang et al., 2008; X. Wang et al., 2018). *PTBP1* is upregulated in breast, prostate and ovarian cancer as well as glioblastomas and *PTBP1* knockdown reduces the proliferation and invasiveness of breast, prostate and ovarian cancers (He et al., 2007, 2014; W. Jin et al., 2000; C. Wang et al., 2008; X. Wang et al., 2018). Interestingly, *PTBP1* knockdown in MDA-MB-231 breast cancer cells upregulates the tumor suppressor PTEN, resulting in decreased phospho-AKT, reducing growth signaling and proliferation (X. Wang et al., 2018). I observe increased exon inclusion at the *PTEN* locus and higher PTEN protein levels coupled with a reduction in phospho-AKT in MV4;11 cells treated with 10 nM pinometostat, suggesting a potential role for PTBP1 in H3K79me2-mediated leukemogenesis.

3.3.3 H3K79me2-regulated alternatively spliced genes have abnormally high H3K79me2 and large pinometostat-induced increases in H3K36me3

Genes differentially alternatively spliced with 10 nM pinometostat treatment had high levels of H3K79me2 that surpassed MLL-AF4 targets or even the highest expressed genes (Figure 3.3A). The profound reductions in H3K79me2 upon 10 nM pinometostat treatment are suggestive of a direct effect of the loss of this modification on alternative splicing, likely through the recruitment of PTBP1. H3K79me2 likely facilitates PTBP1 recruitment to sites harboring PTBP1 consensus sequences to prevent exon inclusion in an H3K79me2-depdendent and cell-type specific manner. It is interesting that PTBP1 is also recruited by H3K36me3 to repress exon inclusion (Luco et al., 2010) and it is possible that this mechanism may also play a role in H3K79me2-regulated alternative splicing.

I observed global increases in H3K36me3 with 10 nM pinometostat treatment. These increases in H3K36me3 were dramatically elevated at H3K79me2-regulated alternatively spliced genes after pinometostat treatment and were much higher than pinometostat-downregulated genes and MLL-AF4 targets and rivaled levels at the highest expressed genes, suggesting that H3K36me3 may also be involved in the alternative splicing events at these loci. Increases in H3K36me3 could potentially recruit splicing factors such as ZMYND11 that promote intron inclusion to antagonize PTBP1-mediated effects (Guo et al., 2014). Or, perhaps globally increased H3K36me3 levels alter the localization of PTBP1 through its interaction with the H3K36me3-binder MRG15 and recruit PTBP1 away from H3K79me2-regulated sites of alternative splicing (Luco et al., 2010). Further investigations are needed to determine if H3K36me3 affects pinometostat-induced alternative splicing.

Crosstalk between H3K79me2 and H3K36me3 was previously observed by Bu et al. where H3K79me2 levels increased after *Setd2* knockdown and resulting global reductions in H3K36me3 in *MLL-AF9* mouse hematopoietic progenitors (Bu et al., 2018). Ectopic expression of *Setd2* increased global H3K36me3 with a coinciding decrease in H3K79me2. The mechanism behind this bidirectional crosstalk is unknown, as is the nature of the cooperation between MLL-fusions and *SETD2* lesions but, it is entirely possible that effects on alternative splicing from changes in the levels of these modifications may play a role in leukemogenesis.

Pinometostat-induced increases in H3K36me3 might reduce the viability of MLL-r leukemia through affects on MLL-fusion mediated gene activation. *SETD2* is often mutated in MLL-r leukemia with about 22% of patients carrying loss-of-function mutations (X. Zhu et al., 2014), strongly suggesting cooperation between these mutations in leukemogenesis. There are some indications of the nature of this cooperation from previous studies. Reductions in

H3K36me2 through conversion of this modification to H3K36me3 by SETD2 might reduce recruitment of LEDGF, a component of the MLL-fusion complex, necessary for localizing the MLL-fusion complex including MLL1 to target genes and leukemogenesis (Okuda et al., 2014). LEDGF has a higher affinity for H3K36me2 than H3K36me3 (L. Zhu et al., 2016). Zhu et al. found that *Setd2* knockdown in MLL-AF9 expressing mouse hematopoietic progenitors increased Mll1 but not MLL-fusion localization to fusion targets and increased the expression of the *Meis1* and *Mef2c* oncogenes and (L. Zhu et al., 2016). Mll1 localization and expression of the *Hoxa9* oncogene was reduced after knockdown of *Ash1l*, the histone methyltransferase responsible for H3K36me2 (L. Zhu et al., 2016). Furthermore, *Setd2* knockdown decreased the latency of leukemia onset and increased the progression of the disease in mouse models (X. Zhu et al., 2014). This suggests that H3K79me2 may promote recruitment of the MLL-fusion complex to target genes through antagonism of H3K36me3 and resulting increases in H3K36me2.

3.4 MATERIALS AND METHODS

3.4.1 Accession numbers

The ICeChIP data has been reported in the Gene Expression Omnibus with accession number GSE162441.

3.4.2 Cell Culture

Human MV4;11 leukemia cells were a gift from the laboratory of Yali Dou at the University of Michigan. Cells were cultured in RPMI-1640 medium containing 10% (v/v) FBessence (Seradigm cat # 3100-500), 1% L-glutamine at 37°C in humidified air containing 5% CO_2.

Human embryonic kidney HEK293 cells were cultured in DMEM 10% (v/v) FBessence. DOT1L inhibitor pinometostat (EPZ5676, Cayman Chemical cat # 16175), was resuspended in DMSO. Doxycycline (Alfa Aesar cat # J60422) was resuspended in water.

3.4.3 Reverse Transcription and Quantitative real-time PCR

RNA was extracted from 10^6 cells using 500 µl Trizol and following the manufacturer's protocol. 1 µg RNA was used for reverse transcription with 0.5 µl MMLV HP reverse transcriptase (Lucigen cat # RT80125K) per 20 µl rxn. RNA was then degraded by alkaline hydrolysis by adding 40 µl 150 mM KOH, 20 mM tris base and heating 95 °C 10 min. then cooling on ice and quenching with 40 µl 150 mM HCl and then adding 100 µl TE. Gene expression was assayed by real-time PCR in 10 µl reactions with 0.5 µl cDNA and 5 µl PowerUP SYBR Green master mix (Applied Biosystems cat # A25742) per reactions. qPCR was run on the Bio-Rad thermocycler CFX96 or CFX384 using the program: 50 °C 2:00, 95 °C 2:00, then 40 cycles 95 °C 0:15, then 60 °C 1:00. Data was normalized to 18S rRNA. Primer sets are listed in Table 4.2.

3.4.4 Cell Proliferation Assay

Cells were seeded at 10^5 cells/ml in 80 µl in clear bottom 96-well plates (Corning 07200566) in 3 replicates. Everyday 40 µl of culture was transferred to 40 µl media in a new plate. On odd days 30 µl of Cell TiterGlo 2 (Promega cat # G924A) was added to the remaining 40 µl culture and incubated 10 min. at room temperature on a shaker at 600 rpm. Luminescence was measured on a Tecan Infinite F200 Pro plate reader and fraction viability was determined from the luminescence of treated over untreated cells.

3.4.5 Western blotting

10 ul whole cell extracts of 2 x 10^5 cells in 40 µl 6X SDS loading buffer were run on 4-14% bis-tris gel (Invitrogen cat # NP0335). Membranes were transferred by semi-dry apparatus (Bio-Rad Transblot cat # 170-3940) at 200 mA, 25 V for 35 min to 0.45 µm nitrocellulose membrane (Millipore cat # IPVH00010). Membranes were then blocked for 1 h with TBS-T 1% ECL Prime blocking reagent (GE Healthcare cat # RPN418) at RT on an orbital shaker and blotted with primary antibody for 1 h at RT with gentle agitation. Membranes were then washed 3 times for 5 min. while shaking with TBS-T and then incubated with secondary antibody at RT for 1 h while shaking. A complete list of antibodies used in this study can be found in Table 4.3.

3.4.6 Plasmid generation

pCMV-Gag-Pol plasmid, encoding HIV-1 derived *gag*, and *pol,* the pCMV-VSV-G vector encoding VSV-G envelope gene and Tet-pLKO were purchased from Addgene. shRNA constructs were created by inserting annealed oligos of shRNA sequences (Table 4.2) purchased from IDT into Tet-pLKO at the AgeI and EcoRI restriction sites.

3.4.7 Transfection for lentiviral particle generation

Lentiviral particles were produced by Fugene transfection of the 293T packaging cell line in a 6-well plate at ~70% confluency with pCMV-Gag-Pol, pCMV-VSV-G and 2 µg of the plasmid encoding the gene or shRNA of interest using a 3:1:4 ratio respectively. Lentiviral particle enriched supernatants were collected 72 hours after transfection for immediate transduction.

3.4.8 Lentiviral transduction

4 x 10^5 MV4;11 cells suspended in 1 ml RPMI-1640 medium containing 10% FBessence in a 6-well plate were transduced by adding 2.5 ml of 0.45 μm filtered viral supernatants from 293T cells. Then 0.8 μl polybrene (EMD Millipore cat. # TR-1003-G)/ml transduction reagent was added to the media and the plates were wrapped with parafilm and spun down at 2000 rpm for 2 hours at room temperature then incubated O/N at 37°C in humidified air containing 5% CO_2. After 12 hours cells were spun down and resuspended in RPMI-1640 10% FBessence. After 24 h 0.5 μg/ml puromycin was added to the wells and this selection media was refreshed every 3 days to select for transduced cells. Individual clones were purified by diluting cell cultures to 1 cell/100 μl and then plating 100 μl aliquots in a 96-well plate. Wells were visually assessed for individual clones and then grown out.

3.4.9 Octamer assembly

500 μg of unmodified and H3K79me2 histone octamers were prepared as previously described (Dyer et al., 2004). Briefly, equimolar quantities of the four core histones purified from *E. coli* or synthesized H3K79me2 (Z. Chen et al., 2015), were combined in unfolding buffer (50 mM Tris-HCl pH 8, 6.3 M Guanidine-HCl, 10 mM 2-mercaptoethanol, 4 mM EDTA) in 3500 MWCO dialysis tubing (Pierce), and twice dialyzed in 500 volumes of refolding buffer (20 mM Tris-HCl pH 7.8, 2M NaCl, 1mM EDTA, 5 mM DTT) overnight (14 hours) at 4°C. The sample was then purified by gel filtration chromatography (Superdex 200 10/300 GL, GE Healthcare). Purified octamer fractions were combined and concentrated with Amicon Ultra-4 centrifugal filters (10k MWCO, Millipore) to a final concentration of 5-15 μM.

3.4.10 Nucleosome reconstitution

Nucleosomes were reconstituted by combining equimolar amounts of histone octamer and biotinylated DNA based on the 601 nucleosome positioning sequence (Lowary & Widom, 1998) to final concentrations of 1 μM in dialysis buttons (Hampton Research). Dialysis buttons were placed in 100 ml 2M NaCl in a graduated cylinder and dialyzed overnight through slow addition 0.5ml/minute of 20 mM Tris-HCl pH 7.5, 1 mM EDTA, 10 mM 2-mercaptoetanol over the course of 12-16 hours until a final concentration of 200 mM NaCl (Ruthenburg et al., 2011). After dialysis, reconstituted nucleosomes were diluted 1:1 with storage buffer (20 mM Na•Cacodylate pH 7.5, 10% v/v glycerol, 1mM EDTA, 200 μM PMSF, with protease inhibitors) and stored at 4°C. Reconstitution efficiencies were observed by running 2 μl of each reconstitution on 5% native polyacrylamide gel electrophoresis. Gels were stained 30 min. with SYBR Gold (ThermoFisher Scientific), imaged and compared by densitometry to DNA only control.

3.4.11 Nuclear extraction

Nuclear extract was purified from HEK293 cells using the Dignam and Roeder protocol (Carey et al., 2009). Briefly, 20 million HEK293 cells were washed in 10mL PBS and spun down for 5 min, 1,200 x g. Supernatant was discarded and cells were resuspended in 2.5 packed cell volumes (PCV) of buffer A (10mM Tris pH 7.9, 1.5mM $MgCl_2$, 10mM KCl, 10μM $ZnCl_2$, 0.1mM TCEP, 1x Roche Protease Inhibitor cocktail) and spun down for 5 min, 1,200 x g at 4°C. Add an equal volume of buffer A 0.2% Triton X-100, followed by incubation on ice for 12 min. with occasional gentle mixing then gently add cells to the top of a 7.5 ml sucrose cushion (30% sucrose (W/V), 1.5 mM MgCl2, 10 mM Tris, pH 7.9, 10 mM KCl, and 0.5 mM DTT) in a 50 ml

tube and spun for 10 min. in a table-top swing bucket centrifuge. Carefully aspirate supernatant to leave the nuclei pellet at the bottom of the tube. Gently resuspend nuclei in 1.5 ml buffer B (20 mM Tris pH 7.9, 25% glycerol, 210 mM NaCl, 1.5 mM MgCl2, 0.2 mM EDTA, 0.5 mM PMSF, and 0.5 mM DTT) then add 1.5 ml buffer C (20 mM Tris pH 7.9, 25% glycerol, 630 mM NaCl, 1.5 mM MgCl2, 0.2 mM EDTA, 0.5 mM PMSF, and 0.5 mM DTT). Rock mixture at 4 degrees C for 30 min. to 1 hour. Spin down the crude extract at 18-25k x g for 15 min. in a fixed angle rotor. Collect the supernatant and dilute with 3 volumes buffer A.

3.4.12 Nucleosome pulldown

Aliquot 57 µl of Myone Streptavidin T1 Dynabeads (Thermo Fisher cat # 65601) (slurry volume). Collect the beads on magnetic racks, and discard the supernatant. Resuspend in 500 µl buffer D (20 mM Tris pH 7.9, 10% glycerol, 100 mM NaCl, 1.5 mM MgCl2, 0.2 mM EDTA, 0.5 mM PMSF, and 0.5 mM DTT) collect the beads on magnetic racks, and discard the supernatant. Resuspend beads in 500 µl buffer D and add 50 pmol of freshly assembled nucleosome per pulldown and incubate at 4 deg. C by end-over-end rotation for 10 minutes. Take a Nanodrop reading of the supernatant to determine amount of free nucleosome in solution or collect supernatant and run on 6% native PAGE, saturation of the beads is assumed if significant amounts of nucleosome are present in the supernatant. Wash beads 2 x 500 µl with buffer D. Resuspend beads in 1 ml of diluted nuclear extract for each pulldown. Wash beads 4 x 1 mL of buffer J (20 mM Tris pH 7.9, 10% glycerol, 300 mM NaCl, 1.5mM MgCl2, 0.2 mM EDTA, 0.1% NP40, 0.5 mM PMSF, and 0.5 mM DTT) with 2 tube transfers (siliconized tubes should be used, the sequence is wash, tube transfer, wash, wash, tube transfer, wash). Elute from beads by resuspending in 30 µl 2X SDS-PAGE loading buffer, boil at 95 deg. C for 10 minutes. Load 3 µl

of each sample on 4%-12% gradient gel (NuPAGE from Invitrogen) and image by silver stain.

4 CONCLUSIONS

4.1 MANY FUNCTIONS OF H3K79ME LACK MECHANISTIC EXPLANATION

Histone post-translational modifications regulate a variety of nuclear functions including gene expression, DNA repair and splicing and are indispensable for the development of complex eukaryotic organisms (Zhao & Garcia, 2015). Methylation at lysine 79 of histone H3 exemplifies the diverse array of crucial roles of chromatin modifications and is necessary for embryogenesis, hematopoiesis and cardiac development while playing crucial roles in cell cycle regulation, DNA repair, transcriptional activation and alternative splicing (Bernt et al., 2011; Daigle et al., 2011; Deshpande et al., 2013; Huyen et al., 2004; Jones et al., 2008; McLean et al., 2014). Surprisingly, given the abundance of studies of this mark (W. Kim et al., 2014; McLean et al., 2014; Vlaming & van Leeuwen, 2016), little is known about the mechanisms by which it affects cellular processes and importantly, the proteins that recognize it. The failure to identify H3K79me2-interacting proteins, whether direct or indirect, hampers efforts to understand the crucial H3K79me2-mediated functions observed in alternative splicing and leukemogenesis. There is generally a profound lack of understanding in the field, not just of the proteins that recognize H3K79me2 but also of the pathways responsible for carrying out the observed functions of this modification.

4.2 THE FLT3-ITD/STAT5A SIGNALING PATHWAY IS ACTIVATED BY MLL-FUSION MEDIATED H3K79ME2 AND IS NECESSARY FOR LEUKEMIA SURVIVAL

Nowhere is an understanding of the pathways affected by H3K79me2 more crucial than in MLL-rearranged (MLL-r) leukemia. Currently accepted models of MLL-r leukemia attribute development and maintenance of leukemia to a common core of transcription factors centered on the pleiotropic factors HOXA9 and MEIS1 (Bernt et al., 2011; Daigle et al., 2011; Deshpande et al., 2013; Guenther et al., 2008; Okada et al., 2005). In this prevailing model, MLL-fusions recruit DOT1L to hypermethylate and activate expression of *MEIS1* and *HOXA9* and these two oncogenes then activate a transcription program that drives leukemogenesis (Bernt et al., 2011; Daigle et al., 2011; Deshpande et al., 2013; Guenther et al., 2008; Okada et al., 2005).

My work addresses several previously-made observations that conflicted with the currently accepted model, such as reductions in the viability of some MLL-r leukemia cell lines at DOT1L inhibitor concentrations much lower than those that affect *HOXA9* or *MEIS1* expression (Daigle et al., 2013) and the long latencies of MLL-fusion induced leukemias (Corral et al., 1996; Dobson et al., 1999) that suggest other mutations may be needed for leukemia onset. In fact, other mutations in histone methyltransferases such as *EZH2* and *SETD2* and growth signaling pathways often coincide with MLL-fusions in patients but, very little is known about how these mutations cooperate or if H3K79me2 is involved (Armstrong et al., 2003; Grossmann et al., 2013; Liang et al., 2006; Stubbs et al., 2008; X. Zhu et al., 2014).

My work uncovers a mechanism of cooperation between MLL-fusions and *FLT3-ITD* lesions. I observed that the exquisite sensitivity of some MLL-r leukemia cells to low-dose DOT1L inhibition is mediated not through downregulation of the canonical leukemic drivers

HOXA9 and *MEIS1* but, reductions in *FLT3-ITD* expression and loss of downstream STAT5A gene activation. I can disrupt FLT3-ITD/STAT5A signaling through downregulation of *FLT3-ITD* by depleting either H3K79me2 or H3K4me3, two modifications necessary for MLL-fusion-mediated gene activation. Because these orthologous perturbations to MLL-fusion function both reduced *FLT3-ITD* expression and low-dose DOT1L inhibition doesn't affect *HOXA9* expression, it is likely that *FLT3-ITD* expression depends on activation by the fusion protein and not HOXA9, even though it is a target of both (Y. Huang et al., 2012; Kerry et al., 2017).

However, additional aspects of this cooperation remain to be investigated. Two previous studies identified significant overlap of HOXA9 and STAT5A binding sites at targets genome-wide (de Bock et al., 2018; Y. Huang et al., 2012). HOXA9 interacts with STAT5A and *HOXA9* knockdown reduced STAT5A binding at common target sites (Y. Huang et al., 2012), suggesting that HOXA9 localization and activation at a subset of targets may depend on STAT5A. However, it is unknown if reductions in STAT5A localization affect HOXA9 target binding. This putative dependence between these transcription factors may be necessary for the activation of common targets such as *PIM1*, an anti-apoptotic protooncogene upregulated in MLL-r leukemia. Given that both PBX3 and C/EBP consensus binding motifs were also significantly enriched at HOXA9 binding sites (de Bock et al., 2018) these four transcription factors including STAT5A, may be part of a large activation complex that upregulates the leukemic expression program. Further investigations are necessary to determine if these transcription factors facilitate *HOXA9/MEIS1* gene activation in leukemia.

Using ICeChIP I was able to quantitatively measure higher levels of H3K79me2 at MLL-AF4 targets such as *FLT3* that were downregulated by 10 nM pinometostat, than MLL-AF4 targets as a whole or even the highest expressed genes. This suggests that some MLL-AF4

targets are more dependent on H3K79me2 for expression but, it is still unknown why some genes are more efficiently methylated by DOT1L or why they their expression is more sensitive to reductions in methylation. With little known about how H3K79me2 activates gene expression it will be difficult to determine why genes are differentially affected by H3K79me2 depletion.

Perhaps H3K79me2-mediated gene activation isn't through recruitment of some activating factor but through exclusion of transcriptional repressors. Chen et al. found that H3K79me2 depletion resulted in localization of the histone deacetylase SIRT1, subsequent loss of H3K9ac and installation of repressive H3K9me3 by the SUVARH1 methyltransferase at MLL-AF4 targets (C. W. Chen et al., 2015). It is still unknown how H3K79me2 prevents localization of SIRT1 and this effect could be the result of reduced gene activation but, this at least provides part of an overall mechanism for how H3K79me2 affects gene expression.

A more complete understanding of the role of H3K79me2 in leukemogenesis and how MLL-fusions cooperate with other leukemic lesions will aid in the development of new treatments for the disease. Currently available treatments for MLL-r leukemia are not very effective and using single agents to treat leukemia patients usually offers little benefit due to the emergence of resistance (Winters & Bernt, 2017). An improved understanding of the pathways and proteins involved in leukemic pathogenesis would provide additional targets for combination therapies that would be less likely to resist treatment. My results suggest that the *FLT3* locus is highly susceptible to DOT1L and MLL1 inhibition and that DOT1L and MLL1 inhibitors might be suitable for use in combination with FLT3 inhibitors to treat ~30% of AML leukemias that bear *FLT3-ITD* mutations.

4.3 PRC2 PATHWAY ACTIVATION BY MLL-FUSION MEDIATED H3K79ME2 PROMOTES LEUKEMIA SURVIVAL

In addition to affecting the FLT3-ITD/STAT5A signaling pathway, I observe that H3K79me2 depletion disrupts PRC2 function by downregulating the PRC2 components *EZH2* and *EED* and globally reducing H3K27me3 (Figure 2.11). The effects of H3K79me2 depletion on *EZH2* and *EED* expression are likely direct as both genes are MLL-AF4 targets (Wilkinson et al., 2013). My observation that *EZH2* overexpression can partially rescue the effects of low dose DOT1L inhibition are consistent with previous findings that global reductions in repressive H3K27me3 reduce the survival of MLL-r leukemia and that PRC2 function is necessary for MLL-AF9 induced leukemia (Neff et al., 2012; Shi et al., 2013; J. Zhou et al., 2011). *EZH2* is upregulated in many cancers and activating mutations have been observed in several types of lymphoma (Gibaja et al., 2016).

Just how this modification cooperates with MLL-r leukemia is not understood. However, I find that treatment of MV4;11 cells with the EZH2 inhibitor EI1, at doses that more thoroughly deplete H3K27me3, causes reductions in *MEIS1* and *HOXA9* expression. It will require further investigation to determine why H3K27me3, a modification that represses transcription and is antagonistic to H3K4me3 (D.-H. Kim et al., 2013) is necessary for expression of these genes. Ironically, H3K4me3 is also necessary for *HOXA9* and *MEIS1* expression suggesting there could be either a complex interplay between these opposing histone modifications at these loci that promotes gene activation or the effect of H3K27me3 is indirect and instead involves perhaps the repression of transcriptional repressor of *HOXA9* and *MEIS1*. Interestingly, Stat5 recruits Ezh2 to the *Igk* promoter to facilitate deposition of H3K27me3 and gene silencing in mouse B-cell progenitors (Mandal et al., 2011). Perhaps this is a common mechanism of gene repression and

reduced activation of STAT5A in response to DOT1L inhibition in MLL-r leukemia relieves H3K27me3 inhibition through reduced targeting of the PRC2 complex at loci of tumor suppressors or differentiation factors.

There are many small molecule inhibitors of EZH2, some in clinical trials for the treatment of lymphoma and leukemia (Gibaja et al., 2016). My work, uncovering cooperation between MLL-rearrangements and PRC2 function, suggests that it may be of benefit to use EZH2 and DOT1L inhibitors in combination for the treatment of MLL-r leukemia.

4.4 H3K79ME2 IS NECESSARY FOR PTBP1-MEDIATED ALTERNATIVE SPLICING EVENTS

In MLL-r leukemia, aberrantly high H3K79me2 levels at hundreds of genes are not only involved in gene activation but, also have a pronounced effect on alternative splicing (T. Li et al., 2018). Previous studies observed enrichment of H3K79me2, that was especially high in some MLL-r leukemia cells lines, at sites of alternative splicing (T. Li et al., 2018; Ye et al., 2014). Depleting H3K79me2 resulted in genome-wide changes in alternative splicing with the majority of effects resulting in exon inclusion (T. Li et al., 2018). These sites of alternative splicing were found to be enriched for the consensus binding sequences of several splicing factors including PTBP1, however there was no elucidation of how H3K79me2 affects alternative splicing and what factors might be involved. Using the Leafcutter software package, I identified 71 previously unknown H3K79me2-mediated alternative splicing events in MV4;11 cells though low-dose DOT1L inhibition, the majority of which were exon inclusion events. As the Leafcutter software uses a stringent method for calling alternative splicing events that relies on the detection of reads that span exon junctions, this value is likely to be conservative and may be just the tip of

the iceberg of genome-wide effects on alternative splicing. The Li et al. study identified hundreds of genes that were enriched for H3K79me2 and alternatively spliced across cell types (T. Li et al., 2018), indicating the potential magnitude of H3K79me2-regulated alternative splicing events. An analysis with less conservative detection software and/or greater sequencing depth would provide a more definitive examination of the scope of H3K79me2-mediated changes in alternative splicing.

Using modified nucleosomes in pulldowns from nuclear extract I identified several splicing factors that interact specifically with H3K79me2 over H3K79me3 and observed that knocking down one of those factors, *PTBP1*, causes similar effects on splicing as DOT1L inhibition at several loci, suggesting that PTBP1 is necessary for H3K79me2-mediated alternative splicing. To my knowledge, this is the first observed interaction between H3K79me2 and splicing factors and the first described mechanism of H3K79me2-mediated alternative splicing. It would be interesting to know if the abundance of splicing and RNA processing factors that were enriched in the H3K79me2 nucleosome pulldowns are part of the same complex or make up different complexes. Separate complexes RNA processing factors may have additional roles in splicing and gene expression that could provide further mechanistic characterizations of known functions of H3K79me2.

PTBP1 also interacts with H3K36me3 through the MRG15 PWWP domain and is recruited to loci enriched with H3K36me3 to repress exon inclusion (Luco et al., 2010). Interestingly, I observe an increase of H3K36me3 within gene bodies genome-wide after 10 nM pinometostat treatment. It is possible that a global increase in H3K36me3 might titrate PTBP1 away from genomic loci where it is involved in alternative splicing events to reduce its effect on splicing. This effect could be in addition to reduced recruitment from

H3K79me2 or might serve as the sole source of H3K79me2 effects on splicing from pinometostat treatment.

Additionally H3K36me3- and/or H3K79me2-mediated effects on the rate of transcriptional elongation through interactions with the FACT nucleosome remodeling complex and associations with components of the transcriptional elongation complex, respectively may affect alternative splicing (Bitoun et al., 2007; Carvalho et al., 2013; Mohan et al., 2010; Mueller et al., 2007, 2009; Pavri et al., 2006). If perturbations to the distribution of H3K36me3 and/or H3K79me2 affect the rate of elongation this could in turn affect alternative splicing as has been shown previously through expression of a slower mutant pol II (De La Mata et al., 2003). Further investigations are needed to determine if pinometostat-induced changes in H3K36me3 or potential changes to the polymerase elongation rate affect H3K79me2-regulated alternative spicing.

In addition to its well-characterized role in splicing, PTBP1 has been implicated in the maintenance of several cancer types. Knockdown of *PTBP1* reduces the proliferation and of breast, prostate and ovarian cancers (He et al., 2007, 2014; W. Jin et al., 2000; C. Wang et al., 2008; X. Wang et al., 2018). In what is to my knowledge the first examination of the role of PTBP1 in MLL-r leukemia survival, I find that *PTBP1* knockdown also reduces proliferation in the MLL-r leukemia cell line MV4;11. How PTBP1 promotes the survival of many cancer types is not well understood (He et al., 2007, 2014; W. Jin et al., 2000; C. Wang et al., 2008; X. Wang et al., 2018). But, PTBP1's effects on growth signaling in breast cancer could be a more common mechanism, typical of this protein's role in promoting proliferation in other malignancies. In the MDA-MB-231 breast cancer cell line *PTBP1* knockdown increases protein levels of the tumor suppressor PTEN, resulting in decreased phospho-AKT, reducing growth signaling and

proliferation (X. Wang et al., 2018). Consistent with this observation I find an increase in PTEN protein expression upon 10 nM pinometostat treatment but, surprisingly, I observe no overall increase in *PTEN* RNA transcript levels. However, H3K79me2 depletion results in a change in *PTEN* splicing toward exon inclusion that might have an effect on protein expression. Along with the increase in PTEN protein levels I observe a decrease in phosphorylated AKT, a component of the PI3K/AKT growth signaling pathway that regulates proliferation. However, we previously observed that *FLT3-ITD,* an activator of AKT signaling (Fathi et al., 2012), is downregulated by 10 nM pinometostat treatment and could be responsible for at least part of the reduction in AKT activation. But, the increase in PTEN protein levels and changes in alternative splicing at the *PTEN* locus suggest that H3K79me2/PTBP1 alternative splicing may play an important role in regulating the PI3K/AKT pathway and proliferation in leukemia.

4.5 H3K79ME2 IS INVOLVED IN EXTENSIVE HISTONE CROSSTALK

Several previous studies have observed crosstalk between histone modifications that either antagonize or promote one another, typically through modulating the enzymatic activity of other histone-modifying complexes (Dover et al., 2002; D.-H. Kim et al., 2013; Ng et al., 2002; Schmitges et al., 2011). The repressive modification H3K27me3 inhibits SET1-like complexes' deposition of H3K4me3 and H3k4me3 in turn inhibits PRC2 deposition of H3K27me3 (D.-H. Kim et al., 2013; Schmitges et al., 2011). Although it is known that H2B ubiquitination facilitates- and H3K27me3 antagonizes H3K79 methylation (S. Chen et al., 2015; Krogan et al., 2002), it is not well understood how H3K79me2 affects other histone modifications often found in close proximity on gene bodies and with similar associations with active transcription such as H3K4me3 and H3K36me3. A study by Bu et al. found SETD2-mediated crosstalk with

H3K79me2 in which perturbations to *SETD2* expression and the resulting changes in H3K36me3 levels were met by reciprocal changes H3K79me2 but, it was not determined if this antagonism was bidirectional (Bu et al., 2018).

Using calibrated ICeChIP-seq, I performed one of the first quantitative studies of the effects of DOT1L inhibitor treatment on the distribution of histone modifications and the first at low-dose inhibitor treatment, closer to the concentration where H3K79me2 depletion becomes apparent and affects might be more directly associated with depletion of the mark. Surprisingly I observed that, upon depletion of transcriptionally activating H3K79me2, H3K27me3 levels decreased globally, H3K4me3 levels increased at promoters and H3K36me3 decreased at promoters but increased in gene bodies.

The reductions in H3K27me3 are likely due to downregulation of the *EZH2* and *EED* components of the PRC2 complex from depletion of transcriptionally activating H3K79me2 at those loci. I was able to slightly recue MV4;11 proliferation by ectopic expression of *EZH2*, the catalytic subunit, suggesting that the reductions in H3K27me3 affect leukemia cell viability, as has been observed previously with EZH2 inihibitor concentrations that more dramatically decreased H3K27me3 (Ueda et al., 2014).

After I treated MV4;11 cells with a high concentration of an EZH2 inhibitor that severely depleted H3K27me3, I observed downregulation of *HOXA9* and *MEIS1*, a surprising and likely indirect effect given that H3K27me3 is a transcriptionally repressive modification. It would be interesting to know how these leukemic drivers were downregulated with more severe reductions in H3K27me3 and also how the much lower pinometostat-mediated reductions in H3K27me3 reduced MV4;11 proliferation if *HOXA9* and *MEIS1* expression was not affected. Even though EZH2 inhibition couldn't recapitulate the increases in expression of MHC class II genes caused

by DOT1L inhibition, reductions in H3K27me3 might still have been involved in the massive number of genes upregulated by 10 nM pinometostat treatment. Interestingly, STAT5A, the activation of which was reduced by pinometostat treatment, can recruit EZH2 to repress gene expression in certain contexts (Mandal et al., 2011). Perhaps the combined effect of reduced STAT5A activation and downregulation of EZH2 resulted in widespread gene activation from low-dose pinometostat treatment.

Pinometostat treatment resulted in H3K4me3 increases at promoters genome-wide, a surprising increase in a mark associated with transcriptional activation that was most pronounced at downregulated genes that had lost the most H3K79me2. It seems likely that this strange antagonism between H3K79me2 and H3K4me3 is mediated by LSD1. It has been previously observed that knockout or inhibition of LSD1 results in apoptosis and differentiation of MLL-r cells including MV4;11 and reductions in MLL-fusion target expression (Z. Feng et al., 2016). LSD1 is an H3K4me2-histone demethylase and a component of the MLL-supercomplex (McGrath et al., 2016). Interestingly, pharmacological inhibition of LSD1 has been observed to increase H3K4me2/3 at MLL-target genes (Fang et al., 2017; Z. Feng et al., 2016; Harris et al., 2012; McGrath et al., 2016). H3K79me2 depletion and a resulting loss of MLL-fusion complex recruitment would likely reduce LSD1 localization at MLL-fusion targets, increasing H3K4me2/3.

The increase in H3K36me3 in gene bodies that I observed from pinometostat treatment are interesting and perhaps very important for understanding MLL-r leukemogenesis. A previous study had found that knocking down or overexpressing *Setd2* could increase or decrease H3K79m2 levels, respectively, in *MLL-AF9* expressing mouse hematopoietic progenitors (Bu et al., 2018). My results show that this antagonism is reciprocal and that reductions in H3K79me2

can cause increases in H3K36me3. Another study be Zhu et al. observed that LEDGF, a component of the MLL-fusion complex, necessary for MLL-fusion targeting and leukemogenesis (Okuda et al., 2014), has a higher affinity for H3K36me2 than H3K36me3 (L. Zhu et al., 2016). This suggests that an increase in H3K36me3, if it is at the expense of H3K36me2, as SETD2 requires H3K36me2 to convert to H3K36me3, could reduce localization of the MLL-fusion complex through a loss of LEDGF-mediated recruitment (Edmunds et al., 2008). Zhu et al. found that *Setd2* knockdown increased the expression of the *Meis1* and *Mef2c* oncogenes and increased Mll1 but not MLL-fusion localization to fusion targets (L. Zhu et al., 2016). Furthermore, knockdown of the histone methyltransferase *Ash1l*, responsible for H3K36me2 at many MLL-fusion targets resulted in reduced Mll1 localization and expression of *Hoxa9* (L. Zhu et al., 2016).

A dependence of MLL-r leukemia on H3K36me2 for proper targeting of the MLL1 complex (a necessary cofactor of the MLL-fusion protein in leukemogenesis), via LEDGF to activate expression of oncogenic drivers, could explain the high incidence of coinciding *SETD2* loss-of-function mutations in MLL-r leukemia (X. Zhu et al., 2014). It is also possible that the role of H3K79me2 in MLL-r leukemia mediated gene activation is through antagonism of H3K36me3 to increase H3K36me2 and facilitate MLL1 recruitment. Crucially, the mechanism of H3K36me3/H3K79me2 antagonism is yet to be resolved and future investigations should determine whether it is a direct enzymatic inhibition, as occurs between the methyltransferases that deposit H3K27me3 and H3K4me3, or if it involves the recruitment of intermediary factors such as demethylases.

Table 4.1: List of 10 nM pinometostat-mediated alternative splicing events

gene	chromosome	intron start	intron end	p.adjust	deltaPSI	classification
AK2	chr1	33031661	33036736	0.0469	-0.0057	exon inclusion
LYST	chr1	235829039	235830226	0.0440	0.0662	exon exclusion
SMYD3	chr1	246053069	246108080	0.0303	0.0006	other
RPS6KA1	chr1	26546035	26546867	0.0433	0.1111	alt. start site
LRRC8D	chr1	89822185	89843638	0.0184	0.3087	alt. start site
MDM4	chr1	204537497	204538209	0.0433	-0.0045	exon inclusion
RPS24	chr10	78040225	78040615	0.0000	-0.0502	exon inclusion
PTEN	chr10	87927599	87931046	0.0134	-0.0284	exon inclusion
ABI1	chr10	26771089	26777065	0.0386	-0.0760	exon inclusion
HNRNPF	chr10	43396590	43409131	0.0052	-0.0818	alt. start site
MS4A6A	chr11	60183331	60184320	0.0433	-0.0570	alt. start site
CHKA	chr11	68081457	68097019	0.0418	0.1629	alt. start site
ARAP1	chr11	72692785	72693325	0.0257	-0.1690	exon inclusion
PFDN5	chr12	53297924	53298045	0.0404	0.0098	other
MYL6	chr12	56160670	56161387	0.0184	-0.0255	exon inclusion
RP11-497G19.1	chr12	116698363	116702793	0.0088	-0.0005	other
FAM60A	chr12	31305123	31326024	0.0196	0.0382	exon exclusion
ACIN1	chr14	23090101	23090522	0.0371	-0.0894	exon inclusion
ZFAND6	chr15	80098578	80120328	0.0369	-0.0122	alt. start site
FES	chr15	90891191	90891554	0.0075	-0.0061	exon inclusion
METTL26	chr16	635774	636094	0.0429	-0.0390	other
XPO6	chr16	28155975	28156074	0.0404	-0.1131	exon inclusion
EIF5A	chr17	7308113	7309615	0.0371	-0.0904	alt. start site
WSB1	chr17	27306882	27309100	0.0404	0.1363	exon inclusion
ZNF207	chr17	32366757	32367772	0.0006	-0.0605	exon inclusion
TMEM11	chr17	21211227	21214091	0.0404	-0.1117	exon inclusion
BECN1	chr17	42814008	42814524	0.0418	-0.0092	other
ARHGAP27	chr17	45404334	45404445	0.0116	-0.2076	exon inclusion
MBTD1	chr17	51259206	51260120	0.0404	0.0444	exon inclusion
SRSF2	chr17	76735875	76736154	0.0386	-0.0047	exon inclusion
ISOC2	chr19	55455845	55456349	0.0374	-0.0566	exon inclusion
XPO1	chr2	61525333	61526420	0.0020	-0.0412	exon inclusion
BAZ2B	chr2	159431156	159432757	0.0194	-0.0959	exon inclusion
MRPL33	chr2	27774530	27779433	0.0188	-0.0336	other
UGP2	chr2	63842204	63856306	0.0404	0.1553	alt. start site
UGGT1	chr2	128156415	128157252	0.0404	-0.0781	exon inclusion
HMGN1	chr21	39347952	39348292	0.0301	-0.0018	exon inclusion
CMC1	chr3	28294529	28316333	0.0418	-0.0085	exon inclusion
MBNL1	chr3	152396224	152414941	0.0000	0.0078	alt. start site

Table 4.1, continued.

EIF4A2	chr3	186788420	186789125	0.0013	0.0376	exon exclusion
SATB1	chr3	18420991	18445518	0.0007	-0.0276	alt. start site
WDR49	chr3	167651746	167653261	0.0404	0.0489	other
TRA2B	chr3	185931852	185937825	0.0006	-0.0207	exon inclusion
DCAF16	chr4	17809692	17810447	0.0303	0.0890	exon inclusion
TMEM165	chr4	55416157	55417072	0.0116	-0.0524	exon inclusion
EMB	chr5	50416090	50428144	0.0075	-0.0043	other
EMB	chr5	50428227	50442952	0.0003	0.0344	alt. start site
H2AFY	chr5	135359628	135360497	0.0000	-0.0004	other
RPS14	chr5	150447735	150449703	0.0039	-0.0240	exon exclusion
DCTN4	chr5	150756487	150779415	0.0088	0.0437	other
AHRR	chr5	420216	422729	0.0386	0.1361	other
PARP8	chr5	50666997	50667085	0.0429	0.0662	alt. start site
PARP8	chr5	50760362	50761821	0.0386	-0.0150	exon inclusion
MATR3,SNHG4	chr5	139308327	139314675	0.0007	-0.0832	other
SIRT5	chr6	13599155	13600834	0.0439	0.0761	exon inclusion
HLA-A,HLA-H	chr6	29943543	29944122	0.0418	-0.1808	other
HLA-A,HLA-H	chr6	29945091	29945234	0.0386	-0.1064	other
LST1	chr6	31587966	31588563	0.0014	-0.0055	exon inclusion
UTRN	chr6	144344304	144403123	0.0404	0.2680	alt. start site
MCM3	chr6	52265385	52266075	0.0404	-0.0213	exon inclusion
SNX14	chr6	85538864	85541985	0.0117	-0.0801	exon inclusion
HNRNPA2B1	chr7	26192338	26192495	0.0043	0.0430	exon inclusion
GSAP	chr7	77326273	77328606	0.0371	-0.2504	alt. start site
RMDN1	chr8	86484961	86486484	0.0113	-0.0510	exon inclusion
PVT1	chr8	127984204	127989162	0.0303	0.0144	other
SLC44A1	chr9	105275518	105299220	0.0088	-0.0281	other
ODF2	chr9	128457437	128459567	0.0418	-0.0558	exon inclusion
GLE1	chr9	128507340	128508876	0.0404	0.0699	exon exclusion
FLNA	chrX	154357274	154357434	0.0088	-0.0428	exon inclusion
NONO	chrX	71285097	71290629	0.0257	-0.0021	exon exclusion
MORF4L2	chrX	103685260	103687989	0.0144	-0.1216	alt. start site

Table 4.2: List of qPCR and shRNA oligonucleotides

qPCR oligos		
gene	**sequence**	**reference**
HLD-DRA qPCR F	CTCAGGAATCATGGGCTATCAA	
HLA-DRA qPCR R	CTCATCACCATCAAAGTCAAACAT	

Table 4.2, continued.

HLA-DRB1 qPCR F	GTGACACTGATGGTGCTGAG	
HLA-DRB1 qPCR R	GCTCCGTCCCATTGAAGAAA	
MEF2C qPCR F	GTCTGAGGACAAGTACAGGAAAA	
MEF2C qPCR R	GAGACTGGCATCTCGAAGTT	
FLT3 qPCR F	ATCATATCCCATGGTATCAGAATCC	
FLT3 qPCR R	GAAGCAGATACATCCACTTCCA	
ARID3B qPCR F	AGACCATACCAAAGATGCTTCC	
ARID3B qPCR R	ATCATCACTCCAGGCCAAAC	
STAT5A qPCR F	CAGATGCAGGTGCTGTACG	
STAT5A qPCR R	TGTCCAAGTCAATGGCATCC	
PIM2 qPCR F	ATGTTGACCAAGCCTCTACA	
PIM2 qPCR R	TCGATACTCGGCCTCGAA	
MEIS1 qPCR F	AGACGATAGAGAAGGAGGATCAA	
MEIS1 qPCR R	CCGTGTCATCATGATCTCTGTT	
HOXA9 qPCR F	AGGCGCCTTCTCTGAAA	
HOXA9 qPCR R	GTTGGCTGCTGGGTTATTG	
PBX3 qPCR F	CCACCAGATCATGACCATCAC	
PBX3 qPCR R	AAGAGCGCTGGTTTCATTCT	
CEBPA qPCR F	CCTTCAACGACGAGTTCCT	
CEBPA qPCR R	GCCCGGGTAGTCAAAGTC	
CSF1R qPCR F	GCCATCCACCTCTATGTCAAA	
CSF1R qPCR R	AGCAGACAGGGCAGTAGT	
B2M qPCR F	CTCTCTCTTTCTGGCCTGGAG	
B2M qPCR R	TCTGCTGGATGACGTGAGTA	
SPI1 qPCR F	TGCCCTATGACACGGATCTA	
SPI1 qPCR R	GTCCCAGTAATGGTCGCTATG	
CSF3R qPCR F	CTATGGCAAGGCTGGGAAA	
CSF3R qPCR R	GGGCTGAGACACTGATGTG	
PIM1 qPCR F	GTGGAGAAGGACCGGATTTC	
PIM1 qPCR R	TTCTTCAGCAGGACCACTTC	
PBX3 qPCR F	CAAAGAAACATGCCCTGAACTG	
PBX3 qPCR R	CTCTGATGCTGAGACCTGTTT	
18S (RNA18S5) F	CGCAGCTAGGAATAATGGAATAGG	
18S (RNA18S5) R	GCCTCAGTTCCGAAAACCAA	
CIITA qPCR F	CTGTGCCTCTACCACTTCTATG	
CIITA qPCR R	GTCGCAGTTGATGGTGTCT	
EZH2 qPCR F	GGAGGATCACCGAGATGATAAAG	

Table 4.2, continued.

EZH2 qPCR R	TTCTGCTGTGCCCTTATCTG	
EED qPCR F	CTGGCACAGTAAAGAAGGAGAT	
EED qPCR R	GCATCAGCATCCACGTAAGA	
SATB1 iso 209 qPCR F	ACATCTCCTGTAGGGCTAGAT	
SATB1 iso 209 qPCR R	CTGAGTTGCCTCGTTCAAATG	
SATB1 iso 205 qPCR F	GGAGCCGTTCTTGGTTTCA	
SATB1 iso 205 qPCR R	GCCTCGTTCAAATGATCCATACT	
SATB1 iso 203 qPCR F	CGGAGAGGTGATCTTTAGACAG	
SATB1 iso 203 qPCR R	CCCTTCGGATCACTCACATT	
H2AFY iso 202 qPCR F	CCCGACAAACACTGACTTCTAC	
H2AFY iso 202 qPCR R	CAGGACAGCTTCCACAAACT	
H2AFY iso 201 qPCR F	TTTGAGGTGGAGGCCATAATC	
H2AFY iso 201 qPCR R	ACTCCTTGCCACCTTTCTTC	
ABI1 qPCR iso 204 F	CCATGGTGTCAAGTGGCTAAA	
ABI1 qPCR iso 204 209 R	CGGTTTCTGAGTAGGAGGATTTG	
ABI1 qPCR iso 209 F	TACACAGTTCTGGATGATGTGG	
PTBP1 qPCR F	TCATCGTGGAGAACCTCTTCTA	
PTBP1 qPCR R	TGTTCTTGGTGAAGGTGATGAT	
shRNA oligos	**sequence**	**reference**
scrambled shRNA F	CCGG TTCTCCGAACGTGTCACGTTT CTCGAG AAACGTGACACGTTCGGAGAA TTTTT	(Yuan et al., 2009)
scrambled shRNA R	AATTAAAAA TTCTCCGAACGTGTCACGTTT CTCGAG AAACGTGACACGTTCGGAGAA	(Yuan et al. 2009)
FLT3 shRNA 2F	CCGG GCATCCCAGTCAATCAGCTTT CTCGAG AAAGCTGATTGACTGGGATGC TTTTT	(Green et al., 2015)
FLT3 shRNA 2R	AATTAAAAA GCATCCCAGTCAATCAGCTTT CTCGAG AAAGCTGATTGACTGGGATGC	(Green et al. 2015)
GFP shRNA F	CCGG GCAAGCTGACCCTGAAGTTCAT CTCGAG ATGAACTTCAGGGTCAGCTTGC TTTTT	(Scheeren et al., 2005)
GFP shRNA R	AATTAAAAA GCAAGCTGACCCTGAAGTTCAT CTCGAG ATGAACTTCAGGGTCAGCTTGC	(Scheeren et al. 2005)
PTBP1 shRNA F	CCGG AACTTCCATCATTCCAGAGAA CTCGAG TTCTCTGGAATGATGGAAGTT TTTTT	(Coelho et al., 2015)
PTBP1 shRNA R	AATTAAAAA AACTTCCATCATTCCAGAGAA CTCGAG TTCTCTGGAATGATGGAAGTT	(Coelho et al. 2015)

Table 4.3: List of antibodies for ChIP-seq and Western blotting

Western blotting			
target	**provider**	**cat #**	**lot #**
HOXA9	Proteintech	18501-1-AP	NA
MEIS1	EMD Millipore	ABE2864	Q2933434
H3	Active Motif	61277	
H3K79me2	Abcam	ab3594	GR173874
FLT3	Cell Signaling	3462S	14
GAPDH	Cell Signaling	5174S	7
STAT5A	Cell Signaling	94205T	1
p-STAT5	Cell Signaling	9359S	9
H3K27me3	Cell Signaling	9733S	14
H3K4me3	Cell Signaling	9751S	9
EZH2	Cell Signaling	5246S	1
LEDGF	Bethyl	A300-848A	A300-848A-1
RBBP5	Bethyl	A300-109A	3
HNRNPK	Abcam	ab70492	GR175966-6
H4	Active Motif	61299	
MBD3	Bethyl	A302-529A	A302-529A-1
PTBP1	ThermoFisher Scientific	32-4800	TG268402
myc	Abcam	ab32	GR3109353-2
anti-rabbit	Cell Signaling	7074S	
anti-mouse	Thermo Scientific	31432	
THRAP3	Bethyl	A300-956A	A300-956A-1
SSRP1	Abcam	ab21584	GR55713-1
ICeChIP-seq			
name	**provider**	**cat #**	**lot #**
H3K79me2	Abcam	ab3594	GR173874
H3K27me3	Cell Signaling	9733	8
H3K4me3	Abcam	12209	GR275790-1
H3K36me3	RevMab	31-1051-00	R-05-01575

APPENDIX A: SOLUTION MASS SPECTROMETRY ANALYSIS OF H3K79ME2-MODIFIED NUCLEOSOME PULLDOWNS FROM NUCLEAR EXTRACT

This appendix describes in brief, the use of reconstituted nucleosomes in pulldown assays from nuclear extract to identify binders of H3K79me2. Nucleosomes were reconstituted with a biotinylated 601 sequence (Lowary & Widom, 1998) with an extra linker for a total of 153 bp and H3 unmodified or containing the H3K79me2 modification (Figure A1.1A). Nucleosomes were bound to streptavidin beads and incubated with HeLa cell nuclear extract. The samples were washed and the nucleosomes and bound proteins were eluted from the beads through heated incubation with a high concentrations SDS buffer. This eluted sample was then sent to MS Bioworks (Ann Arbor, Michigan) where the samples were run on SDS-PAGE, segmented (10 gel segments per sample), subjected to in-gel trypsin digestion followed by LC/MS/MS and database searching for protein identification (Figure A1.1B).

The most enriched proteins in the H3K79me2 pulldowns compared to the unmodified nucleosome controls included many splicing and RNA processing factors (Figure A1.1C). The dimeric FACT complex components SSRP1 and SUPT16H were among the proteins with the highest enrichment and coverage. In separate experiments of nucleosome pulldowns from HEK293 nuclear extract followed by Western blotting I observed H3K79me2-enrichment of the SSRP1 suggesting the FACT complex can recognize H3K79me2 (Figure A1.1D).

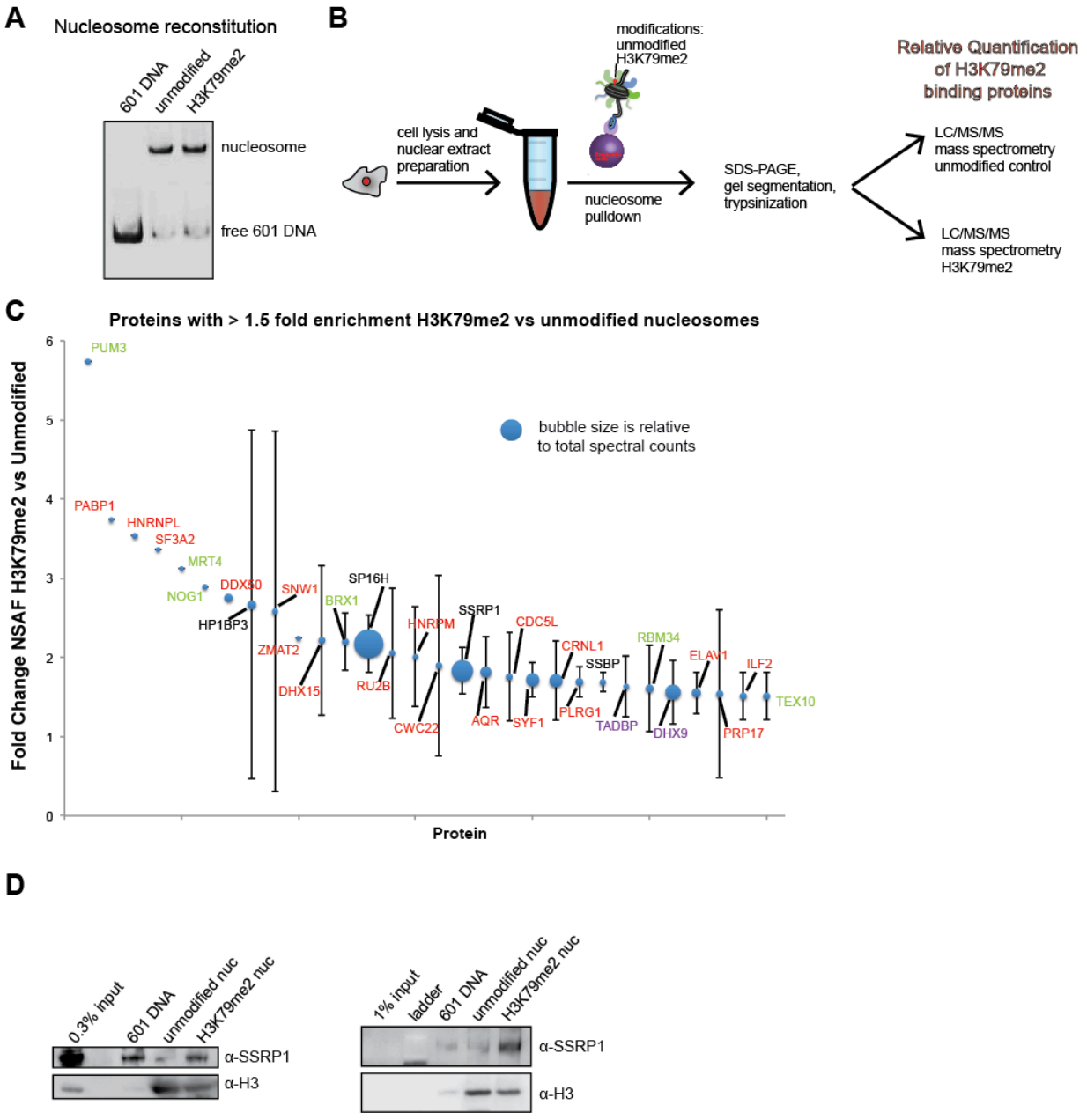

Figure A.1 Solution mass spectrometry analysis of H3K79me2 vs. unmodified nucleosome pulldowns.

A. Experimental workflow for nucleosome pulldowns followed by mass spectrometry. Nuclear extract was obtained from HeLa cells and incubated with reconstituted nucleosomes either unmodified or containing H3K79me2 bound to streptavidin beads. Eluted nucleosomes and bound protein samples were then processed by MS Bioworks. Samples were run on a10% Bis-Tris Novex mini-gel (Invitrogen) in MOPS buffer. The gel was sectioned into 5 slices of increasing molecular weight. These slices were then tripsonized and run by LC/MS/MS using an Orbitrap mass analyzer (Thermo Fisher) and proteins were identified. **B.** 2 µl of 601 DNA, unmodified or H3K79me2 reconstituted nucleosomes were run on a 5% TBE native gel and stained with SYBR gold (DNA) to visualize reconstituted nucleosomes and free DNA. **C.** Plot of

Figure A.1, continued.
the proteins enriched > 1.5-fold for H3K79me2 over unmodified nucleosomes. The y axis is the normalized spectral abundance factor (NSAF = (spectral counts (SpC)/protein length (L))/ sum of SpC/L for all proteins) and the size of each bubble is relative to the total spectal counts. The FACT complex components SSRP1 and SUPT16H are highly enriched for H3K79me2. **D.** Western blot for SSRP1 and H3 as a loading control from DNA or nucleosome pulldowns from HEK293 nuclear extract.

APPENDIX B: MASS SPECTROMETRY ANALYSIS OF HEAVY OXYGEN LABELED NUCLEOSOME PULLDOWNS

The solution mass spectrometry analysis by MS Bioworks identified several proteins that were narrowly enriched (< 4-fold) in the H3K79me2 nucleosome pulldowns. I wanted to find a more quantitative mass spectrometry approach that would improve the resolution and better distinguish H3K79me2 binders from non-specific background or mass spec run bias. Heavy oxygen labeling during trypsinization would differentially label the H3K79me2 and unmodified nucleosome pulldown samples, thereby permitting both control and experimental samples to be run in the same analysis eliminating potential variation between mass spec runs (Figure B1.1A).

I once again performed nucleosome pulldowns using H3K79me2- and H3K36me3-modified nucleosomes incubated with HeLa nuclear extract. The H3K36me3-modified nucleosomes were a more suitable control for pan-methyl binding proteins than the unmodified nucleosomes that were used previously. The ^{18}O labeling, LC/MS/MS and protein identification was done by Don Wolfgeher of the University of Chicago Proteomics Core Facility. The pulldowns were repeated for a total of two replicates and were analyzed in both the forward and reverse labeling scheme for both experiments.

Experiment 1 (the first set of replicates) revealed that 4 out of 6 members of the PAF complex were highly enriched in the H3K79me2 pulldown in both the forward and reverse mass spec analyses (Figure B1.1B). The members of the FACT complex and the RNA processing

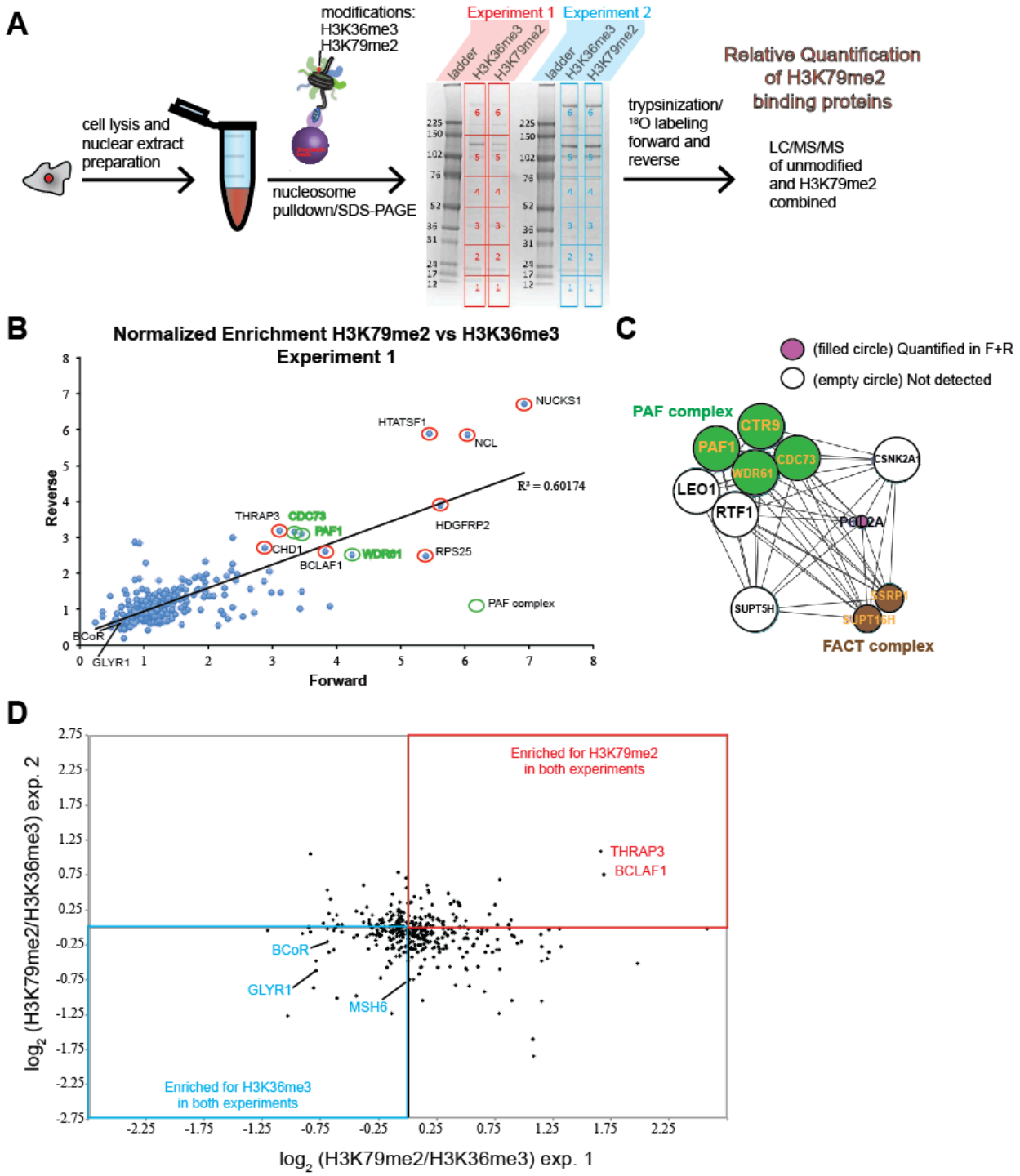

Figure B.1 Heavy oxygen labeling and mass spectrometry analysis of H3K79me2 and H3K36me3 nucleosome pulldowns.

A. Experimental workflow for nucleosome pulldowns followed by ^{18}O labeling and mass spectrometry for 2 experiments. Nuclear extract was obtained from HeLa cells and incubated with reconstituted nucleosomes containing either H3K79me2 or H3K36me3 bound to streptavidin beads. Eluted nucleosomes and bound protein samples were then processed by the

Figure B.1, continued.
University of Chicago Proteomics Core and run by SDS-PAGE. The gel was sectioned into 6 slices of increasing molecular weight. These slices were then split in two for tripsinization in the presence of heavy oxygen water for labeling in the forward and reverse directions. Labeled H3K36me3 and H3K79me2 pulldown samples were then combined and run together for LC/MS/MS and proteins were identified. **B.** A scatterplot of the H3K79me2/H3K36me3 fold-enrichment (normalized to H3) in the forward vs. reverse ^{18}O labeling directions from a mass spectrometry analysis of experiment 1. Several proteins including members of the PAF complex (green outline) and THRAP3 and BCLAF1 are enriched for H3K79me2 nucleosomes. **C.** STRING interactome for PAF1 protein (confidence >0.98). 4 out of 6 members of PAF complex were highly enriched for H3K79me2 in experiment 1. Circle size is proportional to avg. enrichment. Other detected interactors include FACT complex members and POL2A. **D.** Scatterplot of protein $\log_2$ fold-enrichment (H3 normalized) H3K79me2/H3K36me3 from the averages of the forward and reverse ^{18}O labeling mass spectrometry analyses of experiment 1 vs. 2. The red rectangle highlights the quadrant of H3K79me2-enriched proteins in both experiments while the blue rectangle includes those proteins that are enriched for H3K36me3 that includes many known binders of this modification highlighted in blue.

factors THRAP3 and BCLAF1 were also highly enriched for the H3K79me2 pulldown. A STRING interactome analysis for PAF1 reveals known interactions with the H3K79me2-enriched proteins of the FACT complex and POL2A (Figure B1.1C).

A plot of the fold-enrichment of proteins identified in the H3K79me2 vs H3K36me3 pulldowns for both experiments for forward and reverse labeling (a total of 4 analyses), shows a strong enrichment of THRAP3 and BCLAF1 for H3K79me2 (Figure B1.1D). I also observed an enrichment of many known binders of H3K36me3, demonstrating the effectiveness of this methodology in identifying binders of histone modifications.

APPENDIX C: TANDEM PULLDOWNS REVEAL THRAP3 NUCLEOSOME-BINDING COMPLEX MEMBERS

To further examine if THRAP3 and BCLAF1 specifically recognize H3K79me2 I transiently transfected FLAG-tagged THRAP3 and BCLAF1 into HEK293 cells and performed nucleosome pulldowns from nuclear extract followed by Western blotting for FLAG-tagged proteins. Although BCLAF1 was very difficult to express, I eventually observed enrichment of both BCLAF1 and THRAP3 in the H3K79me2-modified nucleosome pulldowns over H3K36me3 or unmodified nucleosomes (Figure B2.1A).

Because neither THRAP3 nor BCLAF1 contain any known methylation-binding domains and in vitro analyses revealed no affinity of purified FLAG-THRAP3 or expressed fragments for H3K79me2-modified nucleosomes (data not shown) I wanted to determine if these proteins were indirectly binding H3K79me2 through another protein. To determine the identity of a putative THRAP3 complex that is capable of binding H3K79me2-modified nucleosomes I performed a tandem pulldown of ectopically expressed FLAG-tagged THRAP3 followed by a nucleosome pulldown of the eluted THRAP3 complex. A mass spectrometry analysis of bands excised from a silver-stained SDS-PAGE of unmodified or H3K79me2-modified THRAP3 tandem pulldowns showed an enrichment of splicing and RNA processing factors in the H3K79me2 samples (Figure B2.1B). However, I was unable to identify any H3K79me2-enriched proteins with known methyl-binding domains.

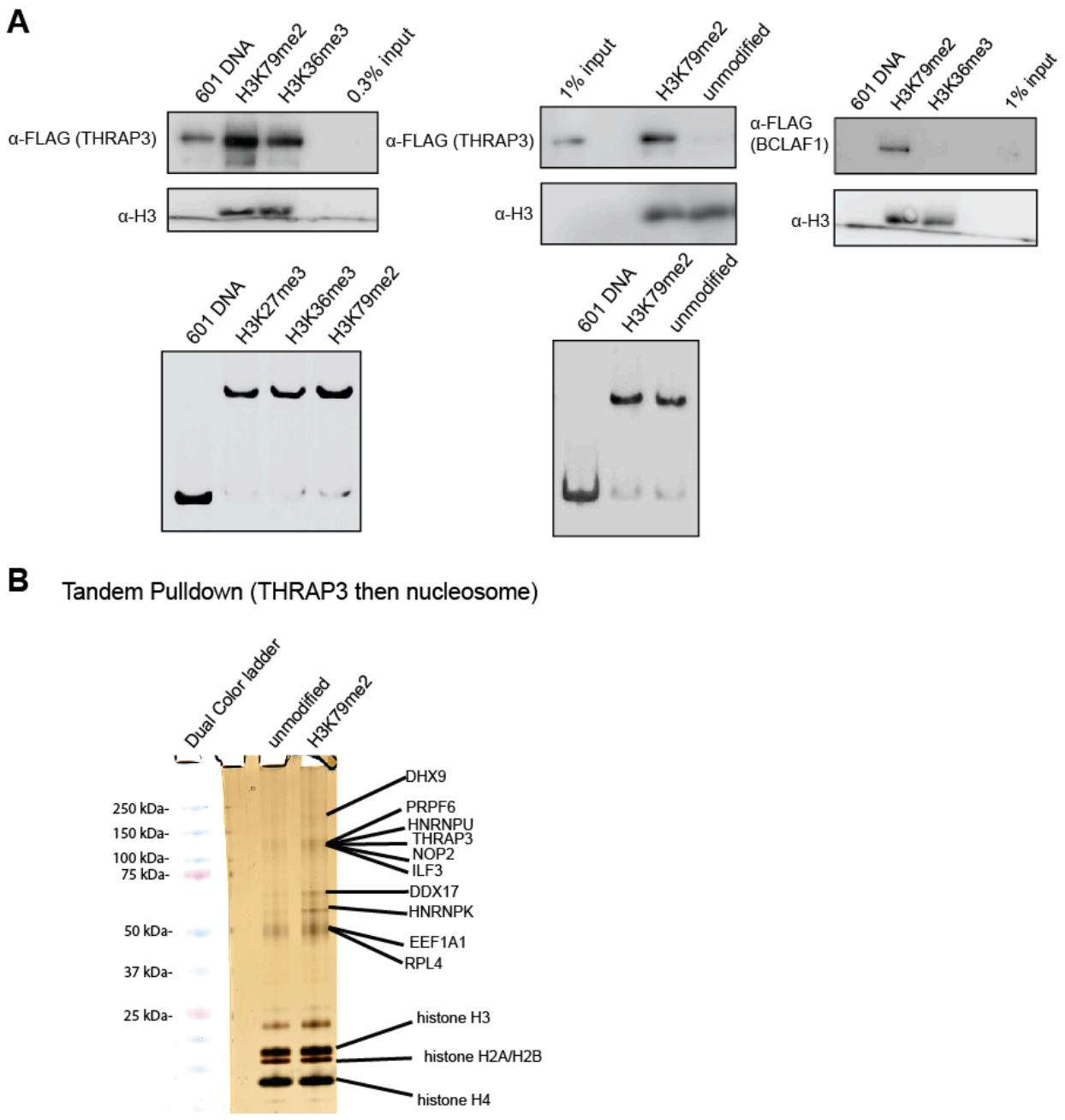

Figure C.1 THRAP3 recognizes H3K79me2-labeled nucleosomes.
A. Western blots for FLAG (THRAP3) or FLAG (BCLAF1) and H3 as a loading control of nucleosome pulldowns from nuclear extract from HEK293 cells transiently transfected with FLAG-THRAP3. (below) SYBR gold DNA staining of 2 µl of each reconstitution of the nucleosomes used for the above pulldowns. **B.** Silver-stained SDS-PAGE of tandem pulldowns in which an α-FLAG pulldown of FLAG-THRAP3 followed by 3X FLAG peptide elution was followed by nucleosome pulldowns of the FLAG-THRAP3 eluate. The proteins indicated were identified as enriched in the H3K79me2 nucleosome pulldowns over the unmodified pulldowns by mass spectrometry analysis of excised bands.

APPENDIX D: MASS SPECTROMETRY ANALYSIS OF H3K79ME2-MODIFIED NUCLEOSOME PULLDOWNS FROM BIOCHEMICALLY FRACTIONATED NUCLEAR EXTRACT

The nucleosome complex, with its abundance of protein and DNA interfaces generates an enormous amount of background, off-target binding that has the potential to dwarf the signal of any binder of the miniscule, uncharged methyl groups on lysine 79 of histone H3. Fractionating the nuclear extract and probing the different fractions for H3K79me2 binders provides the advantage of simplifying the pool of non-specific binders and reducing background. In an attempt to boost the signal of any potential H3K79me2 binder I fractionated HeLa nuclear extract by applying it to a heparin sepharose column and then eluted the bound proteins with stepwise increases in salt concentration. I then probed the different fractions for H3K79me2/3-specific binders through nucleosome pulldowns with unmodified or H3K36me3 as controls for nucleosome and pan-methyl binding proteins. A silver-stained SDS-PAGE gel of pulldowns from the 300 mM and 450 mM salt fractions reveals several bands that are highly enriched in the H3K79me2 pulldowns (Figure C2.1A). Mass spectrometry analyses of these excised bands and other revealed enrichment of the FACT complex and splicing factors over the corresponding section of the gel for the unmodified pulldowns (Figure C2.1B).

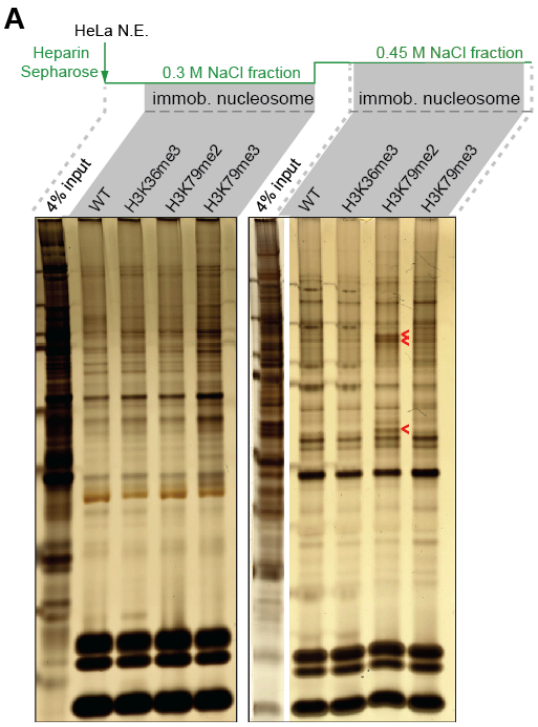

B

Gene	WT (unmodified) Unique Peptide Hits	H3K79me2 Unique Peptide Hits	H3K79me3 Unique Peptide Hits
HNRNPM	0	-	6
TRIM29	0	-	14
SF1	9	-	17
SSRP1	20	44	-
Supt16h	56	128	-

Figure D.1 Salt fractionation of nuclear extract reveals fraction-specific H3K79me2-recognizing proteins.
A. A silver-stained gel from unmodified, H3K36me3, H3K79me2 or H3K79me3 nucleosome pulldowns from the indicated salt elution fractions of HeLa nuclear extract eluted from heparin sepharose resin. Red arrows indicate bands that are unique to H3K79me2 nucleosome pulldowns. **B.** Table displaying the number of unique peptides from proteins enriched in H3K79me2/3 nucleosome pulldowns from fractionated HeLa nuclear extract identified from mass spectrometry analysis of excised gel bands.

APPENDIX E: MATERIALS AND METHODS FOR APPENDICES

Nuclear extraction

Resuspend HeLa cell pellet from 1L of culture in 10 ml of buffer A (10 mM Tris pH 7.9, 1.5 mM MgCl2, 10 mM KCl, and 0.5 mM DTT) and incubate on ice for 15 min. Lyse cells by gentle passage 20X through a 22 G needle mounted on a 20 ml syringe (Syringe and needle works better in my hand than dounce homogenizer in side-by-side comparison). Spin mixture at 1200 x g through a sucrose cushion (Sucrose Cushion: 30% sucrose (W/V), 1.5 mM MgCl2, 10 mM Tris, pH 7.9, 10 mM KCl, and 0.5 mM DTT- 7.5 ml in a 50 ml conical tube) for 10 min. in table-top swing bucket centrifuge. Carefully aspirate the supernatant to isolate the nuclei at the bottom of the tube. Gently resuspend the nuclei in 1.5 ml of buffer B (20 mM Tris pH 7.9, 25% glycerol, 210 mM NaCl, 1.5 mM MgCl2, 0.2 mM EDTA, 0.5 mM PMSF, and 0.5 mM DTT) then add 1.5 ml of Buffer C (20 mM Tris pH 7.9, 25% glycerol, 630 mM NaCl, 1.5 mM MgCl2, 0.2 mM EDTA, 0.5 mM PMSF, and 0.5 mM DTT) and mix well. Rock the mixture at 4 deg. C for 1 hour. Spin down the crude extract at 18-25,000 x g for 15 min. in a fixed angle rotor. Collect the supernatant and dilute with 3 volumes of buffer A. For fractionation on an FPLC spin again at 18-25,000 x g, pass through a 0.45 μm filter and load on the column.

Nuclear fractionation

Equilibrate a 5 ml heparin column with 2 column volumes (CVs) of buffer D (20 mM Tris pH 7.9, 10% glycerol, 100 mM NaCl, 1.5 mM MgCl2, 0.2 mM EDTA, 0.5 mM PMSF, and 0.5 mM DTT). Note: Column equilibration and sample loading is carried out on a peristaltic pump. Load nuclear extract from nuclear extraction on the column and collect the flow through. Elute stepwise with 2 CV of buffer I (20 mM Tris pH 7.9, 10% glycerol, 1.5mM MgCl2, 0.2 mM

EDTA, 0.5 mM PMSF, and 0.5 mM DTT) with 100, 200, 300 and 450 mM NaCl. Dilute the last elution to 300 mM salt with buffer I.

Nucleosome Pulldowns

Aliquot 57 µl of Myone Streptavidin T1 Dynabeads (Thermo Fisher cat # 65601) (slurry volume). Collect the beads on magnetic racks, and discard the supernatant. Resuspend in 500 µl buffer D (20 mM Tris pH 7.9, 10% glycerol, 100 mM NaCl, 1.5 mM MgCl2, 0.2 mM EDTA, 0.5 mM PMSF, and 0.5 mM DTT) collect the beads on magnetic racks, and discard the supernatant. Resuspend beads in 500 µl buffer D and add 50 pmol of freshly assembled nucleosome per pulldown and incubate at 4 deg. C by end-over-end rotation for 10 minutes. Take a Nanodrop reading of the supernatant to determine amount of free nucleosome in solution or collect supernatant and run on 6% native PAGE, saturation of the beads is assumed if significant amounts of nucleosome are present in the supernatant. Wash beads 2 x 500 µl with buffer D. Resuspend beads in 1 ml of diluted nuclear extract for each pulldown. Wash beads 4 x 1 mL of buffer J (20 mM Tris pH 7.9, 10% glycerol, 300 mM NaCl, 1.5mM MgCl2, 0.2 mM EDTA, 0.1% NP40, 0.5 mM PMSF, and 0.5 mM DTT) with 2 tube transfers (siliconized tubes should be used, the sequence is wash, tube transfer, wash, wash, tube transfer, wash). Elute from beads by resuspending in 30 µl 2X SDS-PAGE loading buffer, boil at 95 deg. C for 10 minutes. Load 3 µl of each sample on 4%-12% gradient gel (NuPAGE from Invitrogen) and image by silver stain.

Transfection

HEK293 cells were grown in a 10 cm^2 plate until ~70% confluency and then transfected using 6 µg pRuth3000-FLAG-THRAP3 or pRuth3000-FLAG-BCLAF1 plasmid DNA and 18 µl

Fugene (Promega cat # E2311). After 48 h cells were trypsinized and spun down and pellets were flash frozen and stored at -80 deg C.

Tandem (FLAG followed by nucleosome) pulldowns

100 µl of ANTI-FLAG M2 Affinity Gel slurry (Millipore Sigma cat # A2220) was equilibrated in 1 ml I200 (20 mM Tris pH 7.9, 10% glycerol, 200 mM NaCl, 1.5mM MgCl2, 0.2 mM EDTA, 0.5 mM PMSF, and 0.5 mM DTT) with end-over-end rotation for 10 min. at 4 deg. C and then spun down at 200 x g for 5 min at 4 deg. C. The supernatant was carefully removed and the gel was resuspended in 3 ml HEK293 nuclear extract diluted 1:3 in buffer A (10 mM Tris pH 7.9, 1.5 mM MgCl2, 10 mM KCl, and 0.5 mM DTT) and incubated at 4 deg. C with end-over-end rotation for 1 h. The sample was spun down at 200 x g for 5 min at 4 deg. C and washed 2 x 1 ml buffer I200. The sample was transferred to a 1.5 ml tube and eluted with 500 µl buffer I200 250 µg/ml 3X FLAG peptide for 30 min. at 4 deg. C with end-over-end roation. The sample was spun down at 200 x g for 5 min at 4 deg. C and the supernatant containing the FLAG-tagged protein was carefully transferred to a new tube. Repeat this elution 2 more times for a total of 3 elutions. 20 pmol nucleosomes bound to MyOne T1 streptavidin beads were added to 500 µl of the eluate and incubated 1 hour at 4 deg. C with end-over-end rotation. Wash beads 4 x 1 mL of buffer J (20 mM Tris pH 7.9, 10% glycerol, 300 mM NaCl, 1.5mM MgCl2, 0.2 mM EDTA, 0.1% NP40, 0.5 mM PMSF, and 0.5 mM DTT) with 2 tube transfers (siliconized tubes should be used, the sequence is wash, tube transfer, wash, wash, tube transfer, wash). Elute from beads by resuspending in 30 µl 2X SDS-PAGE loading buffer, boil at 95 deg. C for 10 minutes. Load 5 µl of each sample on 4%-12% gradient gel (NuPAGE from Invitrogen) and image by silver stain.

REFERENCES

Adam, M., Pogacic, V., Bendit, M., Chappuis, R., Nawijn, M. C., Duyster, J., Fox, C. J., Thompson, C. B., Cools, J., & Schwaller, J. (2006). Targeting PIM kinases impairs survival of hematopoietic cells transformed by kinase inhibitor-sensitive and kinase inhibitor-resistant forms of Fms-like tyrosine kinase 3 and BCR/ABL. *Cancer Research*, *66*(7), 3828–3835. https://doi.org/10.1158/0008-5472.CAN-05-2309

ALLFREY, V. G., FAULKNER, R., & MIRSKY, A. E. (1964). Acetylation and Methylation of Histones and Their Possible Role in the. *Proceedings of the National Academy of Sciences of the United States Of*, *51*(1938), 786–794. https://doi.org/10.1073/pnas.51.5.786

Amson, R., Sigaux, F., Przedborski, S., Flandrin, G., Givol, D., & Telerman, A. (1989). The human protooncogene product p33pim is expressed during fetal hematopoiesis and in diverse leukemias. *Proceedings of the National Academy of Sciences of the United States of America*, *86*(22), 8857–8861. https://doi.org/10.1073/pnas.86.22.8857

Anderson, C. J., Baird, M. R., Hsu, A., Barbour, E. H., Koyama, Y., Borgnia, M. J., & McGinty, R. K. (2019). Structural Basis for Recognition of Ubiquitylated Nucleosome by Dot1L Methyltransferase. *Cell Reports*, *26*(7), 1681-1690.e5. https://doi.org/10.1016/j.celrep.2019.01.058

Andersson, A. K., Ma, J., Wang, J., Chen, X., Gedman, A. L., Dang, J., Nakitandwe, J., Holmfeldt, L., Parker, M., Easton, J., Huether, R., Kriwacki, R., Rusch, M., Wu, G., Li, Y., Mulder, H., Raimondi, S., Pounds, S., Kang, G., … Downing, J. R. (2015). The landscape of somatic mutations in infant MLL-rearranged acute lymphoblastic leukemias. *Nature Genetics*, *47*(4), 330–337. https://doi.org/10.1038/ng.3230

Andersson, R., Enroth, S., Rada-Iglesias, A., Wadelius, C., & Komorowski, J. (2009). Nucleosomes are well positioned in exons and carry characteristic histone modifications. *Genome Research*, *19*(10), 1732–1741. https://doi.org/10.1101/gr.092353.109

Anglin, J. L., & Song, Y. (2013). A medicinal chemistry perspective for targeting histone H3 lysine-79 methyltransferase DOT1L. *Journal of Medicinal Chemistry*, *56*(22), 8972–8983. https://doi.org/10.1021/jm4007752

Arents, G., & Moudrianakis, E. N. (1995). The histone fold: A ubiquitous architectural motif utilized in DNA compaction and protein dimerization. *Proceedings of the National Academy of Sciences of the United States of America*, *92*(24), 11170–11174. https://doi.org/10.1073/pnas.92.24.11170

Armstrong, S. A., Kung, A. L., Mabon, M. E., Silverman, L. B., Stam, R. W., Den Boer, M. L., Pieters, R., Kersey, J. H., Sallan, S. E., Fletcher, J. A., Golub, T. R., Griffin, J. D., & Korsmeyer, S. J. (2003). Inhibition of FLT3 in MLL: Validation of a therapeutic target identified by gene expression based classification. *Cancer Cell*, *3*(2), 173–183. https://doi.org/10.1016/S1535-6108(03)00003-5

Armstrong, S. A., Staunton, J. E., Silverman, L. B., Pieters, R., Den Boer, M. L., Minden, M. D., Sallan, S. E., Lander, E. S., Golub, T. R., & Korsmeyer, S. J. (2002). MLL translocations specify a distinct gene expression profile that distinguishes a unique leukemia. *Nature Genetics*, *30*(1), 41–47. https://doi.org/10.1038/ng765

Barski, A., Cuddapah, S., Cui, K., Roh, T. Y., Schones, D. E., Wang, Z., Wei, G., Chepelev, I., & Zhao, K. (2007). High-Resolution Profiling of Histone Methylations in the Human Genome. *Cell*, *129*(4), 823–837. https://doi.org/10.1016/j.cell.2007.05.009

Bernt, K. M., Zhu, N., Sinha, A. U., Vempati, S., Faber, J., Krivtsov, A. V., Feng, Z., Punt, N., Daigle, A., Bullinger, L., Pollock, R. M., Richon, V. M., Kung, A. L., & Armstrong, S. A. (2011). MLL-Rearranged Leukemia Is Dependent on Aberrant H3K79 Methylation by DOT1L. *Cancer Cell*, *20*(1), 66–78. https://doi.org/10.1016/j.ccr.2011.06.010

Birke, M. (2002). The MT domain of the proto-oncoprotein MLL binds to CpG-containing DNA and discriminates against methylation. *Nucleic Acids Research*, *30*(4), 958–965. https://doi.org/10.1093/nar/30.4.958

Biswas, D., Milne, T. A., Basrur, V., Kim, J., Elenitoba-Johnson, K. S. J., Allis, C. D., & Roeder, R. G. (2011). Function of leukemogenic mixed lineage leukemia 1 (MLL) fusion proteins through distinct partner protein complexes. *Proceedings of the National Academy of Sciences of the United States of America*, *108*(38), 15751–15756. https://doi.org/10.1073/pnas.1111498108

Bitoun, E., Oliver, P. L., & Davies, K. E. (2007). The mixed-lineage leukemia fusion partner AF4 stimulates RNA polymerase II transcriptional elongation and mediates coordinated chromatin remodeling. *Human Molecular Genetics*, *16*(1), 92–106. https://doi.org/10.1093/hmg/ddl444

Bonnal, S. C., López-Oreja, I., & Valcárcel, J. (2020). Roles and mechanisms of alternative splicing in cancer — implications for care. *Nature Reviews Clinical Oncology*, *17*(8), 457–474. https://doi.org/10.1038/s41571-020-0350-x

Borkin, D., He, S., Miao, H., Kempinska, K., Pollock, J., Chase, J., Purohit, T., Malik, B., Zhao, T., Wang, J., Wen, B., Zong, H., Jones, M., Danet-Desnoyers, G., Guzman, M. L., Talpaz, M., Bixby, D. L., Sun, D., Hess, J. L., … Grembecka, J. (2015). Pharmacologic inhibition of the menin-MLL interaction blocks progression of MLL leukemia invivo. *Cancer Cell*,

27(4), 589–602. https://doi.org/10.1016/j.ccell.2015.02.016

Botuyan, M. V., Lee, J., Ward, I. M., Kim, J. E., Thompson, J. R., Chen, J., & Mer, G. (2006). Structural Basis for the Methylation State-Specific Recognition of Histone H4-K20 by 53BP1 and Crb2 in DNA Repair. *Cell*, *127*(7), 1361–1373. https://doi.org/10.1016/j.cell.2006.10.043

Brown, S. J., Stoilov, P., & Xing, Y. (2012). Chromatin and epigenetic regulation of pre-mrna processing. *Human Molecular Genetics*, *21*(R1), 90–96. https://doi.org/10.1093/hmg/dds353

Bu, J., Chen, A., Yan, X., He, F., Dong, Y., Zhou, Y., He, J., Zhan, D., Lin, P., Hayashi, Y., Sun, Y., Zhang, Y., Xiao, Z., Grimes, H. L., Wang, Q. F., & Huang, G. (2018). SETD2-mediated crosstalk between H3K36me3 and H3K79me2 in MLL-rearranged leukemia. *Leukemia*, *32*(4), 890–899. https://doi.org/10.1038/leu.2017.339

Caldarelli, A., Müller, J. P., Paskowski-Rogacz, M., Herrmann, K., Bauer, R., Koch, S., Heninger, A. K., Krastev, D., Ding, L., Kasper, S., Fischer, T., Brodhun, M., Böhmer, F. D., & Buchholz, F. (2013). A genome-wide RNAi screen identifies proteins modulating aberrant FLT3-ITD signaling. *Leukemia*, *27*(12), 2301–2310. https://doi.org/10.1038/leu.2013.83

Calvo, K. R., Sykes, D. B., Pasillas, M. P., & Kamps, M. P. (2002). Nup98-Hoxa9 immortalizes myeloid progenitors, enforces expression of Hoxa9, Hoxa7 and Meis1, and alters cytokine-specific responses in a manner similar to that induced by retroviral co-expression of Hoxa9 and Meis1. *Oncogene*, *21*(27), 4247–4256. https://doi.org/10.1038/sj.onc.1205516

Campbell, C. T., Haladyna, J. N., Drubin, D. A., Thomson, T. M., Maria, M. J., Yamauchi, T., Waters, N. J., Olhava, E. J., Pollock, R. M., Smith, J. J., Copeland, R. A., Blakemore, S. J., Bernt, K. M., & Daigle, S. R. (2017). Mechanisms of Pinometostat (EPZ-5676) Treatment–Emergent Resistance in MLL-Rearranged Leukemia. *Molecular Cancer Therapeutics*, *16*(8), 1669 LP – 1679. https://doi.org/10.1158/1535-7163.MCT-16-0693

Cao, F., Townsend, E. C., Karatas, H., Xu, J., Li, L., Lee, S., Liu, L., Chen, Y., Ouillette, P., Zhu, J., Hess, J. L., Atadja, P., Lei, M., Qin, Z. S., Malek, S., Wang, S., & Dou, Y. (2014). Targeting MLL1 H3K4 Methyltransferase Activity in Mixed-Lineage Leukemia. *Molecular Cell*, *53*(2), 247–261. https://doi.org/10.1016/j.molcel.2013.12.001

Cao, R., Wang, L., Wang, H., Xia, L., Erdjument-Bromage, H., Tempst, P., Jones, R. S., & Zhang, Y. (2002). Role of histone H3 lysine 27 methylation in polycomb-group silencing. *Science*, *298*(5595), 1039–1043. https://doi.org/10.1126/science.1076997

Carey, M. F., Peterson, C. L., & Smale, S. T. (2009). Dignam and Roeder nuclear extract preparation. *Cold Spring Harbor Protocols*, *2009*(12), pdb.prot5330. https://doi.org/10.1101/pdb.prot5330

Carrillo Oesterreich, F., Herzel, L., Straube, K., Hujer, K., Howard, J., & Neugebauer, K. M. (2016). Splicing of Nascent RNA Coincides with Intron Exit from RNA Polymerase II. *Cell*, *165*(2), 372–381. https://doi.org/10.1016/j.cell.2016.02.045

Carvalho, S., Raposo, A. C., Martins, F. B., Grosso, A. R., Sridhara, S. C., Rino, J., Carmo-Fonseca, M., & De Almeida, S. F. (2013). Histone methyltransferase SETD2 coordinates FACT recruitment with nucleosome dynamics during transcription. *Nucleic Acids Research*, *41*(5), 2881–2893. https://doi.org/10.1093/nar/gks1472

Cauchy, P., James, S. R., Zacarias-Cabeza, J., Ptasinska, A., Imperato, M. R., Assi, S. A., Piper, J., Canestraro, M., Hoogenkamp, M., Raghavan, M., Loke, J., Akiki, S., Clokie, S. J., Richards, S. J., Westhead, D. R., Griffiths, M. J., Ott, S., Bonifer, C., & Cockerill, P. N. (2015). Chronic FLT3-ITD Signaling in Acute Myeloid Leukemia Is Connected to a Specific Chromatin Signature. *Cell Reports*, *12*(5), 821–836. https://doi.org/10.1016/j.celrep.2015.06.069

Chang, M. J., Wu, H., Achille, N. J., Reisenauer, M. R., Chou, C. W., Zeleznik-Le, N. J., Hemenway, C. S., & Zhang, W. (2010). Histone H3 Lysine 79 Methyltransferase Dot1 Is Required for Immortalization by MLL Oncogenes. *Cancer Research*, *70*(24), 10234–10242. https://doi.org/10.1158/0008-5472.CAN-10-3294

Chang, P.-Y., Hom, R. A., Musselman, C. A., Zhu, L., Kuo, A., Gozani, O., Kutateladze, T. G., & Cleary, M. L. (2010). Binding of the MLL PHD3 Finger to Histone H3K4me3 Is Required for MLL-Dependent Gene Transcription. *Journal of Molecular Biology*, *400*(2), 137–144. https://doi.org/https://doi.org/10.1016/j.jmb.2010.05.005

Chen, C. W., Koche, R. P., Sinha, A. U., Deshpande, A. J., Zhu, N., Eng, R., Doench, J. G., Xu, H., Chu, S. H., Qi, J., Wang, X., Delaney, C., Bernt, K. M., Root, D. E., Hahn, W. C., Bradner, J. E., & Armstrong, S. A. (2015). DOT1L inhibits SIRT1-mediated epigenetic silencing to maintain leukemic gene expression in MLL-rearranged leukemia. *Nature Medicine*, *21*(4), 335–343. https://doi.org/10.1038/nm.3832

Chen, S., Yang, Z., Wilkinson, A. W., Deshpande, A. J., Sidoli, S., Krajewski, K., Strahl, B. D., Garcia, B. A., Armstrong, S. A., Patel, D. J., & Gozani, O. (2015). The PZP Domain of AF10 Senses Unmodified H3K27 to Regulate DOT1L-Mediated Methylation of H3K79. *Molecular Cell*, *60*(2), 319–327. https://doi.org/10.1016/j.molcel.2015.08.019

Chen, Z., Grzybowski, A. T., & Ruthenburg, A. J. (2015). Traceless semisynthesis of a set of histone 3 species bearing specific lysine methylation marks. *ChemBioChem*, *16*(17), 2071–

2075. https://doi.org/10.1002/cbic.201402313

Choudhary, C., Brandts, C., Schwable, J., Tickenbrock, L., Sargin, B., Ueker, A., Böhmer, F. D., Berdel, W. E., Müller-Tidow, C., & Serve, H. (2007). Activation mechanisms of STAT5 by oncogenic Flt3-ITD. *Blood*, *110*(1), 370–374. https://doi.org/10.1182/blood-2006-05-024018

Choudhary, C., Müller-Tidow, C., Berdel, W. E., & Serve, H. (2005). Signal transduction of oncogenic Flt3. *International Journal of Hematology*, *82*(2), 93–99. https://doi.org/10.1532/IJH97.05090

Cibull, T. L., Jones, T. D., Li, L., Eble, J. N., Baldridge, L. A., Malott, S. R., Luo, Y., & Cheng, L. (2006). Overexpression of Pim-1 during progression of prostatic adenocarcinoma. *Journal of Clinical Pathology*, *59*(3), 285–288. https://doi.org/10.1136/jcp.2005.027672

Clark, J. J., Cools, J., Curley, D. P., Yu, J. C., Lokker, N. A., Giese, N. A., & Gilliland, D. G. (2004). Variable sensitivity of FLT3 activation loop mutations to the small molecule tyrosine kinase inhibitor MLN518. *Blood*, *104*(9), 2867–2872. https://doi.org/10.1182/blood-2003-12-4446

Clayton, A. L., Rose, S., Barratt, M. J., & Mahadevan, L. C. (2000). Phosphoacetylation of histone H3 on c-fos- and c-jun-associated nucleosomes upon gene activation. *EMBO Journal*, *19*(14), 3714–3726. https://doi.org/10.1093/emboj/19.14.3714

Coelho, M. B., Attig, J., Bellora, N., König, J., Hallegger, M., Kayikci, M., Eyras, E., Ule, J., & Smith, C. W. (2015). Nuclear matrix protein Matrin3 regulates alternative splicing and forms overlapping regulatory networks with PTB . *The EMBO Journal*, *34*(5), 653–668. https://doi.org/10.15252/embj.201489852

Collinson, A., Collier, A. J., Morgan, N. P., Sienerth, A. R., Chandra, T., Andrews, S., & Rugg-Gunn, P. J. (2016). Deletion of the Polycomb-Group Protein EZH2 Leads to Compromised Self-Renewal and Differentiation Defects in Human Embryonic Stem Cells. *Cell Reports*, *17*(10), 2700–2714. https://doi.org/10.1016/j.celrep.2016.11.032

Corral, J., Lavenir, I., Impey, H., Warren, A. J., Forster, A., Larson, T. A., Bell, S., McKenzie, A. N. J., King, G., & Rabbitts, T. H. (1996). An MII-AF9 fusion gene made by homologous recombination causes acute leukemia in chimeric mice: A method to create fusion oncogenes. *Cell*, *85*(6), 853–861. https://doi.org/10.1016/S0092-8674(00)81269-6

Cutter, A. R., & Hayes, J. J. (2015). A brief review of nucleosome structure. *FEBS Letters*, *589*(20 Pt A), 2914–2922. https://doi.org/10.1016/j.febslet.2015.05.016

Daigle, S. R., Olhava, E. J., Therkelsen, C. A., Basavapathruni, A., Jin, L., Boriack-Sjodin, P. A., Allain, C. J., Klaus, C. R., Raimondi, A., Scott, M. P., Waters, N. J., Chesworth, R., Moyer, M. P., Copeland, R. A., Richon, V. M., & Pollock, R. M. (2013). Potent inhibition of DOT1L as treatment of MLL-fusion leukemia. *Blood*, *122*(6), 1017–1025. https://doi.org/10.1182/blood-2013-04-497644

Daigle, S. R., Olhava, E. J., Therkelsen, C. A., Majer, C. R., Sneeringer, C. J., Song, J., Johnston, L. D., Scott, M. P., Smith, J. J., Xiao, Y., Jin, L., Kuntz, K. W., Chesworth, R., Moyer, M. P., Bernt, K. M., Tseng, J. C., Kung, A. L., Armstrong, S. A., Copeland, R. A., … Pollock, R. M. (2011). Selective Killing of Mixed Lineage Leukemia Cells by a Potent Small-Molecule DOT1L Inhibitor. *Cancer Cell*, *20*(1), 53–65. https://doi.org/10.1016/j.ccr.2011.06.009

Dardaei, L., Longobardi, E., & Blasi, F. (2014). Prep1 and Meis1 competition for Pbx1 binding regulates protein stability and tumorigenesis. *Proceedings of the National Academy of Sciences of the United States of America*, *111*(10). https://doi.org/10.1073/pnas.1321200111

de Bock, C. E., Demeyer, S., Degryse, S., Verbeke, D., Sweron, B., Gielen, O., Vandepoel, R., Vicente, C., Bempt, M. Vanden, Dagklis, A., Geerdens, E., Bornschein, S., Gijsbers, R., Soulier, J., Meijerink, J. P., Heinäniemi, M., Teppo, S., Bouvy-Liivrand, M., Lohi, O., … Cools, J. (2018). HOXA9 cooperates with activated JAK/STAT signaling to drive leukemia development. *Cancer Discovery*, *8*(5), 616–631. https://doi.org/10.1158/2159-8290.CD-17-0583

De La Mata, M., Alonso, C. R., Kadener, S., Fededa, J. P., Blaustein, M., Pelisch, F., Cramer, P., Bentley, D., & Kornblihtt, A. R. (2003). A slow RNA polymerase II affects alternative splicing in vivo. *Molecular Cell*, *12*(2), 525–532. https://doi.org/10.1016/j.molcel.2003.08.001

Deneen, B., Welford, S. M., Ho, T., Hernandez, F., Kurland, I., & Denny, C. T. (2003). PIM3 Proto-Oncogene Kinase Is a Common Transcriptional Target of Divergent EWS/ETS Oncoproteins. *Molecular and Cellular Biology*, *23*(11), 3897–3908. https://doi.org/10.1128/mcb.23.11.3897-3908.2003

Deshpande, A. J., Chen, L., Fazio, M., Sinha, A. U., Bernt, K. M., Banka, D., Dias, S., Chang, J., Olhava, E. J., Daigle, S. R., Richon, V. M., Pollock, R. M., & Armstrong, S. A. (2013). Leukemic transformation by the MLL-AF6 fusion oncogene requires the H3K79 methyltransferase Dot1l. *Blood*, *121*(13), 2533–2541. https://doi.org/10.1182/blood-2012-11-465120

Dillon, L. M., & Miller, T. W. (2014). Therapeutic targeting of cancers with loss of PTEN function. *Current Drug Targets*, *15*(1), 65–79. https://doi.org/10.2174/1389450114666140106100909

Ding, L., Rath, E., & Bai, Y. (2017). Comparison of Alternative Splicing Junction Detection Tools Using RNASeq Data. *Current Genomics*, *18*(3), 268–277. https://doi.org/10.2174/1389202918666170215125048

Dixon, J. R., Gorkin, D. U., & Ren, B. (2016). Chromatin Domains: The Unit of Chromosome Organization. *Molecular Cell*, *62*(5), 668–680. https://doi.org/10.1016/j.molcel.2016.05.018

Dobson, C. L., Warren, A. J., Pannell, R., Forster, A., Lavenir, I., Corral, J., Smith, A. J. H., & Rabbitts, T. H. (1999). The Mll-AF9 gene fusion in mice controls myeloproliferation and specifies acute myeloid leukaemogenesis. *EMBO Journal*, *18*(13), 3564–3574. https://doi.org/10.1093/emboj/18.13.3564

Dosil, M., Wang, S., & Lemischka, I. R. (1993). Mitogenic signalling and substrate specificity of the Flk2/Flt3 receptor tyrosine kinase in fibroblasts and interleukin 3-dependent hematopoietic cells. *Molecular and Cellular Biology*, *13*(10), 6572–6585. https://doi.org/10.1128/mcb.13.10.6572

Dover, J., Schneider, J., Tawiah-Boateng, M. A., Wood, A., Dean, K., Johnston, M., & Shilatifard, A. (2002). Methylation of histone H3 by COMPASS requires ubiquitination of histone H2B by Rad6. *Journal of Biological Chemistry*, *277*(32), 28368–28371. https://doi.org/10.1074/jbc.C200348200

Du, Y., Spence, S. E., Jenkins, N. A., & Copeland, N. G. (2005). Cooperating cancer-gene identification through oncogenic-retrovirus-induced insertional mutagenesis. *Blood*, *106*(7), 2498–2505. https://doi.org/10.1182/blood-2004-12-4840

Dvinge, H. (2018). Regulation of alternative mRNA splicing: old players and new perspectives. *FEBS Letters*, *592*(17), 2987–3006. https://doi.org/10.1002/1873-3468.13119

Dyer, P. N., Edayathumangalam, R. S., White, C. L., Bao, Y., Chakravarthy, S., Muthurajan, U. M., & Luger, K. (2004). Reconstitution of nucleosome core particles from recombinant histones and DNA. *Methods in Enzymology*, *375*, 23–44. https://doi.org/10.1016/s0076-6879(03)75002-2

Edmunds, J. W., Mahadevan, L. C., & Clayton, A. L. (2008). Dynamic histone H3 methylation during gene induction: HYPB/Setd2 mediates all H3K36 trimethylation. *EMBO Journal*, *27*(2), 406–420. https://doi.org/10.1038/sj.emboj.7601967

El Ashkar, S., Schwaller, J., Pieters, T., Goossens, S., Demeulemeester, J., Christ, F., Van Belle, S., Juge, S., Boeckx, N., Engelman, A., Van Vlierberghe, P., Debyser, Z., & De Rijck, J. (2018). LEDGF/p75 is dispensable for hematopoiesis but essential for MLL-rearranged leukemogenesis. *Blood*, *131*(1), 95–107. https://doi.org/10.1182/blood-2017-05-786962

Fang, J., Ying, H., Mao, T., Fang, Y., Lu, Y., Wang, H., Zang, I., Wang, Z., Lin, Y., Zhao, M., Luo, X., Wang, Z., Zhang, Y., Zhang, C., Xiao, W., Wang, Y., Tan, W., Chen, Z., Lu, C., … Gu, J. (2017). Upregulation of CD11b and CD86 through LSD1 inhibition promotes myeloid differentiation and suppresses cell proliferation in human monocytic leukemia cells. *Oncotarget*, *8*(49), 85085–85101. https://doi.org/10.18632/oncotarget.18564

Fathi, A. T., Arowojolu, O., Swinnen, I., Sato, T., Rajkhowa, T., Small, D., Marmsater, F., Robinson, J. E., Gross, S. D., Martinson, M., Allen, S., Kallan, N. C., & Levis, M. (2012). A potential therapeutic target for FLT3-ITD AML: PIM1 kinase. *Leukemia Research*, *36*(2), 224–231. https://doi.org/10.1016/j.leukres.2011.07.011

Feng, Q., Wang, H., Ng, H. H., Erdjument-Bromage, H., Tempst, P., Struhl, K., & Zhang, Y. (2002). Methylation of H3-lysine 79 is mediated by a new family of HMTases without a SET domain. *Current Biology*, *12*(12), 1052–1058. https://doi.org/10.1016/S0960-9822(02)00901-6

Feng, Z., Yao, Y., Zhou, C., Chen, F., Wu, F., Wei, L., Liu, W., Dong, S., Redell, M., Mo, Q., & Song, Y. (2016). Pharmacological inhibition of LSD1 for the treatment of MLL-rearranged leukemia. *Journal of Hematology and Oncology*, *9*(1), 1–13. https://doi.org/10.1186/s13045-016-0252-7

Fingerman, I. M., Li, H. C., & Briggs, S. D. (2007). A charge-based interaction between histone H4 and Dot1 is required for H3K79 methylation and telomere silencing: Identification of a new trans-histone pathway. *Genes and Development*, *21*(16), 2018–2029. https://doi.org/10.1101/gad.1560607

Forster, A., Pannell, R., Drynan, L. F., McCormack, M., Collins, E. C., Daser, A., & Rabbitts, T. H. (2003). Engineering de novo reciprocal chromosomal translocations associated with Mll to replicate primary events of human cancer. *Cancer Cell*, *3*(5), 449–458. https://doi.org/10.1016/S1535-6108(03)00106-5

Frederiks, F., Tzouros, M., Oudgenoeg, G., Van Welsem, T., Fornerod, M., Krijgsveld, J., & Van Leeuwen, F. (2008). Nonprocessive methylation by Dot1 leads to functional redundancy of histone H3K79 methylation states. *Nature Structural and Molecular Biology*, *15*(6), 550–557. https://doi.org/10.1038/nsmb.1432

Galanis, A., Ma, H., Rajkhowa, T., Ramachandran, A., Small, D., Cortes, J., & Levis, M. (2014). Crenolanib is a potent inhibitor of FLT3 with activity against resistance-conferring point mutants. *Blood*, *123*(1), 94–100. https://doi.org/10.1182/blood-2013-10-529313

Gary Gilliland, D., & Griffin, J. D. (2002). The roles of FLT3 in hematopoiesis and leukemia. *Blood*, *100*(5), 1532–1542. https://doi.org/10.1182/blood-2002-02-0492

Gibaja, V., Shen, F., Harari, J., Korn, J., Ruddy, D., Saenz-Vash, V., Zhai, H., Rejtar, T., Paris, C. G., Yu, Z., Lira, M., King, D., Qi, W., Keen, N., Hassan, A. Q., & Chan, H. M. (2016). Development of secondary mutations in wild-type and mutant EZH2 alleles cooperates to confer resistance to EZH2 inhibitors. *Oncogene*, *35*(5), 558–566. https://doi.org/10.1038/onc.2015.114

Godfrey, L., Crump, N. T., Thorne, R., Lau, I. J., Repapi, E., Dimou, D., Smith, A. L., Harman, J. R., Telenius, J. M., Oudelaar, A. M., Downes, D. J., Vyas, P., Hughes, J. R., & Milne, T. A. (2019). DOT1L inhibition reveals a distinct subset of enhancers dependent on H3K79 methylation. *Nature Communications*, *10*(1). https://doi.org/10.1038/s41467-019-10844-3

Green, A. S., Maciel, T. T., Hospital, M. A., Yin, C., Mazed, F., Townsend, E. C., Pilorge, S., Lambert, M., Paubelle, E., Jacquel, A., Zylbersztejn, F., Decroocq, J., Poulain, L., Sujobert, P., Jacque, N., Adam, K., So, J. C. C., Kosmider, O., Auberger, P., … Tamburini, J. (2015). Pim kinases modulate resistance to FLT3 tyrosine kinase inhibitors in FLT3-ITD acute myeloid leukemia. *Science Advances*, *1*(8), 1–14. https://doi.org/10.1126/sciadv.1500221

Grossmann, V., Schnittger, S., Poetzinger, F., Kohlmann, A., Stiel, A., Eder, C., Fasan, A., Kern, W., Haferlach, T., & Haferlach, C. (2013). High incidence of RAS signalling pathway mutations in MLL-rearranged acute myeloid leukemia. *Leukemia*, *27*(9), 1933–1936. https://doi.org/10.1038/leu.2013.90

Grzybowski, A. T., Chen, Z., & Ruthenburg, A. J. (2015). Calibrating ChIP-Seq with Nucleosomal Internal Standards to Measure Histone Modification Density Genome Wide. *Molecular Cell*, *58*(5), 886–899. https://doi.org/10.1016/j.molcel.2015.04.022

Grzybowski, A. T., Shah, R. N., Richter, W. F., & Ruthenburg, A. J. (2019). Native internally calibrated chromatin immunoprecipitation for quantitative studies of histone post-translational modifications. *Nature Protocols*, *14*(12), 3275–3302. https://doi.org/10.1038/s41596-019-0218-7

Guenther, M. G., Lawton, L. N., Rozovskaia, T., Frampton, G. M., Levine, S. S., Volkert, T. L., Croce, C. M., Nakamura, T., Canaani, E., & Young, R. A. (2008). Aberrant chromatin at genes encoding stem cell regulators in human mixed-lineage leukemia. *Genes and Development*, *22*(24), 3403–3408. https://doi.org/10.1101/gad.1741408

Guenther, M. G., Levine, S. S., Boyer, L. A., Jaenisch, R., & Young, R. A. (2007). A Chromatin Landmark and Transcription Initiation at Most Promoters in Human Cells. *Cell*, *130*(1), 77–88. https://doi.org/10.1016/j.cell.2007.05.042

Guo, R., Zheng, L., Park, J. W., Lv, R., Chen, H., Jiao, F., Xu, W., Mu, S., Wen, H., Qiu, J., Wang, Z., Yang, P., Wu, F., Hui, J., Fu, X., Shi, X., Shi, Y. G., Xing, Y., Lan, F., & Shi, Y. (2014). BS69/ZMYND11 reads and connects histone H3.3 lysine 36 trimethylation-

decorated chromatin to regulated pre-mRNA processing. *Molecular Cell*, *56*(2), 298–310. https://doi.org/10.1016/j.molcel.2014.08.022

Haddadi, N., Lin, Y., Travis, G., Simpson, A. M., McGowan, E. M., & Nassif, N. T. (2018). PTEN/PTENP1: "Regulating the regulator of RTK-dependent PI3K/Akt signalling", new targets for cancer therapy. *Molecular Cancer*, *17*(1), 1–14. https://doi.org/10.1186/s12943-018-0803-3

Hanson, R. D., Hess, J. L., Yu, B. D., Ernst, P., Van Lohuizen, M., Berns, A., Van Der Lugt, N. M. T., Shashikant, C. S., Ruddle, F. H., Seto, M., & Korsmeyer, S. J. (1999). Mammalian Trithorax and Polycomb-group homologues are antagonistic regulators of homeotic development. *Proceedings of the National Academy of Sciences of the United States of America*, *96*(25), 14372–14377. https://doi.org/10.1073/pnas.96.25.14372

Harris, W. J., Huang, X., Lynch, J. T., Spencer, G. J., Hitchin, J. R., Li, Y., Ciceri, F., Blaser, J. G., Greystoke, B. F., Jordan, A. M., Miller, C. J., Ogilvie, D. J., & Somervaille, T. C. P. (2012). The Histone Demethylase KDM1A Sustains the Oncogenic Potential of MLL-AF9 Leukemia Stem Cells. *Cancer Cell*, *21*(4), 473–487. https://doi.org/10.1016/j.ccr.2012.03.014

Hayashi, K., Yoshida, K., & Matsui, Y. (2005). A histone H3 methyltransferase controls epigenetic events required for meiotic prophase. *Nature*, *438*(7066), 374–378. https://doi.org/10.1038/nature04112

He, X., Arslan, A. D., Ho, T. T., Yuan, C., Stampfer, M. R., & Beck, W. T. (2014). Involvement of polypyrimidine tract-binding protein (PTBP1) in maintaining breast cancer cell growth and malignant properties. *Oncogenesis*, *3*(1), 1–8. https://doi.org/10.1038/oncsis.2013.47

He, X., Pool, M., Darcy, K. M., Lim, S. B., Auersperg, N., Coon, J. S., & Beck, W. T. (2007). Knockdown of polypyrimidine tract-binding protein suppresses ovarian tumor cell growth and invasiveness in vitro. *Oncogene*, *26*(34), 4961–4968. https://doi.org/10.1038/sj.onc.1210307

Hendzel, M. J., Wei, Y., Mancini, M. A., Van Hooser, A., Ranalli, T., Brinkley, B. R., Bazett-Jones, D. P., & Allis, C. D. (1997). Mitosis-specific phosphorylation of histone H3 initiates primarily within pericentromeric heterochromatin during G2 and spreads in an ordered fashion coincident with mitotic chromosome condensation. *Chromosoma*, *106*(6), 348–360. https://doi.org/10.1007/s004120050256

Herzel, L., Ottoz, D. S. M., Alpert, T., & Neugebauer, K. M. (2017). Splicing and transcription touch base: co-transcriptional spliceosome assembly and function. *Nature Reviews Molecular Cell Biology*, *18*(10), 637–650. https://doi.org/10.1038/nrm.2017.63

Hess, J. L. (2004). MLL: A histone methyltransferase disrupted in leukemia. *Trends in Molecular Medicine*, *10*(10), 500–507. https://doi.org/10.1016/j.molmed.2004.08.005

Hu, D., Gao, X., Morgan, M. A., Herz, H.-M., Smith, E. R., & Shilatifard, A. (2013). The MLL3/MLL4 Branches of the COMPASS Family Function as Major Histone H3K4 Monomethylases at Enhancers. *Molecular and Cellular Biology*, *33*(23), 4745–4754. https://doi.org/10.1128/mcb.01181-13

Huang, D. W., Sherman, B. T., & Lempicki, R. A. (2009a). Bioinformatics enrichment tools: Paths toward the comprehensive functional analysis of large gene lists. *Nucleic Acids Research*, *37*(1), 1–13. https://doi.org/10.1093/nar/gkn923

Huang, D. W., Sherman, B. T., & Lempicki, R. A. (2009b). Systematic and integrative analysis of large gene lists using DAVID bioinformatics resources. *Nature Protocols*, *4*(1), 44–57. https://doi.org/10.1038/nprot.2008.211

Huang, Y., Sitwala, K., Bronstein, J., Sanders, D., Dandekar, M., Collins, C., Robertson, G., MacDonald, J., Cezard, T., Bilenky, M., Thiessen, N., Zhao, Y., Zeng, T., Hirst, M., Hero, A., Jones, S., & Hess, J. L. (2012). Identification and characterization of Hoxa9 binding sites in hematopoietic cells. *Blood*, *119*(2), 388–398. https://doi.org/10.1182/blood-2011-03-341081

Huff, J. T., Plocik, A. M., Guthrie, C., & Yamamoto, K. R. (2010). Reciprocal intronic and exonic histone modification regions in humans. *Nature Structural and Molecular Biology*, *17*(12), 1495–1499. https://doi.org/10.1038/nsmb.1924

Hui, J., Hung, L. H., Heiner, M., Schreiner, S., Neumüller, N., Reither, G., Haas, S. A., & Bindereif, A. (2005). Intronic CA-repeat and CA-rich elements: A new class of regulators of mammalian alternative splicing. *EMBO Journal*, *24*(11), 1988–1998. https://doi.org/10.1038/sj.emboj.7600677

Huyen, Y., Zgheib, O., DiTullio, R. A., Gorgoulis, V. G., Zacharatos, P., Petty, T. J., Sheston, E. A., Mellert, H. S., Stavridi, E. S., & Halazonetis, T. D. (2004). Methylated lysine 79 of histone H3 targets 53BP1 to DNA double-strand breaks. *Nature*, *432*(7015), 406–411. https://doi.org/10.1038/nature03114

Jabbour, E., O'Brien, S., Konopleva, M., & Kantarjian, H. (2015). New insights into the pathophysiology and therapy of adult acute lymphoblastic leukemia. *Cancer*, *121*(15), 2517–2528. https://doi.org/10.1002/cncr.29383

Jacobson, R. H., Ladurner, A. G., King, D. S., & Tjian, R. (2000). Structure and Function of a Human TAF_{II}250 Double Bromodomain Module. *Science*,

288(5470), 1422 LP – 1425. https://doi.org/10.1126/science.288.5470.1422

Jin, Q., Yu, L. R., Wang, L., Zhang, Z., Kasper, L. H., Lee, J. E., Wang, C., Brindle, P. K., Dent, S. Y. R., & Ge, K. (2011). Distinct roles of GCN5/PCAF-mediated H3K9ac and CBP/p300-mediated H3K18/27ac in nuclear receptor transactivation. *EMBO Journal*, *30*(2), 249–262. https://doi.org/10.1038/emboj.2010.318

Jin, W., McCutcheon, I. E., Fuller, G. N., Huang, E. S. C., & Cote, G. J. (2000). Fibroblast growth factor receptor-1 α-exon exclusion and polypyrimidine tract-binding protein in glioblastoma multiforme tumors. *Cancer Research*, *60*(5), 1221–1224.

Jo, S. Y., Granowicz, E. M., Maillard, I., Thomas, D., & Hess, J. L. (2011). Requirement for Dot1l in murine postnatal hematopoiesis and leukemogenesis by MLL translocation. *Blood*, *117*(18), 4759–4768. https://doi.org/10.1182/blood-2010-12-327668

Jones, B., Su, H., Bhat, A., Lei, H., Bajko, J., Hevi, S., Baltus, G. A., Kadam, S., Zhai, H., Valdez, R., Gonzalo, S., Zhang, Y., Li, E., & Chen, T. (2008). The histone H3K79 methyltransferase Dot1L is essential for mammalian development and heterochromatin structure. *PLoS Genetics*, *4*(9). https://doi.org/10.1371/journal.pgen.1000190

Karmodiya, K., Krebs, A. R., Oulad-Abdelghani, M., Kimura, H., & Tora, L. (2012). H3K9 and H3K14 acetylation co-occur at many gene regulatory elements, while H3K14ac marks a subset of inactive inducible promoters in mouse embryonic stem cells. *BMC Genomics*, *13*(1). https://doi.org/10.1186/1471-2164-13-424

Katz, Y., Wang, E. T., Airoldi, E. M., & Burge, C. B. (2010). Analysis and design of RNA sequencing experiments for identifying isoform regulation. *Nature Methods*, *7*(12), 1009–1015. https://doi.org/10.1038/nmeth.1528

Kerry, J., Godfrey, L., Repapi, E., Tapia, M., Blackledge, N. P., Ma, H., Ballabio, E., O'Byrne, S., Ponthan, F., Heidenreich, O., Roy, A., Roberts, I., Konopleva, M., Klose, R. J., Geng, H., & Milne, T. A. (2017). MLL-AF4 Spreading Identifies Binding Sites that Are Distinct from Super-Enhancers and that Govern Sensitivity to DOT1L Inhibition in Leukemia. *Cell Reports*, *18*(2), 482–495. https://doi.org/10.1016/j.celrep.2016.12.054

Kikushige, Y., Yoshimoto, G., Miyamoto, T., Iino, T., Mori, Y., Iwasaki, H., Niiro, H., Takenaka, K., Nagafuji, K., Harada, M., Ishikawa, F., & Akashi, K. (2008). Human Flt3 Is Expressed at the Hematopoietic Stem Cell and the Granulocyte/Macrophage Progenitor Stages to Maintain Cell Survival. *The Journal of Immunology*, *180*(11), 7358–7367. https://doi.org/10.4049/jimmunol.180.11.7358

Kim, D.-H., Tang, Z., Shimada, M., Fierz, B., Houck-Loomis, B., Bar-Dagen, M., Lee, S., Lee,

S.-K., Muir, T. W., Roeder, R. G., & Lee, J. W. (2013). Histone H3K27 Trimethylation Inhibits H3 Binding and Function of SET1-Like H3K4 Methyltransferase Complexes. *Molecular and Cellular Biology*, *33*(24), 4936–4946. https://doi.org/10.1128/mcb.00601-13

Kim, D., Langmead, B., & Salzberg, S. L. (2015). HISAT: a fast spliced aligner with low memory requirements. *Nature Methods*, *12*(4), 357–360. https://doi.org/10.1038/nmeth.3317

Kim, K. T., Baird, K., Ahn, J. Y., Meltzer, P., Lilly, M., Levis, M., & Small, D. (2005). Pim-1 is up-regulated by constitutively activated FLT3 and plays a role in FLT3-mediated cell survival. *Blood*, *105*(4), 1759–1767. https://doi.org/10.1182/blood-2004-05-2006

Kim, W., Choi, M., & Kim, J. E. (2014). The histone methyltransferase Dot1/DOT1L as a critical regulator of the cell cycle. *Cell Cycle*, *13*(5), 726–738. https://doi.org/10.4161/cc.28104

Kizer, K. O., Phatnani, H. P., Shibata, Y., Hall, H., Greenleaf, A. L., Strahl, B. D., & Iol, M. O. L. C. E. L. L. B. (2005). *A novel domain in Set2 mediates RNA polymerase II interaction and couples histone H3 K36 methylation with transcript elongation*. *25*(8), 3305–3316. https://doi.org/10.1128/MCB.25.8.3305

Klimiankou, M., Dannenmann, B., Solovyeva, A., Bernhard, R., Amend, D., Zeidler, C., Mellor-Heineke, S., Kanz, L., Skokowa, J., & Welte, K. (2017). Effects of CSF3R mutations on Myeloid Differentiation and Proliferation of Hematopoietic Cells of Congenital Neutropenia Patients. *Blood*, *130*(Supplement 1), 2278. https://doi.org/10.1182/blood.V130.Suppl_1.2278.2278

Kornberg, R. D., & Lorch, Y. (1999). Twenty-five years of the nucleosome, fundamental particle of the eukaryote chromosome. *Cell*, *98*(3), 285–294. https://doi.org/10.1016/S0092-8674(00)81958-3

Krivtsov, A. V., Twomey, D., Feng, Z., Stubbs, M. C., Wang, Y., Faber, J., Levine, J. E., Wang, J., Hahn, W. C., Gilliland, D. G., Golub, T. R., & Armstrong, S. A. (2006). Transformation from committed progenitor to leukaemia stem cell initiated by MLL-AF9. *Nature*, *442*(7104), 818–822. https://doi.org/10.1038/nature04980

Krogan, N. J., Dover, J., Khorrami, S., Greenblatt, J. F., Schneider, J., Johnston, M., & Shilatifard, A. (2002). COMPASS, a histone H3 (lysine 4) methyltransferase required for telomeric silencing of gene expression. *Journal of Biological Chemistry*, *277*(13), 10753–10755. https://doi.org/10.1074/jbc.C200023200

Kroon, E., Krosl, J., Thorsteinsdottir, U., Baban, S., Buchberg, A. M., & Sauvageau, G. (1998).

Hoxa9 transforms primary bone marrow cells through specific collaboration with Meis1a but not Pbx1b. *EMBO Journal*, *17*(13), 3714–3725. https://doi.org/10.1093/emboj/17.13.3714

Larrosa-Garcia, M., & Baer, M. R. (2017). FLT3 Inhibitors in acute myeloid leukemia: Current status & future directions. *Molecular Cancer Therapeutics*, *16*(6), 991–1001. https://doi.org/10.1158/1535-7163.MCT-16-0876

Lawrence, H. J., Christensen, J., Fong, S., Hu, Y.-L., Weissman, I., Sauvageau, G., Humphries, R. K., & Largman, C. (2005). Loss of expression of the Hoxa-9 homeobox gene impairs the proliferation and repopulating ability of hematopoietic stem cells. *Blood*, *106*(12), 3988–3994. https://doi.org/10.1182/blood-2005-05-2003

Lee, K. K., & Workman, J. L. (2007). Histone acetyltransferase complexes: one size doesn't fit all. *Nature Reviews Molecular Cell Biology*, *8*(4), 284–295. https://doi.org/10.1038/nrm2145

Levis, M., & Small, D. (2003). FLT3: ITDoes matter in leukemia. *Leukemia*, *17*(9), 1738–1752. https://doi.org/10.1038/sj.leu.2403099

Levis, Mark, Allebach, J., Tse, K. F., Zheng, R., Brenda, R., Baldwin, B., Smith, D., Jones-Bolin, S., Ruggeri, B., Dionne, C., & Small, D. (2002). A FLT3-targeted tyrosine kinase inhibitor is cytotoxic to leukemia cells in vitro and in vivo. *Blood*, *99*(11), 3885–3891. https://doi.org/10.1182/blood.V99.11.3885

Li, B. E., Gan, T., Meyerson, M., Rabbitts, T. H., & Ernst, P. (2013). Distinct pathways regulated by menin and by MLL1 in hematopoietic stem cells and developing B cells. *Blood*, *122*(12), 2039–2046. https://doi.org/10.1182/blood-2013-03-486647

Li, T., Liu, Q., Garza, N., Kornblau, S., & Jin, V. X. (2018). Integrative analysis reveals functional and regulatory roles of H3K79me2 in mediating alternative splicing. *Genome Medicine*, *10*(1), 1–11. https://doi.org/10.1186/s13073-018-0538-1

Li, Y. I., Knowles, D. A., Humphrey, J., Barbeira, A. N., Dickinson, S. P., Im, H. K., & Pritchard, J. K. (2018). Annotation-free quantification of RNA splicing using LeafCutter. *Nature Genetics*, *50*(1), 151–158. https://doi.org/10.1038/s41588-017-0004-9

Li, Z., Chen, P., Su, R., Hu, C., Li, Y., Elkahloun, A. G., Zuo, Z., Gurbuxani, S., Arnovitz, S., Weng, H., Wang, Y., Shenglai, L., Huang, H., Neilly, M. B., Wang, G. G., Jiang, X., Liu, P. P., Jin, J., & Chen, J. (2016). PBX3 and MEIS1 Cooperate in hematopoietic cells to drive acute myeloid leukemias characterized by a core transcriptome of the MLL-rearranged disease. *Cancer Research*, *76*(3), 619–629. https://doi.org/10.1158/0008-5472.CAN-15-

1566

Li, Z., Zhang, Z., Li, Y., Arnovitz, S., Chen, P., Huang, H., Jiang, X., Hong, G. M., Kunjamma, R. B., Ren, H., He, C., Wang, C. Z., Elkahloun, A. G., Valk, P. J. M., Döhner, K., Neilly, M. B., Bullinger, L., Delwel, R., Löwenberg, B., … Chen, J. (2013). PBX3 is an important cofactor of HOXA9 in leukemogenesis. *Blood*, *121*(8), 1422–1431. https://doi.org/10.1182/blood-2012-07-442004

Liang, D. C., Shih, L. Y., Fu, J. F., Li, H. Y., Wang, H. I., Hung, I. J., Yang, C. P., Jaing, T. H., Chen, S. H., & Liu, H. C. (2006). K-Ras mutations and N-Ras mutations in childhood acute leukemias with or without mixed-lineage leukemia gene rearrangements. *Cancer*, *106*(4), 950–956. https://doi.org/10.1002/cncr.21687

Linares, A. J., Lin, C. H., Damianov, A., Adams, K. L., Novitch, B. G., & Black, D. L. (2015). The splicing regulator PTBP1 controls the activity of the transcription factor Pbx1 during neuronal differentiation. *ELife*, *4*(DECEMBER2015), 1–25. https://doi.org/10.7554/eLife.09268

Ling, J. P., Chhabra, R., Merran, J. D., Schaughency, P. M., Wheelan, S. J., Corden, J. L., & Wong, P. C. (2016). PTBP1 and PTBP2 Repress Nonconserved Cryptic Exons. *Cell Reports*, *17*(1), 104–113. https://doi.org/10.1016/j.celrep.2016.08.071

López, C., Bergmann, A. K., Paul, U., Murga Penas, E. M., Nagel, I., Betts, M. J., Johansson, P., Ritgen, M., Baumann, T., Aymerich, M., Jayne, S., Russell, R. B., Campo, E., Dyer, M. J., Dürig, J., & Siebert, R. (2016). Genes encoding members of the JAK-STAT pathway or epigenetic regulators are recurrently mutated in T-cell prolymphocytic leukaemia. *British Journal of Haematology*, *173*(2), 265–273. https://doi.org/10.1111/bjh.13952

Lowary, P. T., & Widom, J. (1998). New DNA sequence rules for high affinity binding to histone octamer and sequence-directed nucleosome positioning. *Journal of Molecular Biology*, *276*(1), 19–42. https://doi.org/10.1006/jmbi.1997.1494

Luco, R. F., Allo, M., Schor, I. E., Kornblihtt, A. R., & Misteli, T. (2011). Epigenetics in alternative pre-mRNA splicing. *Cell*, *144*(1), 16–26. https://doi.org/10.1016/j.cell.2010.11.056

Luco, R. F., Pan, Q., Tominaga, K., Blencowe, B. J., Pereira-Smith, O. M., & Misteli, T. (2010). Regulation of alternative splicing by histone modifications. *Science*, *327*(5968), 996–1000. https://doi.org/10.1126/science.1184208

Mandal, M., Powers, S. E., Maienschein-Cline, M., Bartom, E. T., Hamel, K. M., Kee, B. L., Dinner, A. R., & Clark, M. R. (2011). Epigenetic repression of the Igk locus by STAT5-

mediated recruitment of the histone methyltransferase Ezh2. *Nature Immunology*, *12*(12), 1212–1220. https://doi.org/10.1038/ni.2136

Mann, G., Attarbaschi, A., Schrappe, M., De Lorenzo, P., Peters, C., Hann, I., De Rossi, G., Felice, M., Lausen, B., LeBlanc, T., Szczepanski, T., Ferster, A., Janka-Schaub, G., Rubnitz, J., Silverman, L. B., Stary, J., Campbell, M., Li, C. K., Suppiah, R., … Pieters, R. (2010). Improved outcome with hematopoietic stem cell transplantation in a poor prognostic subgroup of infants with mixed-lineage-leukemia (MLL)-rearranged acute lymphoblastic leukemia: Results from the Interfant-99 Study. *Blood*, *116*(15), 2644–2650. https://doi.org/10.1182/blood-2010-03-273532

Marks, D. I., Moorman, A. V., Chilton, L., Paietta, E., Enshaie, A., de Wald, G., Harrison, C. J., Fielding, A. K., Foroni, L., Goldstone, A. H., Litzow, M. R., Luger, S. M., McMillan, A. K., Racevskis, J., Rowe, J. M., Tallman, M. S., Wiernik, P., & Lazarus, H. M. (2013). The clinical characteristics, therapy and outcome of 85 adults with acute lymphoblastic leukemia and t(4;11)(q21;q23)/MLL-AFF1 prospectively treated in the UKALLXII/ECOG2993 trial. *Haematologica*, *98*(6), 945–952. https://doi.org/10.3324/haematol.2012.081877

Marschalek, R. (2011). Mechanisms of leukemogenesis by MLL fusion proteins. *British Journal of Haematology*, *152*(2), 141–154. https://doi.org/10.1111/j.1365-2141.2010.08459.x

McGrath, J. P., Williamson, K. E., Balasubramanian, S., Odate, S., Arora, S., Hatton, C., Edwards, T. M., O'Brien, T., Magnuson, S., Stokoe, D., Daniels, D. L., Bryant, B. M., & Trojer, P. (2016). Pharmacological inhibition of the histone lysine demethylase KDM1A suppresses the growth of multiple acute myeloid leukemia subtypes. *Cancer Research*, *76*(7), 1975–1988. https://doi.org/10.1158/0008-5472.CAN-15-2333

McLean, C. M., Karemaker, I. D., & van Leeuwen, F. (2014). The emerging roles of DOT1L in leukemia and normal development. *Leukemia*, *28*(11), 2131–2138. https://doi.org/10.1038/leu.2014.169

Metzeler, K. H., Sandhöfer, N., Hinrichsen, T., Zellmeier, E., Ksienzyk, B., Dufour, A., Schneider, S., Kakadia, P. M., Greif, P. A., Subklewe, M. S., Bohlander, S. K., Klein, H.-G., Hiddemann, W., & Spiekermann, K. (2012). Analysis of Cooperating Genetic Events in MLLT3-MLL Rearranged Acute Myeloid Leukemia (AML) by Targeted Next-Generation Sequencing of 16 Leukemia-Related Genes Reveals Frequent Mutations Affecting Growth Factor Signalling Pathways and Provides Evidence fo. *Blood*, *120*(21), 1379. https://doi.org/10.1182/blood.V120.21.1379.1379

Meyer, C., Burmeister, T., Gröger, D., Tsaur, G., Fechina, L., Renneville, A., Sutton, R., Venn, N. C., Emerenciano, M., Pombo-De-Oliveira, M. S., Barbieri Blunck, C., Almeida Lopes, B., Zuna, J., Trka, J., Ballerini, P., Lapillonne, H., De Braekeleer, M., Cazzaniga, G., Corral Abascal, L., … Marschalek, R. (2018). The MLL recombinome of acute leukemias in 2017.

Leukemia, *32*(2), 273–284. https://doi.org/10.1038/leu.2017.213

Milne, T. A., Briggs, S. D., Brock, H. W., Martin, M. E., Gibbs, D., Allis, C. D., & Hess, J. L. (2002). MLL targets SET domain methyltransferase activity to Hox gene promoters. *Molecular Cell*, *10*(5), 1107–1117. https://doi.org/10.1016/S1097-2765(02)00741-4

Milne, T. A., Kim, J., Wang, G. G., Stadler, S. C., Basrur, V., Whitcomb, S. J., Wang, Z., Ruthenburg, A. J., Elenitoba-Johnson, K. S. J., Roeder, R. G., & Allis, C. D. (2010). Multiple Interactions Recruit MLL1 and MLL1 Fusion Proteins to the HOXA9 Locus in Leukemogenesis. *Molecular Cell*, *38*(6), 853–863. https://doi.org/10.1016/j.molcel.2010.05.011

Milne, T. A., Martin, M. E., Brock, H. W., Slany, R. K., & Hess, J. L. (2005). Leukemogenic MLL fusion proteins bind across a broad region of the Hox a9 locus, promoting transcription and multiple histone modifications. *Cancer Research*, *65*(24), 11367–11374. https://doi.org/10.1158/0008-5472.CAN-05-1041

Min, J., Feng, Q., Li, Z., Zhang, Y., & Xu, R. M. (2003). Structure of the catalytic domain of human Dot1L, a non-SET domain nucleosomal histone methyltransferase. *Cell*, *112*(5), 711–723. https://doi.org/10.1016/S0092-8674(03)00114-4

Mizuki, M., Schwäble, J., Steur, C., Choudhary, C., Agrawal, S., Sargin, B., Steffen, B., Matsumura, I., Kanakura, Y., Böhmer, F. D., Müller-Tidow, C., Berdel, W. E., & Serve, H. (2003). Suppression of myeloid transcription factors and induction of STAT response genes by AML-specific Flt3 mutations. *Blood*, *101*(8), 3164–3173. https://doi.org/10.1182/blood-2002-06-1677

Mohan, M., Herz, H. M., Takahashi, Y. H., Lin, C., Lai, K. C., Zhang, Y., Washburn, M. P., Florens, L., & Shilatifard, A. (2010). Linking H3K79 trimethylation to Wnt signaling through a novel Dot1-containing complex (DotCom). *Genes and Development*, *24*(6), 574–589. https://doi.org/10.1101/gad.1898410

Moore, M. A. S., Dorn, D. C., Schuringa, J. J., Chung, K. Y., & Morrone, G. (2007). Constitutive activation of Flt3 and STAT5A enhances self-renewal and alters differentiation of hematopoietic stem cells. *Experimental Hematology*, *35*(4 SUPPL.), 105–116. https://doi.org/10.1016/j.exphem.2007.01.018

Mootha, V. K., Lindgren, C. M., Eriksson, K.-F., Subramanian, A., Sihag, S., Lehar, J., Puigserver, P., Carlsson, E., Ridderstråle, M., Laurila, E., Houstis, N., Daly, M. J., Patterson, N., Mesirov, J. P., Golub, T. R., Tamayo, P., Spiegelman, B., Lander, E. S., Hirschhorn, J. N., … Groop, L. C. (2003). PGC-1α-responsive genes involved in oxidative phosphorylation are coordinately downregulated in human diabetes. *Nature Genetics*, *34*(3), 267–273. https://doi.org/10.1038/ng1180

Mossadegh-Keller, N., Sarrazin, S., Kandalla, P. K., Espinosa, L., Richard Stanley, E., Nutt, S. L., Moore, J., & Sieweke, M. H. (2013). M-CSF instructs myeloid lineage fate in single haematopoietic stem cells. *Nature*, *497*(7448), 239–243. https://doi.org/10.1038/nature12026

Mueller, D., Bach, C., Zeisig, D., Garcia-Cuellar, M. P., Monroe, S., Sreekumar, A., Zhou, R., Nesvizhskii, A., Chinnaiyan, A., Hess, J. L., & Slany, R. K. (2007). A role for the MLL fusion partner ENL in transcriptional elongation and chromatin modification. *Blood*, *110*(13), 4445–4454. https://doi.org/10.1182/blood-2007-05-090514

Mueller, D., García-Cuéllar, M. P., Bach, C., Buhl, S., Maethner, E., & Slany, R. K. (2009). Misguided transcriptional elongation causes mixed lineage leukemia. *PLoS Biology*, *7*(11). https://doi.org/10.1371/journal.pbio.1000249

Muhlethaler-Mottet, A., Berardino, W. Di, Otten, L. A., & Mach, B. (1998). Activation of the MHC class II transactivator CIITA by interferon-γ requires cooperative interaction between Stat1 and USF-1. *Immunity*, *8*(2), 157–166. https://doi.org/10.1016/S1074-7613(00)80468-9

Muñoz, M. J., Santangelo, M. S. P., Paronetto, M. P., de la Mata, M., Pelisch, F., Boireau, S., Glover-Cutter, K., Ben-Dov, C., Blaustein, M., Lozano, J. J., Bird, G., Bentley, D., Bertrand, E., & Kornblihtt, A. R. (2009). DNA Damage Regulates Alternative Splicing through Inhibition of RNA Polymerase II Elongation. *Cell*, *137*(4), 708–720. https://doi.org/10.1016/j.cell.2009.03.010

Nagel, G., Weber, D., Fromm, E., Erhardt, S., Lübbert, M., Fiedler, W., Kindler, T., Krauter, J., Brossart, P., Kündgen, A., Salih, H. R., Westermann, J., Wulf, G., Hertenstein, B., Wattad, M., Götze, K., Kraemer, D., Heinicke, T., Girschikofsky, M., … Schlenk, R. F. (2017). Epidemiological, genetic, and clinical characterization by age of newly diagnosed acute myeloid leukemia based on an academic population-based registry study (AMLSG BiO). *Annals of Hematology*, *96*(12), 1993–2003. https://doi.org/10.1007/s00277-017-3150-3

Nagy, Z., & Tora, L. (2007). Distinct GCN5/PCAF-containing complexes function as co-activators and are involved in transcription factor and global histone acetylation. *Oncogene*, *26*(37), 5341–5357. https://doi.org/10.1038/sj.onc.1210604

Nakao, M., Yokota, S., Iwai, T., Kaneko, H., Horiike, S., Kashima, K., Sonoda, Y., Fujimoto, T., & Misawa, S. (1996). Internal tandem duplication of the flt3 gene found in acute myeloid leukemia. *Leukemia*, *10*(12), 1911–1918.

Navaratnam, D. S., Bell, T. J., Tu, T. D., Cohen, E. L., & Oberholtzer, J. C. (1997). Differential distribution of Ca2+-activated K+ channel splice variants among hair cells along the tonotopic axis of the chick cochlea. *Neuron*, *19*(5), 1077–1085. https://doi.org/10.1016/S0896-6273(00)80398-0

Neff, T., Sinha, A. U., Kluk, M. J., Zhu, N., Khattab, M. H., Stein, L., Xie, H., Orkin, S. H., & Armstrong, S. A. (2012). Polycomb repressive complex 2 is required for MLL-AF9 leukemia. *Proceedings of the National Academy of Sciences of the United States of America*, *109*(13), 5028–5033. https://doi.org/10.1073/pnas.1202258109

Ng, H. H., Xu, R. M., Zhang, Y., & Struhl, K. (2002). Ubiquitination of histone H2B by Rad6 is required for efficient Dot1-mediated methylation of histone H3 lysine 79. *Journal of Biological Chemistry*, *277*(38), 34655–34657. https://doi.org/10.1074/jbc.C200433200

Nilsen, T. W., & Graveley, B. R. (2010). Expansion of the eukaryotic proteome by alternative splicing. *Nature*, *463*(7280), 457–463. https://doi.org/10.1038/nature08909

Oberstrass, F. C., Auweter, S. D., Erat, M., Hargous, Y., Henning, A., Wenter, P., Reymond, L., Amir-Ahmady, B., Pitsch, S., Black, D. L., & Allain, F. H.-T. (2005). Structure of PTB bound to RNA: specific binding and implications for splicing regulation. *Science (New York, N.Y.)*, *309*(5743), 2054–2057. https://doi.org/10.1126/science.1114066

Okada, Y., Feng, Q., Lin, Y., Jiang, Q., Li, Y., Coffield, V. M., Su, L., Xu, G., & Zhang, Y. (2005). hDOT1L links histone methylation to leukemogenesis. *Cell*, *121*(2), 167–178. https://doi.org/10.1016/j.cell.2005.02.020

Okuda, H., Kawaguchi, M., Kanai, A., Matsui, H., Kawamura, T., Inaba, T., Kitabayashi, I., & Yokoyama, A. (2014). MLL fusion proteins link transcriptional coactivators to previously active CpG-rich promoters. *Nucleic Acids Research*, *42*(7), 4241–4256. https://doi.org/10.1093/nar/gkt1394

Okuda, H., Stanojevic, B., Kanai, A., Kawamura, T., Takahashi, S., Matsui, H., Takaori-Kondo, A., & Yokoyama, A. (2017). Cooperative gene activation by AF4 and DOT1L drives MLL-rearranged leukemia. *Journal of Clinical Investigation*, *127*(5), 1918–1931. https://doi.org/10.1172/JCI91406

Onishi, M., Nosaka, T., Misawa, K., Mui, A. L.-F., Gorman, D., McMahon, M., Miyajima, A., & Kitamura, T. (1998). Identification and Characterization of a Constitutively Active STAT5 Mutant That Promotes Cell Proliferation. *Molecular and Cellular Biology*, *18*(7), 3871–3879. https://doi.org/10.1128/mcb.18.7.3871

Ono, R., Nakajima, H., Ozaki, K., Kumagai, H., Kawashima, T., Taki, T., Kitamura, T., Hayashi, Y., & Nosaka, T. (2005). Dimerization of MLL fusion proteins and FLT3 activation synergize to induce multiple-lineage leukemogenesis. *Journal of Clinical Investigation*, *115*(4), 919–929. https://doi.org/10.1172/JCI200522725

Orlando, D. A., Chen, M. W., Brown, V. E., Solanki, S., Choi, Y. J., Olson, E. R., Fritz, C. C.,

Bradner, J. E., & Guenther, M. G. (2014). Quantitative ChIP-Seq normalization reveals global modulation of the epigenome. *Cell Reports*, *9*(3), 1163–1170. https://doi.org/10.1016/j.celrep.2014.10.018

Pan, Q., Shai, O., Lee, L. J., Frey, B. J., & Blencowe, B. J. (2008). Deep surveying of alternative splicing complexity in the human transcriptome by high-throughput sequencing. *Nature Genetics*, *40*(12), 1413–1415. https://doi.org/10.1038/ng.259

Panier, S., & Boulton, S. J. (2014). Double-strand break repair: 53BP1 comes into focus. *Nature Reviews Molecular Cell Biology*, *15*(1), 7–18. https://doi.org/10.1038/nrm3719

Papaemmanuil, E., Gerstung, M., Bullinger, L., Gaidzik, V. I., Paschka, P., Roberts, N. D., Potter, N. E., Heuser, M., Thol, F., Bolli, N., Gundem, G., Van Loo, P., Martincorena, I., Ganly, P., Mudie, L., McLaren, S., O'Meara, S., Raine, K., Jones, D. R., … Campbell, P. J. (2016). Genomic Classification and Prognosis in Acute Myeloid Leukemia. *New England Journal of Medicine*, *374*(23), 2209–2221. https://doi.org/10.1056/nejmoa1516192

Pavri, R., Zhu, B., Li, G., Trojer, P., Mandal, S., Shilatifard, A., & Reinberg, D. (2006). Histone H2B Monoubiquitination Functions Cooperatively with FACT to Regulate Elongation by RNA Polymerase II. *Cell*, *125*(4), 703–717. https://doi.org/10.1016/j.cell.2006.04.029

Peltola, K., Hollmen, M., Maula, S. M., Rainio, E., Ristamäki, R., Luukkaa, M., Sandholm, J., Sundvall, M., Elenius, K., Koskinen, P. J., Grenman, R., & Jalkanen, S. (2009). Pim-1 kinase expression predicts radiation response in squamocellular carcinoma of head and neck and is under the control of epidermal growth factor receptor. *Neoplasia*, *11*(7), 629–636. https://doi.org/10.1593/neo.81038

Pieters, R., Schrappe, M., De Lorenzo, P., Hann, I., De Rossi, G., Felice, M., Hovi, L., LeBlanc, T., Szczepanski, T., Ferster, A., Janka, G., Rubnitz, J., Silverman, L., Stary, J., Campbell, M., Li, C. K., Mann, G., Suppiah, R., Biondi, A., … Valsecchi, M. G. (2007). A treatment protocol for infants younger than 1 year with acute lymphoblastic leukaemia (Interfant-99): an observational study and a multicentre randomised trial. *Lancet*, *370*(9583), 240–250. https://doi.org/10.1016/S0140-6736(07)61126-X

Pietschmann, K., Bolck, H. A., Buchwald, M., Spielberg, S., Polzer, H., Spiekermann, K., Bug, G., Heinzel, T., Bo̎hmer, F. D., & Krämer, O. H. (2012). Breakdown of the FLT3-ITD/STAT5 axis and synergistic apoptosis induction by the histone deacetylase inhibitor panobinostat and FLT3-specific inhibitors. *Molecular Cancer Therapeutics*, *11*(11), 2373–2383. https://doi.org/10.1158/1535-7163.MCT-12-0129

Pradeepa, M. M., Sutherland, H. G., Ule, J., Grimes, G. R., & Bickmore, W. A. (2012). Psip1/Ledgf p52 binds methylated histone H3K36 and splicing factors and contributes to the regulation of alternative splicing. *PLoS Genetics*, *8*(5).

https://doi.org/10.1371/journal.pgen.1002717

Qi, W., Chan, H. M., Teng, L., Li, L., Chuai, S., Zhang, R., Zeng, J., Li, M., Fan, H., Lin, Y., Gu, J., Ardayfio, O., Zhang, J. H., Yan, X., Fang, J., Mi, Y., Zhang, M., Zhou, T., Feng, G., … Li, E. (2012). Selective inhibition of Ezh2 by a small molecule inhibitor blocks tumor cells proliferation. *Proceedings of the National Academy of Sciences of the United States of America*, *109*(52), 21360–21365. https://doi.org/10.1073/pnas.1210371110

Quentmeier, H., Reinhardt, J., Zaborski, M., & Drexler, H. G. (2003). FLT3 mutations in acute myeloid leukemia cell lines. *Leukemia*, *17*(1), 120–124. https://doi.org/10.1038/sj.leu.2402740

Rani, A., & Murphy, J. J. (2016). STAT5 in Cancer and Immunity. *Journal of Interferon and Cytokine Research*, *36*(4), 226–237. https://doi.org/10.1089/jir.2015.0054

Rappsilber, J., Ryder, U., Lamond, A. I., & Mann, M. (2002). Large-scale proteomic analysis of the human spliceosome. *Genome Research*, *12*(8), 1231–1245. https://doi.org/10.1101/gr.473902

Rasche, A., Lienhard, M., Yaspo, M. L., Lehrach, H., & Herwig, R. (2014). ARH-seq: Identification of differential splicing in RNA-seq data. *Nucleic Acids Research*, *42*(14), 1–12. https://doi.org/10.1093/nar/gku495

Ribeiro, D., Melão, A., van Boxtel, R., Santos, C. I., Silva, A., Silva, M. C., Cardoso, B. A., Coffer, P. J., & Barata, J. T. (2018). STAT5 is essential for IL-7–mediated viability, growth, and proliferation of T-cell acute lymphoblastic leukemia cells. *Blood Advances*, *2*(17), 2199–2213. https://doi.org/10.1182/bloodadvances.2018021063

Rosen, D. B., Minden, M. D., Kornblau, S. M., Cohen, A., Gayko, U., Putta, S., Woronicz, J., Evensen, E., Fantl, W. J., & Cesano, A. (2010). Functional characterization of FLT3 receptor signaling deregulation in acute myeloid leukemia by single cell network profiling (SCNP). *PLoS ONE*, *5*(10), 10–18. https://doi.org/10.1371/journal.pone.0013543

Rosenblatt, K. P., Sun, Z. P., Heller, S., & Hudspeth, A. J. (1997). Distribution of Ca2+-activated K+ channel isoforms along the tonotopic gradient of the chicken's cochlea. *Neuron*, *19*(5), 1061–1075. https://doi.org/10.1016/S0896-6273(00)80397-9

Rosenfeld, M. G., Lin, C. R., Amara, S. G., Stolarsky, L., Roos, B. A., Ong, E. S., & Evans, R. M. (1982). Calcitonin mRNA polymorphism: Peptide switching associated with alternative RNA splicing events. *Proceedings of the National Academy of Sciences of the United States of America*, *79*(6 I), 1717–1721. https://doi.org/10.1073/pnas.79.6.1717

Ruthenburg, A. J., Allis, C. D., & Wysocka, J. (2007). Methylation of Lysine 4 on Histone H3: Intricacy of Writing and Reading a Single Epigenetic Mark. *Molecular Cell*, *25*(1), 15–30. https://doi.org/10.1016/j.molcel.2006.12.014

Ruthenburg, A. J., Li, H., Milne, T. A., Dewell, S., McGinty, R. K., Yuen, M., Ueberheide, B., Dou, Y., Muir, T. W., Patel, D. J., & Allis, C. D. (2011). Recognition of a mononucleosomal histone modification pattern by BPTF via multivalent interactions. *Cell*, *145*(5), 692–706. https://doi.org/10.1016/j.cell.2011.03.053

Sabra, M., Texier, P., El Maalouf, J., & Lomonte, P. (2013). The Tudor protein survival motor neuron (SMN) is a chromatin-binding protein that interacts with methylated lysine 79 of histone H3. *Journal of Cell Science*, *126*(16), 3664–3677. https://doi.org/10.1242/jcs.126003

Sakharkar, M. K., Chow, V. T. K., & Kangueane, P. (2004). Distributions of Exons and Introns in the Human Genome. *In Silico Biology*, *4*, 387–393.

Sandhöfer, N., Bauer, J., Reiter, K., Dufour, A., Rothenberg, M., Konstandin, N. P., Zellmeier, E., Tizazu, B., Greif, P. A., Metzeler, K. H., Hiddemann, W., Polzer, H., & Spiekermann, K. (2016). The new and recurrent FLT3 juxtamembrane deletion mutation shows a dominant negative effect on the wild-Type FLT3 receptor. *Scientific Reports*, *6*(May), 1–6. https://doi.org/10.1038/srep28032

Santos, S. C. R., Lacronique, V., Bouchaert, I., Monni, R., Bernard, O., Gisselbrecht, S., & Gouilleux, F. (2001). Constitutively active STAT5 variants induce growth and survival of hematopoietic cells through a PI 3-kinase/Akt dependent pathway. *Oncogene*, *20*(17), 2080–2090. https://doi.org/10.1038/sj.onc.1204308

Sassone-Corsi, P., Mizzen, C. A., Cheung, P., Crosio, C., Monaco, L., Jacquot, S., Hanauer, A., & Allis, C. D. (1999). Requirement of Rsk-2 for Epidermal Growth Factor-Activated Phosphorylation of Histone H3. *Science*, *285*(5429), 886 LP – 891. https://doi.org/10.1126/science.285.5429.886

Scheeren, F. A., Naspetti, M., Diehl, S., Schotte, R., Nagasawa, M., Wijnands, E., Gimeno, R., Vyth-Dreese, F. A., Blom, B., & Spits, H. (2005). STAT5 regulates the self-renewal capacity and differentiation of human memory B cells and controls Bcl-6 expression. *Nature Immunology*, *6*(3), 303–313. https://doi.org/10.1038/ni1172

Schmitges, F. W., Prusty, A. B., Faty, M., Stützer, A., Lingaraju, G. M., Aiwazian, J., Sack, R., Hess, D., Li, L., Zhou, S., Bunker, R. D., Wirth, U., Bouwmeester, T., Bauer, A., Ly-Hartig, N., Zhao, K., Chan, H., Gu, J., Gut, H., … Thomä, N. H. (2011). Histone Methylation by PRC2 Is Inhibited by Active Chromatin Marks. *Molecular Cell*, *42*(3), 330–341. https://doi.org/10.1016/j.molcel.2011.03.025

Schübeler, D., MacAlpine, D. M., Scalzo, D., Wirbelauer, C., Kooperberg, C., Van Leeuwen, F., Gottschling, D. E., O'Neill, L. P., Turner, B. M., Delrow, J., Bell, S. P., & Groudine, M. (2004). The histone modification pattern of active genes revealed through genome-wide chromatin analysis of a higher eukaryote. *Genes and Development*, *18*(11), 1263–1271. https://doi.org/10.1101/gad.1198204

Schwartz, S., Meshorer, E., & Ast, G. (2009). Chromatin organization marks exon-intron structure. *Nature Structural and Molecular Biology*, *16*(9), 990–995. https://doi.org/10.1038/nsmb.1659

Scotti, M. M., & Swanson, M. S. (2016). RNA mis-splicing in disease. *Nature Reviews Genetics*, *17*(1), 19–32. https://doi.org/10.1038/nrg.2015.3

Shah, R. N., Grzybowski, A. T., Cornett, E. M., Johnstone, A. L., Dickson, B. M., Boone, B. A., Cheek, M. A., Cowles, M. W., Maryanski, D., Meiners, M. J., Tiedemann, R. L., Vaughan, R. M., Arora, N., Sun, Z. W., Rothbart, S. B., Keogh, M. C., & Ruthenburg, A. J. (2018). Examining the Roles of H3K4 Methylation States with Systematically Characterized Antibodies. *Molecular Cell*, *72*(1), 162-177.e7. https://doi.org/10.1016/j.molcel.2018.08.015

Shen, H., Xu, W., & Lan, F. (2017). Histone lysine demethylases in mammalian embryonic development. *Experimental and Molecular Medicine*, *49*(4), 1–7. https://doi.org/10.1038/emm.2017.57

Shi, J., Wang, E., Zuber, J., Rappaport, A., Taylor, M., Johns, C., Lowe, S. W., & Vakoc, C. R. (2013). The Polycomb complex PRC2 supports aberrant self-renewal in a mouse model of MLL-AF9;Nras G12D acute myeloid leukemia. *Oncogene*, *32*(7), 930–938. https://doi.org/10.1038/onc.2012.110

Singh, P. K., Plumb, M. R., Ferris, A. L., Iben, J. R., Wu, X., Fadel, H. J., Luke, B. T., Esnault, C., Poeschla, E. M., Hughes, S. H., Kvaratskhelia, M., & Levin, H. L. (2015). LEDGF/p75 interacts with mRNA splicing factors and targets HIV-1 integration to highly spliced genes. *Genes and Development*, *29*(21), 2287–2297. https://doi.org/10.1101/gad.267609.115

Smith, C C, Lin, K., Stecula, A., Sali, A., & Shah, N. P. (2015). FLT3 D835 mutations confer differential resistance to type II FLT3 inhibitors. *Leukemia*, *29*(12), 2390–2392. https://doi.org/10.1038/leu.2015.165

Smith, Catherine C, Wang, Q., Chin, C.-S., Salerno, S., Damon, L. E., Levis, M. J., Perl, A. E., Travers, K. J., Wang, S., Hunt, J. P., Zarrinkar, P. P., Schadt, E. E., Kasarskis, A., Kuriyan, J., & Shah, N. P. (2012). Validation of ITD mutations in FLT3 as a therapeutic target in human acute myeloid leukaemia. *Nature*, *485*(7397), 260–263. https://doi.org/10.1038/nature11016

Spiekermann, K., Bagrintseva, K., Schwab, R., Schmieja, K., & Hiddemann, W. (2003). Overexpression and constitutive activation of FLT3 induces STAT5 activation in primary acute myeloid leukemia blast cells. *Clinical Cancer Research*, *9*(6), 2140–2150.

Spiekermann, K., Pau, M., Schwab, R., Schmieja, K., Franzrahe, S., & Hiddemann, W. (2002). Constitutive activation of STAT3 and STAT5 is induced by leukemic fusion proteins with protein tyrosine kinase activity and is sufficient for transformation of hematopoietic precursor cells. *Experimental Hematology*, *30*(3), 262–271. https://doi.org/10.1016/S0301-472X(01)00787-1

Spies, N., Nielsen, C. B., Padgett, R. A., & Burge, C. B. (2009). Biased Chromatin Signatures around Polyadenylation Sites and Exons. *Molecular Cell*, *36*(2), 245–254. https://doi.org/10.1016/j.molcel.2009.10.008

Steger, D. J., Lefterova, M. I., Ying, L., Stonestrom, A. J., Schupp, M., Zhuo, D., Vakoc, A. L., Kim, J.-E., Chen, J., Lazar, M. A., Blobel, G. A., & Vakoc, C. R. (2008). DOT1L/KMT4 Recruitment and H3K79 Methylation Are Ubiquitously Coupled with Gene Transcription in Mammalian Cells. *Molecular and Cellular Biology*, *28*(8), 2825–2839. https://doi.org/10.1128/mcb.02076-07

Stehling-Sun, S., Dade, J., Nutt, S. L., DeKoter, R. P., & Camargo, F. D. (2009). Regulation of lymphoid versus myeloid fate "choice" by the transcription factor Mef2c. *Nature Immunology*, *10*(3), 289–296. https://doi.org/10.1038/ni.1694

Stein, E. M., Garcia-Manero, G., Rizzieri, D. A., Tibes, R., Berdeja, J. G., Savona, M. R., Jongen-Lavrenic, M., Altman, J. K., Thomson, B., Blakemore, S. J., Daigle, S. R., Waters, N. J., Suttle, A. B., Clawson, A., Pollock, R., Krivtsov, A., Armstrong, S. A., DiMartino, J., Hedrick, E., … Tallman, M. S. (2018). The DOT1L inhibitor pinometostat reduces H3K79 methylation and has modest clinical activity in adult acute leukemia. *Blood*, *131*(24), 2662–2669. https://doi.org/10.1182/blood-2017-12-818948

Strahl, B. D., & Allis, C. D. (2000). The language of covalent histone modifications. *Nature*, *403*(6765), 41–45. https://doi.org/10.1038/47412

Stubbs, M. C., Kim, Y. M., Krivtsov, A. V., Wright, R. D., Feng, Z., Agarwal, J., Kung, A. L., & Armstrong, S. A. (2008). MLL-AF9 and FLT3 cooperation in acute myelogenous leukemia: Development of a model for rapid therapeutic assessment. *Leukemia*, *22*(1), 66–77. https://doi.org/10.1038/sj.leu.2404951

Subramanian, A., Tamayo, P., Mootha, V. K., Mukherjee, S., Ebert, B. L., Gillette, M. A., Paulovich, A., Pomeroy, S. L., Golub, T. R., Lander, E. S., & Mesirov, J. P. (2005). Gene set enrichment analysis: A knowledge-based approach for interpreting genome-wide expression profiles. *Proceedings of the National Academy of Sciences of the United States*

of America, *102*(43), 15545–15550. https://doi.org/10.1073/pnas.0506580102

Sullivan, S., & Landsman, D. (2003). Characterization of sequence variability in nucleosome core histone folds. *Proteins*, *52*, 454–465. https://doi.org/10.1002/prot.10441

Sweet, S. M. M., Li, M., Thomas, P. M., Durbin, K. R., & Kelleher, N. L. (2010). Kinetics of re-establishing H3K79 methylation marks in global human chromatin. *Journal of Biological Chemistry*, *285*(43), 32778–32786. https://doi.org/10.1074/jbc.M110.145094

Thiel, A. T., Blessington, P., Zou, T., Feather, D., Wu, X., Yan, J., Zhang, H., Liu, Z., Ernst, P., Koretzky, G. A., & Hua, X. (2010). MLL-AF9-Induced Leukemogenesis Requires Coexpression of the Wild-Type Mll Allele. *Cancer Cell*, *17*(2), 148–159. https://doi.org/10.1016/j.ccr.2009.12.034

Trapnell, C., Pachter, L., & Salzberg, S. L. (2009). TopHat: Discovering splice junctions with RNA-Seq. *Bioinformatics*, *25*(9), 1105–1111. https://doi.org/10.1093/bioinformatics/btp120

Trapnell, C., Roberts, A., Goff, L., & Geo, P. (2013). Differential gene and transcript expression analysis of RNA-seq experiments with TopHat and Cufflinks. *Nature Protocol*, *7*(3), 562–578. https://doi.org/10.1038/nprot.2012.016.Differential

Tse, C., Sera, T., Wolffe, A. P., & Hansen, J. C. (1998). Disruption of Higher-Order Folding by Core Histone Acetylation Dramatically Enhances Transcription of Nucleosomal Arrays by RNA Polymerase III. *Molecular and Cellular Biology*, *18*(8), 4629–4638. https://doi.org/10.1128/mcb.18.8.4629

Tumes, D. J., Onodera, A., Suzuki, A., Shinoda, K., Endo, Y., Iwamura, C., Hosokawa, H., Koseki, H., Tokoyoda, K., Suzuki, Y., Motohashi, S., & Nakayama, T. (2013). The Polycomb protein Ezh2 regulates differentiation and plasticity of CD4+ T helper Type 1 and type 2 cells. *Immunity*, *39*(5), 819–832. https://doi.org/10.1016/j.immuni.2013.09.012

Ueda, K., Yoshimi, A., Kagoya, Y., Nishikawa, S., Marquez, V. E., Nakagawa, M., & Kurokawa, M. (2014). Inhibition of histone methyltransferase EZH2 depletes leukemia stem cell of mixed lineage leukemia fusion leukemia through upregulation of p16. *Cancer Science*, *105*(5), 512–519. https://doi.org/10.1111/cas.12386

Uemura, Y., Oshima, T., Yamamoto, M., Reyes, C. J., Costa Cruz, P. H., Shibuya, T., & Kawahara, Y. (2017). Matrin3 binds directly to intronic pyrimidine-rich sequences and controls alternative splicing. *Genes to Cells*, *22*(9), 785–798. https://doi.org/10.1111/gtc.12512

Ule, J., Stefani, G., Mele, A., Ruggiu, M., Wang, X., Taneri, B., Gaasterland, T., Blencowe, B.

J., & Darnell, R. B. (2006). An RNA map predicting Nova-dependent splicing regulation. *Nature*, *444*(7119), 580–586. https://doi.org/10.1038/nature05304

Van Leeuwen, F., Gafken, P. R., & Gottschling, D. E. (2002). Dot1p modulates silencing in yeast by methylation of the nucleosome core. *Cell*, *109*(6), 745–756. https://doi.org/10.1016/S0092-8674(02)00759-6

van Welsem, T., Frederiks, F., Verzijlbergen, K. F., Faber, A. W., Nelson, Z. W., Egan, D. A., Gottschling, D. E., & van Leeuwen, F. (2008). Synthetic Lethal Screens Identify Gene Silencing Processes in Yeast and Implicate the Acetylated Amino Terminus of Sir3 in Recognition of the Nucleosome Core. *Molecular and Cellular Biology*, *28*(11), 3861–3872. https://doi.org/10.1128/mcb.02050-07

Vermeulen, M., Eberl, H. C., Matarese, F., Marks, H., Denissov, S., Butter, F., Lee, K. K., Olsen, J. V., Hyman, A. A., Stunnenberg, H. G., & Mann, M. (2010). Quantitative Interaction Proteomics and Genome-wide Profiling of Epigenetic Histone Marks and Their Readers. *Cell*, *142*(6), 967–980. https://doi.org/10.1016/j.cell.2010.08.020

Vermeulen, M., Mulder, K. W., Denissov, S., Pijnappel, W. W. M. P., van Schaik, F. M. A., Varier, R. A., Baltissen, M. P. A., Stunnenberg, H. G., Mann, M., & Timmers, H. T. M. (2007). Selective Anchoring of TFIID to Nucleosomes by Trimethylation of Histone H3 Lysine 4. *Cell*, *131*(1), 58–69. https://doi.org/10.1016/j.cell.2007.08.016

Vettese-Dadey, M., Grant, P. A., Hebbes, T. R., Crane-Robinson, C., Allis, C. D., & Workman, J. L. (1996). Acetylation of histone H4 plays a primary role in enhancing transcription factor binding to nucleosomal DNA in vitro. *EMBO Journal*, *15*(10), 2508–2518. https://doi.org/10.1002/j.1460-2075.1996.tb00608.x

Vlaming, H., & van Leeuwen, F. (2016). The upstreams and downstreams of H3K79 methylation by DOT1L. *Chromosoma*, *125*(4), 593–605. https://doi.org/10.1007/s00412-015-0570-5

Voigt, P., LeRoy, G., Drury, W. J., Zee, B. M., Son, J., Beck, D. B., Young, N. L., Garcia, B. A., & Reinberg, D. (2012). Asymmetrically modified nucleosomes. *Cell*, *151*(1), 181–193. https://doi.org/10.1016/j.cell.2012.09.002

Wagner, E. J., & Carpenter, P. B. (2012). Understanding the language of Lys36 methylation at histone H3. *Nature Reviews Molecular Cell Biology*, *13*(2), 115–126. https://doi.org/10.1038/nrm3274

Wahl, M. C., Will, C. L., & Lührmann, R. (2009). The Spliceosome: Design Principles of a Dynamic RNP Machine. *Cell*, *136*(4), 701–718. https://doi.org/10.1016/j.cell.2009.02.009

Walters, D. K., Stoffregen, E. P., Heinrich, M. C., Deininger, M. W., & Druker, B. J. (2017). *Brief report RNAi-induced down-regulation of FLT3 expression in AML cell lines increases sensitivity to MLN518*. *105*(7), 2952–2955. https://doi.org/10.1182/blood-2004-07-2758.Supported

Wang, C., Norton, J. T., Ghosh, S., Kim, J., Fushimi, K., Wu, J. Y., Stack, M. S., & Huang, S. (2008). Polypyrimidine Tract-binding Protein (PTB) differentially affects malignancy in a cell line-dependent manner. *Journal of Biological Chemistry*, *283*(29), 20277–20287. https://doi.org/10.1074/jbc.M803682200

Wang, E. T., Sandberg, R., Luo, S., Khrebtukova, I., Zhang, L., Mayr, C., Kingsmore, S. F., Schroth, G. P., & Burge, C. B. (2008). Alternative isoform regulation in human tissue transcriptomes. *Nature*, *456*(7221), 470–476. https://doi.org/10.1038/nature07509

Wang, G. G., Pasillas, M. P., & Kamps, M. P. (2006). Persistent Transactivation by Meis1 Replaces Hox Function in Myeloid Leukemogenesis Models: Evidence for Co-Occupancy of Meis1-Pbx and Hox-Pbx Complexes on Promoters of Leukemia-Associated Genes. *Molecular and Cellular Biology*, *26*(10), 3902–3916. https://doi.org/10.1128/mcb.26.10.3902-3916.2006

Wang, L., Jin, Q., Lee, J. E., Su, I. H., & Ge, K. (2010). Histone H3K27 methyltransferase Ezh2 represses Wnt genes to facilitate adipogenesis. *Proceedings of the National Academy of Sciences of the United States of America*, *107*(16), 7317–7322. https://doi.org/10.1073/pnas.1000031107

Wang, X., Li, Y., Fan, Y., Yu, X., Mao, X., & Jin, F. (2018). PTBP1 promotes the growth of breast cancer cells through the PTEN/Akt pathway and autophagy. *Journal of Cellular Physiology*, *233*(11), 8930–8939. https://doi.org/10.1002/jcp.26823

Weisberg, E., Sattler, M., Ray, A., & Griffin, J. D. (2010). Drug resistance in mutant FLT3-positive AML. *Oncogene*, *29*(37), 5120–5134. https://doi.org/10.1038/onc.2010.273

Wierenga, A. T. J., Vellenga, E., & Schuringa, J. J. (2008). Maximal STAT5-Induced Proliferation and Self-Renewal at Intermediate STAT5 Activity Levels. *Molecular and Cellular Biology*, *28*(21), 6668–6680. https://doi.org/10.1128/mcb.01025-08

Wilkinson, A. C., Ballabio, E., Geng, H., North, P., Tapia, M., Kerry, J., Biswas, D., Roeder, R. G., Allis, C. D., Melnick, A., de Bruijn, M. F. T. R., & Milne, T. A. (2013). RUNX1 Is a Key Target in t(4;11) Leukemias that Contributes to Gene Activation through an AF4-MLL Complex Interaction. *Cell Reports*, *3*(1), 116–127. https://doi.org/10.1016/j.celrep.2012.12.016

Winters, A. C., & Bernt, K. M. (2017). MLL-rearranged leukemias- An update on science and clinical approaches. *Frontiers in Pediatrics*, *5*(February), 11–13. https://doi.org/10.3389/fped.2017.00004

Wood, K., Tellier, M., & Murphy, S. (2018). DOT1L and H3K79 methylation in transcription and genomic stability. *Biomolecules*, *8*(1), 1–16. https://doi.org/10.3390/biom8010011

Yamamoto, M., Kato, T., Hotta, C., Nishiyama, A., Kurotaki, D., Yoshinari, M., Takami, M., Ichino, M., Nakazawa, M., Matsuyama, T., Kamijo, R., Kitagawa, S., Ozato, K., & Tamura, T. (2011). Shared and distinct functions of the transcription factors IRF4 and IRF8 in myeloid cell development. *PLoS ONE*, *6*(10), 2–11. https://doi.org/10.1371/journal.pone.0025812

Yamamoto, Y., Kiyoi, H., Nakano, Y., Suzuki, R., Kodera, Y., Miyawaki, S., Asou, N., Kuriyama, K., Yagasaki, F., Shimazaki, C., Akiyama, H., Saito, K., Nishimura, M., Motoji, T., Shinagawa, K., Takeshita, A., Saito, H., Ueda, R., Ohno, R., & Naoe, T. (2001). Activating mutation of D835 within the activation loop of FLT3 in human hematologic malignancies. *Blood*, *97*(8), 2434–2439. https://doi.org/10.1182/blood.v97.8.2434

Ye, Z., Chen, Z., Lan, X., Hara, S., Sunkel, B., Huang, T. H. M., Elnitski, L., Wang, Q., & Jin, V. X. (2014). Computational analysis reveals a correlation of exon-skipping events with splicing, transcription and epigenetic factors. *Nucleic Acids Research*, *42*(5), 2856–2869. https://doi.org/10.1093/nar/gkt1338

Yokoyama, A., Wang, Z., Wysocka, J., Sanyal, M., Aufiero, D. J., Kitabayashi, I., Herr, W., & Cleary, M. L. (2004). Leukemia Proto-Oncoprotein MLL Forms a SET1-Like Histone Methyltransferase Complex with Menin To Regulate Hox Gene Expression. *Molecular and Cellular Biology*, *24*(13), 5639–5649. https://doi.org/10.1128/mcb.24.13.5639-5649.2004

Yokoyama, Akihiko, & Cleary, M. L. (2008). Menin Critically Links MLL Proteins with LEDGF on Cancer-Associated Target Genes. *Cancer Cell*, *14*(1), 36–46. https://doi.org/10.1016/j.ccr.2008.05.003

Yokoyama, Akihiko, Somervaille, T. C. P., Smith, K. S., Rozenblatt-Rosen, O., Meyerson, M., & Cleary, M. L. (2005). The menin tumor suppressor protein is an essential oncogenic cofactor for MLL-associated leukemogenesis. *Cell*, *123*(2), 207–218. https://doi.org/10.1016/j.cell.2005.09.025

Yu, B. D., Hess, J. L., Horning, S. E., Brown, G. A. J., & Korsmeyer, S. J. (1995). Altered Hox expression and segmental identity in Mll-mutant mice. *Nature*, *378*(6556), 505–508. https://doi.org/10.1038/378505a0

Yu, W., Chory, E. J., Wernimont, A. K., Tempel, W., Scopton, A., Federation, A., Marineau, J. J., Qi, J., Barsyte-Lovejoy, D., Yi, J., Marcellus, R., Iacob, R. E., Engen, J. R., Griffin, C., Aman, A., Wienholds, E., Li, F., Pineda, J., Estiu, G., … Schapira, M. (2012). Catalytic site remodelling of the DOT1L methyltransferase by selective inhibitors. *Nature Communications*, *3*, 1–12. https://doi.org/10.1038/ncomms2304

Yuan, W., Xie, J., Long, C., Erdjument-Bromage, H., Ding, X., Zheng, Y., Tempst, P., Chen, S., Zhu, B., & Reinberg, D. (2009). Heterogeneous nuclear ribonucleoprotein L is a subunit of human KMT3a/set2 complex required for H3 Lys-36 trimethylation activity in vivo. *Journal of Biological Chemistry*, *284*(23), 15701–15707. https://doi.org/10.1074/jbc.M808431200

Yun, M., Wu, J., Workman, J. L., & Li, B. (2011). Readers of histone modifications. *Cell Research*, *21*(4), 564–578. https://doi.org/10.1038/cr.2011.42

Zeisig, B. B., Milne, T., Garcia-Cuellar, M.-P., Schreiner, S., Martin, M.-E., Fuchs, U., Borkhardt, A., Chanda, S. K., Walker, J., Soden, R., Hess, J. L., & Slany, R. K. (2004). Hoxa9 and Meis1 Are Key Targets for MLL-ENL-Mediated Cellular Immortalization. *Molecular and Cellular Biology*, *24*(2), 617–628. https://doi.org/10.1128/mcb.24.2.617-628.2004

Zeleznik-Le, N. J., Harden, A. M., & Rowley, J. D. (1994). 11q23 translocations split the "AT-hook" cruciform DNA-binding region and the transcriptional repression domain from the activation domain of the mixed-lineage leukemia (MLL) gene. *Proceedings of the National Academy of Sciences of the United States of America*, *91*(22), 10610–10614. https://doi.org/10.1073/pnas.91.22.10610

Zhang, T., Cooper, S., & Brockdorff, N. (2015). The interplay of histone modifications – writers that read. *EMBO Reports*, *16*(11), 1467–1481. https://doi.org/10.15252/embr.201540945

Zhao, Y., & Garcia, B. A. (2015). Comprehensive catalog of currently documented histone modifications. *Cold Spring Harbor Perspectives in Biology*, *7*(9), 1–20. https://doi.org/10.1101/cshperspect.a025064

Zhou, J., Bi, C., Cheong, L. L., Mahara, S., Liu, S. C., Tay, K. G., Koh, T. L., Yu, Q., & Chng, W. J. (2011). The histone methyltransferase inhibitor, DZNep, up-regulates TXNIP, increases ROS production, and targets leukemia cells in AML. *Blood*, *118*(10), 2830–2839. https://doi.org/10.1182/blood-2010-07-294827

Zhou, J., Bi, C., Janakakumara, J. V., Liu, S. C., Chng, W. J., Tay, K. G., Poon, L. F., Xie, Z., Palaniyandi, S., Yu, H., Glaser, K. B., Albert, D. H., Davidsen, S. K., & Chen, C. S. (2009). Enhanced activation of STAT pathways and overexpression of survivin confer resistance to FLT3 inhibitors and could be therapeutic targets in AML. *Blood*, *113*(17), 4052–4062.

https://doi.org/10.1182/blood-2008-05-156422

Zhou, Z., Licklider, L. J., Gygi, S. P., & Reed, R. (2002). Comprehensive proteomic analysis of the human spliceosome. *Nature*, *419*(6903), 182–185. https://doi.org/10.1038/nature01031

Zhu, J., Cote-Sierra, J., Guo, L., & Paul, W. E. (2003). Stat5 activation plays a critical role in Th2 differentiation. *Immunity*, *19*(5), 739–748. https://doi.org/10.1016/S1074-7613(03)00292-9

Zhu, L., Li, Q., Wong, S. H. K., Huang, M., Klein, B. J., Shen, J., Ikenouye, L., Onishi, M., Schneidawind, D., Buechele, C., Hansen, L., Duque-Afonso, J., Zhu, F., Martin, G. M., Gozani, O., Majeti, R., Kutateladze, T. G., & Cleary, M. L. (2016). ASH1L links histone H3 lysine 36 dimethylation to MLL Leukemia. *Cancer Discovery*, *6*(7), 770–783. https://doi.org/10.1158/2159-8290.CD-16-0058

Zhu, X., He, F., Zeng, H., Ling, S., Chen, A., Wang, Y., Yan, X., Wei, W., Pang, Y., Cheng, H., Hua, C., Yang, X., Lu, X., Cao, L., Hao, L., Dong, L., Zou, W., Wu, J., Li, X., … Hospital, C. (2014). Identification of functional cooperative mutations of SETD2 in human acute leukemia. *Nature Genetics*, *46*(3), 287–293. https://doi.org/10.1038/ng.2894.Identification